Queen Mary
University of London

Barts & The London

Biophysical Regulation of Nuclear Architecture in Human Keratinocytes

Oscar Jose Pundel

Centre for Cell Biology and Cutaneous Research, Blizard Institute

Barts and The London School of Medicine and Dentistry

Queen Mary University of London

Supervisor: Dr. John T. Connelly

Co-supervisor: Prof. David Kelsell

Thesis submitted in partial fulfilment of the requirements of the

Degree of Doctor of Philosophy

October 2020, London

Statement of originality

I, Oscar Jose Pundel, confirm that the research included within this thesis is my own work or that where it has been carried out in collaboration with, or supported by others, that this is duly acknowledged below and my contribution indicated. Previously published material is also acknowledged below.

I attest that I have exercised reasonable care to ensure that the work is original, and does not to the best of my knowledge break any UK law, infringe any third party's copyright or other Intellectual Property Right, or contain any confidential material.

I accept that the College has the right to use plagiarism detection software to check the electronic version of the thesis.

I confirm that this thesis has not been previously submitted for the award of a degree by this or any other university.

Signature:

Date: 16th October 2020

Abstract

Epidermal homeostasis is an essential process in the maintenance of healthy skin, and it is regulated by the fine tuning of the proliferation and terminal differentiation of keratinocytes. Various biochemical and biophysical cues regulate the balance between growth and differentiation within the epidermis, and limited adhesion to the extracellular matrix (ECM) is a key trigger for terminal differentiation. Previous studies in our laboratory have shown that keratinocyte adhesion and spreading also influence the size and shape of the nucleus, potentially impacting chromatin remodelling and epigenetic gene regulation. Here, we investigated the direct impact of simple mechanical stimuli on the nuclear architecture of human keratinocytes (HK) using micropatterned substrates to control the adherent surface and cell morphology. When cultured on small micropatterns (20 µm diameter), HKs adopted a rounded morphology and induced terminal differentiation within 24h, while on larger patterns (50 µm diameter) HKs were able to spread and remained undifferentiated. Nuclear morphology is also altered as the nuclear cross-sectional area and volume are both reduced on small patterns.

Immunofluorescence imaging of the nucleoskeletal proteins Lamin A/C showed a clear redisposition towards the nuclear periphery after 24h in HKs on the small patterns but not large patterns. Analysis of immunofluorescence intensity levels of closed and open chromatin markers showed a significant reduction of chromatin markers H3K27Ac, H3K27me3 and H3K9me3 on small patterns after 24h. Furthermore, closed chromatin marker H3K27me3 and H3K9me3 showed differential association into foci; clusters of the marker seem to condense together into fewer and larger foci after 24h on small patterns. Interestingly, we also observed nucleoli fusing on the small patterns, resulting in less numerous and larger nucleoli and reduced translational activity of the HKs. RNAi knockdown of Nesprin-2 and plectin-KO mice cell lines further revealed that these responses depend specifically on the size and shape of the nucleus as influenced by its linkage to the F-actin network. Finally, transcriptional profiling identified corresponding differences in downstream gene expression patterns, notably in ribosome biogenesis, DNA damage repair and retinoic acid signalling pathways accompanied by measurable changes in cellular phenotype.

Together, these findings indicate that biophysical cues directly regulate nuclear architecture in HKs and are translated in differential expression of genes.

Contents

Table of Figures

Table of Tables

List of Abbreviations

ANOVA	Analysis of variance
ATAC	Assay for transposase-accessible chromatin
ATP	Adenosine triphosphate
CT	Chromosome territory
DAPI	4’,6-diamidino-2-phenylindole
DMEM	Dulbecco's modified eagle's medium
DMSO	Dimethylsufoxide
DNA	Deoxyribonucleic acid
DNMT	DNA methyltransferase
DSB	Double strand break
EBS	Epidermolysis bullosa simplex
ECM	Extracellular matrix
EDC	Epidermal differentiation complex
EDTA	Ethylenediaminetetraacetic acid
EGF	Epidermal growth factor
EM	Electron microscopy
ESC	Embryonic stem cells
FBS	Foetal bovine serum
GFP	Green fluorescent protein
GO	Gene ontology
HAT	Histone acetyltransferase
HDAC	Histone deacetylase
HK	Human keratinocytes
HMT	Histone methyltransferase
HP1	Heterochromatin Protein 1
ICF	Immunodeficiency, centromere instability and facial
IF	Intermediate filaments
KD	Knockdown

KO	Knockout
KSFM	Keratinocyte serum free media
LAD	Lamina associated domain
LINC	Linker of nucleoskeleton and cytoskeleton
lncRNA	long non-coding RNA
NAD	Nucleoli associated domain
NOR	Nucleolar Organising Region
NPC	Nuclear pore complex
ORC	Origin recognition complex
PBS	Phosphate-buffered saline
PCA	Principal component analysis
PDMS	Polydimethylsiloxane
PRC	Polycomb repressive complex
PTM	Post translational modifications
RA	Retinoic acid
RNA	Ribonucleic Acid
rRNA	ribosomal RNA
RT-qPCR	Real-time quantitative polymerase chain reaction
SD	Standard deviation
SIR	Silent information regulation
siRNA	Small interfering ribonucleic acid
TAC	Transient amplifying cell
TADs	Topologically associated domains
TET	Ten-eleven translocation
TG	Transglutaminase
WT	Wild type

Acknowledgements

I would like to thank my parents, for their unbridled love and support they have shown me across the years and without with I would certainly not have made it here nor through this project. I do not thank them enough in real life for all that they have given me, so I take this moment to tell them thank you for always being there for me and I love you.

I also thank the rest of my family. My siblings Celia, Claire and Louis, which I am also very thankful to have reconnected so much in the last few years. They made home feel like home every time I came back to visit. I want to thank my grandmother Pilar, who I do not call nearly enough to thank her for all the Spanish charcuterie she sends me over the mail, and for her love and support. Monica and Giancarlo, late additions to the family but definitively not least, and have found a warm spot in my heart.

I thank my supervisor John, for trusting me to conduct this project, his mentoring and support throughout. I count myself very lucky to have had him as my mentor which has helped me grow academically as well as personally. I also thank the rest of the Connelly lab; Atiya, Rosie, Oli, Liisa, Rotimi and Sarah. Partners in the lab and in shenanigans, we had a great supportive ambiance which made lab life much more fun. Ana too, gone but not forgotten, for her invaluable support at the beginning of my thesis which I would not have survived without. My PhD twin, Michael, and our incredibly unproductive collaboration which nevertheless made me fell less alone in the PhD boat. And the rest of the Blizard people (in no particular order): Zak, Lavinia, Jordan, Bjorn, Laura, Rob, Tanwi, Lucas, Chris, Ryan, Hannah, Mat, Jan, Belen, Luke, Gary, Krish, Alida, Eleri, Meg, Beth, Darren, Duncan, Elly, Lottie, Alice, Stef, Mo, Shahid, the post room team, Cleo, Susanne, Kenny, Maria, and many, many more.

I also thank my “real life” friends for their support and friendship over the years. My flatmates and moreover great friends Dan and Casper, which had to endure my antics in the comfort of our home. Sofia and Steve, for always giving me great occasions to blow off some steam. Irene who without our London-Spanish family would not be complete. The rest of the London E3 and EPFL expat teams. All my friends from Balelec, my second family, who did not miss an occasion to come and visit and who I miss dearly. Val, Paulo, Babas, Thaïs, David (x2), Simon (x2), Antoine, Una, Marie, Steph, Mick et puis tous les autres (vous êtes trop).

And Maria. I often wonder how I am so lucky to have met you, and that we are sharing this moment in life. Thank you for all the support, advice, laughs and cuddles. I love you.

Chapter 1: Introduction

The skin homeostasis

The skin is the largest organ in the human body by weight and serves as the primary barrier protecting the interior of the body from the external environment, pathogens and water loss[1], as well as other functions arising from its role as an interface such as somatosensation[2]. It is composed of three major layers; epidermis, dermis and subcutis[1].

The epidermis is the outermost layer of the skin. It sits above the dermis and is separated from it by a basement membrane consisting above all of collagen IV fibrils and laminin 332[1]. The epidermis is mainly composed of keratinocytes that are arranged in stratified layers that overlie a basal layer aptly named stratum basale. The other layers, from innermost to outer, are the spinous layer (stratum spinosum), granular layer (stratum granulosum), clear or translucent layer (stratum lucidum, only present in palms and soles) and finally the cornified layer (stratum corneum)[1].

As the primary interface between the interior and exterior of the body, the epidermis is subjected to intense physical and biochemical insults by foreign bodies and pathogens, creating a substantial need for constant replenishment. This is achieved by what is called epidermal homeostasis. The basal layer of the epidermis is made up mainly of proliferating keratinocytes, as well as a long-term self-renewing population of stem cells. The epidermal stem cells will for the most part stay in an almost quiescent state before undergoing asymmetric division, producing one new stem cell and a transit amplifying cell (TAC)[3]. The latter will keep on proliferating and ultimately differentiate. Once differentiating, keratinocytes will start migrating

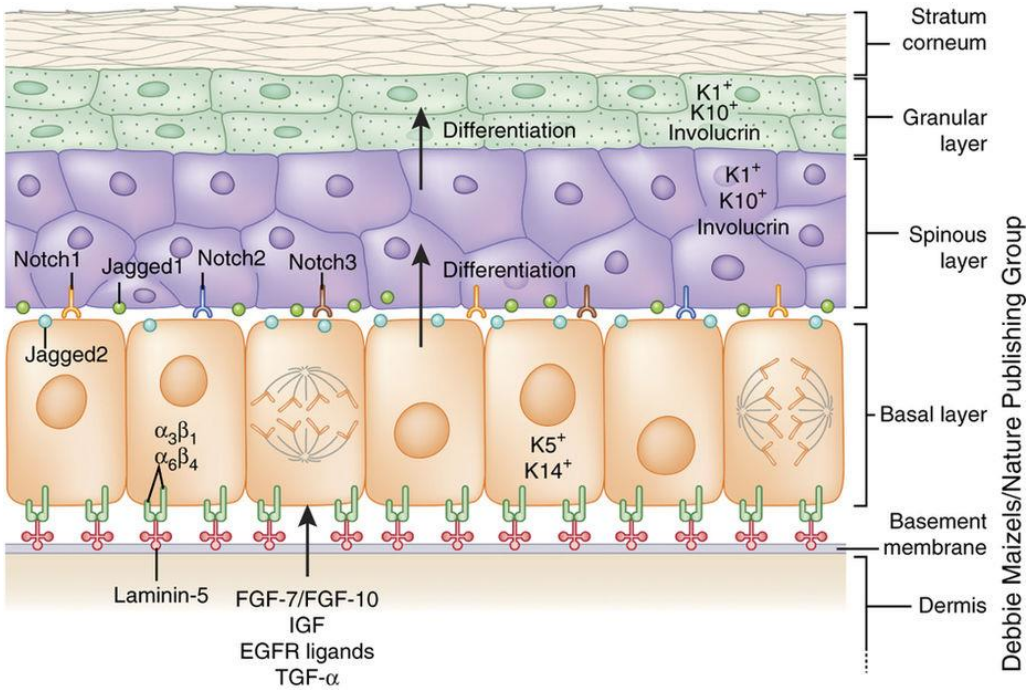

Figure 1.1. *Schematic representation of the epidermal layers. Adapted from Fuchs et al. 2014*

from the basal layer outwards[4]. During this journey they will undergo major changes in phenotype culminating in their transformation into enucleated corneocytes, which compose the stratum corneum, where eventual desquamation or physical trauma will remove them.

The initial asymmetric division and the subsequent entry into the differentiation pathway are primed by extracellular cues. These cues can be inherent to regular homeostasis, i.e to replenish normal loss of skin cells due to desquamation[4] but can also respond to more punctual needs. For example, during early stage development the epidermis is a fast-growing organ and so keratinocytes are in great demand[5]. Physical insults such as wounds will also require elevated levels of proliferation and differentiation to replace the loss of skin[6].

Entry into the differentiation pathway marks several changes in gene expression patterns and phenotype of keratinocytes. Initially a withdrawal from the cell cycle accompanied by a transition from basal to suprabasal layer can be observed. During this initial transition genes coding for intermediate filaments (IF) keratins 5 and 14 will be switched off and replaced by keratins 1 and 10, forming a stronger IF network[7]. This also follows the loss of hemidesmosomes linking the keratinocyte to the basement membrane. A shift in desmosome component isoforms sees desmogleins (Dsg) and descomocollins (dsc) 2 and 3 replaced by Dsg and Dsc 1, while adherens junctions see the loss of P-Cadherin while retaining E-Cadherins[8]. Involucrin and transglutaminase-1 will start being produced as keratinocytes prepare for the last step of differentiation: cornification. Transglutaminase-1 will serve to crosslink several substrates (including involucrin) into the insoluble cornified envelope. When keratinocytes move above the stratum granulosum they produce profilaggrin, the precursor of filaggrin, that serves to bundle keratin filaments and avoid water loss of the epidermis[9], and loricrin, another component of the cornified envelope. Finally, as the cells enter the stratum corneum they undergo nuclear degradation while keratin bundles and lipids secreted by lamellar bodies within the cornified envelope create a strong and impervious layer that protects the ones bellow.

The term homeostasis in skin directly implies that this process is balanced, as the number of cells being removed from the stratum corneum is replaced by a similar number of new cells coming from the stratum basale. All the changes listed here have profound effects on the proper maintenance of the epidermis and can be highlighted by the pathologies that arise from faulty differentiation. For example, keratins 1 and 10 serve to give the epidermis physical resilience through a strong IF network. Mutations in both keratins result in diseases such as Epidermolytic Ichthyosis[10], which can have life threatening effects in early childhood through severe infection, electrolyte imbalances, and sepsis risks while transitioning into a milder form of chronic skin blistering during adulthood. Other examples exist, such as Striate palmoplantar keratoderma (mutations in desmoglein 1 reduces number of desmosomes and perturbs keratin IF

organisation)[11], Lamellar ichthyosis (reduction in Involucrin levels which induces alterations in desquamation process)[12], etc. It is important to note also that as many of these components are shared between epithelial cell types their mutations can also create pathologies in other organs, most notably the gastrointestinal tract[13].

Certain traumas such as wounds can also disturb this balance and require the system to able to withstand punctual changes of diverse magnitude. As with pathologies that arise from improper differentiation, faulty wound healing can also result in dysfunctions of varying severity. A simple example is certain types of skin tumours that arise from overproliferation of keratinocytes after wound healing fails to act properly[6,14].

Nuclear architecture

While entry to the differentiation pathway is partly regulated by extracellular signals that induce changes in gene expression (which will be reviewed later), these changes are maintained by further remodelling of the epigenetic landscape[15,16], which arise from how DNA is stored in the nucleus.

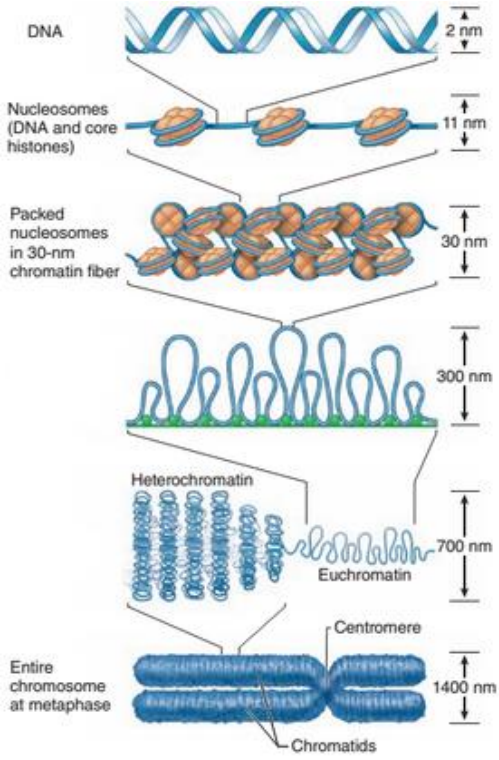

Figure 1.2. *Schematic representation of the different levels of chromatin organisation. Adapted from Junqueira's Basic Histology.*

Indeed, DNA organisation within the nucleus is a highly controlled process, as two meters of it are encased into an organelle that is a few micrometers wide in diameter. For this to be possible the double strands are wrapped around histones, proteins that package DNA into nucleosomes, which in turn form chromosomes[17]. These chromosomes occupy their own distinct territories and share space with several other nuclear bodies such as nucleoli, polycomb bodies or Cajal bodies. Several mechanisms allow for this complex packaging, from DNA methylation, histone covalent post translational modifications (PTMs) and higher order chromosome organisation in 3D such as topologically associated domains (TADs), that are controlled in part by the nucleoskeleton[18]. A striking feature of this compartmentalisation within the nucleus is the absence of physical barriers; contrarily to

cytoplasmic organelles which are encapsulated by membranes, nuclear organelles and territories are segregated through protein-protein or DNA-protein interactions[17]. As DNA accessibility to the transcriptional machinery is in this way tightly controlled, it allows both for "bulk" changes in phenotype of cells as well as for an additional level of fine tuning in the expression of genes above the regular use of transcription factors for example[19].

DNA methylation

At the DNA level the first mechanism of epigenetic control is the methylation of DNA at cytosine and adenine bases. Cytosine methylation is a common occurrence, especially in the context of CpG dinucleotides, and has been widely studied while adenine methylation remains relatively rarer and less well understood[20]. CpG methylation refers to the methylation of a cytosine base 5 prime to a guanine base, and the relative accumulation of both bases upstream of transcriptional start sites is referred to as CpG islands. Hypermethylation of these islands is usually associated with repression of gene expression as well as histone deacetylation and heterochromatin[21] and is catalysed by DNA methyltransferases (DNMT). Inversely hypomethylation at these sites are associated with gene activation and euchromatin, and the removal of methyl groups is catalysed by DNA demethylases. As of now there are 3 known DNMTs (DNMT1, DNMT3A and DNMT3B), each one responsible for specific roles in the maintenance or addition/removal of methylation marks. For example, DNMT1 mediates maintenance of methylation after DNA replication by acting on the hemimethylated strand[22] while DNMT3A and DNMT3B catalyse de novo methylation of CpG islands[23]. As direct DNA demethylation is a controversial topic, mainly since the actual removal of a methyl group is thermodynamically highly unfavourable, the two families of DNA demethylases contribute to the two known indirect demethylation pathways. The first one sees conversion of methylcytosine by deamination into thymine then base excision and eventual insertion of a regular cytosine at the same position[24]. The second one consists of conversion by hydroxylation, catalysed by Ten-Eleven Translocation (TET) enzymes[25].

DNA methylation then plays an important role in gene expression but is also implicated in other processes such as X-chromosome inactivation, genome stability through repression of transposable elements, genomic imprinting or aging. Aberrant DNA methylation is at the center of several pathologies such as cancer[26,27], several autoimmune diseases such as rheumatoid arthritis[28] and multiple sclerosis[29], metabolic disorders like hyperglycemia[30], or age-related diseases like Parkinson[31] or Alzheimer[32]. For example, perturbation of correct X-chromosome inactivation, such as mutations in DNMT3B resulting in incorrect DNA methylation in the inactivated X-chromosome (X_i), has been linked to general hypomethylation within the X_i seen

in Immunodeficiency, Centromere instability and Facial anomalies (ICF) syndrome[33]. This hypomethylation phenomenon results in both improper activation of genes but also in aberrant folding of the X_i, affecting genes that are distant from the original methylation sites.

As of now there is not a clear consensus of how DNA methylation inhibits gene expression but 3 main hypotheses rise: in the first one DNA methylation simply creates steric hindrance vis a vis the translational machinery, for example preventing transcription factor binding[34,35]. In the second one a higher order effect, likely due to electrostatic interactions between DNA and histones, induces chromatin compaction and effectively limits access to the translational machinery, although proof of this is yet to be found. Finally, the third one arises from interactions between chromatin remodelers or histone modifiers and methylated DNA.

There is mounting proof of this concept as these interactions are being actively researched and the fact that DNA methylation does not exist in isolation: this epigenetic mark is correlated with specific histone modifications, most notably lysine methylations, hinting at a direct crosstalk between the epigenetic mark and the histone modification machinery. For example, methylated CpG DNA binding protein MeCP2 (part of the MBD family) is known to associate with Suv39h1/2 histone methyltransferase[36], which implement the H3K9me3 mark on histones, but recent research points towards a much more complex mechanism than simple recruitment of histone methyltransferases[37]. Inversely, non-methylated CpG islands can also direct chromatin structure. For example, it has been shown that the ZF-CxxC domain protein Cfp1, which is known for recruiting Set1a/b H3K4 methyltransferases, binds non-methylated CpG islands in vitro. To further demonstrate the regulatory power of DNA methylation we can note a recent discovery of a reversible DNA-protein cross-link directed by 5-formylcytosine (5fC), the oxidation product of 5-methylcytosine. 5fC displays distinct distribution compared to 5mC, and can form Schiff-base conjugates with lysine residues of proteins with a “short” half-life[38], which indicates a possible additional time-sensible transcriptional regulation characteristic of DNA methylation.

Histones and the histone code

As mentioned before histone PTMs are a well-defined epigenetic mechanism of gene transcriptional control[39]. Histones are alkaline proteins subdivided in five major families: H1/H5, the “linker histones” and H2A, H2B, H3 and H4, the “core histones”. Core histones assemble as dimers using a “handshake” motif: the head domain of one connects to the tail of the other. The four dimers then assemble into a octameric structure; the nucleosome core[40]. 146 base pairs (bp) of DNA can wrap around the nucleosome in a 1.65 left-handed super-helical turn when

tightly bound. The linker histones then “close the loop” by binding the nucleosome and securing the DNA in place. Consequently, there are about 50bp of DNA separating each nucleosome.

Interactions between DNA and the histones account for a great part for how tightly packed the chromatin is and core histones have tails that stick out of the nucleosome and can be modified to modulate these interactions[39]. For example, two of the major histone PTMs are H3K27me3 (Histone 3, Lysine residue 27, tri-methylation) and H3K27Ac (Acetylated version). The first modification induces a positive charge on the histone, thus attracting the negatively charged DNA closer to the nucleosome. This modification is generally found in what is called heterochromatin, or compacted chromatin, and is associated with genes that are transcriptionally silenced. Inversely, H3K27Ac creates a negative charge on the histone, repulsing the DNA and thus opening up the chromatin (the open chromatin state is usually referred as euchromatin), giving transcriptional machinery access to the DNA stored there.

There exists a myriad of histone PTMs that permit a fine tuning of the chromatin opening state, which are dubbed the “Histone Code”. Table 1 summarizes a short list of histone PTMs and their respective effect on chromatin condensation. Note that methylation or acetylation of histone tails do not always have the same effects on activation or repression of nearby genes. It should also be noted that there exists many other modifications such as phosphorylation[41] and ubiquitylation[42], as well as arginine methylation[43] and threonine/serine/tyrosine phosphorilation[44] which will not be discussed here but are merely mentioned to underline the complexity of the histone code. It is also important to note that there exists controversy around the actual significance of the histone code, which would postulate that local chromatin structure as dictated by histone modifications are the main drivers of gene expression and that they are universal, i.e any two genes sharing equal histone PTMs would have similar expression patterns. While the actual importance and moreover reproducibility across genes of local chromatin state remains a hot topic, it is undeniable that the histone code only answers part of the question and that it must be understood as a fragment of all the possible mechanisms of gene expression.

Type of modification	Histone residue							
	H3K4	H3K9	H3K14	H3K27	H3K79	H3K122	H4K20	H2BK5
Mon-methylation	activation	activation		activation	activation		activation	activation
di-methylation	activation	repression		repression	activation			
tri-methylation	activation	repression		repression	activation, repression			repression
Acetylation		activation	activation	activation		activation		

***Table 1.1**. Summary of main histone code methylation and acetylation variants and their effect on gene expression.*

Histone PTMs can be found throughout the genome, and each modification has different roles depending on their location and combination. For example, H3K4me3 is prevalent in

transcriptionally active promoter regions[45]. Both H3K9me3 and H3K27me3 are found at repressed genes but H3K9me3 occupies constitutively repressed genes while H3K27me3 is mostly found at facultatively repressed genes[46]. Combination of activating or repressing marks can help regulate more precisely gene expression. Inversely, chromatin containing both gene repressing and gene activating modifications is often called "poised" and is a marker of cell stemness as it is prevalent in lineage-specific regulatory genes in embryonic stem cells[47]. A classic combination for poised genes is H3K4me3 and H3K27me3[48] but others exist. Combinations of active/active or repressive/repressive marks also occurs when tuning gene expression. H3K27Ac is present at active enhancers containing H3K4me1, effectively distinguishing them from inactive enhancers that only contain H3K4me1[49].

All these modifications are brought about by enzymes that catalyse each specific histone PTM. Depending on the catalysed modification, either addition or removal of a mark, these enzymes are called "writers" or "erasers". Histone methyltransferases (HMTs) and acetyltransferases (HATs) are writers while histone demethylases (HDMs or HDMTs) and deacetylases (HDACs) are erasers. Each family of writers or erasers can be further down classified depending on the amino acid that will receive the PTM (lysine, arginine, etc, as well as their protein domain) and the actual PTM catalysed, i.e mono vs. di vs. trimethylation, etc… which are usually closely related to the sequence homology of their catalytic sites[50]. For example, lysine HMTs (or HKMTs) that are SET domain containing have particular aromatic residues in their catalytic site that determines the final lysine methylation multiplicity state[51]. HKMT SET7/9 with a tyrosine will be sterically hindered to such an extent that only the monomethylated form can fit within the catalytic pocket, while phenylalanine will be able to fit a dimethylated lysine[52]. Owing to the complexity of histone PTMs and their effect in chromatin biology, writer and eraser families are quite populous and sequence homology in shared domain active sites (e.g SET domain) is varied.

The activity of writers and erasers is furthermore regulated through their association with other proteins. We stated before that discrete modifications of histones can have effects on chromatin opening state through electrostatic interactions, but within differentially methylated residues electrostatic charges are the same. Rather, multiplicity of methylation serves as a recognizable mark to direct protein complexes effectively. Akin to writers and erasers, readers are domains that recognize epigenetic markers[53]. Readers are often found on writers and erasers, like for example the bromo domains found in HATs that recognize H4K8Ac [54]. But they can also be part of more diverse proteins that interact with chromatin or DNA in a myriad of other ways, such as Heterochromatin Protein 1 (HP1).

HP1 is a family of proteins heavily associated with heterochromatin maintenance[55] which contains a chromodomain capable of recognizing H3K9me3[56] and a chromo shadow domain, a

distantly related domain that is usually present in chromodomain-containing proteins[57]. The chromo shadow domain is of particular interest as not only it does self-associate, effectively making HP1 a non-covalent linker of heterochromatin nucleosomes thus helping its macromolecular condensation, but also interacts with other chromatin regulating proteins. For example, HP1 interacts with histone methyltransferase SUV39H1[58], serving as a scaffold to further direct chromatin condensation through histone methylation and to help maintain heterochromatin. It also has been found to work with DNMT1[59] as well as other diverse proteins such as methylated CpG binding protein 2 (MECP2) or the origin recognition complex (ORC).

There exists a plethora of multi-subunit histone modifying complexes, such as the polycomb repressive complexes (PRC)[60], Silent Information Regulator (SIR)[61] or SAGA[62] among others. An important result of several readers, writers and erasers working together is the contextualisation of histone modification. Indeed, thanks to this multiplicity of subunits histone modifications can be targeted to the same histone, the same nucleosome or several nucleosomes away[63].

Chromatin remodellers

DNA methylation and the histone code are not only then effective ways to control interactions between DNA, histones and other regulating proteins, but can also affect the higher order structure of chromatin in a "passive" way. But other complexes serve to directly modify chromatin structure using ATP hydrolysis to physically change positions of nucleosomes by mobilizing, exchanging or ejecting them; these are called chromatin remodeller complexes. Their function is mainly to reveal DNA from the tangle of nucleosomes, exposing it to sequence specific regulators. For this they contain the Snf2 family ATPase subunit which effectively mobilizes nucleosomes using ATP[64]. Additionally, they contain several other subunits such as epigenetic, DNA or RNA readers which help guide their activity, domains that regulate the activity of the ATPase and domains that serve as a scaffold to recruit transcriptional apparatus to the DNA. The untangling of DNA for transcription needs to be precise, and sometimes needs to be done fast, which is why chromatin remodellers are very diverse in nature as well as numerous. There is about one remodelling complex per 10 nucleosomes[65] and they are divided in at least 4 families depending on the flanking domains of Snf2, each with their own subfamilies.

The SWI/SNF family have a N-terminus helicase-SANT domain which recruits actin and actin-related proteins Arp7p and Arp9, and a bromo domain. Their name arises from the function that was being screened when they were discovered in yeast (mating-type SWItching and Sucrose Non Fermenting). Eukaryotes have two main members: BAF (Brg1 Associated Factors)

and PBAF (Polybromo-associated BAF), both sharing eight subunits. It has been shown that recognition of acetylated H3 residues by the bromodomain is necessary for the correct configuration of the remodellers before nucleosome sliding but does not need ATP[66]. After that they can either slide[67], transfer[68] or remodel nucleosomes[69]. They have been shown to also interact with other epigenetic modifiers, such as antagonism with the Polycomb Represive Complex (PRC) through direct eviction[70,71]. Mutation of several subunits, for example Brg1 in mice, have shown that they have tumour suppressor capabilities[72], and accordingly specific inactivating mutations of several subunits are found in several types of cancer, such as BRM[73] or BAF180[74]. BAF180 is of special interest as it is thought to give functional specificity to the complex through six tandem bromo domains[75], hinting to a deregulation of targeting, and thus of chromatin remodelling, as the possible initiator of tumorigenesis.

The ISWI family (Imitation SWItch) contain either the SNF2h or SNF2L ATPase domain and a C-terminus SANT domain adjacent to a SANT-like ISWI (SLIDE) domain and a HAND domain, all which participate in regulating targeting of the ATPase domain. For example the SLIDE domain activates the ATPase domain and is needed to slide DNA along the nucleosome[76]. There exist 7 members of the family so far: NURF, CERF, CHRAC, ACF, RSF, WICH and NoRC[77]. They have different activities, for example NURF disturbs nucleosomal structure[78], hereby facilitating access to DNA, while ACF will organize nucleosomes by evenly spacing them[79]. Biologically the whole family participates actively in DNA damage repair mechanisms, such as double strand break repair[80,81]. Albeit the exact mechanisms of these roles are not yet fully understood, most of them arise from either targeting nucleosomes of DNA damage sites, opening of the chromatin and serving as scaffold for other proteins involved in repair. It is then logic to expect that mutations to these complexes end up producing both aberrant chromatin structure as well as cells that are hypersensitive to DNA damage. For example RNF20, a E3 ubiquitin ligase which ubiquitylates K120 of H2B at DNA damage points[82], recruits ISWI family members. Mutations to it are observed in colorectal cancer as well as chromatin cohesion and chromosome instability[83].

The CHD family (Chromodomain-Helicase-DNA binding) have an AT-rich DNA binding domain, two chromo domains in tandem at the N-terminus and additional subunits that further subclassify members into three subfamilies. CHD1 and CHD2 are subfamily one, containing a SNF2 domain. Subfamily two contains CHD3-5 and has dual plant homeodomains (PHD), a reader domain that target trimethylated histones. Finally, subfamily 3 contains CHD6-9 that have Brahma and Kismet domains[84]. They have a broad array of roles ranging transcription control, cellular proliferation and DNA damage repair. A commonly studied complex is NuRD (Nucleosome Remodeling and Deacetylase), which couples chromatin remodelling and histone deacetylase activities. It contains HDAC1 and HDAC2 as well as CHD3 (a.k.a Mi2α) and CHD4

(Mi2β)[85], Methyl-CpG binding domain protein MBD2 or MBD3, metastasis-associated proteins MTA1, MTA2 or mT3, histone binding-proteins Rbbp7 and Rbbp4 and Nuclear zinc-finger protein Gata2a and Gata2b. It also interacts with Lysine Demethylase 1 (LSD1)[86] and Cyclin-Dependent Kinase 2 Associated Protein 1 (CDK2AP1)[87]. Different combinations of core elements and interacting partners give NuRD a vast array of activities and specificities, sometimes even opposed in nature. For example, MTA3 has been shown to upregulate E-cadherin by inhibiting the expression of Snail in tumour invasion[88], while MTA1 can be found at the center of late tumours where E-cadherin is absent[89]. The NuRD complex is a main player in the differentiation of ES cells[90,91] and its role in keratinocyte differentiation will be discussed later.

Finally, the INO80 family (inositol requiring 80) is defined by its split ATPase domain which retains activity and acts as a scaffold for the association of RuvB-like proteins, RBb1 and 2. RuvB is a bacterial helicase, which sets the INO80 family apart by giving it the ability to bind specific DNA structures closely related to Holliday junctions and replication forks, which explains its role in homologous recombination and DNA replication[92]. Furthermore, the INO80 complexes contain more than 15 subunits such as actin-related proteins Arp4, Arp5 and Arp8, Actin itself, TBP-associated factor 14 (Taf14), nonhistone protein 10 (Nhp10) and Ino eighty subunits 1 to 6 (Ies1-Ies6)[93]. As a chromatin remodeller its main role is the exchange of H2A.Z/H2B dimers with H2A/H2B[94] but is implicated in transcription[92], replication[95] and cell division, either through its DNA translocase activity or serving as a scaffold. The inverse dimer exchange reaction is catalysed by SWR1, a member of the SWI/SNF family[96], and both seem to play a role in genome maintenance[97] and control of ESC differentiation[98].

There exist some other chromatin remodeller complexes such as SWR1 or RSC (homologous to the SWI/SNF family[99]) that have yet to be classified into families but have been left out here for the sake of brevity.

Higher order nuclear architecture

While most of the mechanisms of epigenetic gene regulation we have reviewed until now seem to regulate chromatin architecture at the nucleosome or perinucleosomal level they also have profound effects on a higher scale. When describing chromatin within the nucleus, and more importantly chromosomes, the image of a bowl of spaghetti comes easily to mind, where each single spaghetti is the double strand of DNA that compose a chromosome. But unlike the arbitrary position of single spaghetti in the Italian dish the positions of chromosomes and packaging of chromatin in the nucleus is actually very organized (probably because it was not designed by Italians).

Thanks to advances in fluorescence in situ hybridization and moreover the emergence of Chromosome Conformation Capture (3C) technologies it has become obvious that chromatin can be highly compartmentalized. Compartmentalization of chromatin has numerous advantages from the perspective of gene expression regulation. For example, it allows for reagents (e.g enhancers, transcription factors, etc) that might be in low concentration regarding the whole nucleus to have localised high concentration. It can also generate transcription factories where actively transcribed DNA shares space with high concentrations of RNA polymerases, while silent chromatin is kept out. It also better explains certain transcriptional phenomena; per example for a long time enhancer-mediated activation of gene transcription was thought to be a seemingly random event with stochastic kinetics involved. But the apparition of super enhancers[100] or transcriptional bursting[101] demanded a different model of interaction, and compartmentalization through phase separation has been shown to provide a better explanation[102]. As will be discussed later on, compartmentalization through phase separation is not a novel concept; Nucleoli and Cajal bodies have been known for a long time to be membraneless nuclear organelles that form through phase separation orchestrated by proteins and RNA and that can be appreciated with conventional light microscopy.

Several levels of compartmentalization exist within the nucleus: At a more "local" level (i.e within genes and their close regulatory sequences), we start with Insulated Neighbourhoods; chromosomal loop structures held together by the transcription factor CTCF and cohesin. Above it (sub-megabase scale), Topologically Associated Domains (TADs) represent DNA sequences that interact with each other more often than would be expected of a stochastic model and are thought to be formed by several insulated neighbourhoods. Further above it (megabase scale), TADs associate in larger domains called compartments, regions of inactive and active chromatin that are spatially segregated. And finally, we find chromosomal territories; at a nuclear level each chromosome occupies a specific territory, and interphases between chromosomes are also tightly regulated. All these levels of regulation, underlined by what has been previously discussed, form the final 3D architecture of the nucleus.

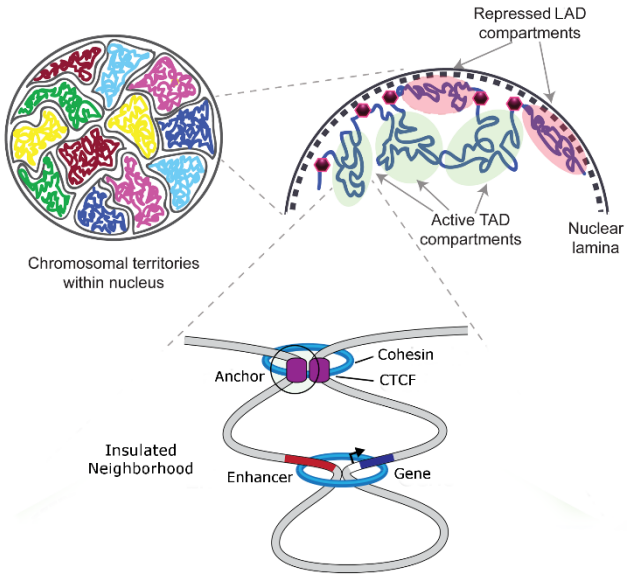

Figure 1.3. *Schematical representation of different levels of chromatin higher order structure. Adapted from Matharu et al. 2015*

Insulated neighbourhoods

Enhancers are segments of DNA that serve as scaffolds to transcription factors and RNA polymerase II, effectively recruiting them to the promoters of their target genes by looping. But in our bowl of spaghetti, how could these loops effectively target the right gene and not another one, proximal or distal, especially considering that most enhancers target genes within their own chromosomes? In the recent years evidence of physical restraint of these chromatin loops, mediated by CTCF dimers and cohesin, has shed some light onto how this phenomenon could be. These loops, termed Insulated Neighbourhoods, span an average of 190 kb and range from 25 to 940 kb and contain between 1 to 10 genes, 3 being the average[103]. After their discovery it was found that most enhancer-gene interactions happen within their boundaries[103,104] and that these boundaries were necessary to effectively control their expression. For example deletion of CTCF anchor of a PRC-repressed gene led to its activation[103].

Moreover, disruption of the boundaries can lead to aberrant gene activation. For example a gain-of-function isocitrate dehydrogenase mutation has been shown to produce hypermethylation at cohesin and CTCF binding sites through interference with TET family 5'-methylcytosine hydroxylases, resulting in activation of receptor tyrosine kinase gene PDGFRA, a prominent glioma oncogene[105]. Also importantly, insulated neighbourhoods seem to be maintained during development. Interestingly, while the boundaries may be very similar between cell types, enhancer-gene interactions within these neighbourhoods can vary as they are cell type specific[106].

Topologically associated domains

TADs are megabase-sized domains that were found through analysis of Hi-C 3C data, a development from 3C technology that pairs proximity-based ligation with massively parallel sequencing, as being regions of high self-interaction[107]. As of now there is much to be understood on the formation and regulation of TADs but key elements have already been laid out.

We know that TADs are very stable, being similarly disposed through cell types, independent of tissue-specific gene expression or histone modifications and are even similar between species, e.g human and mice ESCs share between 50% and 70% of TAD boundaries[108]. This stability raises questions about the maintenance of their boundaries. They are enriched in H3K4me3, H3K36me3, transcription start sites, house-keeping genes, tRNA genes, short interspersed nuclear elements and similarly to insulated neighbourhoods CTCF and cohesin binding sites. Both house-keeping genes and CTCF/cohesin binding sites are specially enriched, which points

both to high level of expression and insulated neighbourhoods as being the underlying elements of TAD boundaries. Other possible factors include DNA supercoiling[109] and how specific compartments of active and inactive chromatin fold, which will be discuss in the next part.

Disruption of TADs has been shown to cause aberrant gene expression as is behind several pathologies[110]. For example, using genome editing to modify CTCF/cohesion binding sites, perturbation of the structure of the WNT6/IHH/EPHA4/PAX3 locus, all within the same TAD, generated mice with severe limb malformations (e.g polydactyly) by causing ectopic interactions between several promoters that are non-interacting in wild type[111].

Analogous to TADs are Lamina-Associated Domains (LADs), which consist of similarly sized (10 to 10'000 kb) genomic regions that interact with itself as well as with the nuclear lamina. LADs are particularly prevalent, representing about one-third of the mouse and human genome[112,113]. These regions are mostly associated with silent heterochromatin, enriched in H3K27me3 as well as CTCF-binding sites at their periphery and H3K9me3 and H3K9me2 throughout[113,114]. Their dynamic interaction with the nuclear lamina offers a unique structural feature which helps define the 3D architecture of the whole genome by helping tether chromosomes to it. LADs can be separated in constitutive (cLADs) and facultative (fLADs), the former being LADs that are conserved across cell types while the later can vary. cLADs are generally more gene-poor than fLADs (less than a gene per Megabase), which foments the idea that their role is mainly structural.

Interestingly, while LADs are nuclear lamina-bound, moving within a micrometer of the nuclear lamina over the space of several hours, part of them can be found deep within the nucleus after mitosis, hinting to a possible reshuffling of the LADs during cellular division[115]. There is also evidence that some LADs might move following a circadian rhythm which is in part regulated by CTCF but is probably not a general feature[116]. More likely, the nuclear-lamina region serves both for cLADs as an anchor point and a transient storage space for repressed genes such as fLADs.

There is still much to learn about how LADs interact with the lamina, but there is mounting evidence that these are multivalent interactions that depend on DNA sequences as well as specific context, i.e chromatin state. For example a study found several cis-elements of the β-globin locus to be necessary for lamina-targeting, but that knock-down of Suv39H, a methyltransferase that regulates H3K9me3, and G9a, responsible for H3K9me2, managed to detach the β-globin locus from the lamina[117]. Similar effects have been found with EZH2 and its associated mark, H3K27me3[118]. Finally it is important to indicate that these elements and marks interact with parts of the nuclear lamina such as lamin A/C[118], Lamin B receptor[119], emerin[120] and several transmembrane proteins[121], several of these will be discussed more in depth later on.

A/B compartments

The introduction of the Hi-C method initially discovered a larger type of nuclear structures; compartments of either actively transcribed, termed A compartment, or inactive B compartment chromosomal regions that are spatially segregated[122]. These compartments are larger than TADs (multi-Megabase scale), which were thought to underline them. A compartments are associated with open chromatin markers, have a high gene and GC content and localize towards the interior of the nucleus while B compartments tend to show the opposite[123]. ATAC-seq and DNaseI digestion experiments confirm that A compartments have open chromatin while B compartments has more condensed chromatin. Genetic composition of the compartments varies depending cell type, and differentiation programs modify it[108].

Unfortunately lack of proof on how these compartments were regulated and research interests in Hi-C technology being more centered around incrementing its resolution power (which ultimately led to the discovery of TADs) left compartments a comparatively unresearched area. Lately it has been shown that removal of cohesin from DNA through inactivation of NIPBL, the factor that loads cohesin onto DNA, can effectively disrupt TADs but that compartments still remain, meaning that TADs are not the underlining structure that form compartments[124].

Chromosome territories

Due to the size of chromosomes compared to the nucleus, the concept of Chromosome Territory (CT) has been apparent for quite some time as simple light microscopy allows for the observation of chromosomal segregation in several species[125,126], but we had to wait for modern technology to get clear proof of their existence[127,128]. Since then much has been developed in their imaging thanks to in situ hybridization[129] and 3D-FISH[130], and finally 3C technology has allowed for in-depth data regarding their relative position with other chromosomes. This led to the realization that chromosomes organize in non-overlapping territories[122], that contacts between chromosomes are limited to the borders of CTs[131] and that interchromosomal contacts are non-random, conserved after mitosis[132] and cell-type dependent[133].

Geometrical analysis of chromosomal territories is of course tricky as the nucleus does not necessarily have apparent poles, so most research is based on radial distribution of individual chromosomes and of intra (giving a sense of shape) versus interchromosomal (determining neighbours) contacts. For example, a very interesting case is the X chromosome; comparison between the inactive and active form of the X chromosome can reveal great insight into the relationship between genome topology, transcriptional activity and the underlying chromatin structure. X chromosome inactivation is mediated by the Xist gene in the inactivated X

chromosome (X_i), which codes for a lncRNA that mediates recruitment of silencing proteins such as PRC 1 and 2. Their accumulation will create a silent nuclear compartment (often referred as the Barr body) where activating histone modifications disappear while heterochromatin markers become prevalent. Finally, there is hypermethylation of CpG islands, rending most genes inside X_i silent[134]. But, not all genes are kept this way: the X chromosome has been shown to localize most genes to the outer rim of its territory and keep its interior relatively gene poor[135]. Interestingly X_i shows little size difference from the active form, but a more condensed state, and can unwrap to resemble the active form after deletion of the Xist locus[136]. As stated before, improper X-chromosome inactivation can result in aberrant gene activation and disease[33]. The radial position of both active and inactive X chromosome is similar although X_i has been shown to localize near the nucleolus in late S-phase[137], and it seems that in certain cell types chromosome size and not gene content regulate radial position[138]. In line with previous concepts gene-poor or inactive chromosomes are found near the nuclear lamina, while gene-rich and actively transcribed chromosomes are mostly located towards the interior of the nucleus[139,140] and their localization and shape changes during differentiation[141,142].

Interchromosome space if of special interest, as it seems to be the hub of transcription factories as well as translocations[131]. EM analysis of this space has revealed it to be much larger than expected (e.g certain measurements put it at 41.7% of nuclear volume for endothelial cells including the nucleoli[143]) and is theorized to create a complex mesh of intranuclear tunnels that mediated free diffusion of components. The contact between separate chromosomal loci has been termed chromosome kissing[144] and is believed to be a driving force of chromosomal territory definition in line with LADs and replicon clusters[145]. Both silencing and active transcription happen at these loci.

For example, the Ikaros/Lyf-1 gene cluster, a gene involved in lymphocyte-activation, has been shown to localize to centromeric heterochromatin, shown by HP1 concentration, and these locus only interact with inactive lymphocyte genes in cis and trans chromosomes[146]. Upon maturation of lymphocytes, the Ikaros cluster begins interaction with activated genes. Another study found that the Igf2/H19 locus (chromosome 7) interacts with Wsb1/Nf1 (chromosome 11) through its imprinting control region, an interaction mediated by CTCF. Inhibition of CTCF or deletion of the ICR in the Igf2/H19 locus effectively perturbated expression of Wsb1/Nf1[147], which could hint at a possible role of CTCF as a building block of transcriptional factories. Similarly, non-mixing of DNA from different chromosome territories is also mediated by chromatin structure has shown by increased chromosomal intermingling after inhibition of HDAC[148].

The nucleolus

The nucleolus is a membraneless organelle in the nucleus whose main role is the compartmentalisation of rRNA synthesis but also plays part in other processes such as cell growth, survival, senescence and stress response[149]. As the rRNA factory, its assembly and size are heavily regulated by the cell type, cycle and transcriptional activity. It increases in size between interphase and prophase and rRNA synthesis accounts for most transcriptional activity, before being disassembled during metaphase[150] and eventually reformed at the beginning of the next cell cycle. In higher eukaryotes the nucleolus contains 3 distinct regions: Fibrillar Centers (FCs), Dense Fibrillar Components (DFCs) and Granular Component (GC). RNA Pol I-mediated transcription of rRNA genes (rDNA) occurs at the interface between FCs and DFCs. The nascent tandem rRNA transcripts create a distinct structure commonly referred to as Christmas Trees[151]. Subsequent processing of pre-rRNA and final assembly with other ribosomal proteins happens in the DFC and GC.

Nucleolus localisation within the nucleus is specified at the genome level by Nucleolar Organizer Regions (NORs); clustered arrays of rDNA repeats found on the short arm of five acrocentric chromosomes that code for 5.8S, 18S, and 28S rRNA. But there exist silent NORs which are extra-nucleolar, revealing that transcriptional activity associated with RNA Pol I is an indicator of nucleolar structure[152,153]. Analog to this, chromatin modulating enzymes and rRNA transcription regulators are also important factors in its architecture. Per example, Upstream Binding Factor (UBF), a TF of rRNA and main component of Pol I machinery, is a marker of the FC. UBF is also of interest to us as it behaves similarly to a chromatin remodeller by removing H1[154]. Fibrillarin (FBL), a small nucleolar ribonucleoprotein[155], and Nucleophosmin (NPM1)[156], a nucleolar histone chaperone, which are crucial for proper rRNA maturation, are markers of DFC and GC respectively. This indicates that RNA Pol I activity on rRNA genes, as modulated by localized chromatin structure, plays an important role in the maintenance and development of nucleoli structure.

Indeed, ribosome synthesis follows punctual needs by the cell for translational capability, and rRNA synthesis can account for most of the transcriptional activity in early developing embryos[157] and is inversely reduced in senescence[158]. This can be modulated by selectively turning on and off NORs using epigenetic reprogramming, and cells that have variant rRNA genes have consistently shown to still have similar levels of rRNA transcription[159]. More intriguingly, which NORs activate (or become “dominant”) seems to be random in nature[160,161], albeit the epigenetic machinery behind these activations acts effectively as both repressed and active rDNA can be adjacent yet have opposed expression profiles[162]. While active or silent rRNA

genomic regions can be found within nucleoli silent NORs are always extranucleolar, indicating a fine tuning of rRNA synthesis within a single nucleolus. Furthermore, the creation of purely synthetic and active NORs and subsequent exogeneous introduction into cells created neonucleoli, irrespective of their site of chromosomal integration[163], further proving that transcriptional activity as mediated by recruitment of binding factors such as UBF is an important effector of nucleoli structure.

Epigenetic regulation of intra and perinucleolar space seems then to be of importance, but little is known for now. A striking feature of perinucleolar space is H3K9me3-marked heterochromatin. These pericentromeric chromocenters are regulated by HP1, and HP1β is found within fibrillarin-positive regions of the nucleolus[164]. More interestingly, epigenetic marks within the nucleolus are differentially maintained compared to interphase nuclear chromatin: inhibition of SUV39h, a histone methyltransferase responsible for H3K9me3, does not modify the positioning of this mark within the nucleolus, nor that of HP1 β, contrarily to the rest of the nucleus[164]. Disturbing DNMT1, but not DNMT3B, effectively disturbs nucleolar structure and subsequently increased levels of H4K16Ac are seen on rRNA genes. SIRT7, a chromatin-silencing factor that interacts with SMARCA5 (SWI/SNF-related matrix-associated actin-dependent regulator of chromatin, subfamily A, member 5), a component of nucleolar heterochromatin-silencing complex NoRC, has been shown to also interact with DNMT1, effectively protecting rDNA array stability[165]. DNMT3b has been implicated in rDNA promoter methylation which stops UBF from binding, destabilizing nucleoli formation[166]. In breast carcinomas, rDNA methylation status is associated with nucleolar size. Considering that escape from senescence pathways need upregulation of ribosomal biogenesis, this is quite interesting[167]. Many other levels of epigenetic control of both rRNA expression and more generally nucleoli structure exist, such as NoRC[168], NuRD[169], HDAC[170], p300[170], but out of brevity we will not discuss them here. One final note will be made regarding interactions between cohesin and nucleoli, indicating a possible, but yet not understood, link between chromatin loops and nucleoli[171].

Nucleoli formation follows a liquid-liquid phase separation dynamic[172]. In line with this, its formation is dependent on several nucleoli-associated protein concentrations within the nucleus[173]. Nuclear enlargement preceding mitosis is a key factor of nucleolar dissociation at this step of the cell cycle. Nucleoli also coalesce following Brownian motion, which accounts for intercellular variation in their number and size, especially in smaller nuclei[174]. Considering that in a relatively well 3-D defined nucleus their coalescence can implicate up to ten chromosomes, this is an indicator of the potential of chromatin to dynamically rearrange. Since different rRNA maturation processes are compartmentalized at the interphase of the nucleolus and the nucleoplasm, the reduction in total surface due to coalescing on ribosomal biogenesis is unclear.

Nuclear architecture changes in keratinocyte differentiation

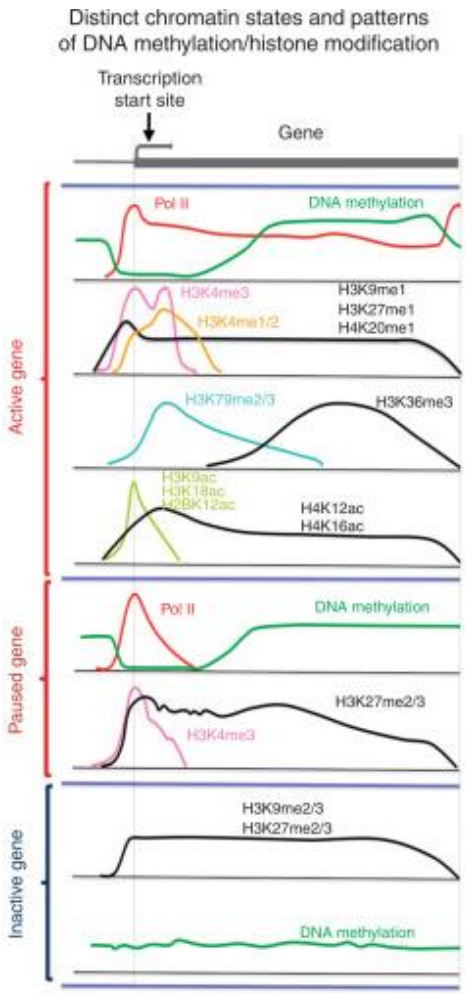

Figure 1.4. *Distribution of different epigenetic marks among the distinct regions of actively transcribed, paused, and inactive genes. Adapted from Gdula et al. 2012*

It should now become apparent that like any other developmental program, HKs differentiation is accompanied by a plethora of changes in their nuclear architecture and epigenetic regulation.

In HKs differentiation, DNA methylation dynamics were first seen by treating them with 5-aza-cytidine, a compound that inhibits DNMTs, which resulted in early differentiation[175,176]. Later, DNMT1 was described as a regulator of proliferation in progenitors and enriched in undifferentiated cells. Knock out of the Dnmt1 gene results in premature keratinocyte differentiation. UHRF1, a protein that directs DNMT1 to hemimethylated DNA has been found to only be expressed in undifferentiated basal cells. Similarly to DNMT1 deletion, depletion of UHRF1 leads to premature HK differentiation as well as a reduction of proliferative potential[22]. Gene-specific analysis of methylation revealed CpG methylation at multiple differentiation gene promoters in progenitor HKs, methylation that was lost upon induction of differentiation[22,177]. This indicates that DNMT1 role is to control entry into the differentiation pathway by inhibiting differentiation genes. DNMT3A and B have recently been shown to bind to super enhancers in a H3K36me3-dependent manner[178] but differ in their mechanism of action and expression profiles during differentiation. DNMT3a partners with p63, interaction mediated by TET2, to maintain DNA hydroxymethylation at the center of enhancers. DNMT3B on the other hand induces DNA methylation along enhancers. Both DNMTs are expressed in basal HKs, but only DNMT3A expression is pursued after entry into the differentiation pathway, albeit a change in targets occur; its activity is shifted from enhancers that control expression of stem cell proliferation genes to differentiation ones,

indicating a dual action. Depletion of either protein inhibits target enhancers as well as reduced H3K27Ac mark. It also induced premature differentiation.

DNMT1 as well as 3A and 3B have been associated with both hyper and hypomethylation in skin cancer, some affecting differentiation-related genes, hinting at a possible role in their regulation in healthy tissue. The promoter of LAMA3, responsible for the laminin α3 subunit and hence of correct anchorage to the basement membrane[179], can get hypermethylated in sun-exposure related melanomas[180]. Interestingly, it has been shown that older subjects that are more exposed to sun have a higher degree of hypomethylation[181]. TGFB1 can inhibit the proliferation of HKs[182] and has been shown to be upregulated in DNMT3A-depleted tumors[183]. The promoter for E-cadherin, which has been shown to be a mediator of differentiation and stratification[184], is also hypermethylated in neoplasms[185].

Markers for actively transcribed chromatin H3K4me3, H3K56Ac as well as RNA Pol II were found to be reduced on suprabasal layers, indicating an overall reduction of transcriptional levels[186].Gene-specific changes in chromatin landscape are also observed. For example, genes that are activated during differentiation (e.g Lef1, Bmp3, Wnt5a, MSx1) show a loss of H3K27me3 while gaining H3K4me3 and H3K79me2 histone marks[187]. Inversely stemness genes (e.g CD34, Sox9, Nfact1) will experience the contrary.

The work of writers and erasers paves in part this process. Histone methyltransferase EZH2 is of importance as its partial ablation has been shown to selectively up-regulate differentiation genes, implying that EZH2-mediated repression maintains stemness in HKs[188,189]. The concept has been tested in vitro with an eraser, JMJD3, which catalyses demethylation of H3K27 and caused HKs to differentiate prematurely and its deletion caused the inverse effect[190]. H4K20me1 is catalysed by the work of Setd8, a histone methyltransferase that inhibits apoptosis in the skin via regulation of p63 expression. It is also a transcriptional target of c-Myc and serves as a mediator in c-Myc induced differentiation. Its ablation effectively stops HK proliferation and differentiation and p63 expression is lost[191].

In parallel, HDAC1 & 2 deletion resulted in failure of epidermal proliferation and stratification by perturbing p63-mediated gene repression while not perturbing p63-activated genes[192]. This is due to HDAC1/2 binding the same promoter regions as p63-repressed genes but not p63-activated ones. Interestingly, inducing global histone hyperacetylation with trichostatin A (TSA) stopped shape-induced differentiation of HKs[193]. This inhibition was shown to be in part p38 MAPK-mediated by affecting Serum Response Factor (SRF) transcriptional activity and the expression of AP-1 TFs. ARNT, a TF that responds to environmental stress, shows reduced expression along the differentiation pathway, suggesting a negative regulatory link between

ARNT and HK terminal differentiation mediated through reduction of EGFR activity. A study using KO of ARNT and TSA, showed that this link is controlled by HDAC activity, whose expression is inversely related to ARNT levels[194]. It also found Filagrin, K10 and loricrin genes to be directly regulated by HDAC. These studies show that histone acetylation has different context-dependent roles in regulating HK differentiation.

Furthering this point, a recent study proposed that p63 and HDAC1 co-expression patterns could potentially be used as a stem cell markers for HKs[195]. ASH1L, which encodes a SET domain-containing protein that catalyses H3K36 demethylation, was found in mice to be required for epidermal homeostasis. Perturbation of the ASH1L gene resulted in excessive keratinocyte proliferation, defective wound healing and skin hyperplasia. The study hinted at a possible reason being disturbance of c-Myc but failed to show a direct link[196].

Concerted work of writers and erasers in complexes with readers and chromatin remodellers adds another level of HK differentiation control. For example, Mi-2β-NuRD has been shown to be of importance during early development of the epidermis, its inhibition induced severe epidermal barrier defects in mice during embryogenesis (notably by the progressive loss of keratin 14), ultimately leading to neo-natal death. It was found to also be of importance for the subsequent maintenance of the self-renewal capability of epidermal precursors[91]. The ATPases Brahma (BRM) or Brahma-related gene 1 (BRG1), share similar functions in later stages epidermis development, as knockdown of both induced severe skin barrier defects in mice[197]. BRG1 was shown not to be of importance in proliferation and early differentiation, but is for late differentiation, ablation generating severe skin permeability barrier effects, indicating a role in lipid structure. Other SWI/SNF regulatory subunits were investigated in a later study, and found BAF250a to direct HK differentiation by opposing Actin-Like Protein 6a (ACTL6a) repressive effect on HK differentiation gene promoters such as KLF34[198].

PRCs are of special interest in HK differentiation pathways. A study showed that PRC1 component CBX4 prevents HK stem cells from exiting the quiescent state and becoming TACs as well as from becoming senescent, but once cells become TACs it is dispensable in inhibiting their proliferation and eventual differentiation[199]. In the same study it was also shown that CBX4 inhibits EZH2, DNMT1, DNp63 and c-Myc, further tying their role in HK differentiation together. Furthermore another study indicated that CBX4 maintains epithelial identity and proliferative activity by repressing selected non-epidermal lineage genes as well as cell-cycle inhibitor genes mediated by p63[200]. PRC2 subunit EZH2 was already discussed before, but a more recent study linked it to other subunits EZH1, EED and SUZ12, stating that in HKs they function largely as part of the PRC2 and not as lone actors as shown by virtually equal effects upon ablation of any individual subunit. PRC2 then becomes a major player in H3K27me3 mark deposition and its

perturbation results in premature formation of the cornified layer, aberrant merkel cell formation and defective hair follicles[201].

Bioinformatic analysis of mRNA assays after induction of differentiation through different pathways identified several chromatin remodellers such as NURF, MORF and LSD1 as of importance in HK differentiation[202]. Further analysis revealed an interaction network between ING5, SMARCA5, BPTF, EZH2 and UHRF1. While the two later were already known to control HK differentiation, the formers, which are subunits of NURF (SMARCA5 and BPTF) and MORF (ING5), were novel and implicated in the control of integrins. In mouse melanocytes, BPTF depletion showed reduced TACs for this specific cell lineage, generating a population of mice with white coat. This was mediated by MITF, a TF that regulates entry into the differentiation pathway of melanocytes, a whose interactome also integrated other NURF complex subunits such as SNF2H, SNF2L and RBBP4[203].

Differentiation also affects the higher order nuclear architecture. Indeed it has been previously shown that the position of chromosomes 18 and 19 change during calcium-induced differentiation[204]. Chromosome 19, which has the highest gene density of all autosomal chromosomes, moves from the interior to a more peripheral position in early differentiating HKs, while chromosome 18, having one of the lowest gene densities, mirrors this transition. Interestingly they both assume similar radial positions in later stages of differentiation. The same study reported variations in size, as both chromosomes shrink in volume by about 20%. Their relative size also varies, from a 5% larger chromosome 18 to over 20% larger in late differentiated cells, virtually the same as the difference in their respective DNA content (76Mbp for chromosome 18 versus 64Mbp for 19). This indicates a change in chromatin compaction that could be coupled with the transcriptional status of HKs during differentiation, from a more active/open state in undifferentiating HKs, to the more transcriptionally silent/closed state of terminally differentiated cells. A dynamic, stepwise change in their pair-wise

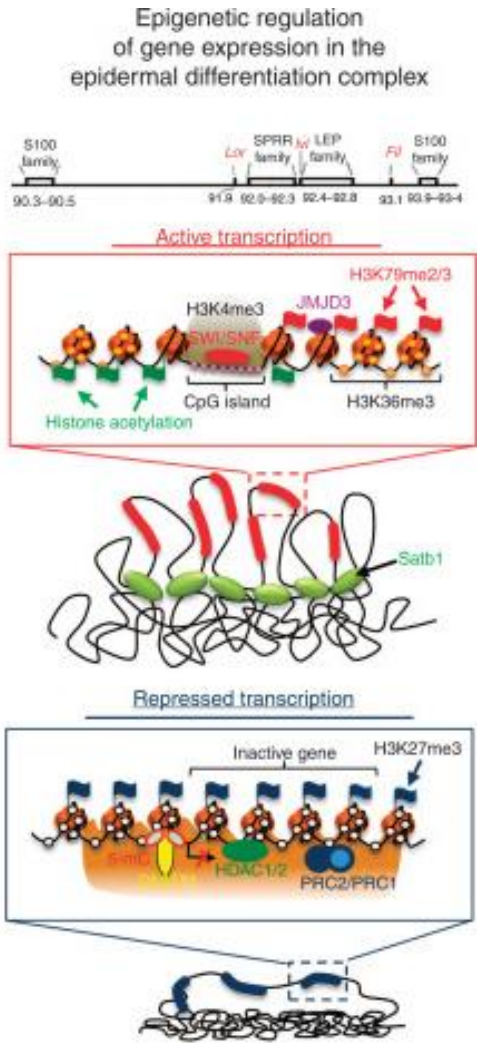

Figure 1.5. *Epigenetic control of expression of terminal differentiation-associated genes in the epidermal differentiation complex locus. Adapted from Gdula et al. 2012*

association was also seen depending on the differentiation state, which could also indicate stepwise change in transcriptional programs, but without any gene-specific information that is pure speculation.

One of the most important higher-order structures in HKs is the Epidermal Differentiation Complex (EDC). This 2Mb region in the 1q21 chromosome contains about 33 known genes responsible for tissue development and repair by regulating keratinocyte terminal differentiation program through concerted signal pathways[205]. 28 genes encode several structural proteins that fall within 3 subfamilies; cornified envelope precursors (loricrin, involucrin and proline-rich proteins), Intermediate Filament (IF) proteins (profilaggrin, and trichohyalin), and the calcium-binding S100A proteins, responsible for and array of cellular functions[206,207]. The remaining 5 genes, as well as 10 additional genes found within a 1-Mb extended region, encode varied proteins such as cytoskeletal tropomysin (TPM3), HAX1, Laminin receptor 6 (LAMRL6), a proteasome subunit (PSMD8L) and 5 initially uncharacterized proteins (NICE-1 through 5). The fact that most of these genes have strong implications in keratinocyte differentiation implies a functional constraint that permits their coordinated expression.

Indeed it has been shown that the EDC in differentiating keratinocytes is located to the exterior of chromosome 1 territory compared to lymphoid cells where the EDC is transcriptionally repressed and found in the interior of the territory[208]. Similarly, basal layer keratinocytes have the EDC much closer to the exterior of the chromosome 1 territory, which could indicate a priming of differentiation. Lately 3C data has allowed to determine a dynamic rearrangement of enhancer 932, situated almost one Mbp downstream of S100A10, with several EDC gene promoters, in a developmental and spatiotemporal fashion[209]. These interactions were also found to be mediated by c-Jun/AP-1. As discussed above the EDC is also regulated locally through the epigenetic machinery[178,192,194,197,199,210].

A study reports that nucleoli vary in number and radial distribution; they become less numerous and tend to congregate towards the nuclear interior as the HK differentiate[186]. The study used mathematical modelling to determine that this is not an effect of nuclear morphology change but a result of active remodelling of the nuclear architecture associated with differentiation. Their reduction in number is accompanied by an increase in average volume.

Finally, macroscopic changes can be observed such as variations in nucleus shape and size. HKs found in the basal and granular layer present more elongated nuclei compared to the spinous layer and Basal HKs, regardless of their proliferative status, seem also to have larger nuclei than suprabasal HKs[186,211]. Interestingly this is not the case in HKs grown on single layer cultures[204].

There is then ample proof of the complex interplay between keratinocyte differentiation and the epigenetic landscape remodelling although there is still much to discover about it. It is also of capital importance to understand that these changes in 3D architecture of chromatin are not a simple by-product of keratinocyte differentiation but also an essential part of it as shown by the pathologies that arise from perturbing them.

The cytoskeleton and mechanotransduction

As mentioned before several environmental cues will regulate the entry of keratinocytes into the differentiation pathway, and a very active line of work in this field is elucidating what cues are these, and through which pathways do they induce differentiation. For example one of the most well-known inducers is calcium[212]. Indeed, a calcium concentration gradient is established throughout the epidermis, which effectively helps control the differentiation process as the keratinocyte migrates through it. Several signalling pathways are controlled by calcium[213], both intra and extracellularly, such as the formation of desmosomes and adherens junctions which serve as extracellular sensing and anchoring apparatuses, the control of activity of several kinases or more directly through the Calcium Receptor, a G-Protein Coupled Receptor. All these ultimately will play a role in regulating the entry into the differentiation pathway.

An essential, yet understudied cue is physical force. As discussed before the epidermal barrier is subject to continuous external physical insults, but more importantly its proper maintenance through homeostasis and its wound-healing potential heavily involve force-sensing of the immediate and proximal environments[214]. For example, asymmetric division perpendicular to the basement membrane has been shown to be a simple method of effectively forcing one of the daughter cells to stratify by being inherently committed and already positioned suprabasaly[211]. Recently it has been shown that adhesion and cortical tension forces generated by neighbouring cell divisions could trigger differentiation and stratification too[184]. Adhesion forces to other cells are regulated by cadherins, that mediate cell-cell contacts, and they also have a role in regulating keratinocyte differentiation[215]. Moreover changes in cadherins expression patterns during differentiation drive subsequent forces that help the migration of differentiating HKs upwards[184]. Adhesion forces can also be influenced by the extracellular matrix (ECM, essentially the basement membrane in vivo) properties, such as stiffness[216,217] or composition[218], and can have effects on differentiation[219]. More interestingly, cellular size and shape as dictated by restricted ECM contact has been shown to induce terminal differentiation[220] and modify nuclear morphology[221].

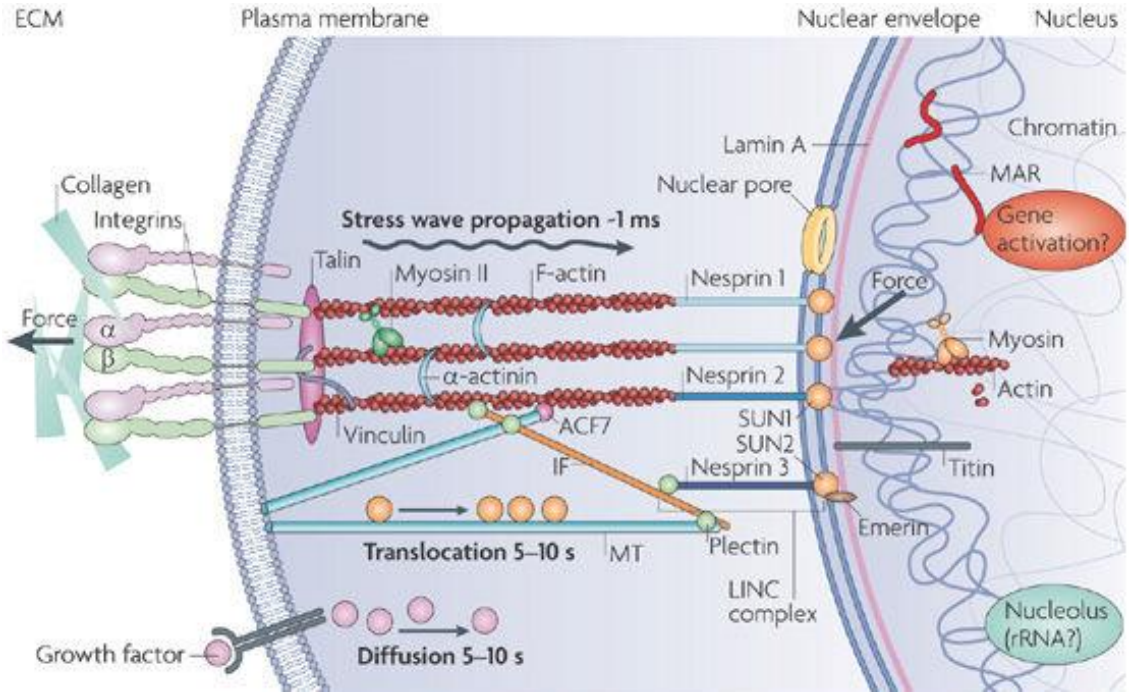

Figure 1.6. *Schematic representation of the molecular connectivity between the Extracellular Matrix (ECM) and the Nucleoplasm mediated by the cytoskeleton and typical propagation times of different stimuli. Ingber et al. 2009*

The cytoskeleton is an important part of mediating these responses to physical stimulus. It is made up of complex networks of interlinking filaments and tubules that helps maintain the structural integrity of the cell[222] as well as having a role in transport[223] and migration[224]. Furthermore, dysfunction in its regulation and mechanical properties not only compromises cell structural integrity but can also have profound effects on tissue structure. It is also important to note, as it will interest us here, that the nucleus also contains its own nucleoskeleton, and like its cytosolic counterpart it has a myriad of other uses apart from structural such as gene regulation[225] [226]. As discussed later, the two are also linked and integrated, which further expands their biological applications.

Keratinocyte cytoskeleton

In epithelial cells three types of filaments form the cytoskeleton: Microfilaments, Microtubules and Intermediate Filaments (IFs). These categories are based on the diameter and biochemical properties of each filament that form them. For a simplified approach, this review will only concern itself with type I and II IFs (keratins), type V (lamins, in the context of the nucleoskeleton) and microfilaments (actin). While microtubules have important roles in intracellular transport[227] and cell division[228], their contribution to mechanical integrity as well as mechanotransduction and differentiation in HKs is limited and not yet very well understood[229,230].

Keratins

Keratinocytes get their name from their comparatively higher amount of keratin[231], IF structural protein, than other cell types, and is the main cytoskeletal proteins that accounts for their mechanical integrity[232]. As a main component of the keratinocyte cytoskeleton, keratin plays an important role in their mechanotransduction[233], compared to other tissues were other cytoskeletal proteins, such as actin, are usually the main actors, allowing for tissue-specific responses to physical force. In this regard keratin has been heavily studied as a structural element of the cytoskeleton and is relatively well understood while its role in other processes such as migration, tissue stability or metastasis remains the focus of active research.

Keratins originated from primordial nuclear Lamin like many other IF genes[234]. Of all IF human genes (70), most (54) encode keratins, and a majority (37) of them are expressed in the skin. Gene evolution brought two types; type I and II, which are divided upon their isoelectric points[235]. They have a central α-helical rod subdivided by 3 short linker segments[236,237]. Rods are flanked by larger non-helical domains; head (N-terminal) and tail (C-terminal).

They are expressed as pairs (one type I and one type II) as they intrinsically form acid-base heterodimers. These then assemble into anti-parallel tetramers as their head rods overlap and finally into “unit length filaments”; short (60nm) keratin cylinders 10nm thick which will become the basic component of the rope-like IFs. This self-organization process usually starts near focal adhesions at the periphery of the cell, then polymerization will allow for the elongation and thickening of the keratin filaments towards the nucleus. Along the way and at the destination they will cross link other keratin filaments, transforming into bundles and finally creating a mesh around the nucleus[238].

It is important to note that depending on their differentiation phase keratinocytes will express different pairs of keratins[231]. These changes in keratin populations and hence in their properties are paramount to the process of differentiation. Keratin 5 and keratin 14 (K5/14) are indicators of basal keratinocytes[7] and are the main pair that interact with hemidesmosomes, proteins that attach basal keratinocytes to the underlying basement membrane[239]. When the keratinocyte enters differentiation, both hemidesmosomes and K5/14 are downregulated, facilitating keratinocyte detachment from the basement membrane and initiating its journey outwards. K5 can form heterodimers with K15, which seems to be a secondary basal HK keratin and whose synthesis might be upregulated in the absence of K14[240] and has been linked to a more mature type of basal HKs[241]. K1/K10 are produced in the suprabasal layers of the epidermis and represent an important mediator in stratification as well as differentiation. Interestingly they are incapable of forming a keratin network on their own and hence rely on the previous K5/14

network to assemble[242]. This is mediated by K1 as its expression precedes K10. Ectopic K10 expression has been shown to prevent cell proliferation, a phenotype that is rescued by expression of K16[243]. K10 can also form heterodimers with K2, which is also a regular component of the suprabasal cells[244] and is upregulated in mechanically stressed epithelia[245]. Both K1 and K2 can form heterodimers with K9, which is also involved in mechanically stressed epithelia[246]. Finally K77 and K79 have been found in terminally differentiated HKs[247]. Many other keratins exist that are found in hair follicle (e.g. K71-74,75, K6, K25-28, K81-86) but will not be discussed here.

As stated before keratins are the main influencer of keratinocyte architecture and mechanical properties. They are viscoelastic and have high flexibility but can react to external physical forces by stiffening. This transition is quick in both directions (i.e. they also recover quickly after cessation of deformation)[248], probably mediated by their ability to initiate bundling by itself[249]. Fluorescence and FRAP experiments have revealed that in living cells the keratin network is in continuous growth[250]; moving by what can be likened to waveform propagations, usually directed towards the cell center[251]. New keratin fibers are found to be initiated towards the cell periphery, but join a more mature, central network along their propagation. The more dynamic peripheral filaments are thus more capable of reacting to extracellular impulses, while relying on the stability of the central network[252]. The initiation of the keratin filament follows a nucleation of soluble monomers close to focal adhesions[253]. The nucleation product, possibly similar to other IF unit length filament, is devoid of polarity so will grow from both ends until they integrate the larger network[252].

There exists a duality of keratin filaments and keratin bundles, which give rise to different mechanical properties. Bundles are more stable and have reduced turnover, giving a more resilient and durable cytoskeleton and are formed by lateral association of keratin filaments[254–256]. These bundles are usually seen perinuclearly and bundling efficiency can be affected by several factors that can influence cell behaviour. The first one is the composition of keratin dimers within the keratin bundle, as seen by ectopic production of different tissue keratins[257]. Second would be interacting molecules, such as cytolinkers[258] like epiplakin[259] or plectin, which acts as a linker between keratin and the other cytoskeletal networks of microtubules and actin[260]. Finally, keratin PTMs can also influence their assembly dynamics. For example PKC ζ has been shown to increase keratin dynamic exchange of subunits leading to thicker bundles in response to sheer stress by phosphorylating a K18 serine residue[261].

The pool of keratin monomers is replenished by disassembly of filaments usually near the nucleus[255,262]. Part of this pool will cycle back to the cellular periphery while the rest will maintain the perinuclear mesh. Cycling is controlled by factors that govern either keratin bundle assembly

or disassembly. As stated before PKC ζ can accelerate this assembly in response to sheer stress. P38 MAPK has a similar effect and is also activated by stress factors or during mitosis[263]. This cycling is proposed as the main driving force of keratin IF cytoskeletal function. In static cells, the cycling is slow and supposed to "check" the presence of other cells through focal adhesions and desmosomes, or of the basement membrane through hemidesmosomes. In motile cells the cycling is faster and facilitates growth toward the leading edge. For example, in line with the three factors stated before, it has been reported that keratin isotypes, whose function is further modulated by protein kinase C α, can affect desmosome stability, intercellular contacts and thus whole tissue mechanics[264].

Keratins also have a function in control of homeostasis. It has been shown that repression of K14 expression induced reduced production of keratin pair K5, premature differentiation and delay in the cell cycle[265]. These effects were mediated through modulation of Akt-mediated cell proliferation and Notch1-dependent differentiation. Recently it has been found that K17 localizes within the nucleus[266,267]. It is for now unclear what exact role its nuclear compartmentalization does, but one can speculate. For example, K17 has been shown to associate with transcriptional regulator AIRE and with p65.

Adaptor proteins mediate interactions between cytoskeletal proteins and other cellular constructs. Keratins can for example use desmoplakin to attach to desmosomes, which link cells to other cells, or through plectin to hemisdesmosomes, that link the cell with the basement membrane[239]. These interactions effectively allow for 3D organisation of keratinocytes throughout the epidermis and mutation in both keratins and adaptor proteins can compromise both cellular and tissue integrity. For example mutation of desmoplakin has been shown to decrease cell-substrate and cell-cell forces as well as cell stiffness both in pairs and sheets[268]. Inhibition of keratin levels effectively modulated the adhesive properties of desmoglein 3, a desmosomal cadherin, modifying intercellular forces in HKs. Interestingly, this led to the discovery that cellular adhesion forces mediated by desmosomes are controlled in part by p38 MAPK-dependent phosphorylation of keratins. Plectin has been shown to be an important player in the coordination of hemidesmosome disassembly during HK differentiation[269]. Mutations in the keratin genes and associated adapters have been linked to several malformations of skin with varying severities, from mild to lethal. One of the better known diseases linked to keratin mutations is Epidermolysis Bullosa Simplex, where skin becomes fragile and easily blisters upon physical trauma[270]. As keratins are also involved in cellular motility their analysis can also give insights into tumour progression and metastasis[271].

Moving away from the cellular periphery to the nucleus, keratin can also physically link to the nuclear envelope. Indeed, through plectin[272], keratin can interact with nesprin-3, an outer-

nuclear envelope member of the LINC (Linker of Nucleoskeleton & Cytoskeleton)[273], creating an indirect physical link between the extracellular space and the nucleus. Interestingly it has been shown that plectin mediates in the nuclear morphology of HKs by modulating the perinuclear mesh of keratin, a phenomenon in part controlled by the crosstalk with F-actin[221]. Indeed, cells grown on microengineered surfaces which reduced their available adhesive surface showed nuclear deformation and removal of plectin incremented the amount of nuclear deformation. This effect was found not the be caused by improper link to the nucleus through the LINC, but rather by a diminished keratin network surrounding the nucleus that dampens tensile and compressive forces. It is important to note that removal of plectin also affected the integration of the keratin network to the other cytoskeletal proteins and that previous studies also have linked it to elevated MAPK activity[274], which is a modulator of nuclear area. Since the LINC complex is heavily implicated with the nucleoskeleton and other cytoskeletal proteins, it will be discussed in its own section further down.

Actin

Actin represents a family of globular proteins that form microfilaments and are of great importance in the cytoskeleton across mammalian cells, both for mechanical integrity and motility. They are usually found in two forms; either as a free monomer (G- actin, for Globular) or as a polymer (F-actin, for Filamentous), both with their respective roles in cell biology[275]. Actin shares some structural roles with keratins, as discussed in some examples before[269], albeit it is not a major player in keratinocyte mechanical integrity[232]. It is nevertheless of importance for skin tissue morphology[276] and has important roles in migration[277] and transport with myosin motors where it serves as a dynamic track[278]. Actin also works as a mediator in the mechanosensory machinery as well as having some gene regulation roles, which is why we will mostly discuss these roles here.

G-actin, who functions primarily as an ATPase, folds into two α/β domains separated by a cleft where ATP is hydrolysed. Because of their role in F-actin these are referred as the outer and inner domains and the whole structure is referred as the “ATPase fold”. G-actin is also particular as it is capable of a comparatively very extended array of interactions with other proteins, giving it a wide field of applications which also translates into its filamentous form[279].

F-actin is a very dynamic polymer, to such an extent that elucidating its 3D structure has proved monumentally difficult as its symmetry is incompatible with the formation of crystals and the wide interactome it possesses create distinct structural states, but some general features have been elucidated. F-actin is classically described as a polar double-stranded right-handed helical structure with two ends; barbed and pointed. The barbed end is the most dynamic as it

elongates about ten times faster than the pointed end[280]. This elongation can be quite rapid, with filaments reaching lengths that are relevant to the cell scale in seconds[281], creating a force capable of giving cells motility for example. Polymerisation of G-actin into F-actin is mediated by three classes of actin nucleation factors: actin-related protein 2/3 (Arp2/3) in complex with nucleation-promoting factos (NFPs), formins and tandem-monomer-binding nucleators. They are further modulated by other proteins such as profilin[282], cofilin[283] or molecular motors like myosins[284].

Depending on nucleation factors and associated proteins, the actin cytoskeleton can develop three distinct networks coexisting in the cytoplasm with different functions[285]. The first one features a small branched architecture that drives a "rolling" of the cell towards its edges. A second one features a broader network that is parallel to IFs in the reverse direction (towards the nucleus) allowing the cell to "pull" from the ECM. The fibrils that compose the later are referred as stress fibres since they react primarily by associating to protect the cell from mechanical stress as well as other biological roles such as mechanotransduction[286]. Finally, we have filopodial bundles that help expand the cell by "poking" outwards. These 3 different types of networks have different roles and all derive from the same pool of G-actin and some shared polymerization factors, indicating that their regulate finite mechanical and mechanosensory properties of cells[287]. An example that is of particular interest to us is that different organizations of the actin filament network in stem cell versus TAC HKs have been shown to modulate their response to EGF through EGFR signalling, effectively modulating cell fate decisions[288].

F-actin polymers exhibit different mechanical properties, giving rise to differential responses to mechanical stimulus. Arising first from their different networks, stress fibers will experiment pulling forces, as opposed to compressing forces for lamellipodium. Their structure is also different depending on their organization and binding factors[289], and can be further modified by mechanical stress. For example, applying tensile force to a single filament in vitro demonstrated reduced cofilin severing activity[290]. Inversely another study showed that stretching filaments within cells incremented their affinity for myosin II[291]. Furthermore, not only mechanical stress modifies actin affinity to other proteins, but other proteins can also have their affinity with actin modified this way. Talin is an integrin-binding protein part of focal adhesions, a similar ECM-binding complex to hemidesmosomes which connects the ECM to the actin network. Upon stretching, talin exposes several cryptic binding sites for vinculin, an actin-binding protein[292]. A similar mechanism has also been observed in adherent-junction protein α-catenin, demonstrating that force was needed for actin-binding to the complex[293]. Finally we will note that actin crosslinking proteins as well as polymerization factors also react to force[294,295]. All of

this taken together shows that the actin network is particularly sensible to extracellular forces and makes it an ideal candidate to modulate cellular response.

Actin is also a regulator of gene expression which is modulated by its polymerisation activity. This was demonstrated when G-actin was found to bind the SRF coactivator MAL, which moves to the nucleus once in its unbound form. Reducing the pool of G-actin through several ways such as stabilization of F-actin or Rho-pathway activation induced translocation of MAL to the nucleus and activation of SRF[296]. This pathway can also be activated as a response to extracellular force as shown by the induction of HK differentiation on small micropatterns through the activation of SRF-MAL[220]. PREP2, another TF, has been shown to interact with actin similarly to MAL[297], while YY1, a negative regulator of SRF and interacting partner of INO80 in DNA repair, responds inversely by shuttling out of the nucleus following actin polymerisation[298].

But actin is not limited to the cytosol; when bound to profilin, an interacting protein that facilitates F-actin depolymerisation, it can also shuttle to the nucleus where it has a wide interactome. TIP60, a INO80 chromatin remodeller involved in DNA repair[299], and p400, a SWI/SNF that interacts with c-myc and polycomb protein[300], both interact with actin and with each other, an interaction that is of utmost importance in colorectal cancer[301]. HDAC1 and 2, both part of the NuRD complex, have been shown to be inhibited by nuclear actin levels, albeit this is probably mediated by actin-interacting proteins[302]. Actin also interacts with RNA Pol I[303], II[304], and III[305], and reducing its active transport into the nucleus has been shown to effectively diminish transcriptional levels[306]. This is further corroborated by indications that actin may play an active role in ribosome biogenesis, as shown by defective rRNA production in actin-KO mice[307]. These mice also showed aberrant epigenetic reprograming mediated by chromatin-bound nuclear myosin 1 (NM1) and SNF2h, a subunit of the chromatin remodelling complex B-WICH, at rRNA locus. It is unclear if actin and B-WICH interact but ChIP-Seq data showed that its subunits localize to the same rRNA genome regions.

Physical cues can also modify actin localization, having profound effects on gene expression and organization. In HKs, mechanical strain can induce a nuclear export of actin and emerin, a protein involved in LAD maintenance, towards the exterior of the nuclear lamina, where it will polymerize with non-muscle myosin IIA[308]. This induces a change in LAD chromatin landscape where H3K9me2,3 is exchanged to H3K27me3 by PRC2, causing a detachment of the chromatin from the nuclear lamina and a rearrangement of chromosomal territories towards the nuclear interior. PRC2-mediated silencing targets preferentially lineage-commitment genes, effectively blocking initiation of differentiation, and depletion of nuclear actin reduces transcriptional activity through its interactions with RNA polymerases. While the study did not measure this, both the resulting extensive F-actin network outside of the nuclear membrane as well as the

dissociation of LADs probably created a change in rheological properties of HKs, but did demonstrate a mechanosensing, actin-dependent, gene-control mechanism.

Actin polymerization can also happen within the nucleus, albeit at a much lesser extent than in cytosol, and exhibits gene-regulation properties. For example, nuclear actin polymerization as mediated by formins has been shown to also activate SRF through MAL[309]. The inverse is also possible; depolymerization of nuclear actin filaments through redox modification mediated by MICAL-2 is correlated with reduced SRF activity, albeit this time mediated thought myocardin-related transcription factor-A (MRTF-A)[310]. Finally we will note that extracellular cues can also direct nuclear actin polymerisation; cellular spreading has been shown to induce nuclear actin polymerization via the LINC and is mediated by integrin signaling[311]. Since actin binds both focal adhesions containing integrin and the LINC this pathway shows an intriguing self-regulating response of actin to physical stimulus with gene-regulation potential. Nuclear export of actin is mediated by exportin 6, and detection of basement membrane laminin 111, has been shown to inhibit exportin 6 activity effectively incrementing nuclear actin levels[312]. Interestingly laminin 111 has been shown to be detected by integrins integrated in hemidesmosomes, which interact with keratins, hinting at a possible crosstalk between the two cytoskeletal networks.

Higher order chromatin movements can also be mediated by actin. As of now there is proof that this phenomenon is implicated in chromosomal segregation during meiosis in oocytes[313] but more important to us is that it has been linked to radial chromosome territory relocation in partnership with nuclear myosin[314]. It has also been shown that the actin cytoskeleton can mediate in chromatin stretching following force application, a phenomenon that has transcription regulation potential[315].

Regarding whole nuclear mechanics actin actively participates in regulating structural integrity of the nucleus. Cell spreading shows a dynamic response by the nucleus, which flattens over time. Inhibition of actin and myosin light chain kinase showed to limit spreading of the cell and flattening of the nucleus. Expansion of nuclear volume as well as chromatin reorganisation following mitosis exit is also dependent on actin polymerisation[316]. As of now the molecular mechanisms of actin influence on nuclear structure are yet to be elucidated. Considering its low propensity to form filaments within the nucleus, it is more likely it may play an interacting role with lamins, the main component of the nucleoskeleton[317], which will be discussed in the next section.

We will mention briefly actin-related proteins (Arps), which are part of the actin superfamily as they share extensive sequence homology (80 to 40%)[318]. In the cytoplasm they interact mainly with actin by modulating its polymerisation and filament branching in the cytoplasm, but in the

nucleus they are components of several chromatin remodelling complexes belonging to the INO80, SWR1 and SWI/SNF families[319].

As indicated before F-actin interacts with other cytoskeletal proteins, like cadherin-based adherents junctions, through adaptor proteins like vinculin, or to LINC through Nesprin, making a very similar connection between the extracellular space and the nucleus to that of keratins. There is also experimental proof of interaction between the two[320], which might be mediated through plectin[321]. These interactions add to the versatility of the cytoskeleton and its mechanotransductive properties. Some research has been done towards understanding the cross-talk between the two networks but much is still to be understood[221].

The nucleoskeleton

As we now know the cytoskeletal network connect to LINCs extranuclearly, and within the nucleus LINCs connect to nucleoplasmic proteins such as Lamins. Lamins are nuclear IFs which are the main component of the nucleoskeleton[322]. There are two families; Lamins A and B, which in vitro form separate and functionally distinct filaments. They originate from 3 lamin genes that code four major and three minor isoforms: LMNA, which codes isoforms A and C as well as AΔ10 and C2, LMNB1, which codes isoform B1, and LMNB2, which codes for B2 and B3. Lamin isoforms share between 53 and 61% sequence homology, which intriguingly makes them numerically similarly distinct from each other (albeit this might just be pure coincidence)[323].

All lamins have a small amino-terminal head domain, a long-coiled coil rod domain and a large carboxy-terminal globular tail domain. The tail domain contains several motifs that set lamins aside as IFs such as a nuclear localization signal, an immunoglobulin (Ig)-fold motif and a CaaX motif which undergoes farnesylation in order to further modulate polymerisation and localisation[324,325].

They dimerize through their rod domain, then associate head to tail to form linear polymers, which in turn associate laterally in groups of 3 or 4 in a staggered antiparallel manner to form 10nm width filaments[326]. Polymerisation dynamics and the resulting higher order structures also seem to be isoform-dependent. For example while computational analysis of Lamins A/C homology point towards possible heterodimer formation, they strictly undergo homodimerization in vivo[327] and moreover lamins A and B polymerise in distinct microdomains[328].

The nucleoskeleton is between 5 and 10 times stiffer than its cytoskeleton counterpart, and while other nucleoskeletal proteins exist (e.g Titin, Actin) this rigidity is mostly due to lamins A[329], as their knockout generates a 11-fold softer nucleus. Lamins B are thought to inversely give

the nucleus elasticity and the ability to deform. While this hints to a separation of roles on each isoform, controversy exists in elucidating which roles exactly do they play. Lamins A/C and B both localize mainly at the inner nuclear membrane but are also distributed in the nucleoplasm where they perform several other roles than structural as well as having different dynamics[328]. For example Lamin B1 can be found in the nucleolus where it is supposed to play a role in modulating its plasticity[330] and stiffness[331]. Lamins A are also much more dynamic compared to their relatively static lamin B counterparts within the nucleoplasm[332].

PTMs have a role in explaining some of these differences. Lamin C does not have a farnesylation site, which could explain why, while computation analysis of sequence homology would predict at least 25% heterodimer formation, lamins A and C strictly form homodimers in vivo[327]. Lamins also undergo phosphorylation, most notably during mitotic disassembly of the nuclear lamina as mediated by CDK1[333], and SUMOylation, which was demonstrated to alter lamin A dynamics and localization in the context of cardiomyopathies[334]. Regarding nuclear mechanical integrity, some studies point towards lamin A being the major player[335] while the creation of a lamin C-only mouse exhibited only mild nuclear fragility[336]. While these results might seem contradictory, they more likely reveal that lamin polymerisation is cell type and cycle dependent[336,337] as well as responsive to extracellular cues from the environment[335], and as we will discuss now also strongly dependent on interacting partners.

Indeed, several observations indicate that lamins and their polymerisation dynamics are heavily modulated by their interactome. As shown before lamin A and C do not form heterodimers in vivo, but they do in vitro[338]. Similarly lamin bundles vary in thickness and spacing between in vivo and in vitro studies[339,340]. This points at a modulation of their higher order structure of lamins by other proteins. Interaction analysis have uncovered that there are over a hundred lamin-binding partners, creating a wide potential for modulation of lamin dynamics[341,342]. Mutations in lamins have been shown to cause the misassembly of lamin filaments in several ways, such as changes in subunit spacing or localization and lead to several laminopathies[343,344]. Laminopathies can vary in degree of severity but are usually linked by a common loss of mechanical resistance of the cell in general and the nucleus in particular, such as is seen in Emery-Dreifuss muscular dystrophy[345]. These mutations are also accompanied by mislocalization of other proteins such as inner nuclear membrane-bound emerin[343], hinting towards the fact that their interplay is crucial in proper nucleoskeletal maintenance.

This regulation, and moreover the mechanosensitive properties of the nucleoskeleton, is dependent on the integration of the nucleoskeleton to the nuclear lamina. The nuclear lamina is a proteinaceous mesh that encompasses the fibrillar networks of lamins and other nucleoskeletal proteins as well as nuclear envelope-associated polypeptides. Among the later

we will remark LINCs, Nuclear Pore Complexes (NPCs), LEM-domain proteins (such as Emerin), LAP1 and LBR, but many other Nuclear Envelope Transmembrane proteins (NETs) exist. While the first ones are universal, some NETs are only expressed in certain tissues and cell types, incrementing the potential for the role of the nuclear lamina. LINCs, which link through SUN domain proteins to the nucleoskeleton in the INM and nesprins in the outer nuclear membrane (ONM) to the cytoskeleton[346], serve as a direct connection between both networks. As so they play an important role in mechanotransdution which will be discussed below. NPCs are the main actors in mediating active transport in and out of the nucleus, and while they have a certain role in the positioning of open chromatin[347,348] as well as a response to mechanical stimulus[349,350], we will not discuss them here out of brevity and limited interest towards our research as they seem to react more to ECM stiffness than anything else[351]. The other proteins act mainly as anchorage and adaptor proteins between different elements of the lamina as well as chromatin. The complex network results in a mechanically rigid but responsive mesh that not only ensures the structural integrity of the nucleus but has important roles in transducing mechanical stimuli as well 3D organisation of the genome.

As stated before lamins interact with LADs through lamin A/C[118,352], LBR[119], emerin[120] and several transmembrane proteins[121]. Interestingly enough, while lamin A and B type produce distinct networks they have been shown to be able to interact, or at least colocalize, with the same genome regions[353] and both are impacted similarly by the reshuffling of LAD territories after mitosis[354]. But the KO of lamins in embryonic mice did not affect LAD and interLAD region formation, revealing that NETs could possibly tether chromatin independently of lamin, at least at first[355]. Furthermore the high mobility of lamins A in the nucleoplasm is an indicator that they probably do not interact with chromatin by thermselves[332], albeit it has been shown that the tail of lamin C can interact with core histones directly, this interaction being likely modulated by a third party[352].

Indeed LBR was shown to initiate chromatin tethering to the nuclear lamina, but needed lamins A to maintain it and was crucial in genome organization during differentiation[119]. While the genomic regions of tethering are still debated it has been demonstrated that LBR can recognize H4K20me2[356], which indicates a chromatin landscape-dependant mechanism. Emerin is also of importance as it has been shown, like other LEM-domain proteins, to interact both with lamins and with chromatin through BAF, a DNA-bridging protein[357]. Mutations in emerin are also quite common in EDMD[358], and general disruption of emerin results in abnormal nuclear morphology[359,360] as well as defective gene regulation[361]. Emerin has also been shown to interact with HDAC3, meaning that it not only directly interacts with chromatin but also can regulate its organisation[362]. Furthermore, as stated before emerin plays a role in nuclear lamin regulation[308].

Finally other NETs can also promote the location of chromosomes to the nuclear periphery, and their activity seems to be cell type and cycle dependant[121]. All of this then points to a dynamic tethering of chromatin to the nuclear lamina, where lamins play a scaffold role. Moreover, lamins also modulate transcription by interacting with promoters as well as modifying local chromatin landscape[363].

The nuclear lamina then represents an ideal mediator of biophysical cues to chromatin. Indeed, we already discussed how emerin, in complex with non-muscle myosin IIA and actin can control gene silencing and chromatin compaction in a mechanosensory manner[308]. Moreover it has been shown that emerin-deficient cells had impaired mechanosensory responses to strain, which eventually lead to increased apoptosis[360]. Emerin is also implicated in ECM-stiffness sensing and the subsequent modification of chromosome territories, a role it partly shares with lamin B2[364]. Similarly it has been shown that lamins A are upregulated on tissue stiffness and regulate matrix-directed differentiation[335], a relationship that is not shared with lamins B. It was later demonstrated that this upregulation, and increment in nuclear integrity was mediated by myosin-II activity that promotes lamins A dephosphorylation, leading to reduced turnover[365].

Shear stress can change nuclear shape and induces upregulation of lamin A as well as a major redisposition towards the nuclear lamina, creating a stiffer nuclei that is more likely to resist deformation[366]; this shift in localisation could have gene expression effects. On one side, congregation of lamin toward the nuclear periphery can serve as a "trap" for certain molecules. For example, lamin A/C and c-Fos can effectively arrest Activating Protein 1 (AP-1) at the nuclear lamina[367]. Interestingly, AP-1 has been shown before to be necessary for EDC activation[209], and AP-1 is a known target of SRF, which as we have discussed before is activated following mechanical stimulation of HKs[220]. Considering that serum stimulation can effectively modulate release of AP-1 from its lamin A/C trap throught ERK1/2 and c-Fos[368], this mechanosensitive mechanism of arrest is thwarted, but taking into account that there exist other proteins that are arrested in such a way[369] this could still be a possibility.

Another likely effect is the removal of lamin-binding partners from the nucleoplasm. For example lamin A binds Lamina-Associated Polypeptide 2 α in the nuclear interior[370], and these complexes have been shown to be required for maintenance of proliferative state in human fibroblasts[371]. As discussed before emerin is an important lamin A/C interacting partner as well as with actin, incrementing its polymerisation rate[372]. Lamin A/C and emerin can thus regulate Megakaryoblastic Leukaemia 1 (MKL1)[373], a mechanosensitive TF that has been shown to up-regulate SRF genes[309].

Finally, another possible pathway is modification of chromatin tethering to the nuclear lamina. As of now such a mechanosensitive pathway is still to be discovered, but in light of the observations made before it seems a likely occurrence.

It is important to note that transmission of these extracellular forces require physical connections between the cytoskeleton and the nucleus. The LINC complex mediates these connections. It contains nesprins, KASH domain proteins in the ONM that connect to actin either directly or through microtubule motor proteins, and to keratins through plectin. Inside the nucleus, SUN domain proteins connect to lamins and other nuclear lamina proteins.

Disruption of the LINC complex induces abhorrent nuclear morphology and impaired force transmission to the nucleus[374], but there have been contradicting reports as to the actual effect on mechanosensation. For example, an initial study that used KO of nesprins and KASH proteins showed normal activity of mechanosensitive genes following physical stimulation[374], indicating that the mechanically initiated signal must be transmitted through another channel. But another study which looked into different magnitudes of strain found that high frequency but low magnitude mechanical signals could activate mechanosensory genes through the LINC complex, while higher magnitudes did not[375]. Mice lacking Nesp4 or Sun1 showed that outer hair cells of the ear, highly specialized cells required for hearing (i.e responsive to sound waves), would degenerate as hearing matured and would lead to hearing loss[376]. Both studies point towards the ability of the cell to differentiate between mechanical signals and their magnitudes and the importance of the LINC complex in this pathway.

While many aspects of what cellular machineries are implicated in the translation of biophysical cues from the environment to the nuclear interior and how these cues might be translated into finite changes of gene expression, much is still left to understand about how the general 3D nuclear architecture is affected. Past studies have showed that modulation of adhesive surface available to HKs can effectively specify 3D nuclear morphology[221], and moreover induce HK entry into the terminal differentiation pathway[193]. The present work will try to further develop those studies to elucidate how changes in cellular morphology following reduction in available adhesive surface of human keratinocytes will impact its nuclear architecture.

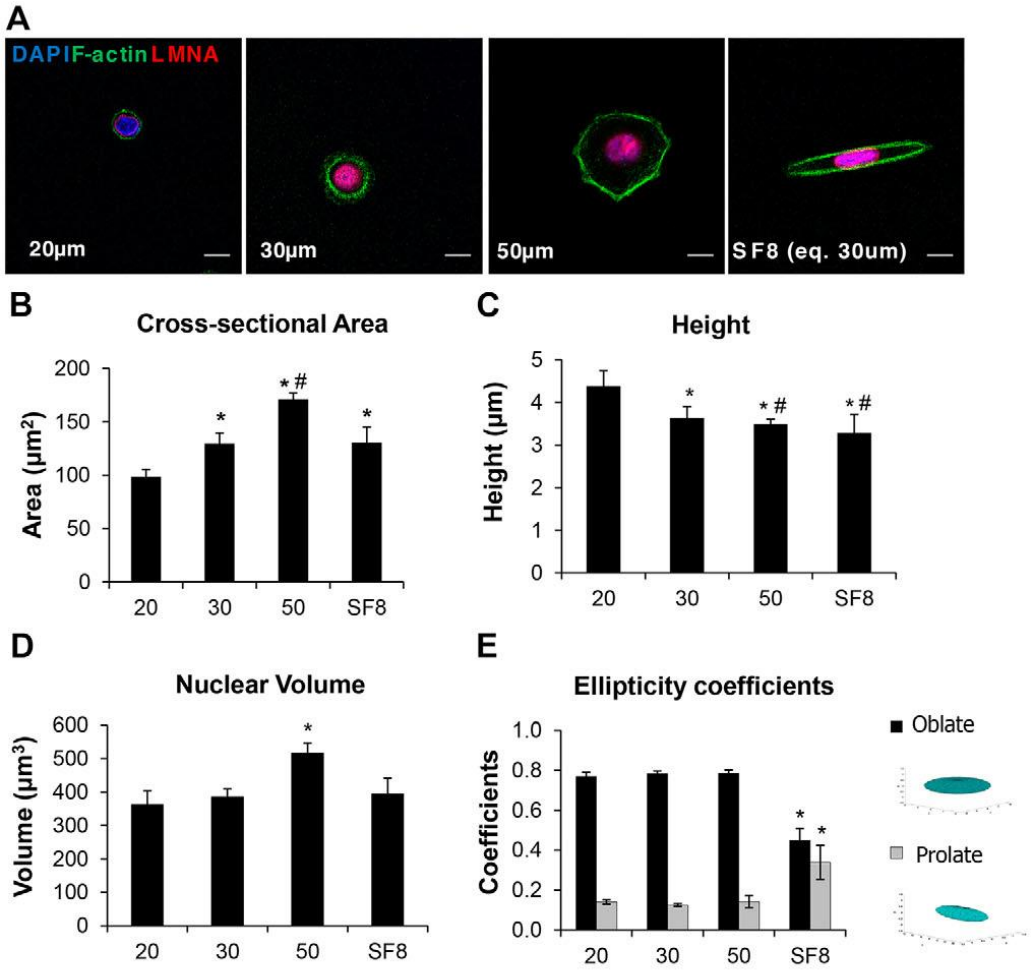

Figure 1.7. *Reduction of available adhesive area through micro-engineered substrates allows for modulation of nuclear morphology. Primary HKs cultured on either circular collagen islands with diameters of 20, 30 and 50 µm, or ellipses (SF8 with equivalent area of 30 µm). (**A**) Representative immunofluorescence images of F-actin (green), lamin A/C (red) and DAPI (blue) (**B–E**) Quantification of the maximum (**B**) cross-sectional area, (**C**) height, (**D**) volume and (**E**) geometrical shape coefficients. Adapted from Almeida et al. 2015.*

Aims of project and development of plan

Past studies have demonstrated that entry into the terminal differentiation pathway by keratinocytes is accompanied by changes in their nuclear morphology and chromatin landscape. It has also been shown that biophysical cues can mediate the entry into the pathway, but as of now little is know on how do biophysical cues affect nuclear architecture and epigenetic gene regulation. The aim of this PhD thesis will therefore be to investigate that relationship using a model system based on micropatterned surfaces to apply simple, defined physical constraints on single keratinocytes.

1. Characterise the effects of cellular shape on nuclear architecture and chromatin remodelling.

   Single HKs will be grown in fully spread/compacted configuration on micropatterned substrates. Confocal imaging of open (H3K27Ac, H3K4me3) and closed (H3K27me3, H3K9me3) markers as well as nucleoskeletal proteins (Lamin A/C, B1) and the nucleolus (Nucleolin).

2. Identify specific genomic regions affected by biophysical cues.

   Here RNA-seq will be used to profile the transcriptome of HKs exposed to defined adhesive cues and further experiments will validate affected pathways.

3. Determining the role of the cytoskeleton in biophysical regulation of nuclear architecture.

   Here using previous findings and general knowledge of the cytoskeleton we will perform different perturbations to analyse changes in the system and gain additional insight. Using inhibitors of the different cytoskeletal proteins/complexes we will study how keratinocytes cope with the loss of their structural integrity and analyse the impact on mechanotransductive regulation of nucleus morphology. Cell lines with knockout of plectin or expressing defective keratin, as well as siRNA knockdown of lamin A/C and nesprin 2, will be used to verify any findings from the inhibitor treatments.

Chapter 2: Materials and Methods

J2 3T3 cell culture

J2 clone of Swiss 3T3 cells were culture in High glucose DMEM with L-glutamine (Gibco) and supplemented with 1% Pen/Strep (Gibco) and 10% Foetal Bovine Serum (Biosera) in T75 cell culture flasks. Cells were passaged bi-weekly, at confluence, and replated at 1/10 split ratio. Cell culture media was removed and cells trypsinized using 5mL pre-warmed (37 °C) 0.05% trypsin in 0.48 mM EDTA solution (Gibco) for 5 minutes. Cells were detached from cell culture flask using light tapping. Trypsination was quenched by addition 10 mL of Foetal Bovine Serum (FBS, Biosera). Total 15 mL was then transferred to a centrifuge tube and cells spun down at 1.2E3 rpm for 5 minutes. Supernatant was removed and cells resuspended in 10 mL fresh media. 1mL of suspension was then added to 9 mL of fresh media in new T75 cell culture flask. Cells were maintained until 25th passage before being discarded. All cell lines were maintained in 5% CO2 at 37ºC.

Primary keratinocyte cell culture

A Feeder Layer was prepared as previously described[377]. Feeder layer was composed of confluent T75 of J2 clone of Swiss 3T3 cells. Confluent J2 3T3s were Mitomycin C treated (0.4 mg/ml in PBS x100 diluted in cell culture media) for 2 to 5 hours before being splitted as previously described. 3E6 of Mitomycin C-treated J2s were seeded onto a new T75 the day before primary keratinocyte splitting. Primary keratinocytes were seeded onto the J2 feeder layer at a density of 5E5 keratinocytes per T75 and co-cultured in FAD medium, composed of 3 parts DMEM (Gibco) and one part F12 (Gibco) supplemented with 1% Pen/Strep (Gibco), 10% Foetal Bovine Serum 1.8E-4 M adenine, 10E-10 M Cholera Toxin (Sigma), 10 ng/ml Epidermal Growth Factor (Peprotech), 0.5 µg/ml Hydrocortisone (Fisher) and 5 µg/ml Insulin (Sigma). When passaging co-cultures, media was aspirated off and cells washed with pre-warmed PBS (Gibco). Cells were then washed thrice with pre-warmed 0.48 mM EDTA solution (Gibco). Each wash was accompanied with tapping, to detach Mitomycin C-treated J2s. By the third wash most J2s should have detached, or else washing cycles were continued until detachment was acceptable. Remaining HKs were then trypsinized using pre-warmed 0.10% trypsin in 0.48 mM EDTA solution (Gibco) for 5 minutes. Trypsinization was then quenched using 10 mL of FBS and cells spun down as indicated previously. Supernatant was aspirated off and cells resuspended in 10 mL fresh FAD media. Primary keratinocytes used were from existing stocks of cells extracted from neonatal foreskin samples. All samples were obtained following routine circumcision procedures at the Royal London Hospital, under the ethical reference number LREC 08/H0704/65. Cells were used from passage 2 to passage 8 before being discarded.

Immortalized keratinocyte HaCaT cell culture

HaCaTs are a SV40-induced immortalized keratinocyte cell line, whose generation has been described elsewhere[378]. HaCaTs were cultured in High glucose DMEM with L-glutamine (Gibco) and supplemented with 1% Pen/Strep (Gibco) and 10% Foetal Bovine Serum (Biosera). They were passaged bi-weekly, splitted using 5mL pre-warmed (37 °C) 0.25% trypsin in 0.48 mM EDTA solution (Gibco) for over 10 minutes and then in a similar fashion to J2s. Previously stably-infected HaCaTs with K14-WT-GFP or K14-R416P-GFP were cell-sorted by FACS to select the higher-expressing population prior to being plated unto T75 cell culture flasks and stably selected using Neomycin (500 µg/ml, Sigma). Stable infection of HaCaTs was performed previously by past members of our laboratory and described elsewhere[379]. Cells were used from passage 2 to passage 20 before being discarded.

Plec KO mouse keratinocyte cell culture

Plec KO and WT mouse keratinocytes were provided by Prof. Gerhard Wiche. Cell cultures were established from $Plec^{-/-}/p53^{-/-}$ and $Plec^{+/+}/p53^{-/-}$ mice, as described elsewhere[380]. They were cultured in EpiLife medium (Gibco) supplemented with 1% Pen/Strep (Gibco) and KSFM supplements (5 mg/cl Bovine Pituitary Extract (BPE), 0.5 µg/cl EGF, Human Recombinant, ThermoFisher). Cell culture flasks were type I collagen-coated before seeding cells. For this T75 cell culture flask was treated with 5 mL PBS (Gibco) containing 30 µg/mL type I collagen (Corning) for 1 hour at 37°C before being washed off with PBS. Cells were passaged once weekly, splitted in the same way as J2 3T3 cells. Cells were used from passage 2 to passage 20 before being discarded.

RT-qPCR

Cells were washed once with PBS and subsequently lysed with RLT Plus lysis buffer (Qiagen) before RNA extraction. RNA was extracted from samples using RNeasy Plus Micro kit (Qiagen) as per manufacturer's instructions and eluted in 14 µL RNAse-free water. RNA was then reverse transcribed using LunaScript™ RT SuperMix kit (NEB). RT-qPCR was performed using qPCRBIO SyGreen Mix (PCR Biosystems). Reaction mix was composed of 10 µL 2x qPCRBIO SyGreen Mix Hi-ROX, 1 µL reverse-transcribed cDNA, 0.8 µL of 10 µM forward and reverse primer and 7.6 µL PCR grade dH2O. All probes were done in duplicates, and no-template controls were introduced for all probes. RT-qPCR was performed in a StepOnePlus RT-qPCR System. Program was as follows: 1 Cycle at 95 °C for 2 minutes. Then 40 cycles of 95 °C for 5 seconds followed by 60 °C to 65 °C for 20 seconds. Melt curve was acquired following this. RT-qPCR data was analysed using StepOne™ Software v2.3 (Applied Biosystems). ΔCt was calculated from averaged Ct of duplicates (Ct_{target}) and compared to reference housekeeping gene (Ct_{ref}) as: $\Delta Ct = 2^{(Ct_{ref}-Ct_{target})}$.

qPCR probe list

Gene	Forward (5' to 3')	Reverse (5' to 3')
K1	ATTTCTGAGCTGAATCGTGTGATC	CTTGGCATCCTTGAGGGCATT
K10	TGATGTGAATGTGGAAATGAATGC	GTAGTCAGTTCCTTGCTCTTTTCA
K16	TGCCCACCTTTCCTCCCAGCAA	CCGGGTCTGACGGCTCGAAG
K5	CTGCTGGAGGGCGAGGAATGC	CCACCGAGGCCACCGCCATA
K14	TGGACGTGAAGACGCGGCTGG	GATTTGGCGGCTGGAGGAGGTC
INV	CTGCCTCAGCCTTACTGTGA	GGAGGAGGAACAGTCTTGAGG
GAPDH	ACCCACTCCTCCACCTTTG	CTCTTGTGCTCTTGCTGGG
TGM1	TCACTGTTTCATTGTCTCCA	CCCTCACCAATGTCGTCTTC
DNp63	GAAGAAAGGACAGCAGCATTGAT	GGGACTGGTGGACGAGGAG
LRIG1	GGGGACAGAAAGGAGGAAGT	GCCTCTCAGAAGCAGCAAAT
B2M	ATGGAGGTTTGAAGATGCC	CTAAGTTGCCAGCCCTCCT
7SK	GAGGGCGATCTGGCTGCGACAT	ACATGGAGCGGTGAGGGAGGAA
H3.1	TCCGCCGTTATCAGAAGTCC	GTGTCCTCAAATAGCCCTACC
BRCA1	TATCACCACTGAATCTCTACCG	GACCTCAAACTCTGAGATCCAC
ATR	GAACACCACTGAGAAGCGTG	CCACATGGCTCCACATGCAA
ATM	TGCTGACAATCATCACCAAGTTC	TCTCCCTTCGTGTCCTGGAA
RARG	GCCCTTCTGTACTGTCCATGT	AGAAGCCCAATGGATAGGGTA
CRABPII	TGATGAGGAAGATCGCTGTG	TTCCACTCTCCCATTTCACC
NCL	TGTCAGCCCTGTTCCATGTC	GCTTGCCTCATAGGAGACCC
RPL36	CTGGTGCCAGACGTGTTACT	TGGAAACACGCACTAAGCCA
RRP1B	AAGAACACGCCCCACTTCAA	AGCAGAAATGTCCTCCGCAA
H47S pre-rRNA	GCTGACACGCTGTCCTCTG	TCGGACGCGCGAGAGAAC
45S pre-rRNA (Mouse)	GTTCCCGTGTTTTTCCGCTC	CATCGGAGAGCATCAGCCAT
RPL36 (Mouse)	CATCGGAGAGCATCAGCCAT	ATCATGTCCCGCACGAACTT
NCL (Mouse)	TGATAGGCTGAGGCCCATTTT	TTCCCTTCCCTCCCCAATAAAC
RRP1B (Mouse)	GCTCATCATCCGTGTCGCTA	CGGGGTGCTTTTTGAGTTGG

De Novo protein synthesis assay

Nascent protein levels were determined using Click-iT™ HPG Alexa Fluor™ 488 Protein Synthesis Assay Kit (ThermoFisher). 30 minutes before levels were to be determined, cell media was switched with methionine-free media supplemented with L-homopropargylglycine. After 30 minutes cells were washed once with PBS, fixed and permeabilised as per normal IF protocol. Samples were then washed once with 3% bovine serum albumin (BSA, Sigma) in PBS. Nascent protein was then labelled using 1X Click-iT® HPG reaction cocktail (ThermoFisher) for 30 minutes at room temperature, before being aspirated off and cells washed with Click-iT® reaction rinse buffer (ThermoFisher). Cells were subsequently labelled for their nucleus using HCS NuclearMask™ Blue Stain (1:2000 dilution in PBS, 30 minutes at room temperature), subsequently washed with PBS, ddH2O and mounted onto coverslips using Mowiol. Samples

were then imaged by epifluorescence as indicated below. Nascent levels of protein were assessed by measuring Alexa-488 nm fluorescence levels.

Retinoic acid reporter assay

800E3 primary HKs were transfected in T25 cell culture flasks with 0.5 µL TK-*Renilla* Luciferase control (addgene plasmid #16539) and 1.5 µL Retinoic Acid Response Element – Luciferase (addgene plasmid #13458) using JetPRIME transfection reagent (Polyplus, 114-07) as described below. After 4 hours, cells were seeded onto micropatterned islands. Positive control was treated with 1 µM all-*trans*-retinoic acid (ATRA) introduced in culture media after seeding. Negative control was not transfected. Cells were lysed and subsequently luciferase activity was measured using Dual Luciferase assay system (Promega) and normalized with *Renilla*. 100 µL of 1x Passive Lysis Buffer was added to micropatterned islands in 24-well plate containing HKs. Plate was rocked gently for 15 minutes at room temperature. Lysis solution was then transferred to 1.5 mL Eppendorf tube. 100 µL of Luciferase Assay Reagent was introduced in wells of transparent 96-well plate. 20 µL of lysate was subsequently added and the resulting solution mixed thrice by pipetting. Each lysate was analysed in triplicate. 96-well plate was introduced into illuminometer (CLARIOstar, BMG Labtech) and emission recorded at 750 nm wavelength for 10 seconds after 2 second delay. Plate was taken out of illuminometer and 100 µL of Stop & Glo Reagent introduced in each well. Plate was re-introduced into illuminometer, shaken for 10 seconds then emission recorded as previously stated. *Renilla* signal (post Stop & Glo) was used as normalisation for RARE-Luciferase signal.

siRNA treatment

1E6 primary HK were seeded unto a type I collagen coated T25 cell culture flask. 24 hours later first siRNA transfection was performed using JetPRIME transfection reagent (Polyplus, 114-07). siRNAs were: Silencer™ Select LMNA (s8221), SYNE2 (s23328), Negative Control (4390843). Cell culture media was aspirated and 2mL fresh media introduced. 200 µL of jetPRIME buffer and 2 µL of 20 µM siRNA were introduced in a 500 µL Eppendorf and vortexed for 10 seconds before addition of 4 µL jetPRIME reagent. Solution was vortexed for an additional 10 seconds then left to incubate at room temperature for 10 minutes before being introduced in cell culture flask. Final siRNA concentration in flasks: 20 nM. 48 hours after seeding, 2nd transfection was performed. 72 hours after seeding cells were washed and fresh media added. 96 hours after initial seeding cells were detached from cell culture flask and seeded upon micropatterned islands as previously described.

PDMS stamps

A silicon wafer (Sigma) was cleaned using isopropanol then acetone and blown dry with pressurized nitrogen gas. Silicon wafer was then coated with SU-8 2010 (MicroChem) using a spin coater (10 seconds at 4000 rpm). SU-8 2010 was then soft-baked by heating silicon wafer at 100 °C for 5 minutes before being cooled down at room temperature for 2-3 minutes. Photomask containing islands was cleaned using pressurized nitrogen gas then put in contact with mask and sealed using clamps. Wafer was then exposed to UV (UV-KUB 6, 100% power for 10 seconds) before being baked at 100 °C for 5 minutes. Patterns were developed by submerging the wafer in PEGMA (Sigma) for 2 to 4 minutes, before being washed with isopropanol and dried with pressurized nitrogen gas. Correct generation of patterns was verified using profilometer (Profilm3D). Finally PDMS stamp was generated by casting 10% PDMS (Sylgard 184 silicone elastomer, Farnell) over the micropatterned wafer and incubating overnight at 70 °C before being cut using a microtome blade. Stamp was used for up to two months before being discarded.

Micropattern generation

Micropatterns were generated through the application of an initiator layer onto gold-coated coverslips using PDMS stamps generated through photolithography. This layer served to generate a reaction of surface-initiated polymerisation and atom transfer radical polymerization (ATRP), generating polymer brushes that were cell-phobic. Gold coated coverslips were generated through thermoevaporation using a custom thermoevaporator from Moorfield. Coverslips (24x60 mm, 0.17 mm thickness, MUTO pure chemicals) were initially cleaned using a plasma cleaner (Henniker plasma HPT-200, 100% power, 10 minutes) then coated with 5 nm of chromium before being covered with 15 nm of gold. Brush polymerization solution was prepared by dissolving 320 mg 2,2'-bypiridine (Acros), 18mg $CuBr_2$ (Sigma), 12 mg Oligo(ethylene glycol) methyl ether methacrylate (mean molecular weight 300, Sigma) in 24 mL H_2O and 6 mL EtOH. Solution was degassed using gentle N_2 flow under agitation for 30 minutes. After this 82 mg of CuCl were added and solution left to degas for additional 15 minutes.

PDMS stamps were used to depose ω-mercaptoundecylbromoisobutyrate initiator layer on gold covered coverslips. These were introduced onto degassed brush polymerization solution and left to react for 15 minutes. After that micropatterned coverslips were removed and washed first with H_2O followed by EtOH and stored for a maximum of one month.

Micropattern preparation before seeding

Micropatterns were cut using diamond tipped pen, introduced in either 24-well (1 square cm approx.) or 6-well (4 square cm approx.) before being sterilized using 70% EtOH solution for 15

minutes followed by double wash with sterile PBS (Gibco). After this 30 µg/mL sterile solution of Type I Collagen (Corning) in PBS is added and left to incubate overnight at 4 °C. Following day micropatterns were washed by dilution (i.e solution was added onto micropatterns and excess aspirated off while carefully leaving enough in the well so that micropatterns would not dry) thrice using sterile 1 mM HCl solution and twice with PBS before being incubated in FAD medium a minimum of 30 minutes at 37°C before seeding cells.

Seeding of cells unto micropatterns

After splitting and resuspension, cells were diluted to appropriate concentrations (2E5 cells/mL for 20 µm islands, 4E4 cells/mL for 50 µm islands) in media. Media was aspirated off micropatterns and cellular solution introduced in wells. Cells were left to attach for 1-2 hours before excess cells being washed off by removing micropattern and dipping it into fresh media several times before introducing it into a new well containing fresh media.

Cytoskeletal Inhibitors

HKs were seeded unto micropatterned islands as described above. 2 hours after seeding, non-adherent cells were washed off and fresh media containing 50 µM Blebbistatin (Millipore), 10 µM Y-27632 (Sigma) or 1 µL/mL DMSO (Sigma) was added. 24 hours later cells were washed with PBS and subsequently fixed, permeabilised, blocked and stained as described below.

Nucleoli live imaging

Immortalized keratinocyte HaCaT cells were transfected with 3 µg of GFP-Nucleolin plasmid (addgene, plasmid #28176) using JetPRIME transfection reagent (Polyplus, 114-07) as described previously, 24 hours before seeding cells on micropatterned islands. Micropatterned islands were fitted onto a bottomless round confocal dish (VWR) using silicone adhesive sealant (Momentive). 45 minutes after seeding excess cells were washed off with fresh media and remaining attached cells introduced into Zeiss 880 Laser Scanning Confocal Microscope with incubator chamber attached to maintain 5% CO2 and 37 ºC during imaging. Up to 5 cells per island size were imaged per experiment. Z-stacks were taken every 15 minutes for a total of 3 hours (12 stills per cell).

Immunofluorescence staining

After washing samples with PBS cells are fixed using 4% PFA solution in PBS for 10 minutes before being washed twice in PBS. Cells are permeabilized using 0.2% Triton X100 (Sigma) in PBS for 5 minutes. If staining for Nucleolin 0.1% Triton X100 for 15 minutes were used. Cells were then blocked using 10% FBS in PBS solution with added 25µL cold fish gelatin (Sigma) for 1 hour at room temperature. Primary antibody cocktail in blocking solution was then applied and left for incubation overnight at 4°C. Next day samples were washed in PBS before applying

secondary antibody cocktail and DAPI (Biotium) for 1 hour at room temperature. Finally, samples were washed in PBS followed by H_2O before being mounted onto microscope slides using 5 µL of Mowiol (Sigma).

Fluorescence imaging and processing

Epifluorescence images were acquired using Leica DM4000 Epi-Fluoresce Microscope. Epi-fluorescence images were taken using 40x objective. Confocal images were acquired using Zeiss 880 Laser Scanning Confocal Microscope. Confocal images were taken using AiryScanFast2D configuration, Plan-Apochromat 63x/1.4 Oil DIC M27 objective, 2.3x digital zoom. Images were 1024x1024 pixels, 17.4522 pixels per micron. Middle section of nuclei was determined using Z-stack range indicator. Z-stack slices were spaced by 1 µm.

Primary analysis of images was performed using ImageJ software (v.1.51w, National Institutes of Health). Images had their background removed first (rolling ball radius 50 pixels), before delimiting region of interest with magic wand tool and measuring intensity. DAPI levels were used to normalise all intensity measurements, before being normalised to control condition (50 µm islands). Morphological analysis was performed by first generating a binary image (Make binary). If analysing Z-stacks middle section was used to calculate threshold. Then holes in mask were filed and mask visually inspected to verify correct generation. Mask area was then measured. For nuclear volumes 3D geometrical measure plugin was used.

Mean Fractional assay was performed using CellProfiler software (v.2.2.0, www.cellprofiler.org, BROAD Institute). Images had to be converted to .tif format using a custom script in imageJ. Images were then uploaded to software. Software was instructed to generate a mask based on DAPI images (Nuclei, object between 200 and 2000 pixel units) and to measure mask size and intensity values of all images within that mask (DAPI, chromatin markers, lamin A/C). These measures served as verifications of manually acquired intensity measurements in imageJ. Finally, software was instructed to measure radial intensity distribution within the DAPI-generated mask of images of interest (chromatin markers, lamin A/C) by dividing the nuclear area in 20 bins of equal radial distance.

Foci analysis was performed using InCell Developer Toolbox (v.1.9.2 build 2415, GE Healthcare). Nuclei masks were obtained by performing object segmentation on DAPI images with large kernel size and subsequently passed through a sieve to discriminate objects based on size. Finally, the mask was eroded to remove part of the nuclear periphery. Foci were determined by performing object segmentation on chromatin marker images with a small kernel size. Sieve was used to discriminate between foci deemed too small (close to optical resolution limit) or too big.

Objects that did not share more than 90% boundary with mask obtained from DAPI staining were removed. Number of objects was finally normalised to DAPI levels.

Statistical analysis

Statistical analysis of data was performed using Prism (version 8.4.3, GraphPad). All measurements were averaged per experiment, then entered as column analyses (2 conditions) or grouped data (4 or more conditions). When comparing 2 conditions, significance was investigated through unpaired t-tests. When comparing 4 conditions or more, significance was investigated using 2-way ANOVAs. Multiple comparisons were investigated through Tukey's multiple comparisons test when comparing 4 conditions. When comparing 6 conditions (i.e siRNA and cytoskeletal inhibitors), Sidak's multiple comparisons test was used. Radial intensity distribution assays were entered as XY data, and significance investigated using Kolmogorov-Smirnov test.

Antibodies - Primary

Antibody	Species	Fixation Method	Dilution (IF/WB)	Manufacturer	Reference
Lamin A/C	Mouse	PFA 4%	1:200/1:1000	Santa Cruz	sc-7292
Lamin A	Rabbit	PFA 4%	1:500	Abcam	ab26300
Lamin B1	Rabbit	PFA 4%	1:500	Abcam	ab16048
Nesprin 2	Rabbit	N.A	/1:1000	Abcam	ab103020
H3K27me3	Rabbit	PFA 4%	1:200	Millipore	07-449
H3K27Ac	Rabbit	PFA 4%	1:500	Abcam	ab4729
H3K9me3	Rabbit	PFA 4%	1:400	Abcam	ab8898
H3K4me3	Rabbit	PFA 4%	1:200	Millipore	07-473
Total H3	Rabbit	PFA 4%	1:1000	Abcam	ab1791
Transglutaminase 1 (BC1)	Mouse	PFA 4%	1:1000	CRUK	N.A
Involucrin (DHI B6)	Rabbit	PFA 4%	1:1000	CRUK	N.A
GAPDH	Mouse	N.A	/1:20000	Millipore	MAB374
Nucleolin	Rabbit	PFA 4%	1:400	Abcam	ab22758
Collagen I	Mouse	PFA 4%	1:2000	Abcam	ab90395
LAMA3	Rabbit	PFA 4%	1:200	Sigma	HPA009309
Fibronectin	Rabbit	PFA 4%	1:400	Sigma	F3648
γH2AX	Mouse	PFA 4%	1:1000	Millipore	5636
53BP1	Rabbit	PFA 4%	1:200	Bethyl	A300-273A
P16	Rabbit	PFA 4%	1:500	CRUK	N.A
Keratin 14 (LL002)	Rat	PFA 4%	1:500	eBioscience	CBL197
Pan Keratin (H-240)	Rabbit	PFA 4%	1:500	Santa Cruz	sc-15367
Plectin (10F6)	Mouse	MeOH	1:200	Santa Cruz	sc-33649

Antibodies -Secondary

Antibody	Species	Dilution	Manufacturer
Alexa 488/555 Anti-Mouse	Donkey	1:1000	Molecular Probes

Alexa 488/568 Anti-Rabbit	Goat	1:1000	Molecular Probes
Anti-mouse HRP	-	1:5000	Dako
Anti-rabbit HRP	-	1:5000	Dako
DAPI	Dye	1:1000	Molecular Probes
Phalloidin 488	Dye	1:200	Molecular Probes

Reagents and buffers

Buffers and Solutions	Composition	Application
Mowiol mounting media	Mowiol 40-88, Glycerol, 0.2 Tris-HCl (pH 8.5).	Immunohistochemistry
RIPA	**Sodium chloride (Sigma), 1% Triton-X 100, 0.5% sodium deoxycholate (Sigma), 0.1% sodium dodecyl sulphate (SDS) (Sigma), Tris, phosphatase inhibitor (Roche) at 10x and protease inhibitor (Sigma) (pH 8.0)**	Total Cell Lysate
Running Buffer	2.5 mM Tris, 20 mM Glycine, 0.1% SDS, ddH2O, pH 8.3	Western Blotting
Transfer Buffer	25 mM Tris, 20 mM Glycine, MeOH	Western Blotting

Western Blots

For all western blots 200E3 cells were seeded unto 6-well plates which were previously type I collagen coated. 24 hours after seeding cells were washed using cold PBS (Gibco) then adherent cells scrapped off and lysed using 75 µL of lysis buffer. Lysis buffer consisted of 67.5 µL RIPA buffer (ThermoFisher), 7.5 µL phosphatase inhibitor (phosphoSTOP, Roche) and 0.375 µL Protease inhibitor Cocktail (Sigma). Lysates were then sonicated (30 second intervals for 5 minutes in ice water, high setting on diagenode Bioruptor) before being spun down (2500 RPM, 30 min at 4 °C) and supernatant collected. Total protein concentration was quantified using standard Pierce BCA assay (ThermoFisher). Samples were mixed with 4x sample buffer (Life Technologies) and β-mercaptoethanol (Sigma) and heated at 95 °C for 5 minutes to denature and break cysteine-cysteine bonds. They were subsequently loaded onto 4-15% gradient Mini-Protean gels (Bio-Rad). Gels were run in a Bio-Rad Mini-Protean Tetra Cell System for 90 minutes at 100 V. Gel was then transferred onto a nitrocellulose membrane (GE Healthcare) by current (300 mA for 1 hour) in cold transfer buffer. Correct transfer was assessed by staining nitrocellulose membrane with Ponceau reagent for several minutes. Ponceau reagent was washed off using TBS-T (TBS supplemented with 0.5% Tween-20) and membrane incubated in

5% non-fat dry milk (Marvel) in TBS-T for 1 hour under mild shaking for blocking. Membrane was then incubated with primary antibody in 5% milk/TBS-T overnight at 4 °C. Following day membrane was washed thrice with TBS-T for 5 minutes per wash, before secondary antibody incubation in milk/TBS-T (1 hour, room temperature). Membrane was subsequently washed thrice with TBS-T before being soaked in HRP substrate peroxide/HRP substrate luminol reagent (50:50, Millipore) for 30 seconds. Excess reagent was removed, and membrane imaged using ChemiDoc™ Gel Imaging System (Bio-Rad) using signal accumulation mode.

RNAseq – Sample preparation and data pipeline

Primary HKs were seeded onto micropatterned islands as previously described. 4 hour and 24-hour samples were washed with PBS before being lysed using RLT Plus Lysis Buffer (Qiagen). RNA extraction was performed using RNeasy Plus Micro Kit (Qiagen) and RNA eluted in RNAse-free H2O. Initial quality control was performed using Nanodrop 2000 before sending samples to Genome Center (QMUL, London, UK) for sequencing. RNA was sequenced using NextSeq 500 High Output Run (150 cycles), 40M reads per sample, 75 bp read length, paired end. Data generated was transferred to Basespace sequencing data storage hub. FASTQ files were uploaded to Galaxy (https://usegalaxy.org/) and different lanes of same sample/read direction were concatenated. Concatenated files were then aligned using HISAT2 to hg19 genome to produce BAM files. Average alignment concordance was used as first quality control of data (overall >90% reads aligned concordantly 1 time or more). BAM files were then downloaded and analysed in SeqMonk (Babraham Bioinformatics, version 1.45.0) using R (R Project, version 3.5.3). RNA-Seq QC Plot was used to further verify correct alignment. Biological replicates were then grouped together, and probes quantitated. Differential expression of genes was performed by DeSeq2 with raw counts between couples of individual conditions (alpha set at 0.05 level). Lists of differentially expressed genes were then uploaded to the Gene Ontology Resource (http://geneontology.org/) to further analyse affected pathways. Top pathways were then selected based on relevance.

Chapter 3: Characterisation of the Effects of Cellular Morphology on Nuclear Architecture and Chromatin Remodelling.

Introduction

The nucleus is a central mechanosensory unit in the cell, due to its innermost position within the cytoskeleton to which it is physically linked through LINC proteins. The cytoskeleton can transmit forces generated from physical deformations of the cellular membrane to the nucleus, which will dynamically respond by itself changing in morphology. Inside the nucleus, the nucleoskeleton will mediate this change and by doing so interact with chromatin, the packaging system of DNA. These interactions modulate gene expression and can have profound consequences on cellular fate[193].

Chromatin is a highly dynamic polymer gel, modifying its structure at different organizational levels in response to internal and external cellular cues to control overall transcriptional state of the cell. At the gene level openness of chromatin is a potent regulator of gene expression directing accessibility of genes to the transcriptional machinery. Post-translational modifications to histones tails, the core components of nucleosomes which are the building blocks of chromatin, help modulate the level of openness and serve as markers for active and repressed genes. Association of open and close chromatin regions through phase separation can then help compartmentalize specific processes, such as transcriptional factories or rRNA synthesis in nucleoli. At the nuclear level, radial positioning of chromatin from the more transcriptionally active center to the repressed nuclear periphery serves as another level of transcriptional control. Changes in these structures are mediated by histone readers, erasers and chromatin remodelling complexes, whose activity can be modulated by cyto and nucleoskeletal proteins.

While highly synthetic in nature, micropatterned substrates offer a simple system to effectively control cell shape and thus create physical stimulus. Previous data has showed that reduction in available adhesive area effectively modifies cell and nuclear size and shape and can induce terminal differentiation in HKs[220]. Work by previous members of our laboratory demonstrated these changes to be directly mediated by the cytoskeleton. The studies presented here characterize the structural changes in nuclear organisation and global chromatin remodelling in HKs following nuclear deformation.

Differentiation and nuclear deformation

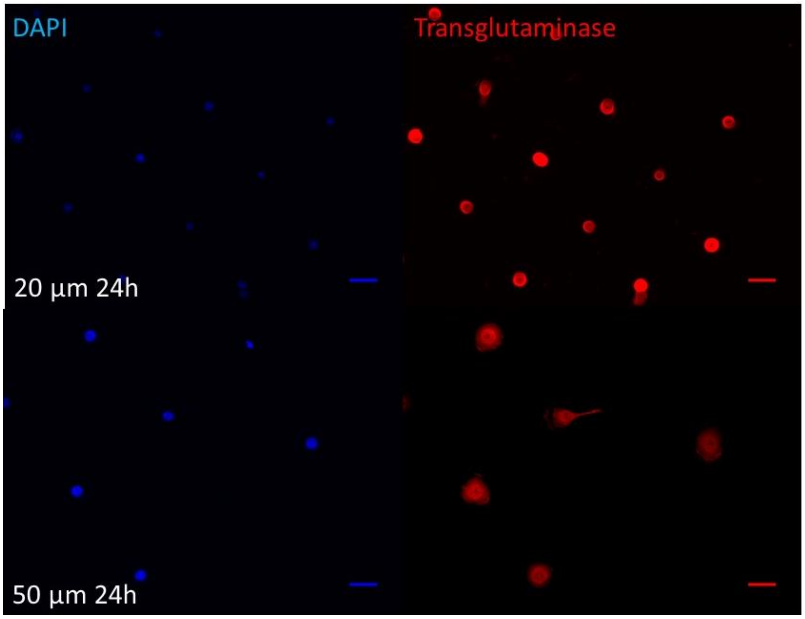

Figure 3.1. *Example of epifluorescence-imaged cells grown on 20 µm and 50 µm islands at 24h time point, stained for Nucleus (DAPI) and Transglutaminase. Scale bar = 50 µm.*

Previous data demonstrated that HKs grown on micro-patterned collagen islands of 20 µm adopt a rounded morphology and initiate terminal differentiation after 24 hours compared to spread cells grown on 50 µm islands in the same time period[220] and have reduced nuclear cross-sectional area and volume[221]. To confirm this experimental model, primary HKs grown on micropatterns were labelled by immunofluorescence for the differentiation marker Transglutaminase (TG) and imaged by epifluorescence microscopy after 4 and 24 hours. General differentiation statistics for each condition are summarized in Table 3.1. Example of epifluorescence imaging can be found in Figure 3.1.

Island Size	TG + (4h)	TG + (24h)	Nuclear Cross-Sectional Area	Nuclear Volume
20 µm	18% (±2%)	55% (±17%)	85.13 ± 19.38 μm^2	372.83 ± 34.23 μm^3
50 µm	11% (±10%)	15% (±8%)	142.91 ± 36.67 μm^2	541.87 ± 86.29 μm^3

Table 3.1. *Transglutaminase-positive cells, Nuclear Cross-Sectional Area and Nuclear Volume at different island size and time. N = 3 experiments for differentiation statistics, N = 12 cells for morphological measurements. Shown as mean ± SD*

Similarly, modified nuclear cross-sectional area and volume were investigated by confocal imaging in the same conditions, results are summarized in table 3.1.

Consistent with previous results[220,221], these data confirmed that limited adhesion promotes HK terminal differentiation and causes a reduction in nuclear volume. Thus, we concluded that the technique was working similarly and proceeded to confocal imaging of chromatin markers.

Changes in overall chromatin marker levels

To determine changes in overall open and closed chromatin states we performed immunofluorescence labelling of chromatin markers H3K27me3, H3K27Ac, H3K9me3 and H3K4me3 and imaged them using confocal microscopy at 4h and 24h time points after seeding of HKs on micropatterned substrates. Cells were fixed and stained for each marker plus TG to serve as a discriminator between differentiating and non-differentiating populations. Statistics were derived from at least three separate experiments with at least 20 cells analysed per condition per experiment. Primary HKs used were all from the same donor (passage 2-8).

H3K27me3 and H3K27Ac levels

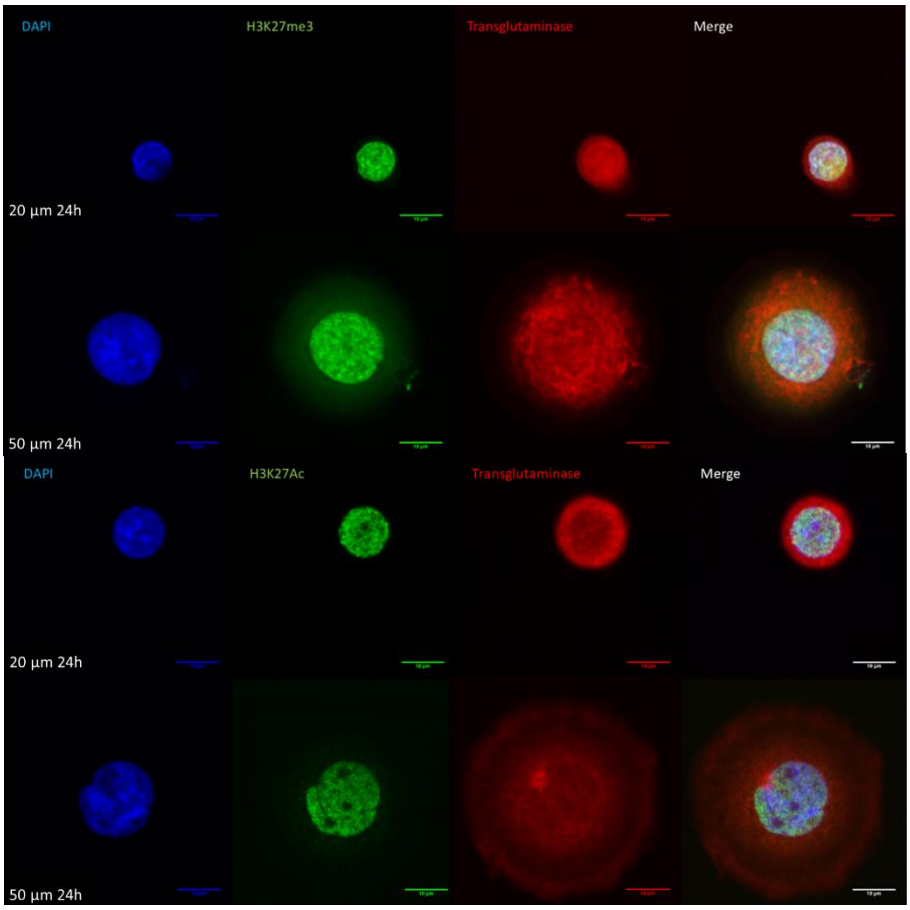

Figure 3.2. *Representative confocal microscopy images of cells grown on 20 µm and 50 µm islands at 24h time point, stained for Nucleus (DAPI), H3K27me3 (Top) or H3K27Ac (Bottom) and Transglutaminase. Scale bar = 10 µm.*

We initially analysed open H3K27me3 and closed H3K27Ac chromatin markers as both have been described extensively in HK differentiation and are markers involved in facultatively repressed genes and active transcription respectively, hence prime candidates to analyse change in gene expression mediated by induction of differentiation. Example of confocal images of both can be found in Figure 3.2 and bar graph of measured integrated intensities are summarised in Figure 3.3. Our measurements of integrated intensity fluorescence showed no

statistically significant differences between 20 µm and 50 µm islands at 4-hour timepoint for both H3K27me3 and H3K27Ac (Figure 4.3.A-B). At 24 hour time point both markers were significantly downregulated on smaller islands which is consistent with previous reports[193]. As both markers target the same lysine a simultaneous costain of both markers was performed to verify that the observed reduction in overall fluorescence intensity was not a product of incorrect targeting. Example of confocal images can be found in Figure 3.3. Finally, as entry into the differentiation pathway is accompanied by major chromatin modifications[381], we performed a discrimination between non-differentiating and terminally differentiating cells on the smaller islands after 24 hours: Both markers showed no difference in integrated fluorescence levels

between differentiated and non-differentiated cells (Figure 3.3 C and D) and thus this type of analysis was not applied to the following experiments.

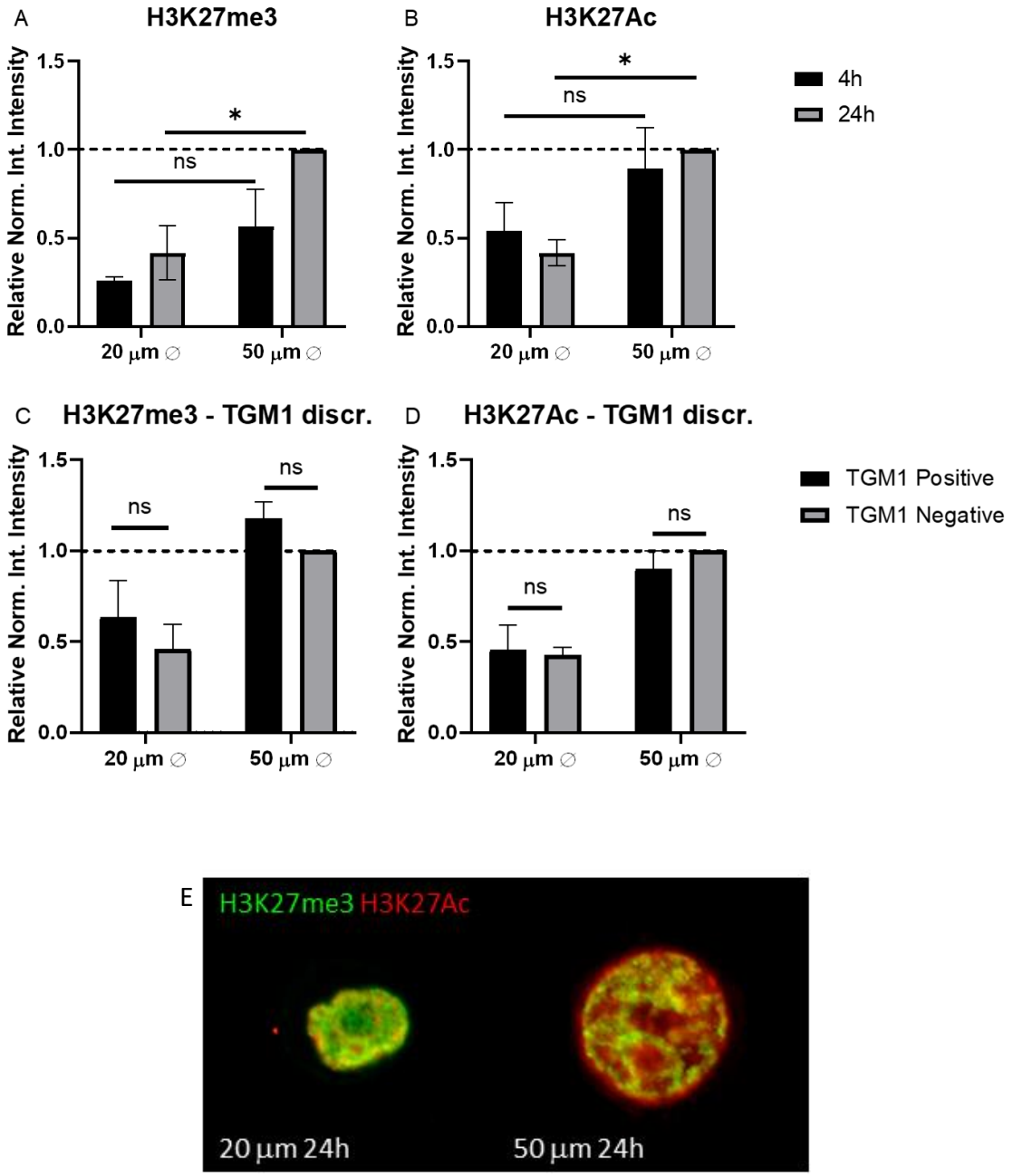

Figure 3.3. *Normalised integrated intensity measurements of confocal images of H3K27me3 (**A**) and H3K27Ac (**B**) markers as well as discriminated by TGM1 levels (**C** & **D** respectively). Shown as mean + S.E.M. N = 3 experiments. n.s: non-significant. *: p-value<0.05. (2-Way ANOVA, Tukey multiple comparisons test). **E**: Representative confocal microscopy images of cells grown on 20 μm and 50 μm islands at 24h time point, stained for H3K27me3 and H3K27Ac.*

H3K4me3 and H3K9me3 levels

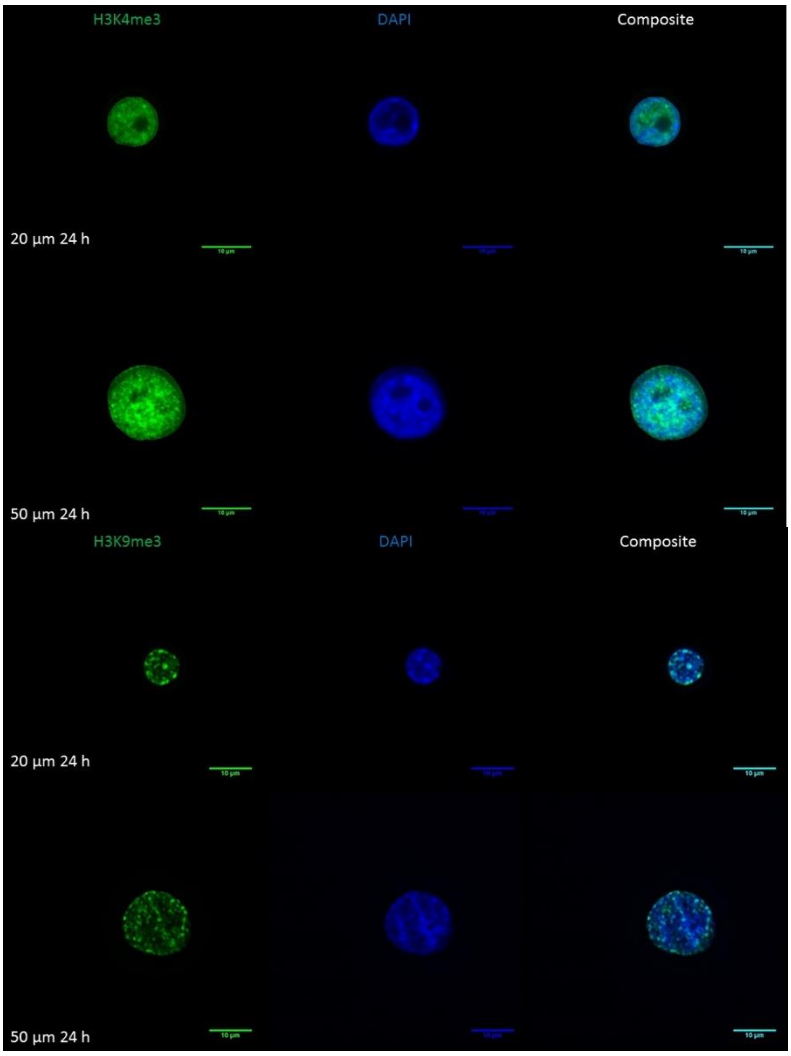

Figure 3.4. *Example of cells grown on 20 µm and 50 µm islands at 24h time point, stained for Nucleus (DAPI) and H3K4me3 (Top) or H3K9me3 (Bottom). Scale bar = 10 µm.*

We next expanded our analysis by measuring integrated fluorescence intensity of both H3K4me3, an open chromatin marker associated with transcriptionally active promoters, and H3K9me3[382], a closed chromatin marker associated with constitutively repressed genes. Examples of confocal images of both stainings can be found in Figure 3.4 and bar graph quantification of measured integrated intensities can be found summarised in Figure 3.5.

Our measurements showed no statistically significant differences between 20 µm and 50 µm islands at 4-hour timepoint for both H3K9me3 and H3K4me3 (figure 3.5.A-B). We found no differences between island sizes at 24 hours for euchromatin marker H3K4me3 but found a statistically significant increment for heterochromatin marker H3K9me3 on large islands compared to small. When comparing between time points, we observed no difference between 4h and 24h in both island sizes for H3K9me3. H3K4me3 did not exhibit change between time

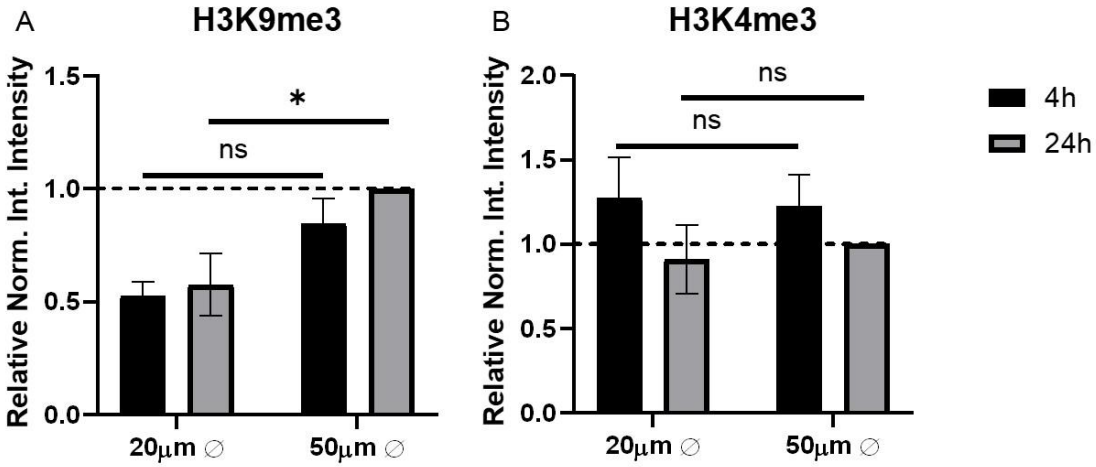

Figure 3.5. *Normalised integrated intensity measurements of confocal images of H3K9me3 (A) and H3K4Ac (B) markers. Shown as mean + S.E.M. N= 3 experiments. n.s: non-significant. *: p-value<0.05. (2-Way ANOVA, Tukey multiple comparisons test).*

points for either island size, albeit a non-statistically significant decrease between 4h and 24h for 20 μm islands can be appreciated (figure 3.5.B). As previous markers did not show any change when discriminated by differentiation markers, we did not apply that analysis modality to the available datasets.

Total Histone 3

In addition to specific histone modifications, we also examined total histone 3 levels by immunofluorescence and confocal microscopy. Representative confocal images and bar graph of measured integrated intensities can be found in Figure 3.6.

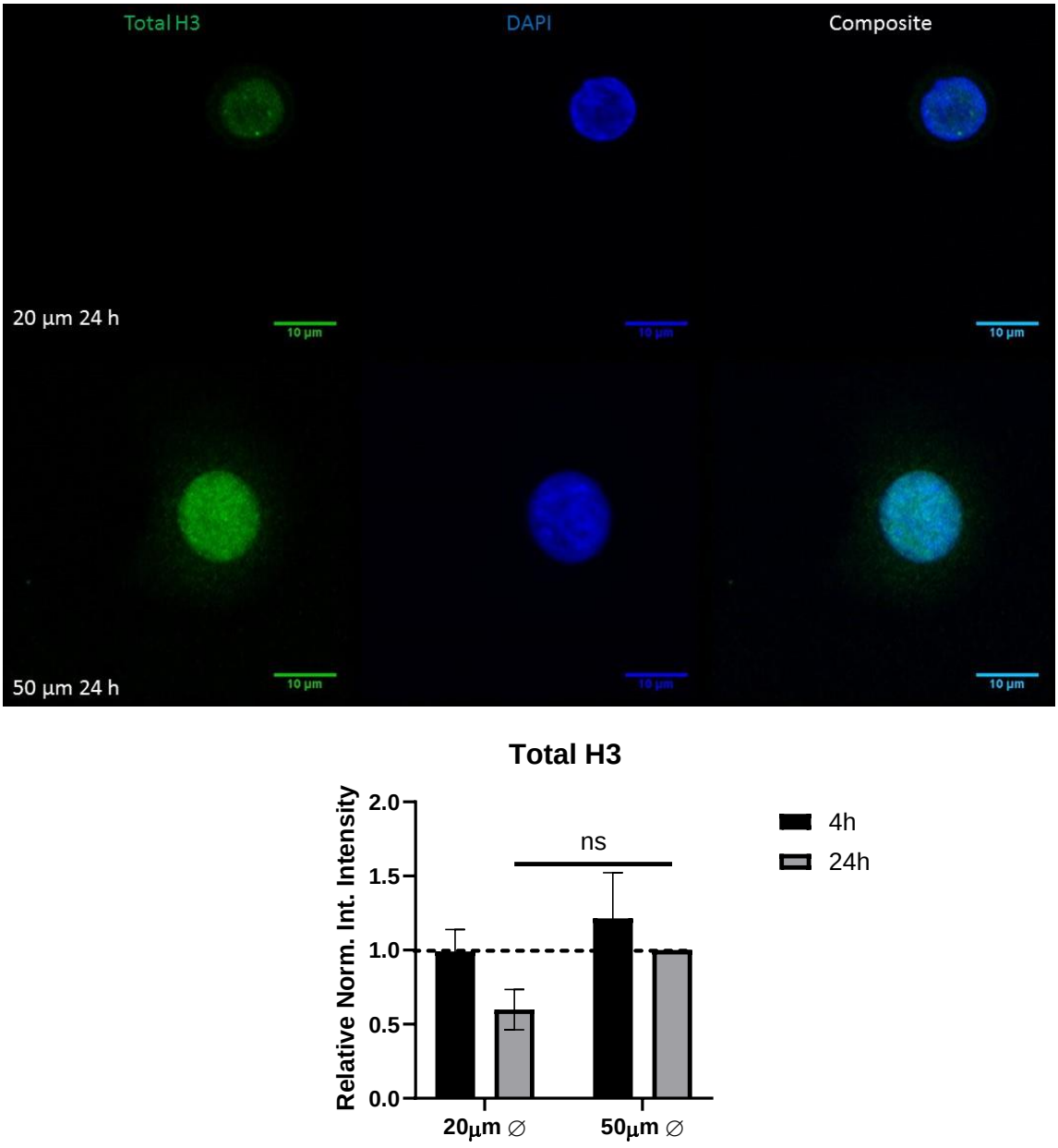

Figure 3.6. *Top: Example of cells grown on 20 µm and 50 µm islands at 24h time point, stained for Nucleus (DAPI) and Total Histone 3. Scale bar = 10 µm. Bottom: Normalised integrated intensity measurements of confocal images of total histone 3. Shown as mean + S.E.M. N = 3 experiments. n.s: non-significant. (2-Way ANOVA, Tukey multiple*

We found total histone 3 to be downregulated in 20 µm islands after 24 hours albeit not significantly. This observation suggests that previous changes in chromatin markers could be influenced by total histone 3 levels being reduced in smaller islands and thus PTM levels could be proportionally higher than measured by immunofluorescence imaging. We theorized the

reduction in total histone 3 levels to be an effect of reduced transcriptional activity of HKs growing on smaller islands, as lack of space may produce physical hindrance of the transcriptional machinery. But qPCR of H3 as well as several other housekeeping genes did not show significant changes across island size (Figure 3.7), hinting that the transcriptional machinery has similar activities.

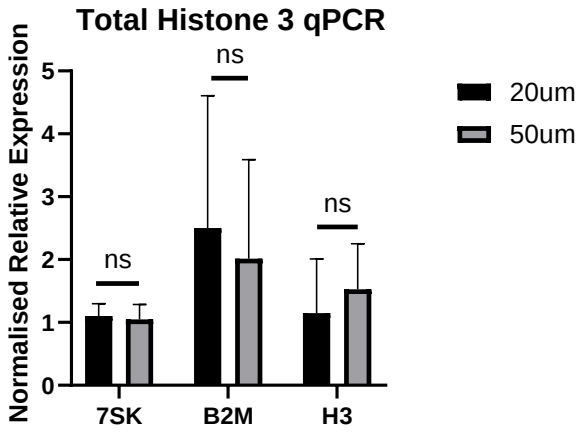

Figure 3.7. *Relative expression of 7SK lncRNA, β2-Microglobulin (B2M) and Histone 3 (H3) to GAPDH. N = 3 experiments, each done in duplicates. n.s: non-significant (two-tail t-test, unequal variance assumed).*

Visual observation of confocal images of chromatin markers also revealed bright fluorescence foci of both heterochromatin markers, which appeared larger and less numerous in small islands (Figure 3.8 Top), while euchromatin ones were more uniform and did not change much in appearance (Figure 3.8 Bottom). We investigated this response by using the InCell Developer image analysis software to quantify foci size and number of heterochromatin and euchromatin markers. Results are summarised in Figure 3.9.

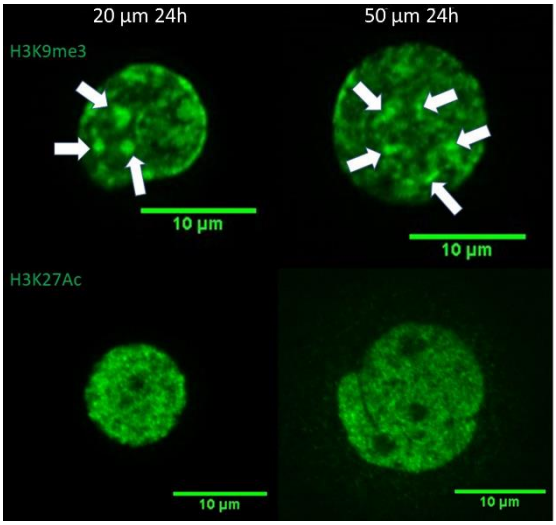

Figure 3.8. *Closeup of confocal images of heterochromatin marker H3K9me3 (top) and H3K27Ac (bottom). Arrows indicate local concentration of marker, or "foci". Heterochromatin markers exhibited larger and less numerous foci on smaller islands after 24h (top) while euchromatin markers seemed comparatively unperturbed (bottom).*

Indeed, foci of H3K27me3 and H3K9me3 showed a clear reduction in number on 20 µm versus 50 µm islands after 24h as well as an increment in size on smaller islands. These differences were stable between time points for H3K9me3, but not for H3K27me3: foci on 50 µm islands incremented in number and reduced in size between 4 and 24 hours, indicating that coalescence

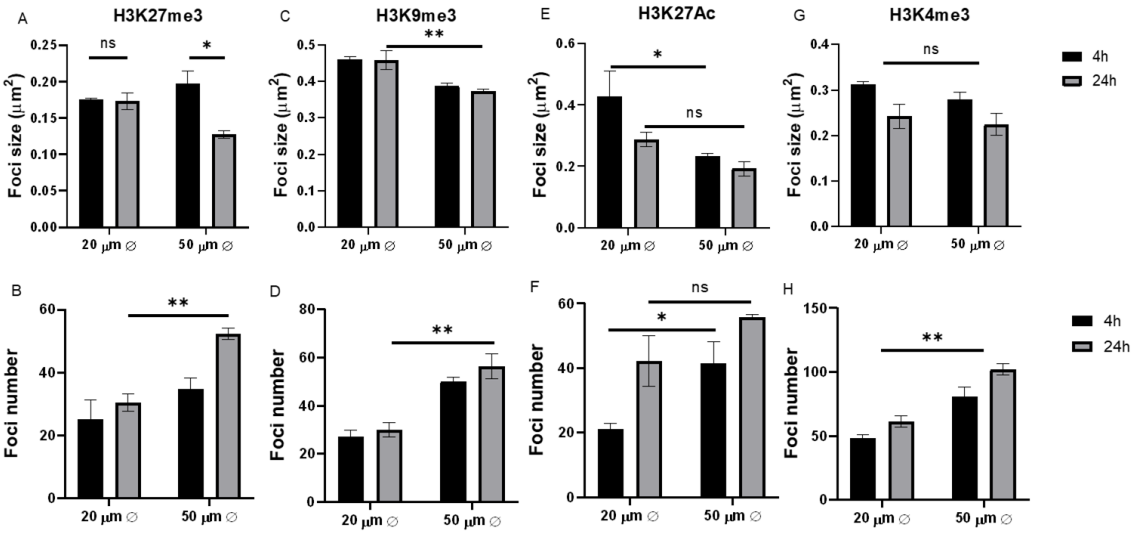

Figure 3.9. *Analysis of foci number and size of different chromatin markers. Shown as mean + S.E.M. N = 3 experiments. n.s: non-significant. *: p-value<0.05. **: p-value<0.01. (2-Way ANOVA, Tukey multiple comparisons test).*

of fluorescence foci might be an effect of cells with reduced adhesion, which is lost upon spreading.

Regarding open chromatin markers we observed a similar effect at 4-hour time point which is then lost. H3K27Ac fluorescence foci showed a significant difference in number between 20 µm and 50 µm islands at 4-hour time point but none at 24 hours. When comparing between time points, 20 µm islands displayed a lower amount of foci at the 4-hour time point. Foci on 20 µm islands after 4 hours also seem to be larger, but the difference was not statistically significant. 50 µm islands showed no difference in foci number between time points, but interestingly their size also seemed to decrease between 4h and 24h although the difference was also not significant. H3K4me3 foci showed a decrease in number in 20 µm versus 50 µm islands after 24h but no change in size. Over time both 20 µm and 50 µm islands foci became more numerous, albeit only significantly on large islands, and smaller in size but not significantly. These experiments indicate that limited adhesion causes heterochromatin marks to associate into fewer and larger foci while euchromatin foci are less affected.

Dynamic radial redisposition of chromatin markers

We next asked if the radial disposition of the chromatin markers was influenced by nuclear size. Closed chromatin markers usually associate more with the nuclear lamina where active gene silencing takes place, while open chromatin markers are found more towards the nuclear interior where transcription usually occurs. We used a radial distribution feature of the CellProfiler suite to measure fractional mean intensity, i.e the mean fluorescence of a radial region compared to the mean fluorescence of the whole nucleus. Values over 1 indicate a higher than average fluorescence intensity and vice versa. Results are summarized in figure 4.9. A striking feature of all chromatin markers at 24 hours is the similar distribution regardless of island size (Figures 3.10 A-D) with minor concentration towards the nuclear periphery. When considering their initial state at the 4h time point, we observe a noisier distribution, particularly for 20 µm islands (Figures 3.10 A-D). This finding suggests that over time markers reset to a stable radial distribution that is not dependent on nuclear volume.

Of all chromatin markers H3K9me3 showed the most interesting behaviour: a localised peak towards the nuclear lamina at 0.9-0.95 normalized distance from center for 20 µm and 50 µm islands at 24h, albeit a more pronounced one on 20µm islands. H3K9me3 showed a higher than average fluorescence towards the nuclear center for 50 µm islands at both time points while distribution remained flat for 20µm islands at 24h. A striking feature of the 4h curve for 20µm

islands is the oversized peak towards the nuclear lamina. Considering recent reports on the mechanoresponsive properties of H3K9me3[383], this could indicate an early response to reduction of nuclear volume which is later on dispersed.

From these findings we conclude that cell shape does not appear have a major impact on the radial distribution of histone PTMs within the nucleus after 24 hours.

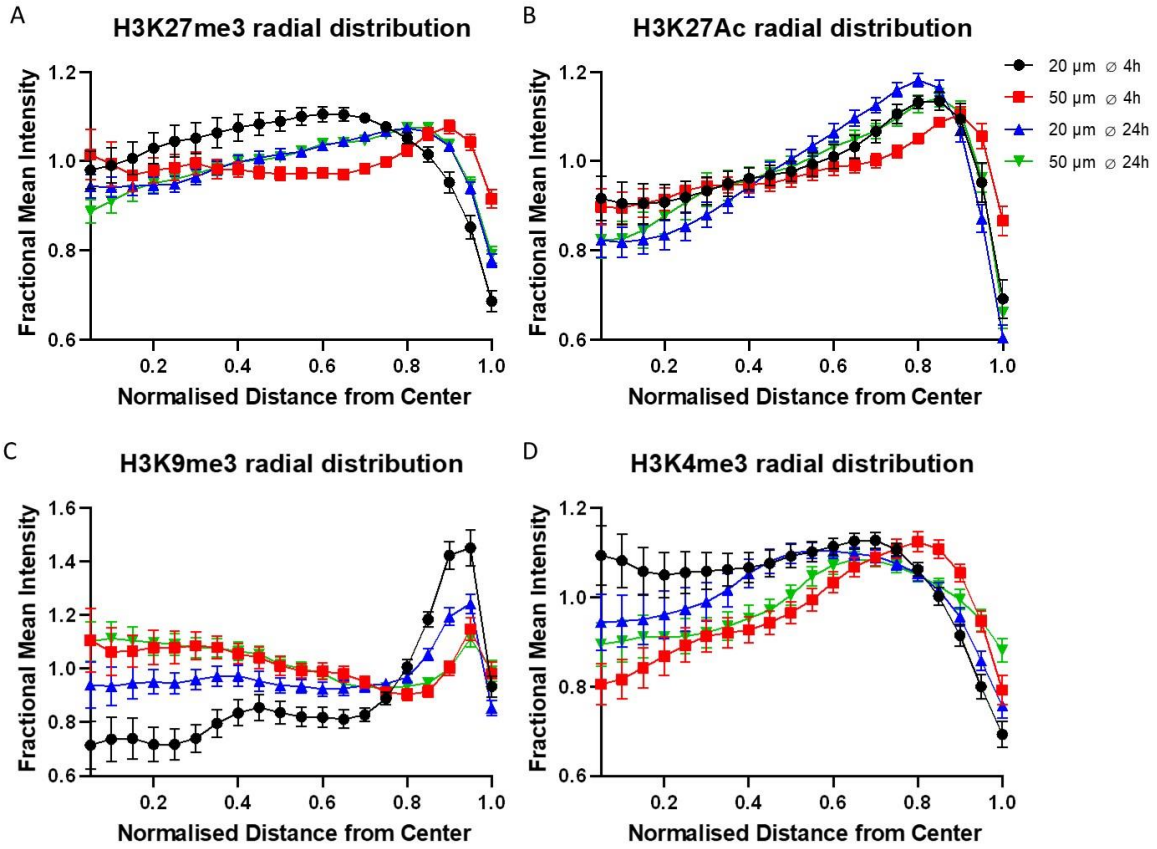

Figure 3.10. *Radial distribution of chromatin markers plotted as radial mean fractional intensity: values over 1 indicate a higher than average fluorescence intensity and vice versa.* ***A****. H3K27me3.* ***B****. H3K27Ac.* ***C****. H3K9me3* ***D****. H3K4me3. Shown as average + S.E.M. N = 3 experiments.*

Lamin levels and radial distribution

Following our characterization of chromatin markers, we investigated nucloskeletal proteins Lamin A/C and B1. Lamin A/C has been shown to be a major regulator of nuclear stiffness and associates with LADs. Inversely, Lamin B1 contributes significantly less to nuclear mechanic integrity but associates with TADs of euchromatin. We initially measured integrated intensity from immunofluorescence stainings of both lamins imaged with confocal microscopy. Example of confocal images can be found in figure 3.11 and quantification of measured integrated intensities can be found in Figure 3.12. Total levels of Lamin A/C showed no significant difference between island size and timepoints (Figure 4.12.A-B). Lamin B1 did exhibit a difference between island size as indicated by 2-way ANOVA, but not between time points.

Analysis of the Lamin A/C radial distribution showed a major redisposition towards the nuclear periphery on 20 µm islands after 24 hours, compared to a lesser redistribution also towards the

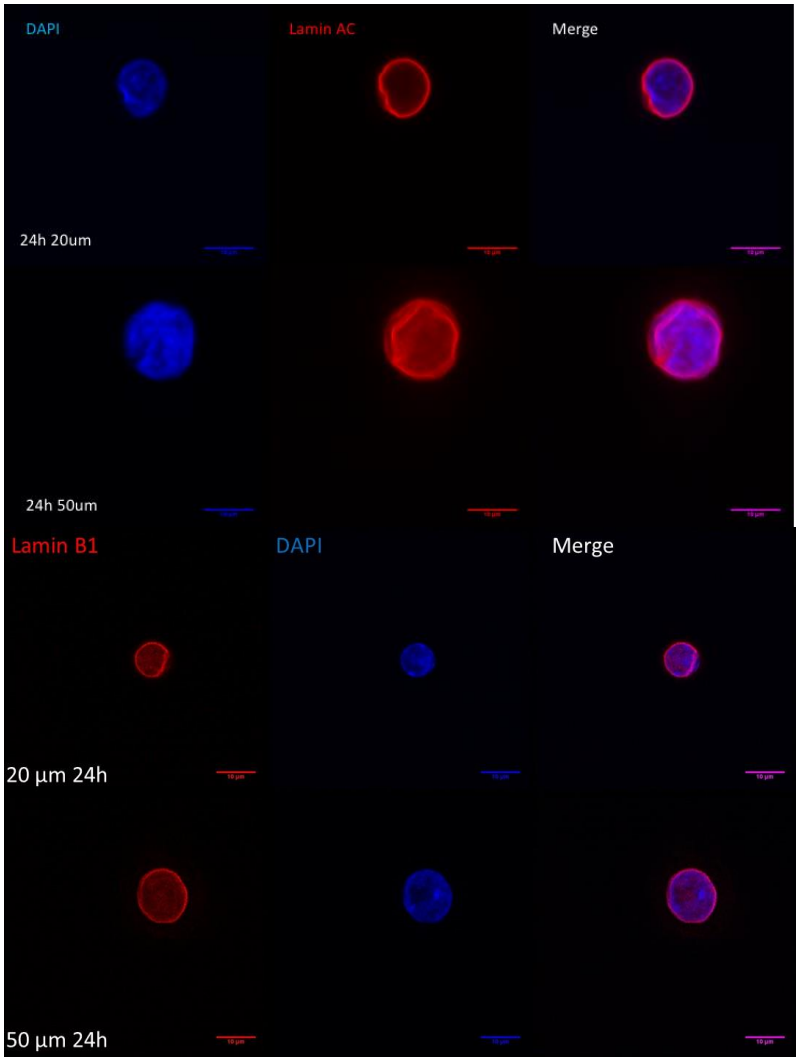

Figure 3.11. *Example of cells grown on 20 µm and 50 µm islands at 24-hour time point, stained for Nucleus (DAPI) and Lamin AC (Top) or Lamin B1 (Bottom). Scale bar = 10 µm.*

nuclear lamina on 50 µm islands (figure 3.13.B). This change is dynamic, as differences are less striking at the 4h time point, although we can already discern an increment in mean fractional intensity towards the nuclear periphery on 20 µm islands (figure 3.13.B). While Lamin B1 also

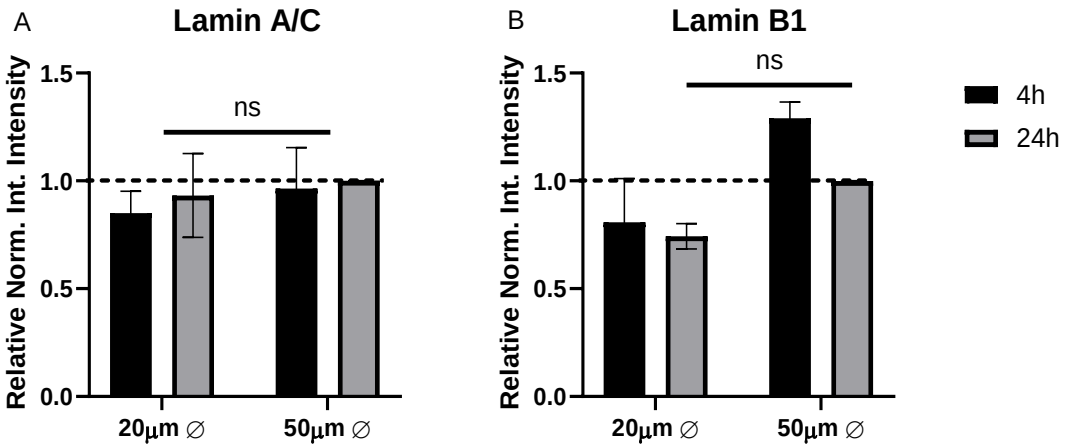

*Figure 3.12. Normalised integrated intensity measurements of confocal images of Lamin AC (**A**) and Lamin B1 (**B**). Shown as mean + S.E.M. N= 3 experiments. n.s: non-significant. *: p-value<0.05 (2-Way ANOVA, Tukey multiple comparisons test).*

displayed a clear localization towards the nuclear periphery, this was a common feature regardless of island size or time point. Considering the role of both lamins in nuclear architecture these data indicate that Lamin B1 does not reorganize dynamically following physical confinement while Lamin A/C does.

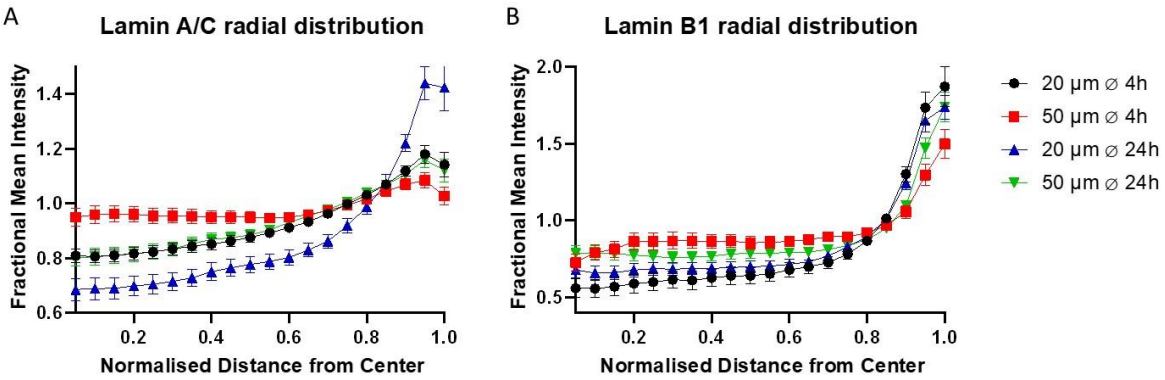

*Figure 3.13. Radial distribution of nucleoskeletal proteins plotted as radial mean fractional intensity: values over 1 indicate a higher than average fluorescence intensity and vice versa. **A**. Lamin AC. **B**. Lamin B1. Shown as average + S.E.M. N = 3 experiments.*

Nucleoli condensation

As nucleoli are large structures within the nucleus and have important roles in ribosomal biosynthesis and thus in transcriptional control, we next quantified the morphology of nucleoli. Example of confocal images can be found in figure 3.14 and measurements of nucleoli size and number can be found on table 3.2, a bar graph representation of both number and relative size of nucleoli on figure 3.15.

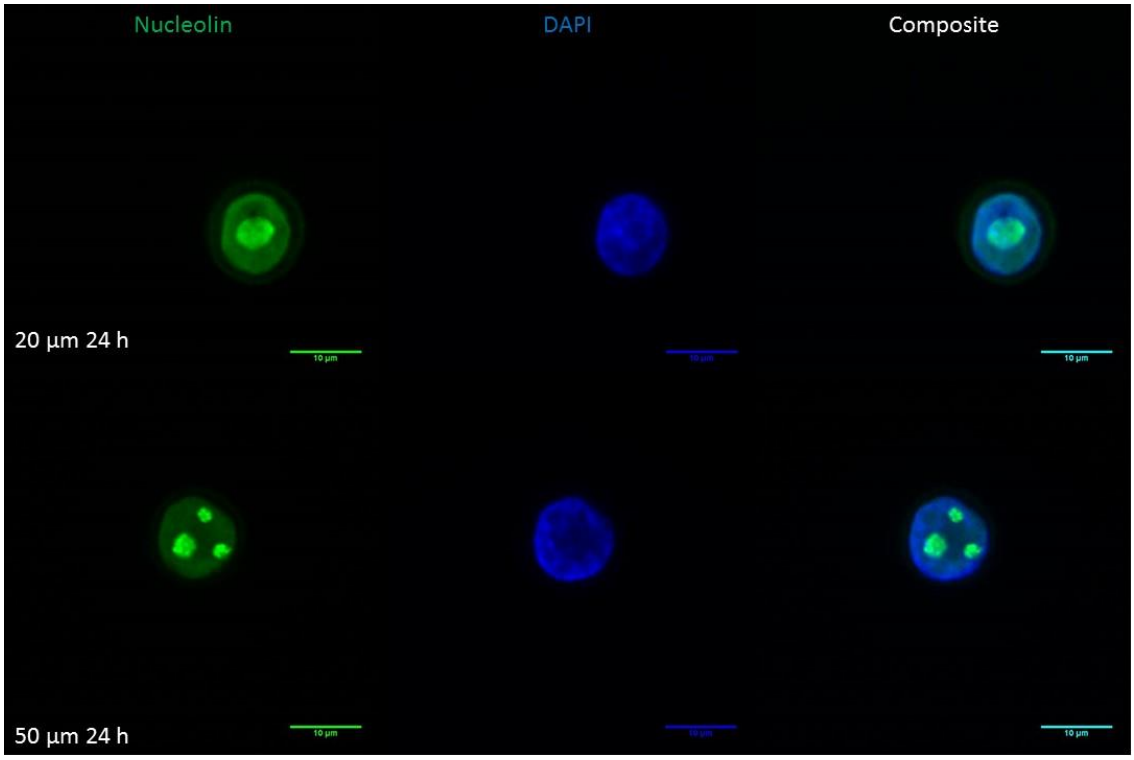

Figure 3.14. *Example of cells grown on 20 µm and 50 µm islands at 24-hour time point, stained for Nucleus (DAPI), Nucleolin and Transglutaminase. Scale bar = 10 µm.*

Nearly all cells grown on 20 µm islands had a single, large nucleolus compared to cells from 50 µm islands, which usually had between 1 and 3 nucleoli of varying sizes (Table 3.2, Figure 3.15). As the nuclear volume of restricted cells is reduced, the relative size to the nucleus of nucleoli is thus increased in 20 µm islands. This difference between relative area to the nuclear area is significant between nucleoli of 20 µm and 50 µm islands at 4 and 24 hours (Figure 3.15.B). There is a significant reduction in nucleoli number between 20 µm and 50 µm islands at 24-hour time point (Figure 3.15.A) but also between 4 and 24-hour time points in 20 µm islands (Figure 3.15.B) indicating a fusing in between those time points. Aspect ratio of nucleoli is reduced in both 20 µm and 50 µm islands between 4h and 24h (Table 3.2).

	20 µm - 4h	20 µm - 24h	50 µm - 4h	50 µm - 24h
n° of nucleoli per nucleus	1.46 ± 0.76	1.09 ± 0.33	1.89 ±1.05	1.69 ± 0.99
Area of Nucleoli (μm^2)	11.24 ± 8.22	12.21 ± 6.72	11.90 ± 9.45	11.67 ± 7.97
Area of Nucleus (μm^2)	85.66 ± 18.11	86.22 ± 16.52	149.43 ± 35.15	143.39 ± 35.15
Relative size to Nucleus (%)	13.85 ± 8.72	17.35 ± 8.81	8.99 ± 6.73	8.67 ± 6.57
Aspect Ratio	1.45 ± 0.39	1.24 ± 0.25	1.47 ± 0.49	1.33 ± 0.27

Table 3.2. *Morphological statistics derived from nucleolin and DAPI stainings. N = 3 experiments. Shown as mean ± SEM.*

As nucleoli size and shape is thought to be regulated by phase separation dynamics we theorized that the overall reduction in nuclear volume forces nucleoli to fuse together We transfected HaCat cells with a Nucleolin-GFP construct and performed live imaging at early time points post seeding to observe nucleoli fusion. An example of the phenomenon can be seen in Figure 3.16.A and a quantification of measured fusion events in Figure 3.16.B-C. To further demonstrate the universality of this mechanism we seeded other cell lines on the same micropatterned surfaces and observed a similar trend across all of them (Figure 3.17).

Finally, we noted a lack of nucleolin staining in the interior of nucleoli on 20 µm islands, unlike fully stained nucleoli on 50 µm islands, suggesting that sub-nucleolar structure may also be altered.

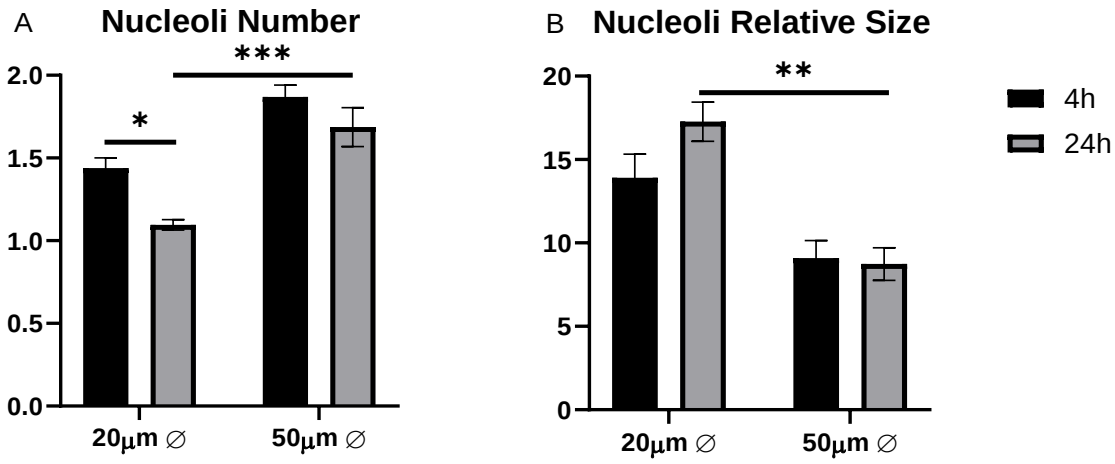

Figure 3.15*. Nucleoli number (A) and relative size (B). Shown as mean + S.E.M. N = 3 experiments *: p-value<0.05. **: p-value<0.01. ***: p-value<0.001 (2-Way ANOVA, Tukey multiple comparisons test).*

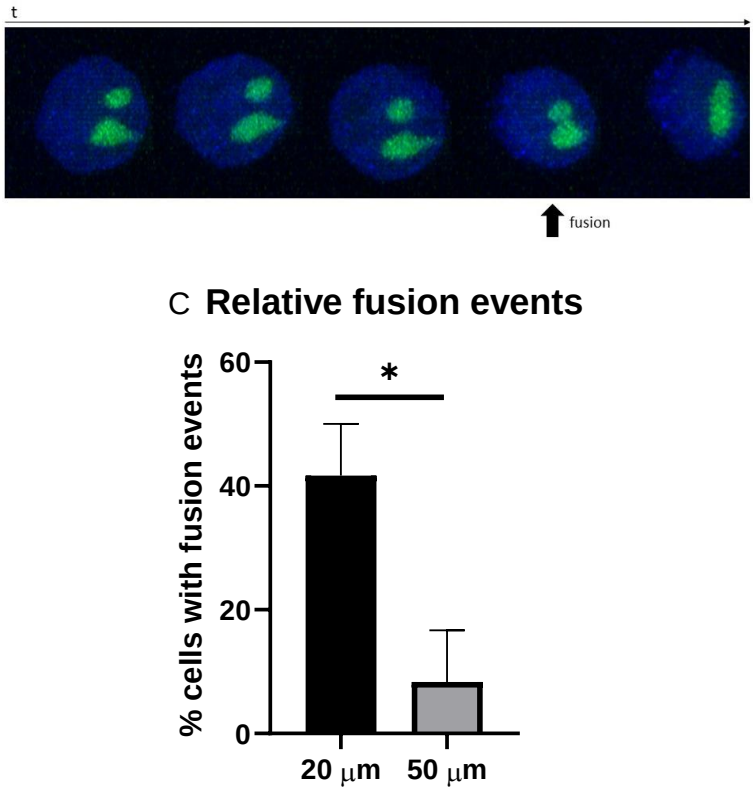

Figure 3.16. *Top: Representative images of nucleoli fusing in HaCat cells transfected with Nucleolin-GFP construct seeded on 20 μm islands. Bottom: % of cells with observed fusion events. Shown as mean + S.E.M. N = 3 experiments, 4 cells imaged per island size per experiment. *: p-value<0.05 (two-tail t-test, equal variance assumed).*

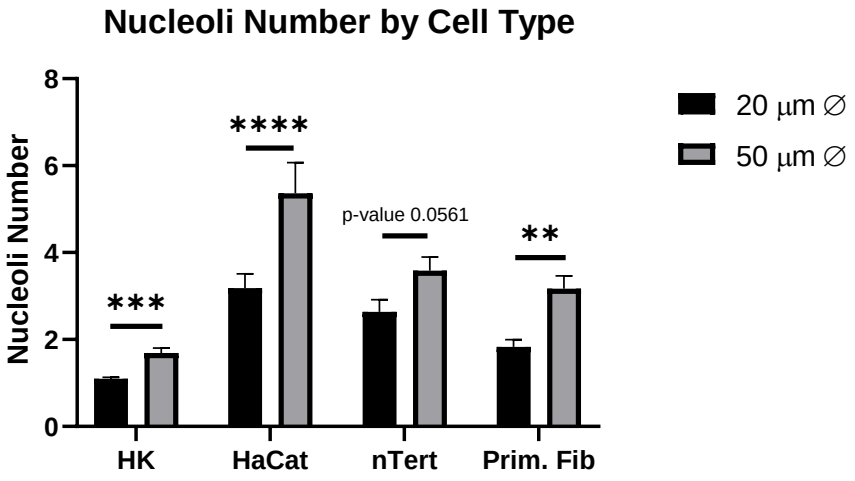

Figure 3.17. *Nucleoli number of diverse cell types grown on micropatterned surfaces. Shown as mean + S.E.M. N = 3 experiments. n.s: non-significant. **: p-value<0.01. ***: p-value<0.001. ****: p-value<0.0001 (2-Way ANOVA, Tukey multiple comparisons test).*

Discussion

Here, we have made a first step towards understanding how reduction of nuclear volume as generated through constraining of HKs can create changes in chromatin remodelling and architecture. For this, we characterized several key components of nuclear architecture, such as heterochromatin and euchromatin markers, nucleoskeletal proteins as well as nucleoli. We have described several dynamic changes to these components following cellular confinement, and we aim to investigate the mechanisms of these changes in following chapters to better elucidate the intricate relationship between biophysical cues, nuclear architecture and HK biology.

We have observed minute changes in overall heterochromatin markers, with both H3K27me3 and H3K9me3 being downregulated on restricted cells. A similar trend is appreciated for euchromatin marker H3K27Ac, but no apparent change in H3K4me3 marker was found. Global changes in histone acetylation have already been reported during keratinocyte differentiation, specifically H4K20Ac[384], but here we saw no differences between non-differentiated and terminally differentiating cells. While H3K27me3 showed a downregulation on small islands, discrimination upon differentiation also showed no differences, further pointing that changes (or lack thereof) are not necessarily differentiation related. However, the lack of correlation between histone PTMs and differentiation here may also be due to a mismatch or delay in the timing of expression for differentiation markers such as TG. Future studies will have to analyse a broader spectrum of chromatin markers and timings to get a more precise picture of the possibly complex dynamic chromatin changes that arise from modifying available adhesive space of HKs. Moreover, considering that changes in histone PTMs are often gene-specific, other techniques, mainly ChIPseq, would provide information that would be more relevant.

Interestingly, total histone 3 showed a non-significant downregulation on small islands, putting a certain doubt on the specificity of histone PTM changes. This downregulation is non-significant compared to the changes in PTMs, albeit this may be due perhaps to a low N number. Changes in overall H3 may also not necessarily impact the chromatin markers that were studied. Indeed, they might indicate a reduction in free floating H3 or perhaps do not incorporate the PTMs studied. Dual staining of both total histone 3 and chromatin markers would be able to give us a definite ratio to which re-evaluate the data.

Nevertheless, analysis of global changes in histone PTMs is a very limited tool as we know that most of these PTMs are gene and context specific. RNAseq data of constrained or non-constrained HKs will provide more gene-specific information, and CHIP-seq analysis in future studies would provide a more detailed information on gene-specific regulation.

Foci analysis as well as radial profile of these markers provided further geometrical information. We observed a significant heterochromatin foci association, and a similar but less pronounced effect on euchromatin foci distribution. In contrast, the radial distribution of PTMs was not affected by nuclear shape. In Chapter Six, perturbation of the system with cytoskeletal inhibitors will be used to investigate whether these effects are purely biophysical responses or consequences of other signalling pathways.

We theorize that the phenomenon of both euchromatin and heterochromatin downregulation and foci aggregation is an attempt by the nucleus to both reduce chromatin volume and save space in a smaller nucleus, while maintaining essential gene transcription relatively unperturbed. Indeed, compaction of chromatin could potentially create kinks and breaks in DNA, and recent studies have shown that reduction of dense chromatin can effectively protect DNA from mechanical loading of the nucleus[383]. Counterintuitively, heterochromatin foci compaction would theoretically increment chromatin viscosity[385], but perhaps this phenomenon is better explained by the reduced intranuclear volume. Cell survival is directly dependent on maintaining transcriptional activity stable, and physical hindrance of transcriptional machinery accessibility to chromatin because of compaction would effectively perturb the system. Hence, reducing closed chromatin and compacting the remaining could effectively both increment chromatin deformability and optimize storage, leaving more space for open chromatin to be transcribed without hindrance.

Further proof of this is needed, such as rheological analysis of the compacted nucleus, counter-staining of RNA polymerases to analyse the distribution of transcriptional factories or de novo RNA and protein synthesis measurements to verify if transcriptional levels are hindered. One hint at this is the reduced levels of total histone 3. As of now we see little biological sense for the cell to effectively reduce its levels of a core nucleosome protein, as it will further hinder DNA storage. There has been reports of histone levels being downregulated after DNA damage[386], but it seems unlikely here. Rather, we believe this to be a consequence of a defect in translation. Further to this point, nucleoli aggregation and condensation could also affect ribosomal biogenesis. qPCR analysis of H3, several housekeeping genes as well as rRNA did not show any major changes, but this could be an artefact of transcriptional levels being downregulated similarly for all genes. We will investigate this further by using de novo protein synthesis assays in the next chapter.

Nucleoskeletal proteins showed a dual response, Lamin A/C exhibiting redistribution to the nuclear periphery on small islands, but no change in expression, while lamin B1 the exact opposite (no redisposition but changes in overall levels). This provides an interesting system to further probe how biophysical cues could modify either position or expression of proteins. The

functional role of Lamin A/C in chromatin remodelling and gene expression will be investigated in Chapter 5.

Finally, nucleoli condensation following nuclear compaction is a novel phenomenon which we report here for the first time. While nucleoli fusing together due to proximity is not a novel concept, almost nothing is known of nucleoli reacting to biophysical cues. Reports indicate possible interactions with Lamin B1[330], H3K9me3[387] and nuclear actin[388], and which will be prime candidates to be analysed with our model. New insights here have the potential to expand our knowledge of their regulation which is intrinsically linked to ribosomal biogenesis and global protein synthesis.

In summary, we have described the initial parameters of our model and gained primary information on chromatin condensation processes due to nuclear compaction (Figure 3.17). These initial observations will serve as a starting point to interrogate the mechanical regulation of these responses and the downstream effects on gene expression.

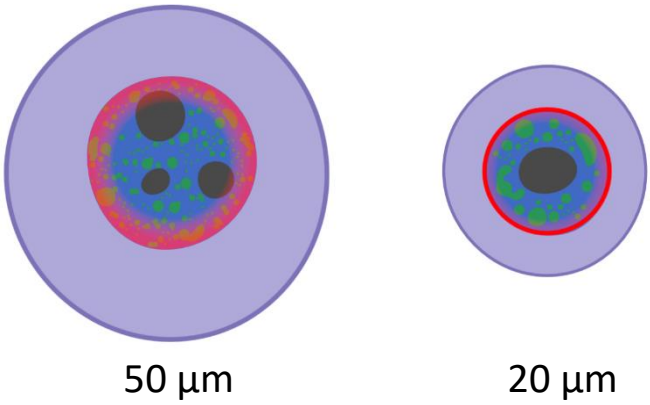

Figure 3.17. *Schematic representation of chromatin condensation. Left: HKs grown on 50 µm islands. Right: HKs grown on 20 µm islands. Blue: DAPI. Red: Lamin A/C. Green: Heterochromatin. Purple: cytoplasm.*

Chapter 4: Analysis of Gene Expression Programmes Regulated by Cell Morphology

Introduction

In the previous chapter we reported observed global chromatin structural changes in HKs following nuclear deformation. Changes in chromatin organization are often accompanied with changes in downstream transcriptional activity, and both phenomena occur in differentiating HKs. Indeed, gene clustering by function, such as seen in the EDC, will see a change in their position within the nucleus and a change in their chromatin state during differentiation[208], which will eventually lead up to activation of transcription of the whole cluster. Genes can also be affected by biophysical cues while not necessarily exhibiting perceptible changes in macroscopic chromatin structure and observed chromatin structural changes do not tell us how individual gene transcription is affected. Therefore, more gene specific information is needed to fully assess the impact of altered nuclear morphology on epigenetic gene regulation.

We expect that cell and nuclear morphology significantly affect gene transcription. As stated previously HK compaction following reduced available adhesive area induces terminal differentiation which is accompanied by major changes in gene expression. Lamin A/C regulates LADs and its relocation towards the nuclear lamina could potentially change the transcription of nuclear lamina associated genes. Condensation of heterochromatin foci, and changes in euchromatin foci could also be indicative of modifications in accessibility of genes. Finally, merging of nucleoli likely would impact ribosomal RNA biogenesis and ribogenesis, which could ultimately affect whole cell translational capabilities.

In the following chapter we will use next-generation RNA sequencing (RNA-seq) to characterize the transcriptome of HKs grown on micropatterned surfaces and subsequently investigate how these changes affect key signalling pathways and phenotype.

Changes in transcriptional profile of HKs due to available adhesive space

Main Affected Pathways

Total RNA was extracted from HKs grown on 20 µm and 50 µm islands at 4h and 24h time points in biological triplicates. RNA was then sequenced using next generation sequencing (paired end, 75 bp read length, 30 M reads per sample). Reads were aligned to genome (Homo Sapiens GRCh37 assembly) using HISAT2 and differential analysis, PCA and hierarchical clustering of gene expression was performed using SeqMonk. Scatterplot of differentially expressed genes between 20 µm and 50 µm at 24 h time point is shown in Figure 4.1. We compared genes differentially expressed between island sizes at the early 4h time point and found only two, both more expressed on smaller islands. In comparison, similar statistical analysis revealed 1820

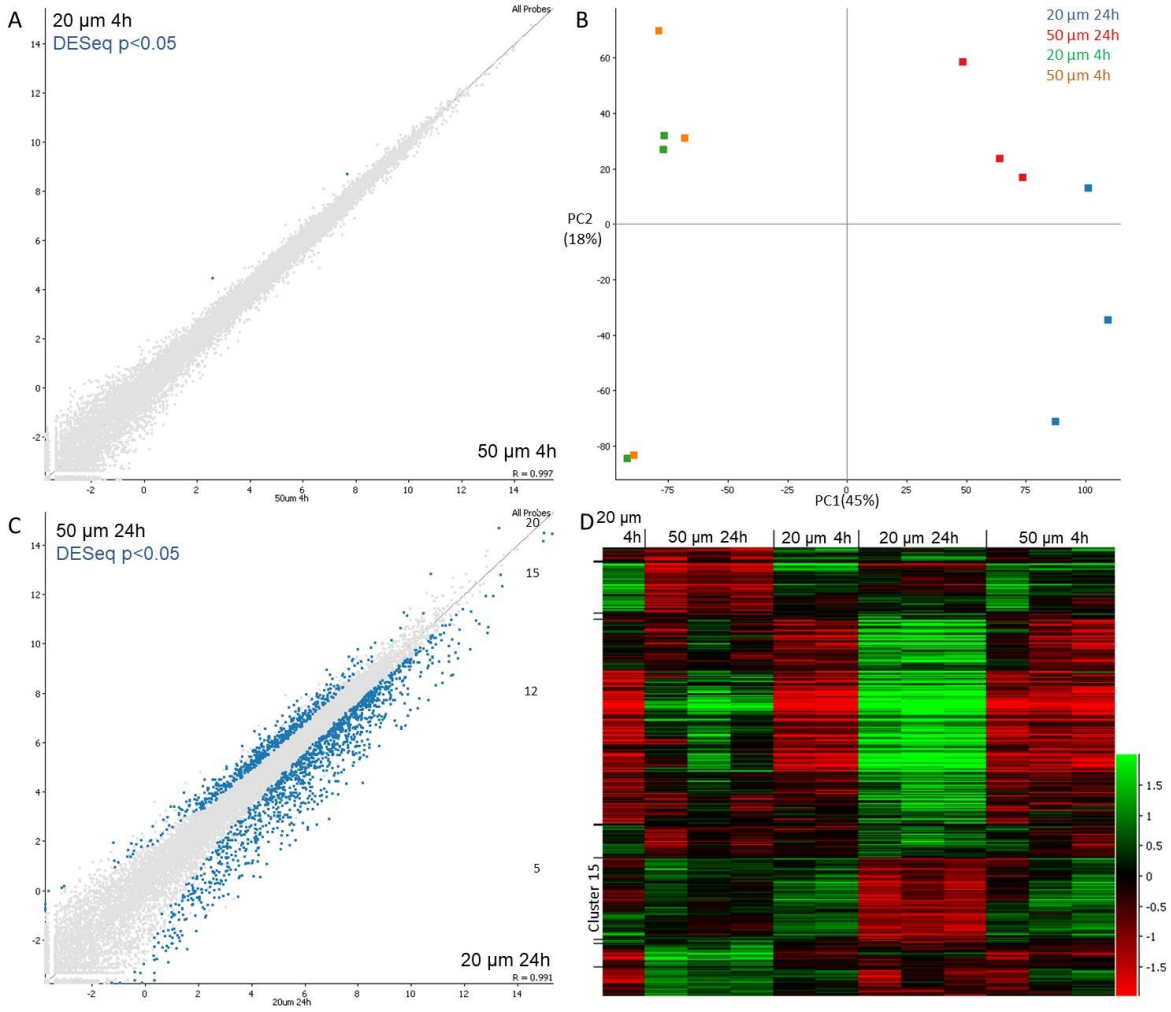

Figure 4.1. *Scatterplot of differentially expressed genes between 20 µm and 50 µm islands at 4-hour (**A**) and 24-hour (**C**) time points. Highlighted in blue are DESEQ significantly differentially expressed genes. **B**: PCA plot of highlighting PCA 1 versus PCA 2. Blue: 20 µm 24h. Red: 50 µm 24h. Green: 20 µm 4h. Orange: 50 µm 4h. **D**: Unsupervised hierarchical clustering plot of all samples with highlighted clusters of interest. **Next page**: three most enriched GO terms of non-clustered data and 4 largest hierarchical clusters.*

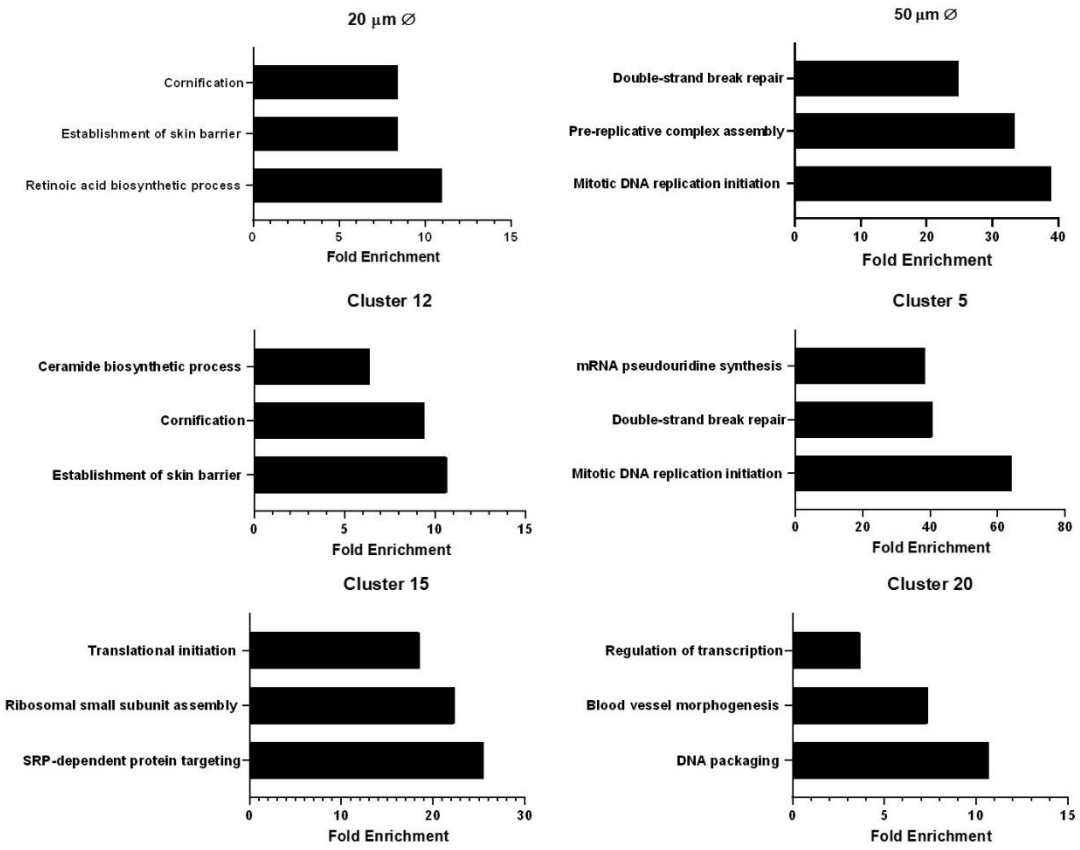

genes to be differentially transcribed between island sizes at 24h time point. A majority of these (1261) were upregulated on 20 μm islands.

Principal component analysis (PCA) of all samples revealed first component to be time as it separated samples based on time point. Second component separated 24-hour samples by island size while being less effective for 4-hour samples. The PCA clustering plot is shown on Figure 4.1. The results suggest that HKs grown on micropatterns are initially a homogenous population when seeded and then separate into different transcriptional programs based on available adhesive area. We then performed unsupervised hierarchical clustering of differentially expressed genes at 24-hour timepoint which revealed 20 clusters of similarly varying transcript levels. Heat map of clusters can be found in Figure 4.1. As can be perceived visually, hierarchical clustering correctly categorised samples based both time and island size. Subsequently the largest clusters (10 or more genes) were analysed using the Gene Ontology (GO) resource (http://geneontology.org/). Cluster 12 was the largest (831 genes) and only upregulated in small islands at 24 h. Most enriched GO terms within that cluster were cornification and establishment of skin barrier. Cluster 5 was the second largest (332 genes) and only upregulated in large islands. One of the most enriched GO terms was found to be DNA replication, indicative of basal keratinocytes. These patterns of gene expression confirm that this model effectively induces HK terminal differentiation on smaller islands and validate the RNA-seq analysis.

There appeared to be a small but measurable amount of differentiation even on the large islands, as we observe that 28 genes linked to cornification are upregulated on large islands at 24h time point compared to 4h. However, when looking at small islands we find 55 genes to be upregulated in this category, which indicates that HKs grown on small islands are differentiating to a greater extent. In parallel, 8 genes linked to hemidesmosome formation and 11 to basement membrane organisation are upregulated on large islands after 24h compared to 4h, suggesting that this population is also attempting to form stable basal-like adhesions. Small islands in comparison do not show an upregulation in genes that are linked to basement membrane attachment, and furthermore exhibit a downregulation of DNA replication genes, which are good indicators of a differentiating population.

We then interrogated which other pathways were being affected. GO analysis of clustered and non-clustered data revealed a plethora of affected pathways (over 100 for both clustered and non-clustered, often overlapping in nature) but we focused our subsequent investigation on the following three. The first one was the DNA double strand break repair pathway, third and second most upregulated GO term on non-clustered and clustered data, respectively. It was selected because there has been mounting support for mechanosensitive roles of lamin A/C in DNA repair mechanisms in the past years[389] as well as recent reports indicating that reduction of heterochromatin following mechanical stimuli was an effective DNA-protecting phenomenon[383]. Retinoic acid (RA) biosynthesis was the most enriched GO term of 20 µm island non-clustered data. It is of interest as RA has been found to be implicated in lamin A/C regulation[390]. Finally, ribogenesis was chosen as analysis of cluster 15, third largest cluster and upregulated in small islands, found ribosomal small subunit assembly and initiation of translation the second and third most enriched GO terms. Cluster 5 also found ribogenesis to be an enriched GO term. This could be intrinsically connected to nucleoli fusion, as ribogenesis is housed within the nucleolus,

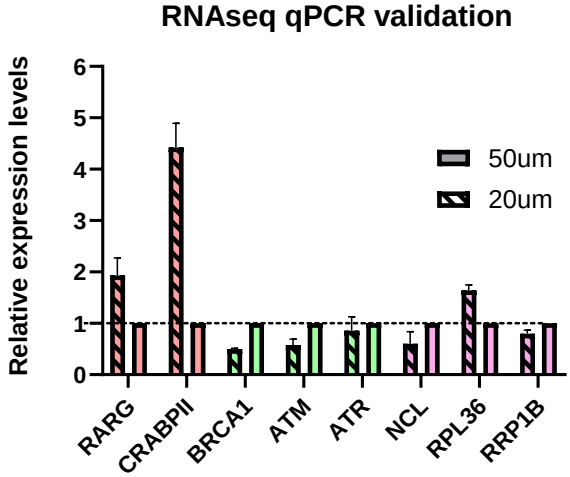

Figure 4.2. *Relative expression levels of genes on 20 µm islands compared to 50 µm islands after 24 hours from qPCR. All genes normalised to GAPDH transcript levels. Shown as mean + S.E.D. N = 3 experiments.*

while interestingly the pathway seemed to be upregulated in both large and small islands. As a final validation of our RNA-seq analysis we selected a few genes from each pathway to measure RNA transcripts by qPCR in independent follow-up experiments. The list of differentially expressed genes in selected pathways can be found in table 4.1 and qPCR results found on figure 4.2.

Pathway	Genes	Log2 Fold Change
Retinoic Acid pathway	**Retinoic Acid Receptor Gamma (RARG)**	-1.684
	Cellular retinoic acid-binding protein 2 (CRABP2)	-1.787
	Dehydrogenase/reductase SDR family member 9 (DHRS9)	-2.868
	Retinol-binding protein 1 (RBP1)	-1.41
	Aldehyde dehydrogenase family 1 member A3 (ALDH1A3)	-1.765
	Retinal dehydrogenase 2 (ALDH1A2)	-1.495
	Aldehyde Dehydrogenase 3 Family Member B1 (ALDH3B1)	-3.148
	Cytochrome P450 Family 1 Subfamily B Member 1 (CYP1B1)	-1.657
	Cytochrome P450 Family 2 Subfamily W Member 1 (CYP2W1)	-3.167
DNA damage response	Flap endonuclease GEN homolog 1 (GEN1)	1.012
	Telomere-associated protein (RIF1)	0.918
	DNA replication licensing factor (MCM6)	0.877
	Breast cancer type 1 susceptibility protein (BRCA1)	1.315
	Breast cancer type 2 susceptibility protein (BRCA2)	1.533
	DNA replication licensing factor (MCM4)	0.897
	Fanconi anemia group J protein (BRIP1)	1.001
	Fanconi anemia group B protein (FANCB)	1.337
	Structural maintenance of chromosomes flexible hinge domain-containing protein 1 (SMCHD1)	0.866
	Poly [ADP-ribose] polymerase 1 (PARP1)	0.984
	DNA replication licensing factor (MCM5)	0.72
	DNA mismatch repair protein (MSH2)	0.688
	Bloom syndrome protein (BLM)	1.134
	DNA repair protein (XRCC2)	1.628
	Protein MMS22-like (MMS22L)	0.892
	Sororin (CDCA5)	0.784
	Claspin (CLSPN)	1.72
	Cell division control protein 45 homolog (CDC45)	0.78
	DNA repair protein RAD51 homolog 1 (RAD51)	0.812
	N-acetyltransferase ESCO2 (ESCO2)	0.952
	DNA polymerase theta (POLQ)	1.344
	DNA repair protein RAD50 (RAD50)	0.931
	DNA replication ATP-dependent helicase/nuclease DNA2 (DNA2)	1.131
	DNA-dependent protein kinase catalytic subunit (PRKDC)	0.941
	Serine-protein kinase ATM (ATM)	1.232
	Serine/threonine-protein kinase ATR (ATR)	0.862
	DNA repair and recombination protein RAD54-like (RAD54L)	0.981
	DNA replication licensing factor MCM3 (MCM3)	1.053
	Flap endonuclease 1 (FEN1)	0.687
	DNA replication licensing factor MCM7 (MCM7)	0.648
	DNA replication licensing factor MCM2 (MCM2)	0.712

	Poly [ADP-ribose] polymerase 2 (PARP2)	1.052
	DNA polymerase alpha catalytic subunit (POLA1)	0.825
	Chromatin assembly factor 1 subunit A (CHAF1A)	1.035
	Denticleless protein homolog (DTL)	1.331
	ATP-dependent DNA helicase DDX11 (DDX11)	0.901
	E3 ubiquitin-protein ligase UHRF1 (UHRF1)	1.238
Ribogenesis	Ribosomal Protein S2 (RPS2)	-0.732
	Ribosomal Protein S4X (RPS4X)	-0.672
	Ribosomal Protein S5 (RPS5)	-0.899
	Ribosomal Protein S9 (RPS9)	-0.829
	Ribosomal Protein S10 (RPS10)	-0.85
	Ribosomal Protein S12 (RPS12)	-0.882
	Ribosomal Protein S27 (RPS27)	-1.013
	Ribosomal Protein S28 (RPS28)	-0.713
	Ribosomal Protein S29 (RPS29)	-1.249
	Ribosomal Protein L13 (RPL13)	-0.685
	Ribosomal Protein L29 (RPL29)	-0.652
	Ribosomal Protein L32 (RPL32)	-0.708
	Ribosomal Protein L36 (RPL36)	-0.941
	Ribosomal Protein L37 (RPL37)	-0.786
	Ribosomal Protein L39 (RPL39)	-1.198
	Ribosomal Protein L41 (RPL41)	-0.882
	Ribosomal Protein LP0 (RPLP0)	-0.788
	Ribosomal Protein LP2 (RPLP2)	-0.706
	Ribosomal Protein L28 (RPL28)	-0.664
	Nucleolin (NCL)	0.856
	Nucleolar Protein 8 (NOL8)	1.131
	RNA Binding Motif Protein 19 (RBM19)	0.791
	RNA Binding Motif Protein 28 (RBM28)	0.824
	Ribosome Biogenesis Factor BMS1 (BMS1)	0.792
	mRNA turnover protein 4 homolog (MRTO4)	0.665
	Nucleolar protein 14 (NOP14)	0.968
	Nucleolar protein 2 (NOP2)	0.756
	NOP2/Sun RNA Methyltransferase 2 (NSUN2)	0.633
	Nucleolar pre-ribosomal-associated protein 1 (URB1)	0.972
	Nucleolar pre-ribosomal-associated protein 2 (URB2)	0.78
	Nucleolar and coiled-body phosphoprotein 1 (NOLC1)	1.046
	Nucleolar MIF4G domain-containing protein 1 (NOM1)	1.143
	Ribosome biogenesis regulatory protein homolog (RRS1)	0.909
	Ribogenesis Regulating Protein 1 B (RRP1B)	0.613
	Ribosomal L1 domain-containing protein 1 (RSL1D1)	0.819
	Large subunit GTPase 1 homolog (LSG1)	0.704
	H/ACA ribonucleoprotein complex subunit DKC1 (DKC1)	0.763
	DEAD-Box Helicase 31 (DDX31)	1.019
	DEAD-Box Helicase 21 (DDX21)	0.75
	DEAD-Box Helicase 11 (DDX11)	0.901

Table 4.1. *Differentially expressed genes from HKs grown on 20 and 50 µm micropatterned islands after 24h belonging to selected pathways and respective fold changes of RNA expression in small islands compared to large islands. Highlighted selected genes for qPCR validation of RNA-seq analysis.*

DNA Double Strand Break Repair pathway

GO analysis of RNAseq revealed up to 50 gene transcripts that are upregulated in large islands to be implicated in DNA double strand break (DSB) repair as well as general DNA repair pathways. Interestingly, when comparing between time points on small islands, we can also observe up to 137 genes related do DNA repair being downregulated at 24-hour time point. In contrast, there is no such change between time points for 50 µm islands.

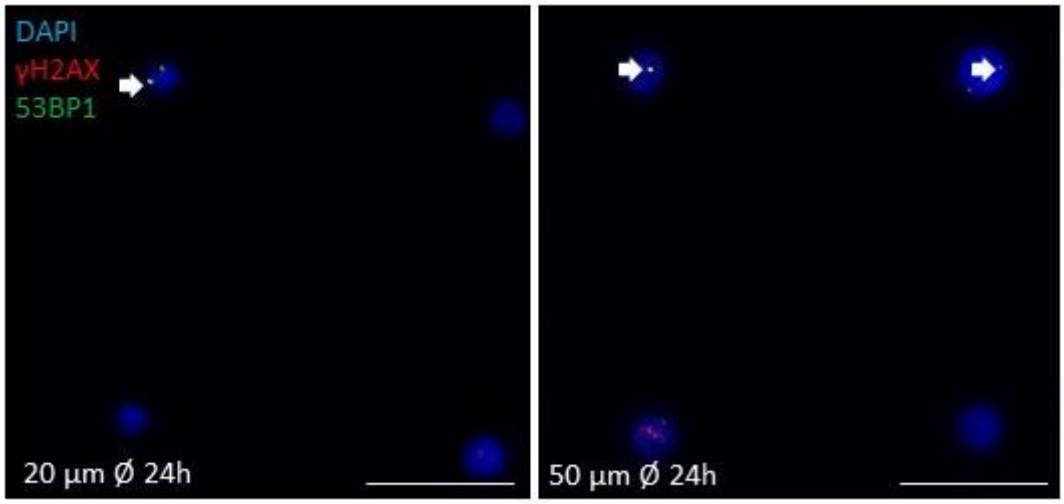

***Figure 4.3**. Example of epifluorescence imaging of HKs grown on 20 µm and 50 µm islands at 24h time point, stained for phosphorylated histone isoform γH2AX and 53BP1. Double foci indicative of active DNA DSB repair sites are highlighted. Scale bar = 20 µm.*

To determine associate functional changes in DNA damage repair we performed parallel immunofluorescence labelling of phosphorylated histone isoform γH2AX and TP53BP1 and imaged them using epifluorescence microscopy at 4h and 24h after seeding of HKs on

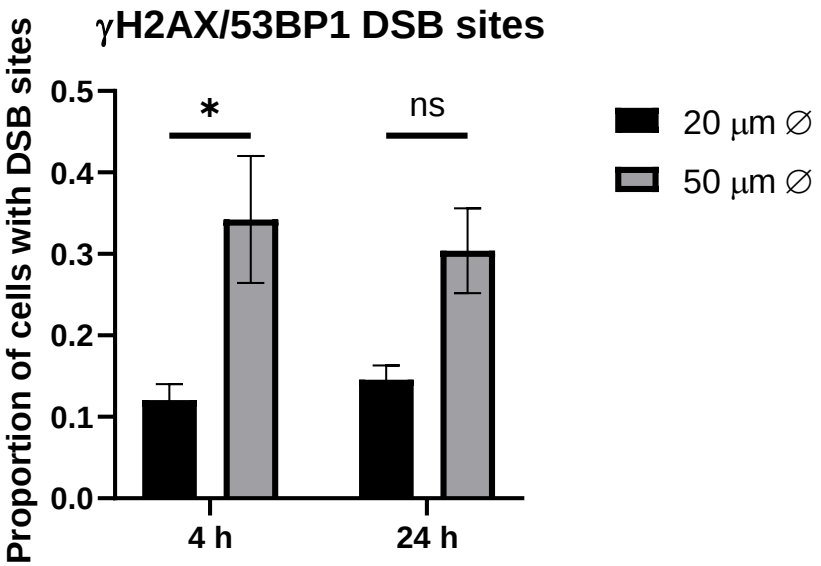

***Figure 4.4.** Proportion of HKs grown on 20 µm and 50 µm islands with active DSB repair sites, as determined by colocalizing double foci of γH2AX and 53BP1. Shown as mean + S.E.M, N = 3 experiments. n.s: non-significant. *: p-value < 0.05 (2-Way ANOVA, Tukey multiple comparisons test).*

micropatterned substrates. Histone isoform H2AX is a member of the H2A histone family and is phosphorylated to become γH2AX upon DNA DSB. TP53BP1 is subsequently recruited to γH2AX and promotes DSB repair through non-homologous end-joining[391]. When both proteins localise to the same region it is highly likely that that is a region undergoing DSB repair. Thus, the number of double foci is a good indicator of how much DNA DSB repair is happening within the nucleus. Representative images of double foci are shown in Figure 4.3 and bar graph of measured proportion of cells with DBS repair sites are summarised in Figure 4.4.

Initial observation confirms that there are significantly more DSB repair site on HKs grown on large islands both at 4 hour and 24-hour timepoint, albeit only significant in the former. This suggests that large available adhesive space support DNA damage repair processes on HKs.

Retinoic Acid biosynthesis

The next pathway to be investigated was related to Retinoic Acid (RA) biosynthesis. RA biosynthesis was the most enriched GO term of HKs grown on 20 µm islands. It revealed 8 genes related to RA biosynthesis to be upregulated with a 10.99-fold enrichment over reference list.

To measure if these changes in gene expression were accompanied by changes in intracellular RA signalling, HKs were transfected with a firefly luciferase reporter containing a RA responder element and its activity measured 24 hours after seeding. RA binding to the response element activates transcription and luciferase expressed, whose activity can be quantitated using a

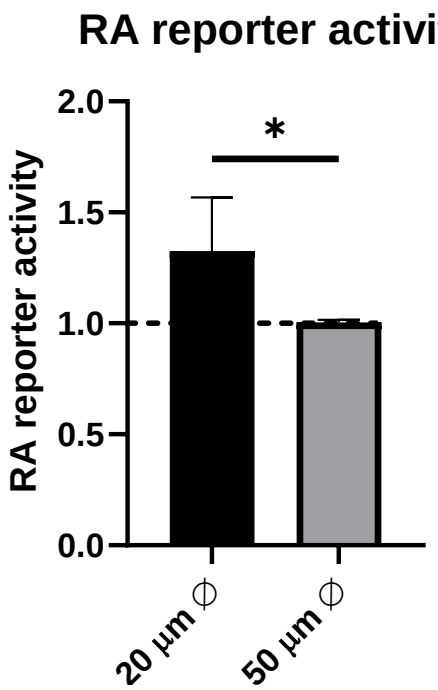

***Figure 4.5**. Retinoic Acid reporter activity as measured from fluorescein bioluminescence assay. Shown as mean + S.E.M. N = 4 experiments. *: p-value < 0.05. (two-tail t-test, equal variance assumed).*

bioluminescence assay. Measured luciferase activity is represented in bar graph form in Figure 4.5.

Elevated RA reporter activity on small islands was observed, indicating intranuclear elevated levels of RA. This suggests that smaller available adhesive space can induce upregulation of RA biosynthesis in HKs.

Ribogenesis

The final pathway to be analysed was ribogenesis. Interestingly, we found genes related to this GO term to be upregulated in both large and small islands after 24h. Translational initiation was one of the most enriched GO terms on small islands, with 25 genes upregulated, all of them ribosomal proteins. Similarly, rRNA processing was one of the most enriched GO terms for large islands with 31 upregulated genes. None of those were ribosomal proteins, but strikingly most were ribogenesis regulators.

We saw in the previous chapter that common housekeeping genes transcript levels were not significantly changed across island size, but observed a slight downregulation in H3 levels, hinting at a possible translational defect. As a proxy measure of ribosomal activity, we measured total amount of rRNA transcripts by qPCR using a primer pair targeting 47S pre-rRNA. Regardless of rRNA splicing and maturation, changes to nascent rRNA transcripts would likely be translated in changes in total ribosomes. qPCR results can be found summarised in bar graph form in Figure 4.6.

We can observe a significant drop of 47S pre-rRNA transcripts on HKs grown on small islands compared to large islands after 24 hours. Taking into consideration that ribogenesis modulators

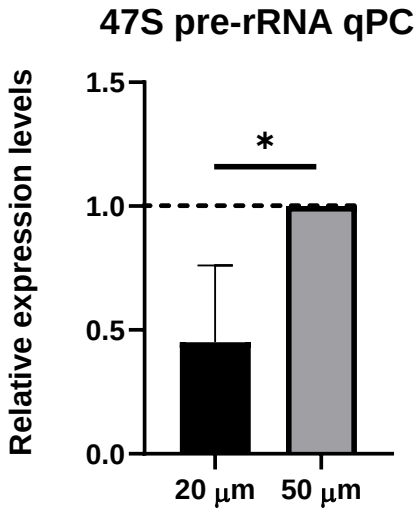

Figure 4.6. *Relative expression levels of 47S pre-ribosomal RNA as quantified from qPCR experiments. Shown as mean + S.E.M. N = 3 experiments. *: p-value < 0.05 (twin-tail t-test, equal variance assumed).*

such as splicing factors are upregulated on large islands; this proxy measure of ribosomes could explain the reduced translational capabilities of HKs grown on small islands.

To further explore this phenomenon, we investigated if the translational capabilities of the cells were being affected. We measured de novo protein synthesis using a commercial kit based on click-it chemistry. After seeding, HKs are exposed to a methionine homolog containing an alkyne bond which is integrated in nascent proteins. Using click chemistry, a fluorophore containing an azyde moiety is attached to the proteins through the alkyne bond, whose levels we measure with epifluorescence microscopy. Bar graph of measured fluorescence intensity are summarised in Figure 4.7.

We can observe a drop in integrated fluorescence on small islands after 24 hours compared to large islands. This difference is not observed at the earlier 4-hour timepoint. This indicates a drop in nascent proteins, which hints at the abovementioned defect in translation.

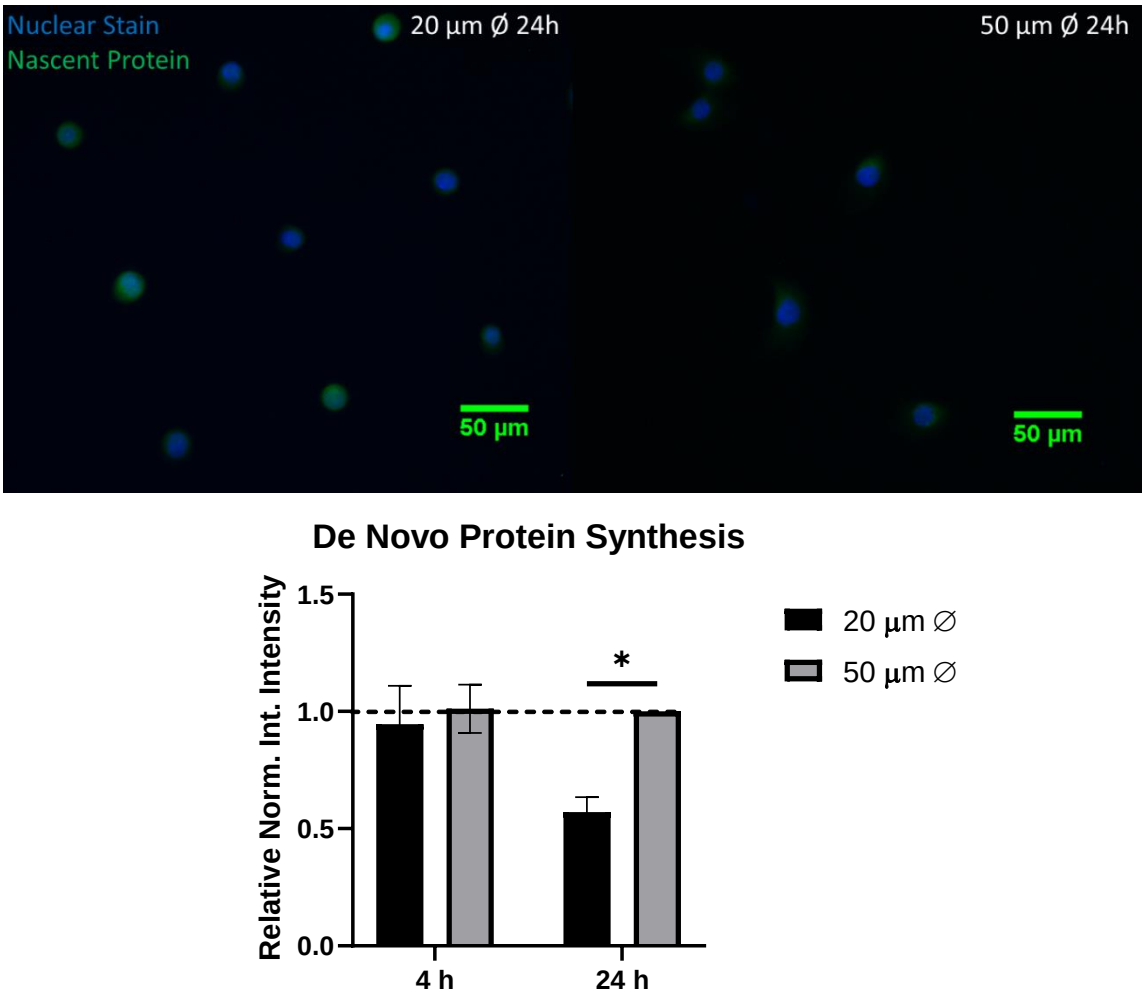

Figure 4.7. *Top: Representative epifluorescence images of HKs grown on micropatterned surfaces stained for nucleus and nascent protein. Bottom: Normalised integrated intensity measurements of epifluorescence microscopy images of nascent proteins. N = 3 experiments. n.s: non-significant. *: p-value < 0.05 (2-Way ANOVA, Tukey multiple comparisons test).*

Discussion

We have shown in this chapter that growing single HKs on micropatterned surfaces limiting their adhesive area effectively changes their transcriptional profile and is accompanied by quantifiable changes in their phenotype. Bulk analysis of differentially expressed genes indicate that reduced adhesive space leads to HK premature differentiation and confirmed this facet of the model. In addition, we have identified several other affected pathways which were not related to HK differentiation, notably DNA damage repair, retinoic acid biosynthesis and ribogenesis. We theorize that these pathways are modulated by the adhesive space made available to the HKs.

Initial analysis of the data was aimed at verifying that the model can induce HK differentiation. We observed that only 2 genes were significantly differentially expressed between island sizes at the early 4-hour time point, indicating that both populations have a homogenous origin and that island size does not induce a selection bias. GO analysis revealed both island sizes to have upregulated differentiation profiles after 24 hours compared to 4-hour samples, but proportionally higher in smaller islands. As discussed before, we believe this to be due to the heterogenous populations found on both island sizes. Indeed, small islands only see about half of HKs differentiate after 24h. On the other hand, multicellular islands are a common occurrence on large islands, and they often differentiate. To aggravate this further, since multicellular islands have more cells than monocellular islands, even a small amount of them would have an overrepresentation on bulk analysis. Nevertheless, these discrepancies were not large enough that differences could not be perceived between both island sizes and permitted to extract valuable information such as a plethora of affected pathways.

The first affected pathway we investigated was DNA damage repair. Interestingly, this pathway was upregulated on large islands compared to small ones after 24 hours. Such a difference could not be perceived at the earlier 4-hour time point, indicating either that small islands have their DNA damage repair capabilities reduced over time or that their need is diminished. We quantified DNA DSB repair sites from colocalization of γH2AX and 53BP1 foci to explore if changes to RNA transcript levels did translate in changes in DNA repair activity. We found that indeed HKs grown on large islands had more DSB repair sites compared to smaller islands, albeit only significantly so at the early 4-hour time point.

A number of recent studies in the mechanobiology field have described the protective mechanical role of lamins in DNA damage[392], but also of how substrate stiffness can induce said damage[389]. Indeed, substrate stiffness can modulate focal adhesion number and maturity. This in turn can generate DNA damage by having the actin cytoskeleton pull on the nucleus from

more mature focal adhesions. Aspects of both phenomenons may be seen here. On one hand lamin A/C redistribution in small islands could be enhancing their DNA protecting role by providing the nucleus with higher mechanical integrity. On the other hand, HKs grown on larger islands could have more focal adhesions and cytoskeletal tension used to pull on the nucleus and thus generate DNA damage. Finally, as discussed before reduction of heterochromatin could also give more deformability and resilience to chromatin thus protecting it. Combination of all three could explain why the amount of DNA damage is higher on large islands. Verification of the first two could be done quite easily; Lamin A/C knock down using siRNA would elevate DNA damage if true, and similarly blocking actin contractility using blebbistatin would reduce it. Blocking histone demethylases thus hindering loss of heterochromatin markers would also give insight into this phenomenon. Unfortunately, if it is true that all three factors are working synergistically then changes might be too small to perceive it. There is also the possibility that a hidden mechanism, maybe such as impaired translational capabilities of HKs grown on small islands, is behind the reduced DNA DSB repair sites. Similarly, maybe DNA damage mechanisms are downregulated in differentiating HKs as they do not undergo DNA damage checks which are part of the cell cycle. Inducing DNA damage, e.g using UV light, and then comparing how both island sizes react would help clear this doubt. Finally, it is interesting to note that substrate stiffness and cellular differentiation are also linked[393] and that here we discuss available hard substrate as a parameter of DNA damage induction. One could entertain the thought of how our model would change if we could change the elastic modulus of the micropatterned islands and how in turn that would affect both HK differentiation and DNA damage.

The second affected pathway was retinoic acid biosynthesis, which was upregulated on small islands. Using a transfected luciferase reporter system, we measured elevated intracellular levels of RA in HKs grown on 20 µm islands. Considering that RA has been shown to inhibit HK differentiation[394], this upregulation in a differentiating population is intriguing. RA signalling has been implicated in lamin biogenesis and to be mechanoresponsive[390], and we believe that lamin radial redistribution may be responsible for the upregulated RA pathway. Further proof of this will be needed, such as knock down of lamin A/C using siRNA, or hopefully disturbing the radial redistribution by perturbing force transmission between the cytoskeleton and the nucleus using cytoskeletal inhibitors.

The final affected pathway that we investigated was ribogenesis. This pathway was particularly interesting as nucleoli fusion was one of the main findings from the initial macroscopic characterisation of our model. Thus, it was important to ask how ribogenesis and protein synthesis would be affected. It was intriguing then to see a mixed response, with 25 ribosomal protein genes being upregulated on small islands, while 31 ribogenesis regulators on the large

islands. The model was initially interrogated for total de novo protein synthesis and found them reduced on small islands after 24 hours. We then aimed at discerning if these decreased levels were due to either reduced total levels of ribosomes or at reduced ribosomal activity. For this we used an estimation of total 47S rRNA transcripts as a proxy measure of total ribosomes and found them to be downregulated on small islands.

Together, these data suggest that there is indeed a reduced number of total ribosomes in HKs grown on 20 μm islands, and that this is translated in overall reduced translational activity. We also note that changes in ribogenesis modulators as revealed by transcriptome data very probably also hint at a perturbed ribosomal splicing and maturation which probably also have effects on ribosomal activity. We theorise that the mixed response in mRNA transcripts could originate from an unknown compensation or feedback mechanism. It would of course be most useful if a direct measurement of total ribosomes could be performed. Unfortunately, it was found that a direct measure by northern blot or gradient centrifugation would not be appropriate considering the low amount of starting materials we can get off the micropatterned surfaces. These methods, coupled with rRNA-seq, would resolve many of the doubts that have arisen from the data presented here. The next step in our investigation here will be to link HK nuclear size with nucleoli condensation and ribogenesis.

In summary, this chapter adds a transcriptomic dimension to the characterization of the HKs nuclear compaction model following reduced available adhesive space. Combined with the initial findings of Chapter 4, we have now drawn a rough outline of the main macroscopic and genomic changes that can be observed. The last chapter of this thesis will dissect the relationship between these changes and force transmission through the cytoskeleton to the nucleus.

Chapter 5: Investigation of the Cytoskeletal-Nucleoskeletal Linkage in Biophysical Regulation of Nuclear Architecture

Introduction

In the first chapter we described the nucleus as a central mechanosensing unit due to its innermost position within the cell and mechanical integration with the cytoskeleton. Biophysical cues sensed by the cytoskeleton are ultimately transmitted to the nucleus through a chain of mediators, from focal adhesions to the LINC. Both cytoskeletal components and mediators are diverse in nature and roles, making several of them redundant[395]. This redundancy allows the cell to maintain part of its mechanosensory ability as well as mechanical integrity shall any of the components fail (e.g such as in genetic abnormalities). This fail-safe approach is furthermore strengthened by the existence of compensation mechanisms[396]. Taken together, both factors make perturbation experiments difficult to interpret as the effect of a perturbation might be minimized by a compensation mechanism. Inversely, this diversity is a double-edged sword: it gives us a comparatively large pool of targets to choose from. Comparisons between distinct perturbations should allow to extract more clear relationships between cytoskeletal components and nuclear architecture.

We have selected several key mediators in force transmission to the nucleus that we will probe in this chapter. Initially, cytoskeletal inhibitors will be used to perturb F-actin, a major cytoskeletal component. These results will be compared with cell lines that express a mutant version of keratin 14, which exhibits defective keratin filament assembly as found in EBS[397]. This mutation has been shown to generate a more severe effect than complete KO of keratin type I KO[398]. This approach will give insight into how the main cytoskeletal networks regulate force transmission. Next, we will investigate mouse cell lines which have had plectin, a major cytolinker, knocked out genetically. Loss of plectin has been shown to increase actin filament assembly thus providing a contrasted picture upon which we can compare previous actin inhibition results. Moreover, they exhibit enlarged nuclei due to increased nuclear deformability[221], which will provide crucial data on how nuclear morphology affects previously observed changes. Finally, small interfering RNA (siRNA) will be used to knock down nesprin 2 and lamin A/C. Nesprin 2 is a central component of the LINC, and its knockdown will diminish force transmission to the nucleus via F-actin filaments. Lamin A/C knockdown will on the other hand help disconnect chromatin through LADs from the nuclear envelope[118,352] and diminish nuclear mechanical integrity[329]. Comparison of the two should allow us to analyse the role of the nuclear envelope.

Our aim in this chapter will be to determine how the previously established cell shape-induced changes in nuclear architecture depend on specific components of the cytoskeleton and nucleoskeleton. Taken together, these analyses should provide causational links between

cytoskeletal components and changes in nuclear architecture following biophysical cues from the extracellular space.

Disruption of cytoskeletal organisation

Blebbistatin and Y-27632

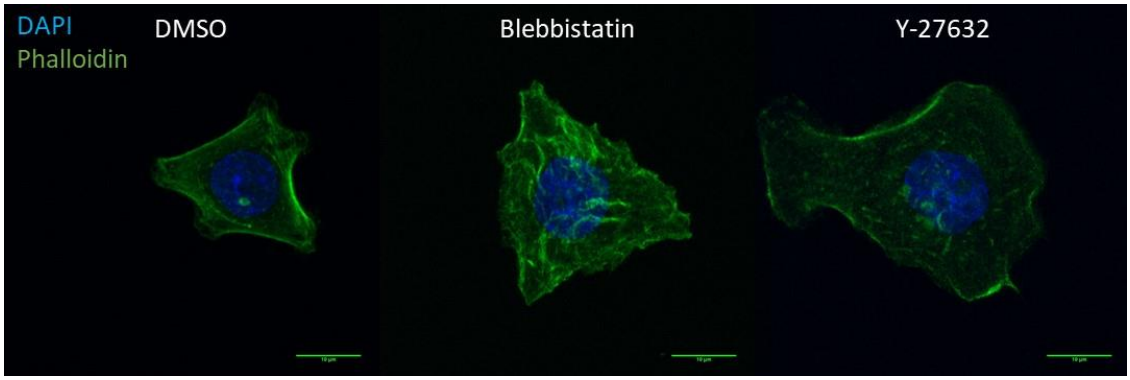

***Figure 5.1**. Representative confocal images of HKs treated with DMSO (1 µL/mL), Blebbistatin (50 µM) and ROCK inhibitor Y-27632 (10 µM) after 24 hours labelled for actin cytoskeleton. Scale bar = 10 µm.*

To determine the role of the actin cytoskeleton in mediating shape-induced changes in nuclear architecture, we first used common cytoskeletal inhibitors to perturb actin dynamics. Actin has been shown to be a major mediator in mechanotransduction as well as being a regulator of nuclear size[399], and thus perturbing its network would give additional insights. We chose blebbistatin, a small molecule inhibitor of myosin II, and Y-27632, a ROCK-inhibitor, which inhibits both contractility and F-actin polymerisation. Representative images of HKs treated with inhibitors and stained for actin (phalloidin) can be found in Figure 5.1. Visual inspection of treated cells confirmed perturbation. After treatment with blebbistatin cells showed disrupted actin network. HKs treated with ROCK inhibitor exhibited more disperse actin, elevated cell spreading and the apparition of lamellipodia-like protrusions.

Nuclear morphology, H3K27Ac and H3K9me3 levels

Quantification of changes in nuclear morphology was initially performed before analysing chromatin markers H3K27Ac and H3K9me3 of HKs grown on micropatterned islands treated with cytoskeletal inhibitors for 24 hours. We selected heterochromatin marker H3K9me3 and euchromatin marker H3K27Ac from previous experiments as they were the most sensitive to changes in cellular shape. Representative images of HKs treated with inhibitors and stained for H3K27Ac can be found in Figure 5.2. Bar graph summary of nuclear volume and H3K27Ac immunofluorescence intensity changes can be found in Figure 5.3. Representative images of HKs treated with inhibitors and stained for H3K9me3 and bar graph summary of H3K9me3 immunofluorescence intensity changes can be found in Figure 5.4.

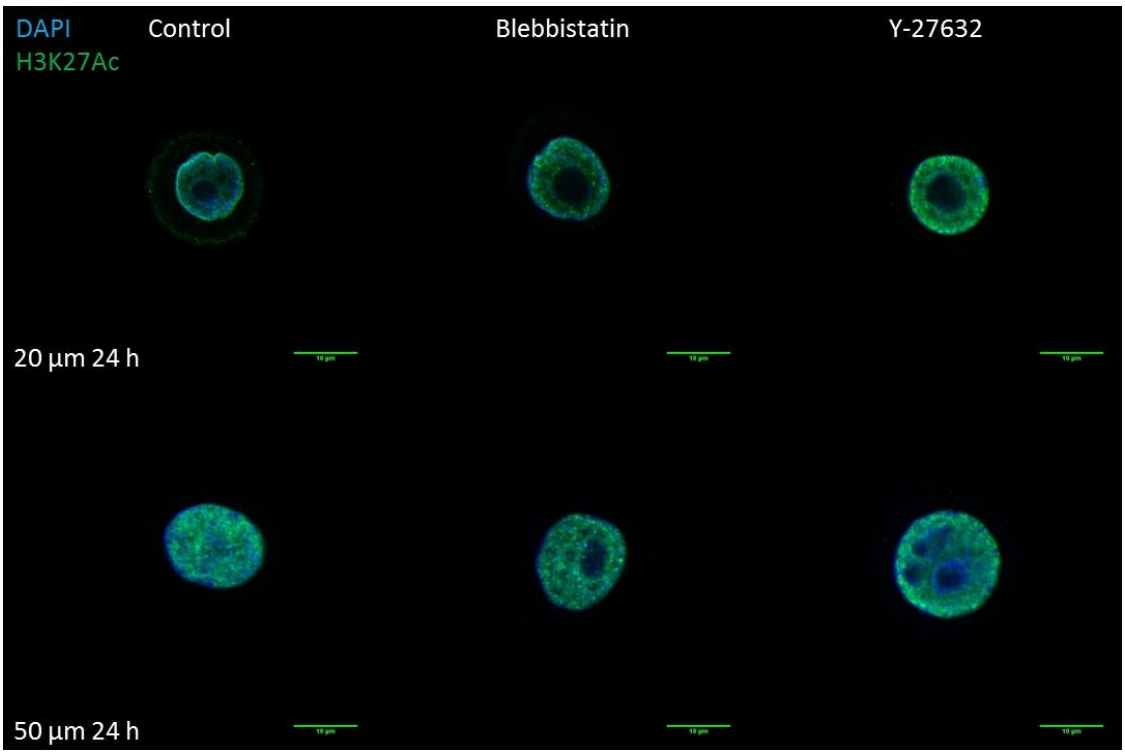

Figure 5.2. *Representative confocal microscopy images of HKs grown on micropatterned islands and treated with DMSO (1 µL/mL), Blebbistatin (50 µM) and ROCK inhibitor Y-27632 (10 µM) after 24 hours labelled for H3K27Ac and DAPI. Scale bar = 10 µm.*

Initial analysis showed that while previous trends of smaller nuclear volume and lower H3K27Ac and H3K9me3 intensity levels for smaller islands compared to large ones on control conditions can be appreciated they were not statistically significant here. Nevertheless, trends can be observed, as small islands seem to have smaller nuclear volume and lower H3K27Ac and H3K9me3 intensity levels compared to large islands across conditions, and 2-Way ANOVA indicated island size to be a source of significant variation for all three measures (Nuclear Volumes p-value: 1.31E-2, H3K27Ac: 2.2E-3, H3K9me3: 1.47E-2). Nuclear volume of HKs grown on large islands appeared reduced after treatment with cytoskeletal inhibitor Blebbistatin, which was to be expected as the acto-myosin network tension on the nucleus was hindered.

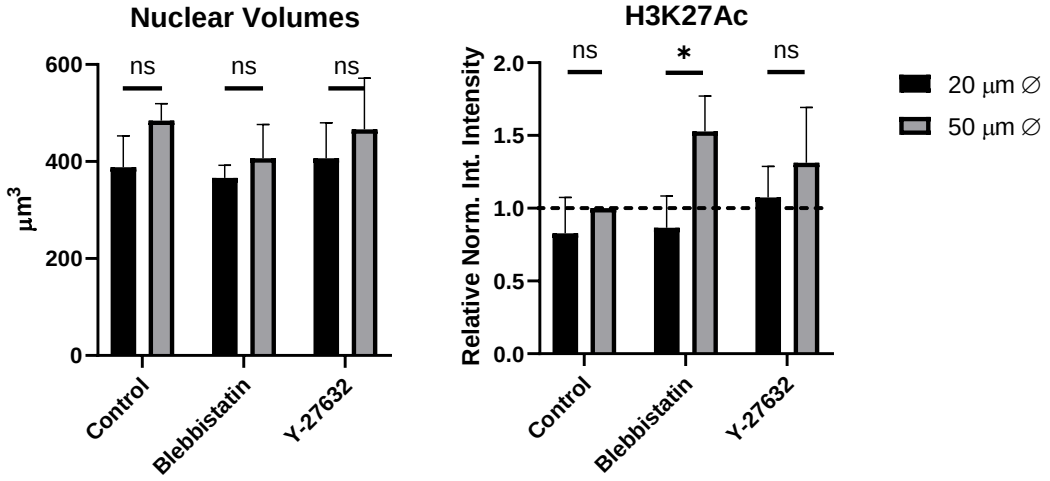

Figure 5.3. *Bar graph of nuclear volumes (right) and H3K27Ac (left) relative fluorescence integrated intensities. Shown as mean + S.E.M. N = 3 experiments. n.s: non-significant. *: p-value < 0.05 (2-Way ANOVA, Sidak multiple comparisons*

This was accompanied by non-statistically significant increments in their H3K27Ac levels for both Blebbistatin and ROCK inhibitor. H3K9me3 levels remained comparatively unperturbed across conditions, with a non-significant reduction of intensity levels on large islands treated with ROCK inhibitor.

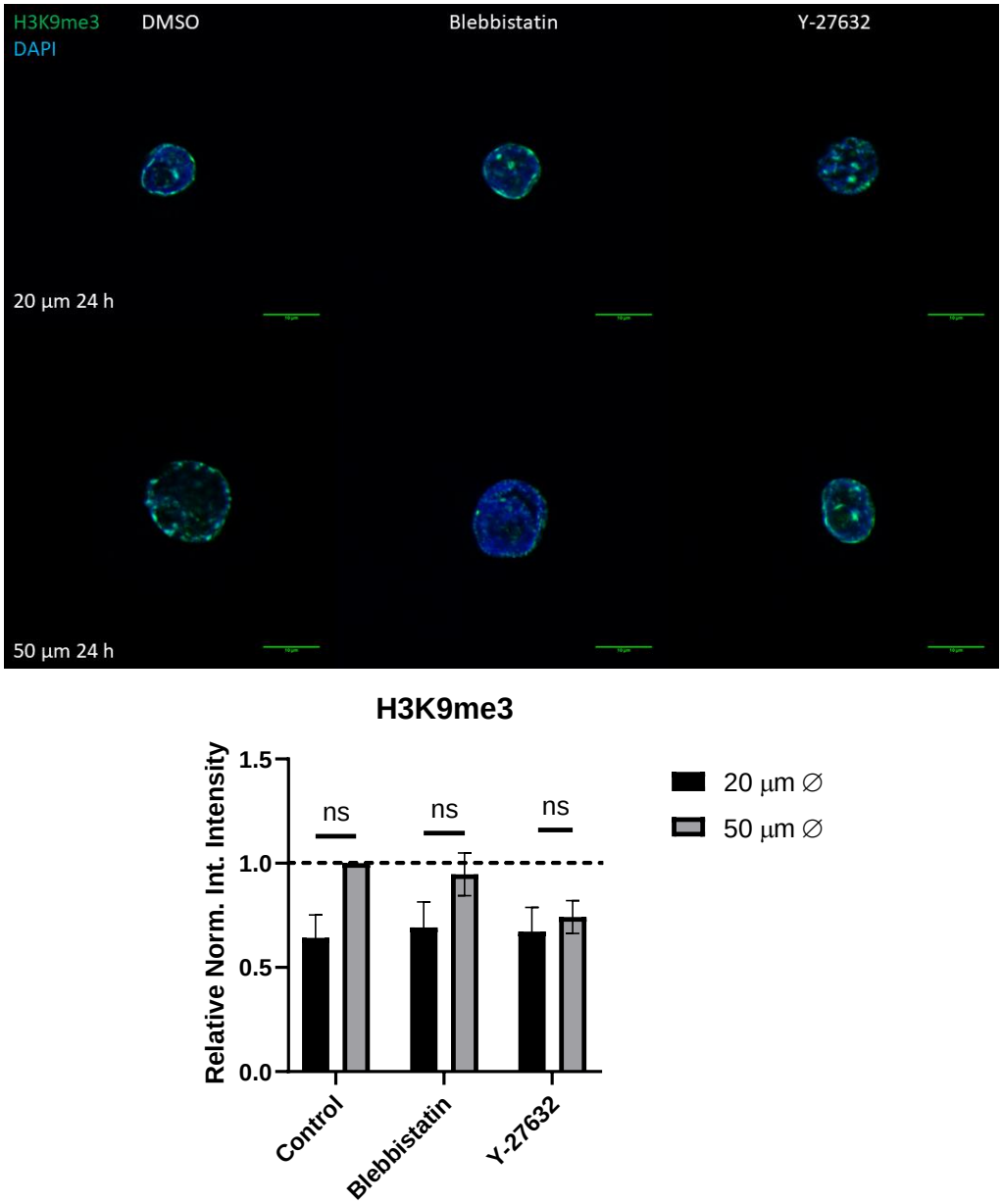

Figure 5.4. ***Top:*** *Representative confocal microscopy images of HKs grown on micropatterned islands and treated with DMSO (1 µL/mL), Blebbistatin (50 µM) and ROCK inhibitor Y-27632 (10 µM) after 24 hours labelled for H3K27Ac and DAPI. Scale bar = 10 µm.* ***Bottom:*** *Bar graph of H3K9me3 relative fluorescence integrated intensities. Shown as mean + S.E.M. N = 3 experiments. n.s: non-significant. (2-Way ANOVA, Sidak multiple comparisons test).*

Lamin A/C levels and radial distribution

Next, nucleoskeletal response to perturbation of actin was analysed by confocal imaging of lamin A/C. Representative images and bar graph summary of immunofluorescence intensity measurements and radial distribution can be found in Figure 5.5. Cytoskeletal inhibitor treatment did not seem to have significant effects on lamin A/C intensity levels. On the other hand, radial distribution of lamin A/C in small islands was significantly reduced near the nuclear periphery after cytoskeletal inhibitor treatment, while large islands were comparatively unaffected. These results suggest that overall lamin A/C levels do not change in response to biophysical cues induced by micropatterned substrates. Furthermore, perturbation of F-actin leads to more disperse lamin within the nucleus, specifically on small micropatterns.

Overall, these results raise interesting questions. Easing of F-actin tension onto the nucleus did not appear to have significant effects, and was expected for blebbistatin[221]. In contrast differences in H3K27Ac levels between island sizes became more pronounced. Both these observations suggest that nuclear volume and H3K27Ac levels are not intrinsically linked, and it is likely chromatin markers are regulated by balanced compressive and tensive forces upon the nucleus. Similarly, lamin A/C appeared to not be affected by cytoskeletal inhibitor treatment but exhibited a slight altered radial profile on small islands which resembled more their larger counterparts, possibly due to perturbation of F-actin tension.

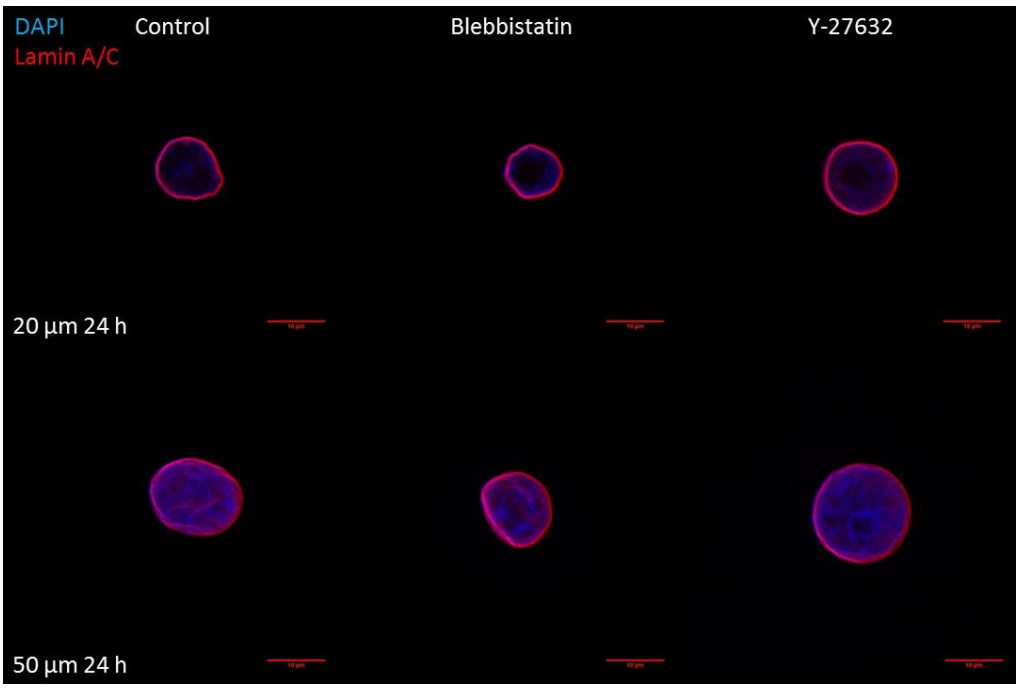

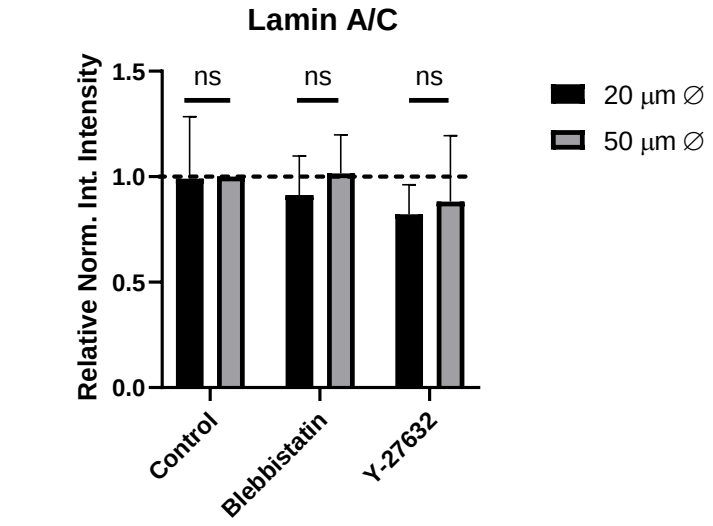

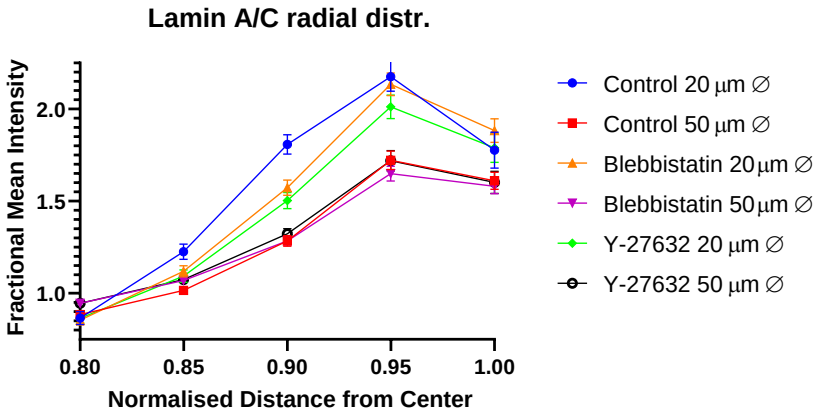

Figure 5.5.Top: *Representative confocal microscopy images of HKs grown on micropatterned islands and treated with DMSO (1 µL/mL), Blebbistatin (50 µM) and ROCK inhibitor Y-27632 (10 µM) after 24 hours labelled for lamin A/C and DAPI. Scale bar = 10 µm.* ***Center:*** *bar graph of relative normalised integrated intensity of Lamin A/C. Shown as mean + S.E.M. N = 3 experiments. n.s: non-significant. (2-Way ANOVA, Sidak multiple comparisons test).* ***Bottom:*** *Radial distribution of lamin A/C plotted as radial mean fractional intensity: values over 1 indicate a higher than average fluorescence intensity and vice versa. Significance calculated using Kolmogorov-Smirnov test. N = 3 experiments.*

Disruption of keratin cytoskeleton stability

Nuclear morphology

We next investigated the role of the keratin cytoskeleton in nuclear mechanotransduction using the HaCaT immortalized keratinocyte cell lines with stable overexpression of keratin 14 with the dominant R416P point mutation. This mutation is localised in the central rod domain of the K14 protein, allowing its filament formation but becoming very unstable. This results in the formation of K14 aggregates under mild forces, as can be appreciated in Figure 5.6 compared to overexpression of the wild type control. As keratins, and namely keratin 14 in basal keratinocytes, are the main cytoskeletal proteins accountable for HKs mechanical integrity[232], this mutation is theorised to have effects on how forces are transmitted to the nucleus. The point mutation is also based on a common mutation found in severe Dowling-Meara form of EB thus adding clinical relevance to the model[400].

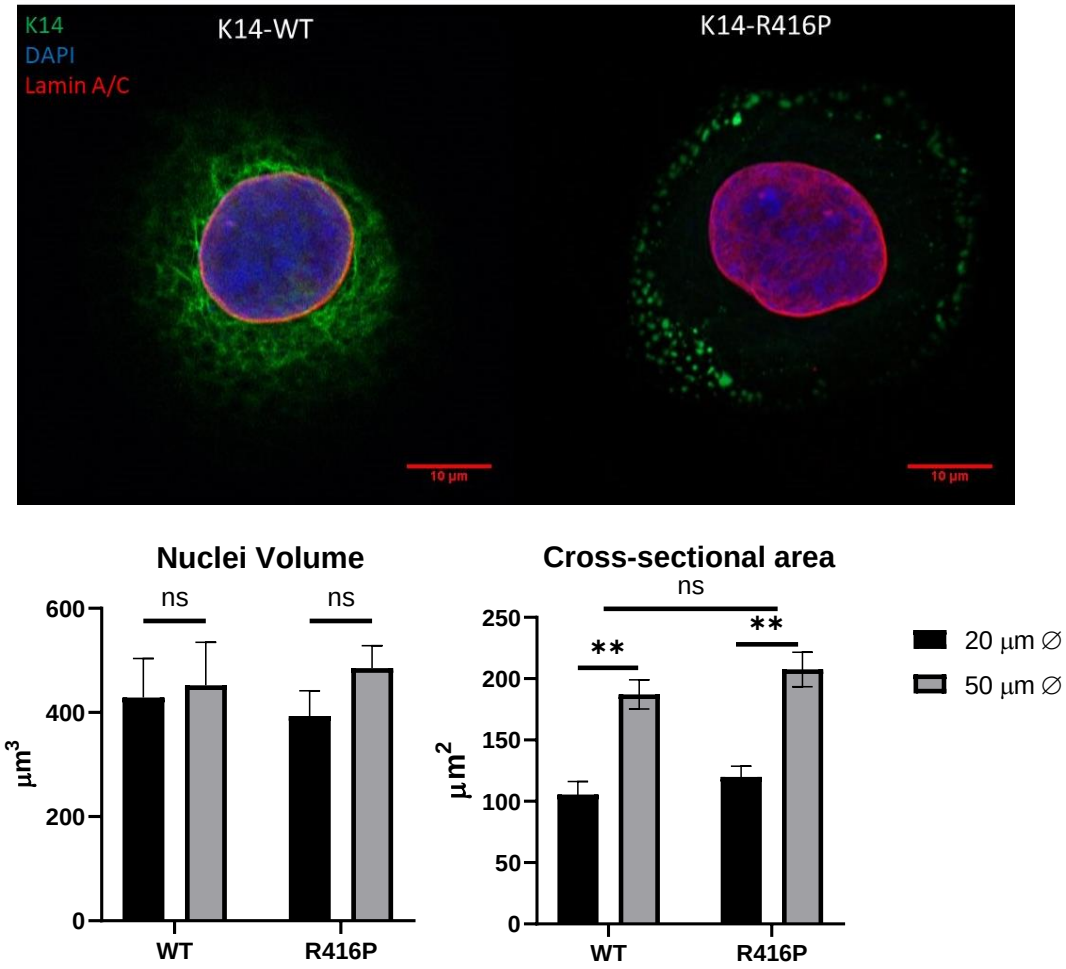

Figure 5.6. Top: *Representative confocal images of HaCaTs transfected with WT K14-GFP (left) or K14-R416P-GFP (left) seeded on large micropatterns after 24 hours labelled for K14, DAPI and lamin A/C. Scale bar = 10 µm.* ***Bottom left:*** *Bar graph of nuclear volumes. Bottom right: Bar graph of nuclear cross-sectional area. Shown as mean + S.E.M. N = 3 experiments. n.s: non-significant. **: p-value < 0.01 (2-Way ANOVA, Tukey multiple comparisons test).*

Effects of this mutation on nuclear morphology was initially investigated. Findings are summarised in Figure 5.6. The K14-R416P mutation does not appear to have significant effects on nuclear volume. However, no differences could be appreciated between island sizes for WT in contrast with previous findings. We further investigated changes in cross-sectional area and observed significant changes across islands size, but not between keratin WT and mutant. This indicate that HaCaT nuclei can react to cellular spreading by incrementing their cross-sectional area but their lack of change in nuclear volume indicate that they are incompressible.

H3K9me3 levels

Next, heterochromatin marker H3K9me3 reaction to keratin cytoskeletal network perturbation was investigated. Measured relative integrated intensities can be found in Figure 5.7 in bar graph form. Similarly to nuclear volumes there seems to be little effect from K14 mutation. While there is a significant downregulation of H3K9me3 intensity on small islands compared to large ones for WT, that significance is lost for cells transfected with the mutated form. Nevertheless, trends between conditions are similar, and differences between same island size but different constructs are not significant.

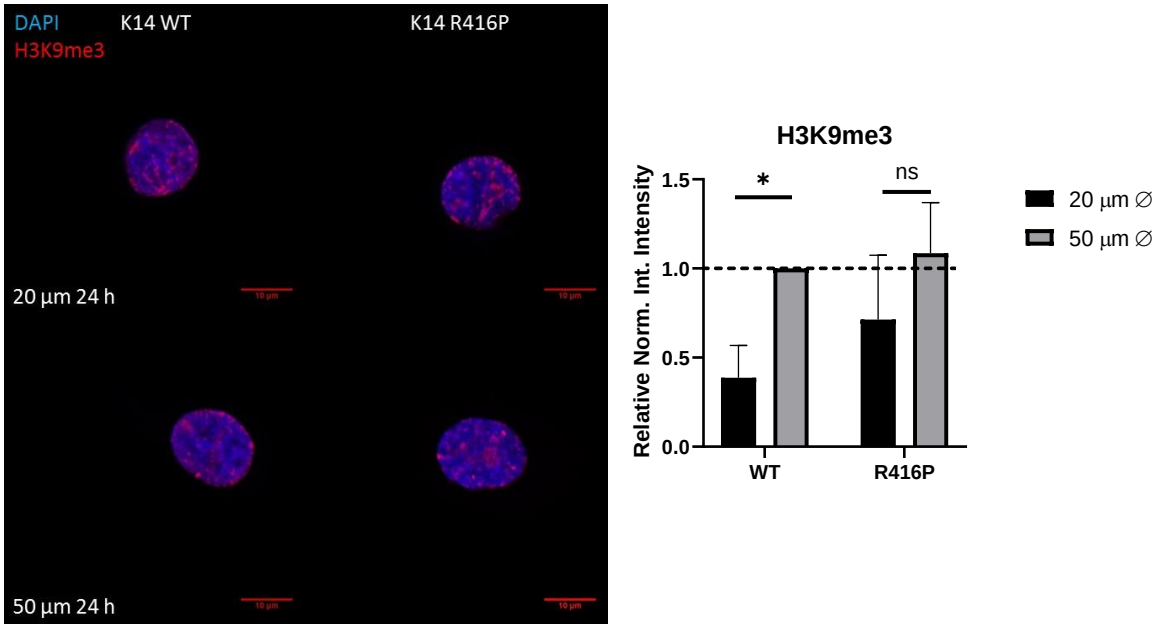

Figure 5.7. Left: *Representative confocal images of HaCaTs expressing WT K14-GFP or K14-R416P-GFP seeded on micropatterned islands after 24 hours labelled for DAPI and H3K9me3. Scale bar = 10µm.* ***Right:*** *Bar graph of H3K9me3 relative fluorescence integrated intensities. Shown as mean + S.E.M. N = 3 experiments. n.s: non-significant. *: p-value < 0.05 (2-Way ANOVA, Tukey multiple comparisons test).*

Lamin A/C levels and radial distribution

After this, changes in lamin A/C levels and radial distribution were quantified. Bar graph of relative integrated intensities as well as radial profiles can be found in Figure 5.8. Here lamin A/C intensity levels were significantly upregulated in R416P cells compared to WT on large islands, and 2-way ANOVA indicated K14 R416P mutation to be a source of significant variance. When observing changes in radial profile no significant changes were perceived between R416P cells compared to WT.

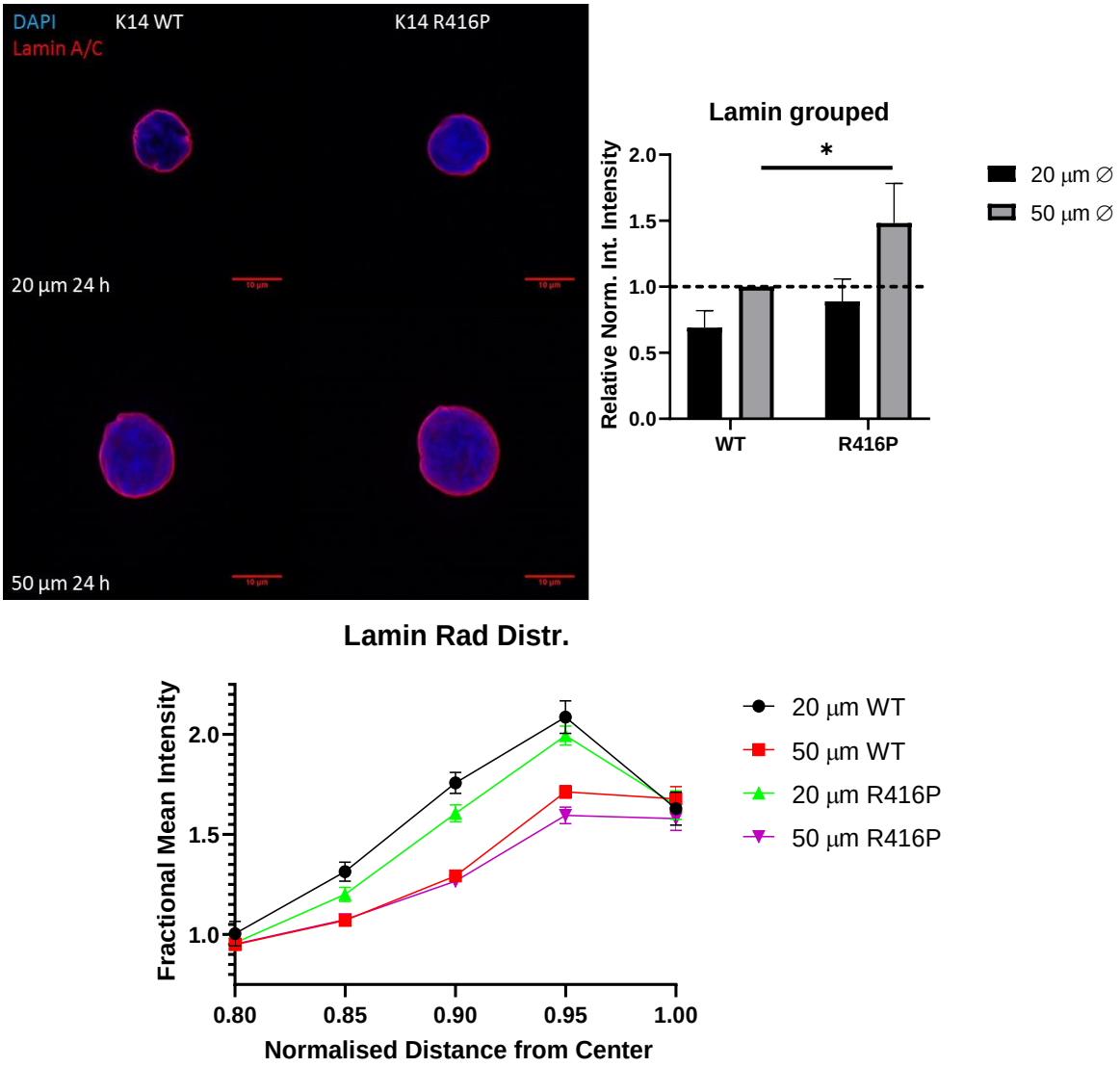

Figure 5.8. Top left: *Representative confocal images of HaCaTs expressing WT K14-GFP or K14-R416P-GFP seeded on micropatterned islands after 24 hours labelled for DAPI and lamin A/C. Scale bar = 10 µm.* ***Top right:*** *Bar graph of lamin A/C relative fluorescence integrated intensities. Shown as mean + S.E.D. N = 3 experiments. n.s: non-significant. *: p-value < 0.05 (2-Way ANOVA, Tukey multiple comparisons test).* ***Bottom:*** *Radial distribution of lamin A/C plotted as radial mean fractional intensity: values over 1 indicate a higher than average fluorescence intensity and vice versa. N = 3 experiments.*

Nucleoli number

Finally, the role of the keratin cytoskeleton in the regulation of nucleoli numbers was investigated. Bar graph of measured average nucleoli number per cell can be found in Figure 5.9. A larger number of nucleoli on large islands was observed, albeit only significantly so in R416P cells, consistent with previous experiments. In summary, no significant effect of K14-R416P mutation was observed.

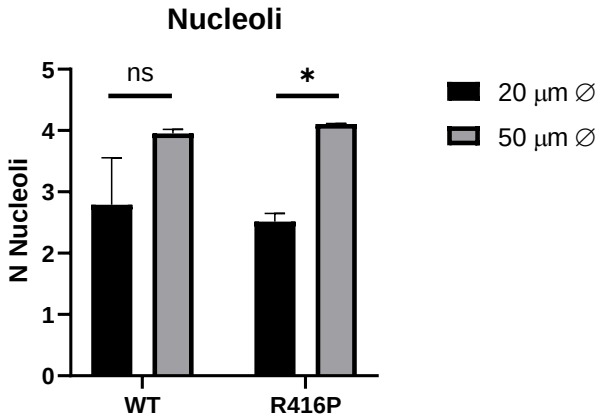

Figure 5.9. *Bar graph of average nucleoli number per cell of K14 WT versus K14 R416P cells. Shown as mean + S.E.M. N = 3 experiments. n.s: non-significant. *: p-value<0.05. (2-Way ANOVA, Tukey multiple comparisons test).*

Altogether, results show that HaCats expressing K14 with R416P point mutation do not exhibit dramatic changes in nuclear volume, lamin A/C radial distribution, H3K9me3 levels and nucleoli number. However, changes in overall lamin A/C levels could be observed. Previous reports have pushed the idea that the perinuclear keratin network protects the nucleus from deformation[221,400] but unfortunately we did not observe significant changes in nuclear volume. But changes in lamin A/C levels could be indicative of a compensation mechanism to protect the nucleus from deformation. Our previous results also indicated a relation between nuclear size and nucleoli number, so the lack of change in nucleoli number was expected. H3K9me3 appears until now to be unaffected by perturbations to the actin and keratin cytoskeletons.

Cytolinker Plectin KO

Nuclear morphology

As an alternative model of keratin disruption, a mouse keratinocyte cell line with a total knock out of the *Plec* gene for the cytolinker plectin was next employed. Plectin links F-actin and keratin and anchors intermediate filaments to hemi-desmosomes[260,401]. *Plec* KO has been shown to destabilise keratin IF network through loss of connection to other cytoskeletal networks, which helps stabilise their network formation. It induces larger nuclear deformability in the context of micropatterned surfaces by means of perinuclear keratin organisation perturbation[221]. Furthermore, *Plec* KO upregulates F-actin as can be appreciated in Figure 5.10.

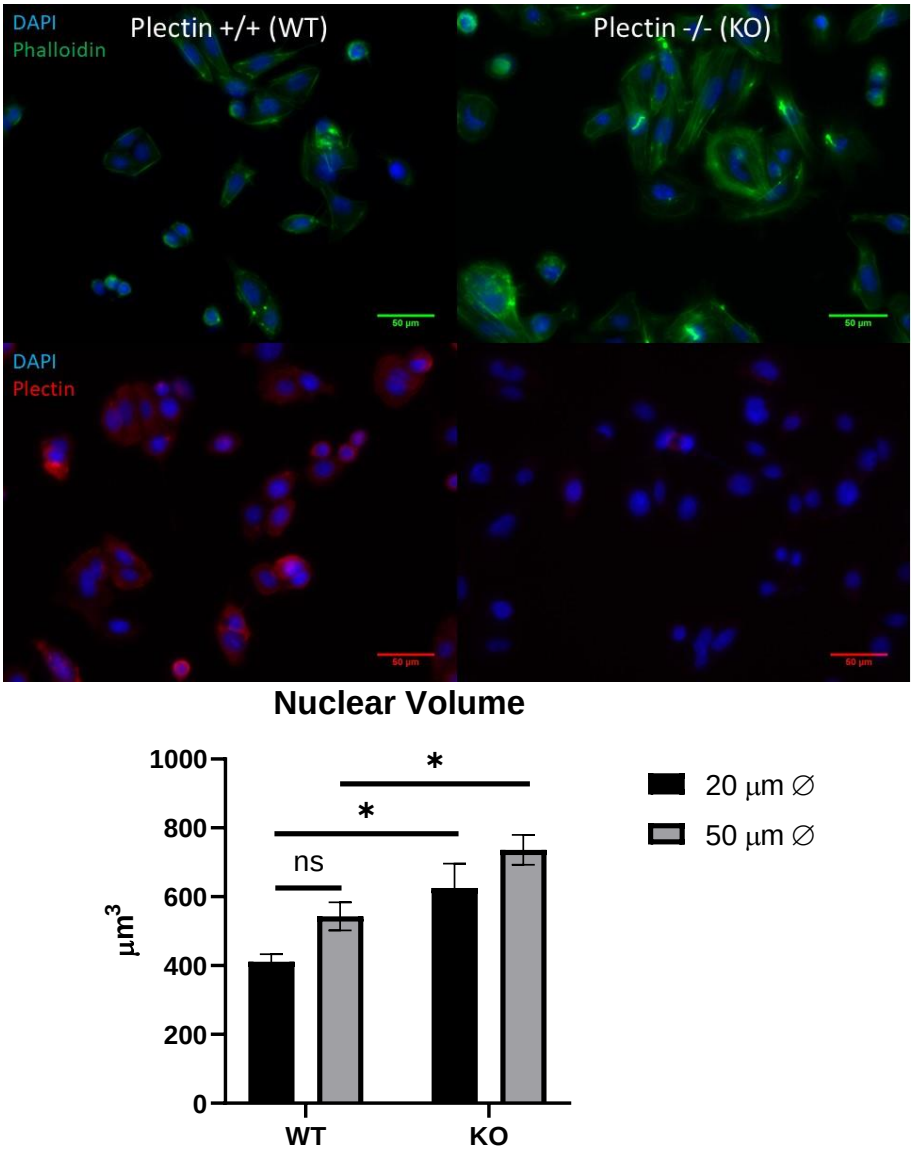

Figure 5.10. Top: *Representative confocal microscopy images of* Plec *WT and* Plec *KO keratinocytes grown on micropatterned surfaces stained for DAPI and H3K9me3.* ***Bottom:*** *Bar graph of nuclear volumes of WT versus* Plec *KO cells. Shown as mean + S.E.M. N = 4 experiments. n.s: non-significant. *: p-value < 0.05 (2-Way ANOVA, Tukey multiple comparisons test).*

Increased F-actin tension on the nucleus likely increases deformation. As of such, this model provides an important contrast to the F-actin inhibitors, which decrease acto-myosin contractility, and K14 disruption.

The effect of *Plec* KO on nuclear morphology was initially investigated. Representative images of *Plec* KO cells grown on micropatterns can be found in Figure 5.11 and graph bar of observed nuclear volumes can be found in Figure 5.10.

2-way ANOVA indicated that both island size and *Plec* KO had significant effects on nuclear volume variation, albeit differences between individual conditions were only significant between *Plec* KO and WT. Visual inspection indicates that there are larger nuclei on larger islands and *Plec* KO cells. This increment was expected, as *Plec* KO cells have been shown to have more deformable nuclei, possibly due to upregulated F-actin network and perturbed perinuclear keratin[221].

H3K27Ac and H3K9me3 levels

Next levels of chromatin markers H3K27Ac and H3K9me3 were analysed. Bar graph summary of measured relative intensities can be found in Figure 5.11. While H3K27Ac was minimally affected by *Plec* KO, a significant downregulation of H3K9me3 can be appreciated for *Plec* KO cells compared to WT across both pattern sizes. Like previous experiments, the general trend of lower intensities for lower available adhesive space held true. It is interesting to note that *plec* KO had the opposite effect on H3K9me3 compared to the K14-R416P mutation.

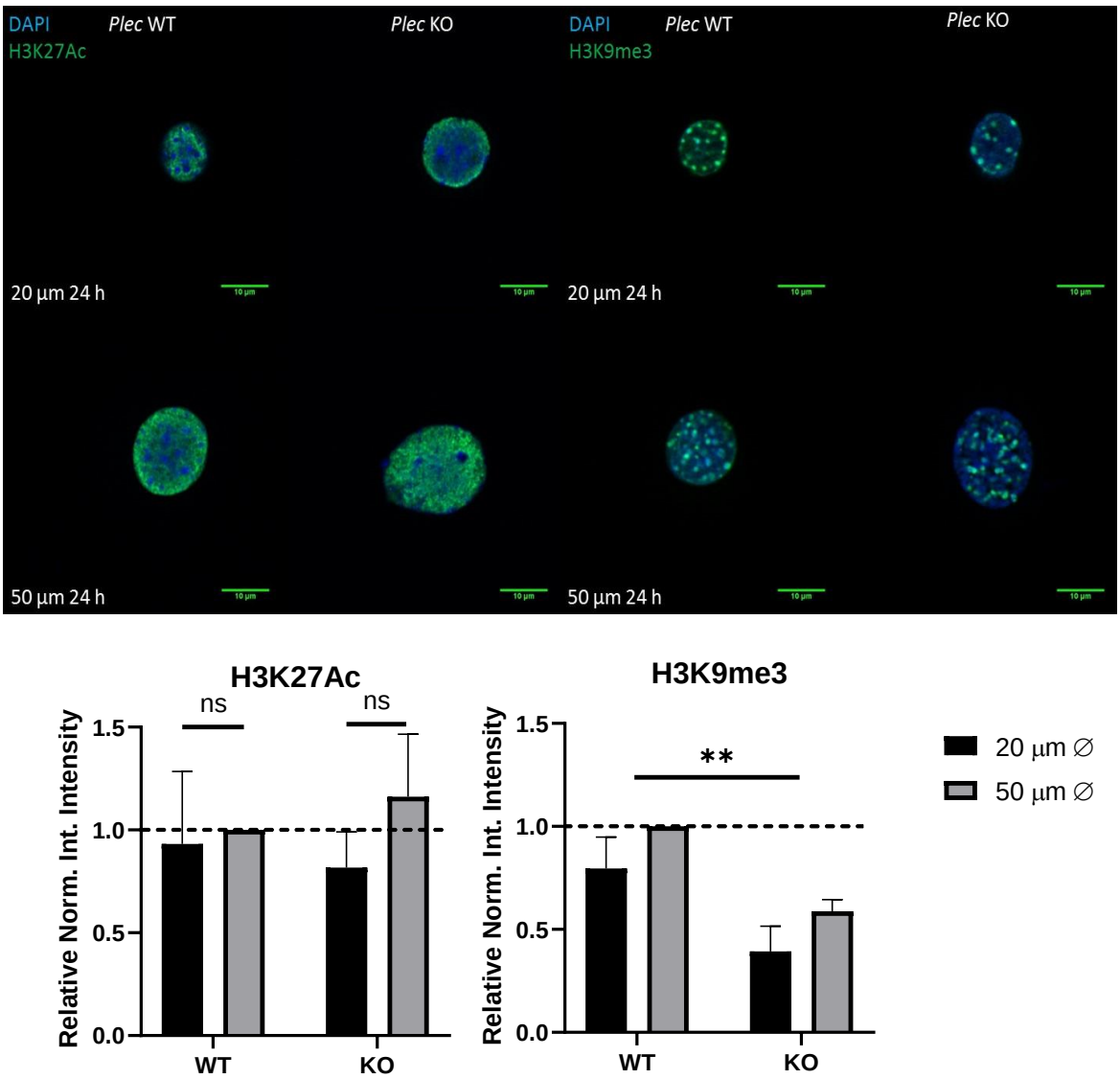

Figure 5.11. Top**: Representative confocal microscopy images of* Plec *WT and* Plec *KO keratinocytes grown on micropatterned surfaces stained for DAPI and H3K27Ac.* ***Bottom: *Bar graph of H3K27Ac (left) and H3K9me3 (right) relative fluorescence integrated intensities. Shown as mean + S.E.M. N = 3 experiments. n.s: non-significant. **: p-value < 0.01 (2-Way ANOVA, Tukey multiple comparisons test).*

Heterochromatin foci distribution

Considering that *Plec* KO has a significant effect on nuclear volume, we analysed next the distribution of size and number of foci for heterochromatin marker H3K9me3 as previously done. Bar graph summary can be found in Figure 5.12.

Unfortunately, no significant changes due to *Plec* KO could be appreciated. Indeed, changes in foci size across island size and between *Plec* KO and WT were not significant. Foci number was significantly affected by island size as revealed by 2-way ANOVA but not by *Plec* KO. As expected, there were more numerous foci on larger islands, although only significantly so for the WT cells.

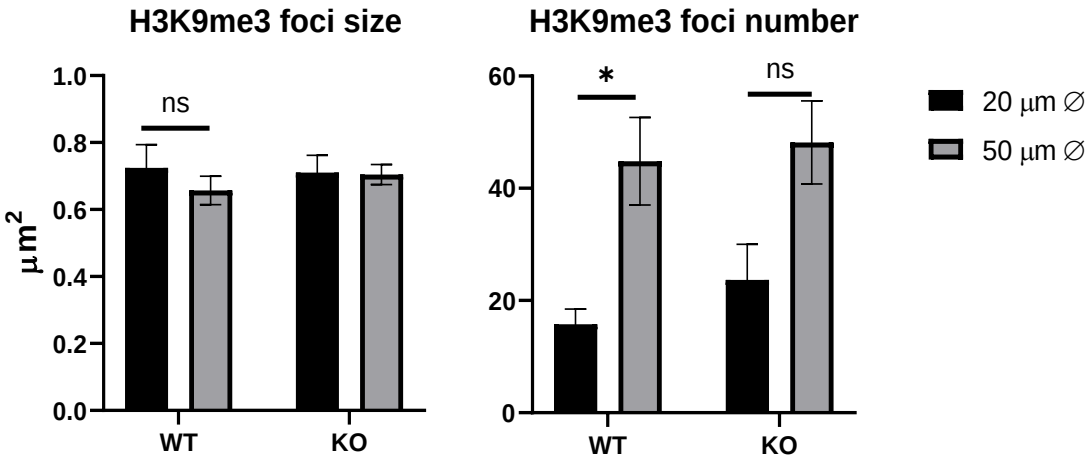

Figure 5.12. *Analysis of foci size and number of H3K9me3. Shown as mean + S.E.M, N = 3 experiments. n.s: non-significant. *: p-value<0.05 (2-Way ANOVA, Tukeys multiple comparisons test).*

Lamin A levels and radial distribution

Next, we investigated the nucleoskeletal protein lamin A. Representative confocal images, bar graphs of measured fluorescence and radial profile can be found in Figure 5.13.

Overall levels as measured by immunofluorescence do not appear to be significantly affected by either island size or *Plec* KO, albeit a small non-significant increment in *Plec* KO cells compared to WT can be visually appreciated. Analysis of radial distribution revealed that *Plec* WT cells behaved similarly to primary HKs, with cells grown on small islands displaying a higher distribution near the nuclear periphery compared to cells grown on large islands which had a more disperse distribution. In contrast, *Plec* KO cells showed a more disperse distribution for both island sizes. It is interesting to note that these variations in lamin A radial distribution seem to scale with nuclear volume, but moreover we believe that increased tension onto the nuclear

envelope from the upregulated actin cytoskeleton as generated by the KO of plectin could be behind the reduction of peripheral lamin A.

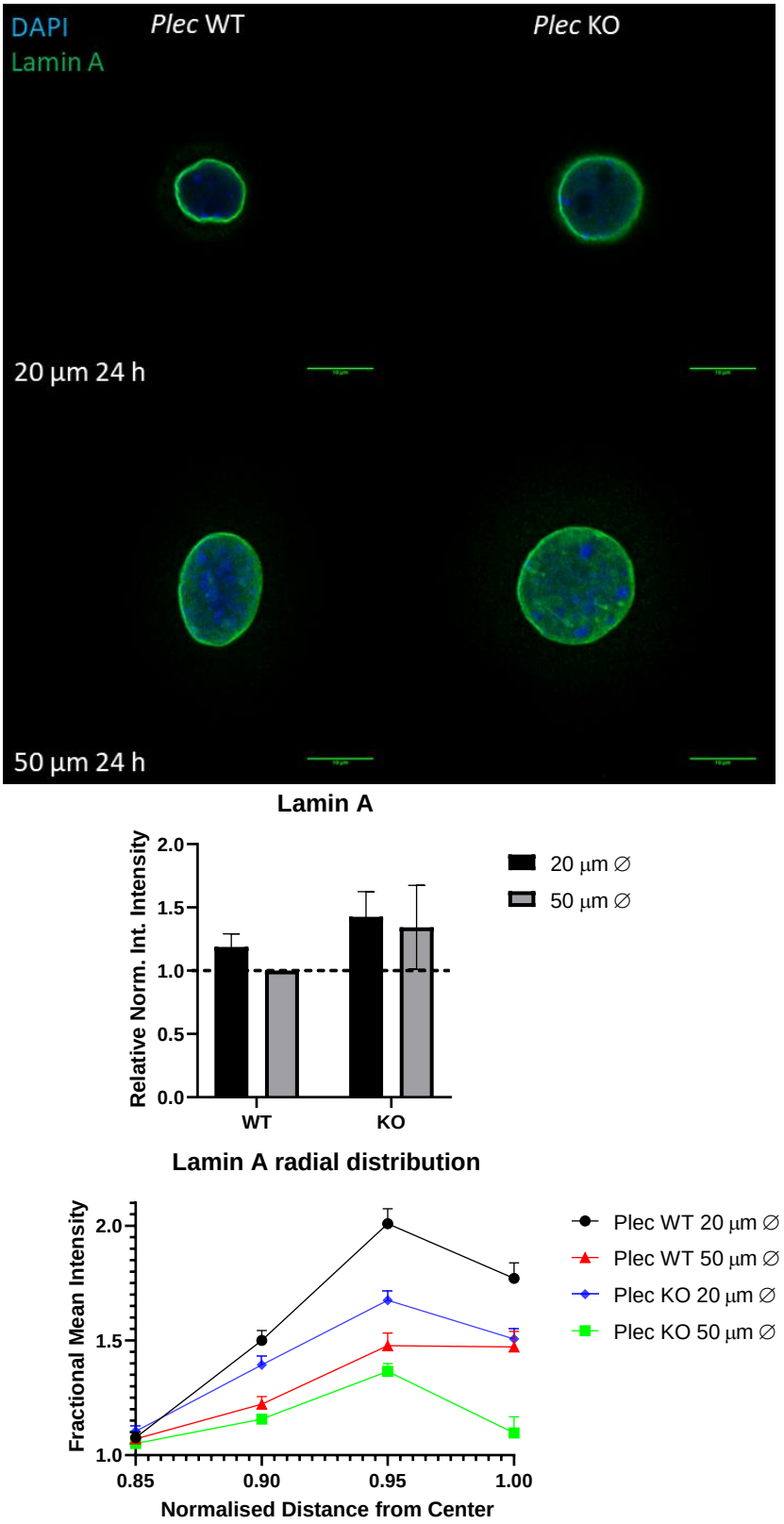

Figure 5.13. ***Top***: *Representative confocal images of* Plec *WT versus* Plec *KO mouse keratinocytes seeded on micropatterned islands after 24 hours labelled for DAPI and lamin A. Scale bar = 10 µm.* ***Center:*** *Bar graph of Lamin A relative immunofluorescence integrated intensities. Shown as mean + S.E.M. N = 3 experiments.* ***Bottom:*** *Radial distribution of lamin A plotted as radial mean fractional intensity: values over 1 indicate a higher than average fluorescence intensity and vice versa. N = 3 experiments.*

Nucleoli number

As observed changes in nuclear morphology should correlate with changes in nucleoli number, average number of nucleoli per cell was measured next. Bar graph summary can be found in Figure 5.14. A significant increase in nucleoli number was observed for *Plec* KO cells compared to WT for both island sizes. Similarly to previous results, larger islands exhibited a larger number of nucleoli compared to smaller ones. As theorised these results indicate that nucleoli number appear to scale with nuclear volume.

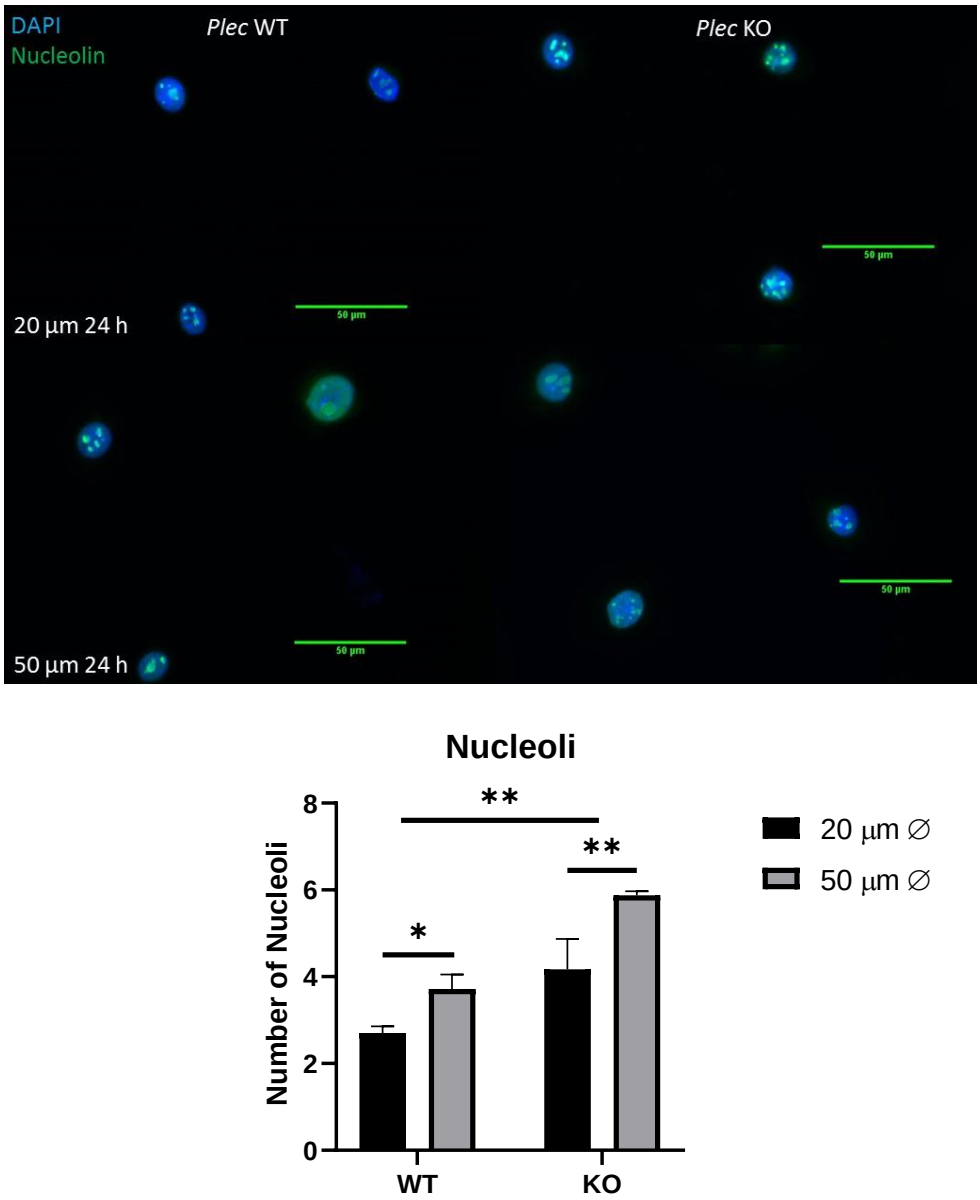

Figure 5.14. Top: *Representative epifluorescence microscopy images of* Plec *WT and* Plec *KO keratinocytes grown on micropatterned surfaces stained for DAPI and Nucleolin.* ***Bottom:*** *Bar graph of nucleoli number of WT versus* Plec *KO cells. Shown as mean + S.E.M. N= 3 experiments. *: p-value<0.05. **: p-value<0.01 (2-Way ANOVA, Tukey multiple comparisons test).*

Protein synthesis

To further explore the link between nuclear volume, nucleoli number and translational capabilities, de novo protein synthesis levels were acquired as previously done. Bar graph of measured normalised fluorescence intensities are summarised in Figure 5.15.

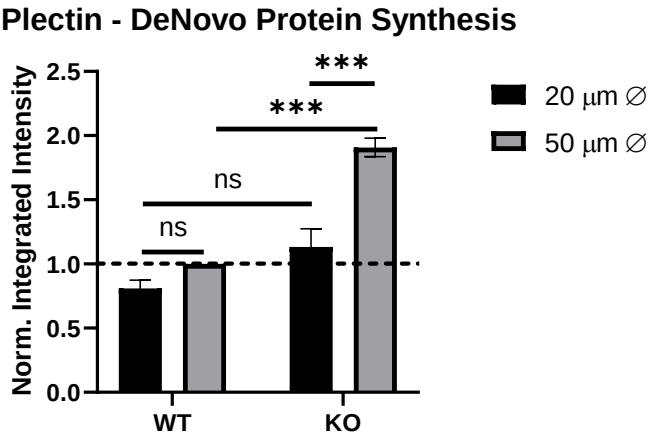

Figure 5.15. *Bar graph of normalised integrated intensity measurements of epifluorescence microscopy images of nascent proteins of* Plec *WT versus* Plec *KO cells grown on micropatterned surfaces. N = 3 experiments. n.s: non-significant. ***: p-value < 0.001 (2-Way ANOVA, Tukey multiple comparisons test).*

Plec WT cells behaved similarly to the previously observed trends in primary keratinocytes, with cells grown on small islands showing reduced protein synthesis levels, albeit differences were not significant. *Plec* KO cells followed a similar trend, but differences between island size were significant. 2-way ANOVA confirmed island size to be a significant source of variation. While differences between WT and KO cells grown on small islands were not significant, an increment could be visually appreciated. *Plec* KO cells grown on large islands in contrast had significantly larger levels of nascent proteins compared to all conditions. As expected, 2-way ANOVA also indicated *Plec* KO to be a significant source of variation. These results appear to scale with nucleoli number and with nuclear volume.

Ribogenesis genes expression

We then questioned if ribogenesis genes were being affected as previously observed in HK primary cells. We investigated this by performing qPCR on pre-ribosomal RNA 45S, Nucleolin, RPL36 and RRP1B. Bar graph of the relative expression levels can be found in Figure 5.16.

qPCR revealed no significant changes across conditions nor island sizes, but trends could be appreciated. Indeed, we observe a non-significant increase of pre-ribosomal RNA 45S on both island sizes for *Plec* KO cells compared to WT. Similarly, RRP1B expression appears to be non-significantly increased for KO cells compared to WT. Both Nucleolin and RPL36 remain comparatively unchanged. Unfortunately, these results do not allow to extract a clear link between pre-ribosomal RNA, ribogenesis effectors and nuclear volume. Moreover, they might indicate a limitation of working with *Plec* KO cells. Indeed, NCL, RPL36 and RRP1B were chosen from the previous RNA sequencing data done on primary human keratinocytes. *Plec* KO cells are also p53-null, which has potentially chromatin-organisation effects that could hinder the expected biophysical response. Nevertheless, we will note a non-significant increment in 45S pre-ribosomal RNA, in accordance with our hypothesis.

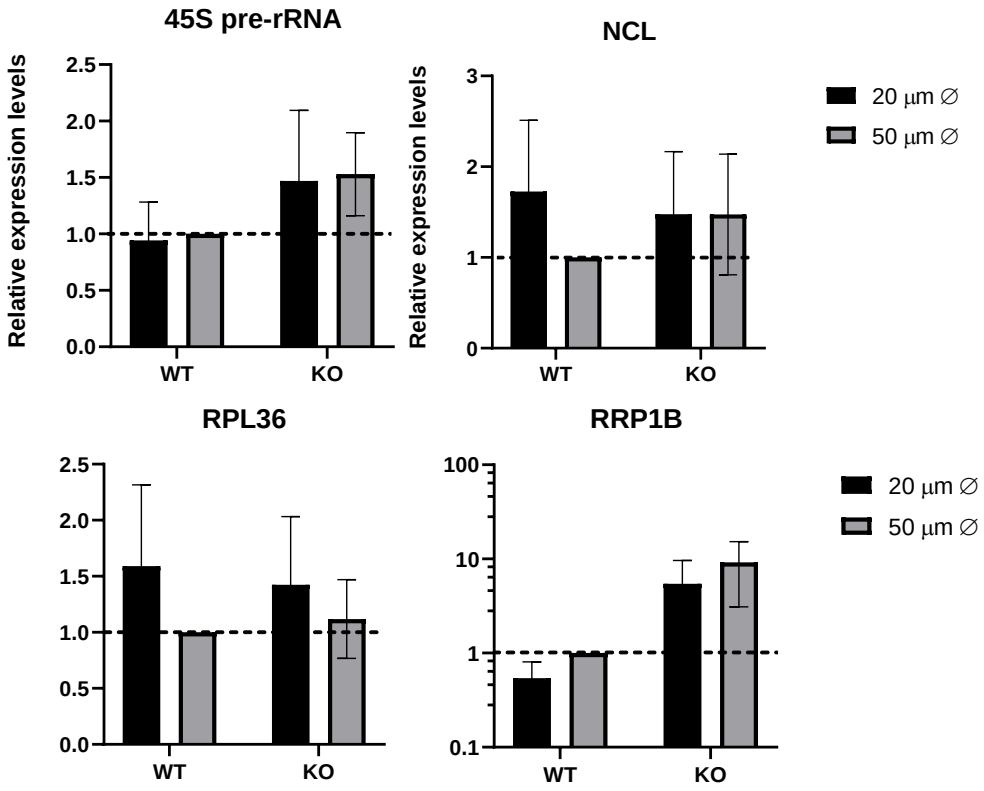

Figure 5.16. *Bar graph of relative expression levels of 45S pre-ribosomal RNA (top left), Nucleolin (top right), Ribosomal Protein Large 36 (bottom left) and Ribogenesis Regulating Protein 1B (bottom right) of WT versus Plec KO cells grown on micropatterned surfaces as evaluated by qPCR. All genes were normalised to 7SK transcript levels. Shown as mean + S.E.M, N = 3 experiments.*

Perturbation of nucleoskeletal proteins

Nuclear morphology

The final set of studies used siRNA to knockdown (KD) LMNA and SYNE genes, which code for lamin A/C and nesprin 2, respectively. Lamin A/C serves both as the principal component of mechanical integrity of the nucleus in keratinocytes as well as an anchorage point for chromatin. LMNA KD was predicted to induce higher deformability of the nucleus as well as disconnection of the chromatin from the nuclear lamina, perturbing force transmission to it. Nesprin 2 serves as one of the main extranuclear components of the LINC, linking the F-actin network to the nucleus. SYNE2 KD would then see a disconnection of the nucleus from the cytoskeleton and perturb force transmission to it while leaving its mechanical integrity untouched. Comparative analysis of both data should reveal specific facets of force transmission to the nucleus.

HKs were transfected with SYNE2, LMNA or non-targeting siRNAs 72 and 48 hours before seeding upon micropatterned islands. 24 hours after seeding they were fixed and immunolabeled. Subsequently they were imaged using confocal microscopy allowing us to measure changes in nuclear morphology. Analysis of protein levels by Western Blot and bar graph summary of measured nuclear volumes after siRNA treatment can be found in Figure 5.17.

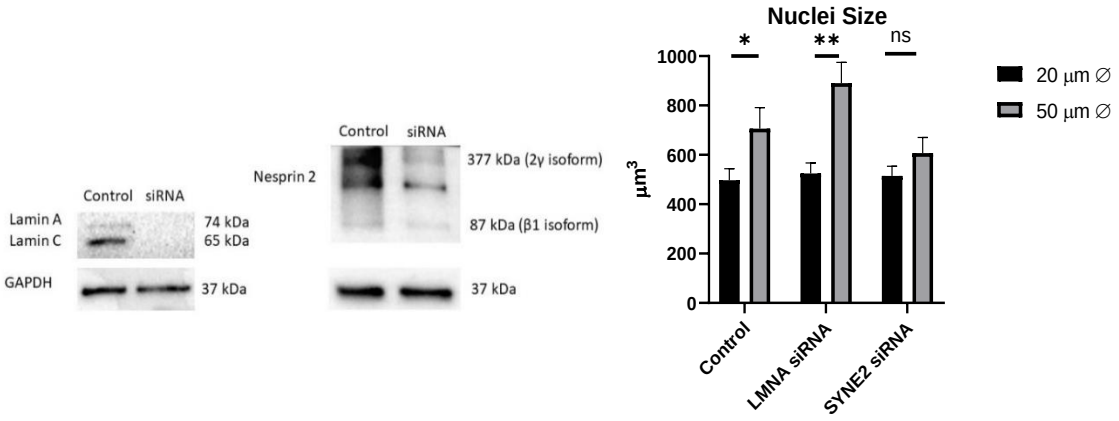

Figure 5.17. *Left: Western blot of lamin A/C and Nesprin II after siRNA treatment of HKs compared to control nonspecific siRNA. Right: Bar graph of nuclear volumes of HKs grown on micropatterns after siRNA treatment. Shown as mean + S.E.M. N= 3 experiments. ns: non-significant. *: p-value < 0.05. **: p-value < 0.01 (2-Way ANOVA, Sidak multiple comparisons test).*

As can be observed, siRNA treatment had significant effect on protein levels. LMNA KD was accompanied with a reduction in both lamin A and C isoforms. SYNE2 KD saw mainly a reduction in nesprin 2 2γ isoform, which is mainly located at the nuclear envelope[402].

While nuclear volume was unperturbed on small islands siRNA KD significantly altered nuclear morphology in spread cells on large islands. Compared to non-targeting controls, HKs grown on large islands treated with LMNA siRNA have larger nuclear volumes, while those treated with SYNE2 siRNA are smaller, like those of smaller islands. This finding suggests tensive forces from the F-actin cytoskeleton expand the nucleus on large islands, and disconnection from the cytoskeleton by SYNE2 KD reduces nuclear volume. Inversely, LMNA KD disrupts the primary structural component of the nucleus, making it more susceptible to deformation.

H3K27Ac and H3K9me3

Overall levels

We next interrogated if the disruption in force transmission and subsequent changes in nuclear morphology would have an effect in overall chromatin marker levels of H3K27Ac and H3K9me3. Representative confocal images and bar graph summary of relative integrated intensity measurements are shown in Figure 5.18.

The foremost characteristic that we can observe from fluorescence intensity measurements is that both closed and open chromatin markers are upregulated on both siRNA treatments. 2-way ANOVA revealed siRNA to be the only significant source of variation for both markers, while interestingly island size was not. Moreover, only LMNA siRNA-treated cells had individual values

which differed significantly from non-targeting siRNA. It is interesting to note that the response of both chromatin markers appears to be uncoupled from nuclear volume regulation.

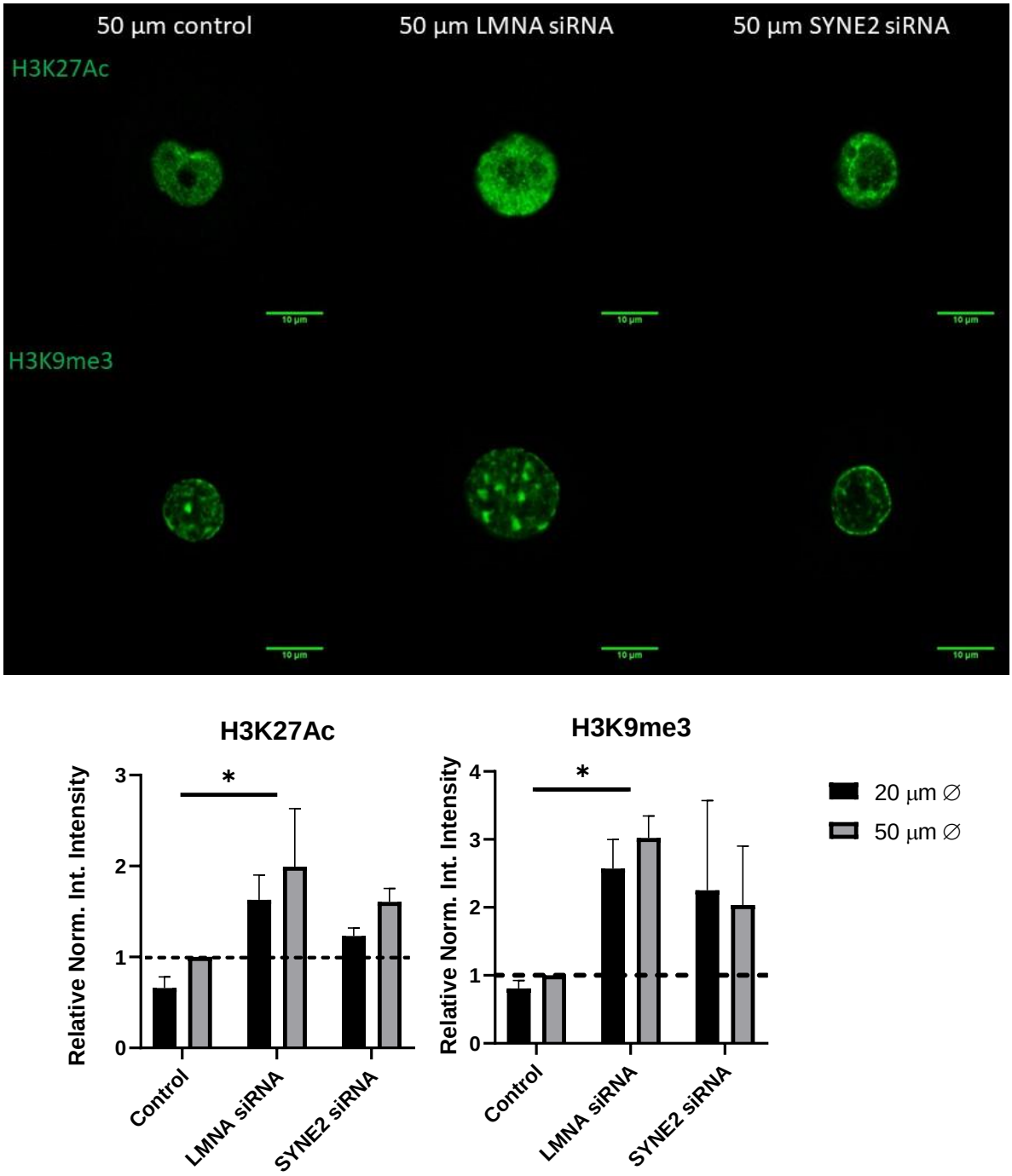

Figure 5.18. Top: *representative confocal images of HKs grown on 50 µm micropatterned islands after 24 hours immunolabelled for open chromatin marker H3K27Ac and close chromatin marker H3K9me3. Scale bar = 10 µm.* ***Bottom:*** *bar graph of relative normalised integrated intensity of H3K27Ac (left) and H3K9me3 (right). Shown as mean + S.E.M. N = 3 experiments. *: p-value < 0.05 (2-Way ANOVA, Sidak multiple comparisons test).*

We then expanded our analysis of heterochromatin marker H3K9me3 by investigating their association into foci as previously done. Bar graph summary of foci number and area can be found in Figure 5.19.

HKs treated with non-targeting siRNA behaved similarly as reported in Chapter 3. Both hetero and euchromatin foci were significantly less numerous on small islands compared to larger ones. They also appeared to be smaller, albeit not significantly. This trend was also similar for LMNA siRNA-treated cells. HKs treated with SYNE2 siRNA had indistinguishable foci number and foci size across island size. Unlike chromatin marker overall levels H3K9me3 foci number appears to be correlated with nuclear volume.

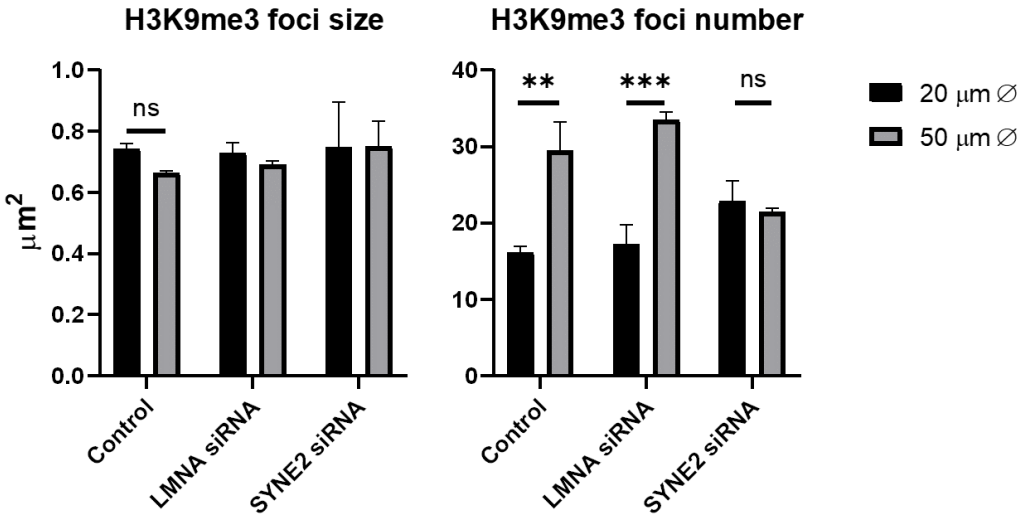

Figure 5.19. *Analysis of foci number and size of H3K9me3 of HKs treated with control, LMNA and SYNE2 siRNA and grown on micropatterned surfaces. Shown as mean + S.E.M, N = 3 experiments. n.s: non-significant. **: p-value<0.01. ***: p-value<0.001 (2-Way ANOVA, Sidak multiple comparisons test).*

We next investigated how lamin A/C levels and radial distribution could be affected by SYNE2 KD. We expected SYNE2 KD to induce a similar lamin A/C profile on 50 µm islands compared to 20 µm. Representative confocal images and bar graph summary of immunofluorescence intensity measurements can be found in Figure 5.20. Radial distribution plots can be found in figure 5.21.

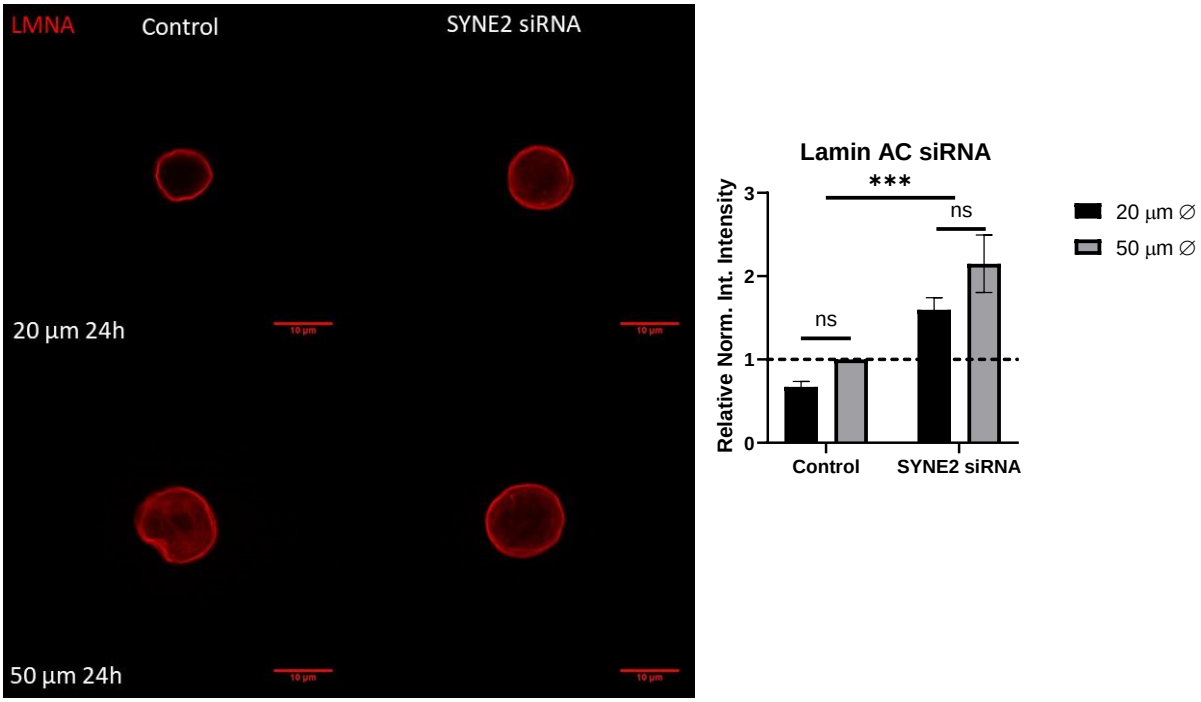

Figure 5.20. Left: *representative confocal images of HKs treated with control and SYNE2 siRNA grown on 50 and 20 µm micropatterned islands after 24 hours immunolabelled for lamin A/C. Scale bar = 10 µm.* ***Right:*** *bar graph of relative normalised integrated intensity of lamin A/C. Shown as mean + S.E.M. N = 3 experiments. n.s: non-significant. ***: p-value < 0.001 (2-Way ANOVA, Tukey multiple comparisons test).*

Unexpectedly, an upregulation of lamin A/C can be observed in HKs treated with nesprin 2 siRNA for both island sizes at 24 hours. We theorise that the upregulation of lamin levels may be a compensation mechanism to reinforce mechanical integrity of the nucleus.

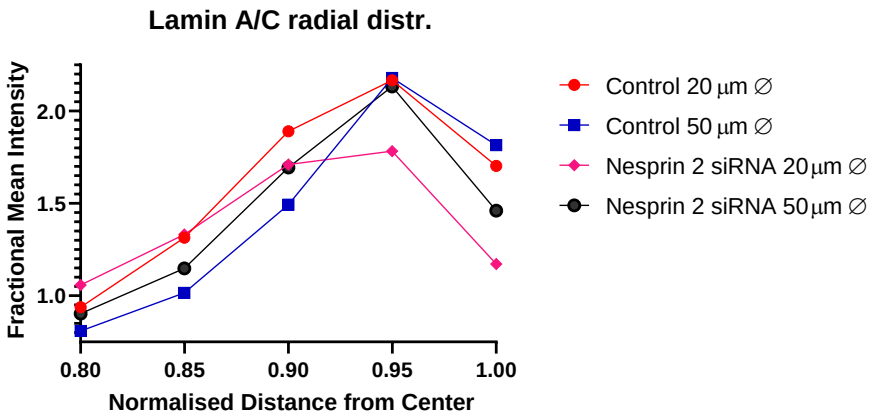

Figure 5.21. *Radial distribution of lamin A/C plotted as radial mean fractional intensity: values over 1 indicate a higher than average fluorescence intensity and vice versa. n>50 cells per condition, N=3 experiments.*

Initial observation of lamin A/C radial distribution does not reveal major differences between island size in non-targeting siRNA treated cells. Similarly, SYNE2 siRNA treated HKs do not exhibit major differences in lamin A/C radial profile, albeit a slight downregulation towards the nuclear periphery can be observed. Nevertheless, SYNE2 siRNA does not appear to have major effects on lamin A/C radial distribution.

Nucleoli number

The next set of studies investigated the role of lamin A/C and nesprin 2 in the regulation of nucleolar morphology. Nucleoli number was analysed using confocal imaging of HKs immunostained for nucleolin. Representative images can be found in Figure 5.22 and the bar graph summary can be found in Figure 5.23.

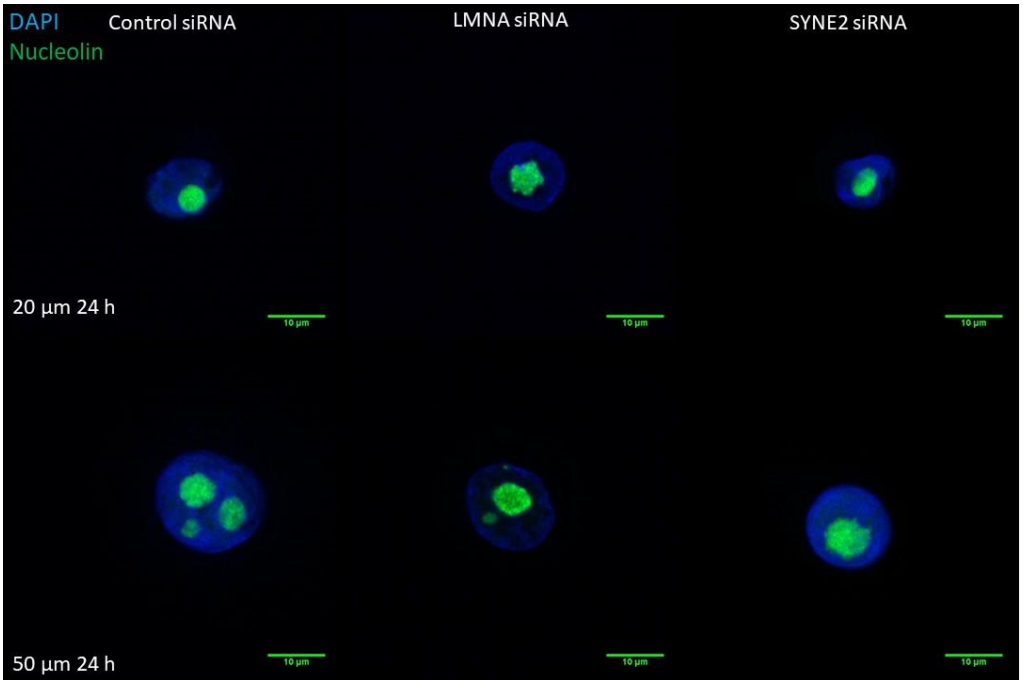

Figure 5.22. *Representative confocal images of HKs treated with control, LMNA and SYNE2 siRNA grown on 50 and 20 µm micropatterned islands after 24 hours immunolabelled for Nucleolin. Scale bar = 10 µm.*

HKs treated with control siRNA behaved similarly to previous measures with HKs growing on small islands exhibiting significantly smaller number of nucleoli. Nucleoli number was significantly reduced in HKs treated with SYNE2 siRNA on 50 µm islands and like the number of nucleoli on 20 µm islands. In contrast LMNA siRNA treatment did not affect nucleoli number. As expected, it appears that nucleoli number correlates with nuclear volume.

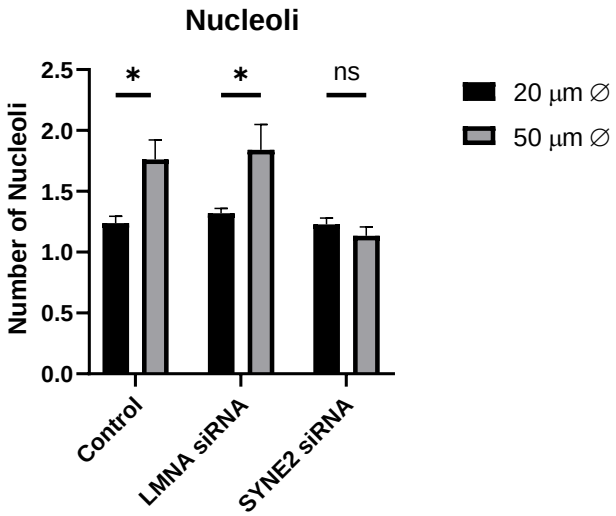

Figure 5.23. *Bar graph of nucleoli number. Shown as mean + S.E.M. n > 60 cells for each condition, N = 3 experiments. n.s: non-significant. *: p-value<0.05. (2-Way ANOVA, Sidak multiple comparisons test).*

Ribogenesis genes expression and protein synthesis

Following the previous results, we investigated if KD of nesprin 2 and its subsequent effects on nuclear volume and nucleoli number could potentially affect ribogenesis and translation. Changes in transcript levels of 47S pre-ribosomal RNA, NCL, RPL36 and RRP1B were first quantified. Bar graph summary of relative transcripts levels can be found in Figure 5.24.

47S pre-ribosomal RNA showed significant differences between island sizes for control siRNA in accordance with previous data. But interestingly differences between island size disappeared after treatment with SYNE2 siRNA, both being at an intermediary expression level. As expected, a 2-way ANOVA indicated the interaction to be a significant source of variance. Similarly to *Plec* KO, nesprin 2 KD by siRNA did not appear to have significant effects on expression levels of ribogenesis effectors NCL and RPL36. RRP1B had no significant differences between island sizes, albeit a slight downregulation of expression levels could be appreciated on small islands compared to large. More importantly, SYNE2 siRNA-treated cells appeared to have lower expression levels than control, and a 2-way ANOVA indicated SYNE2 siRNA treatment to have a significant effect on RRP1B expression. Taken with the previous *Plec* KO data, these results indicate that nuclear morphology may have quantifiable effect on pre-ribosomal RNA and RRP1B but not NCL and RPL36.

To further this analysis, changes in nascent protein levels were quantified as previously done. Bar graph summary of measured fluorescent intensities can be found in Figure 5.25.

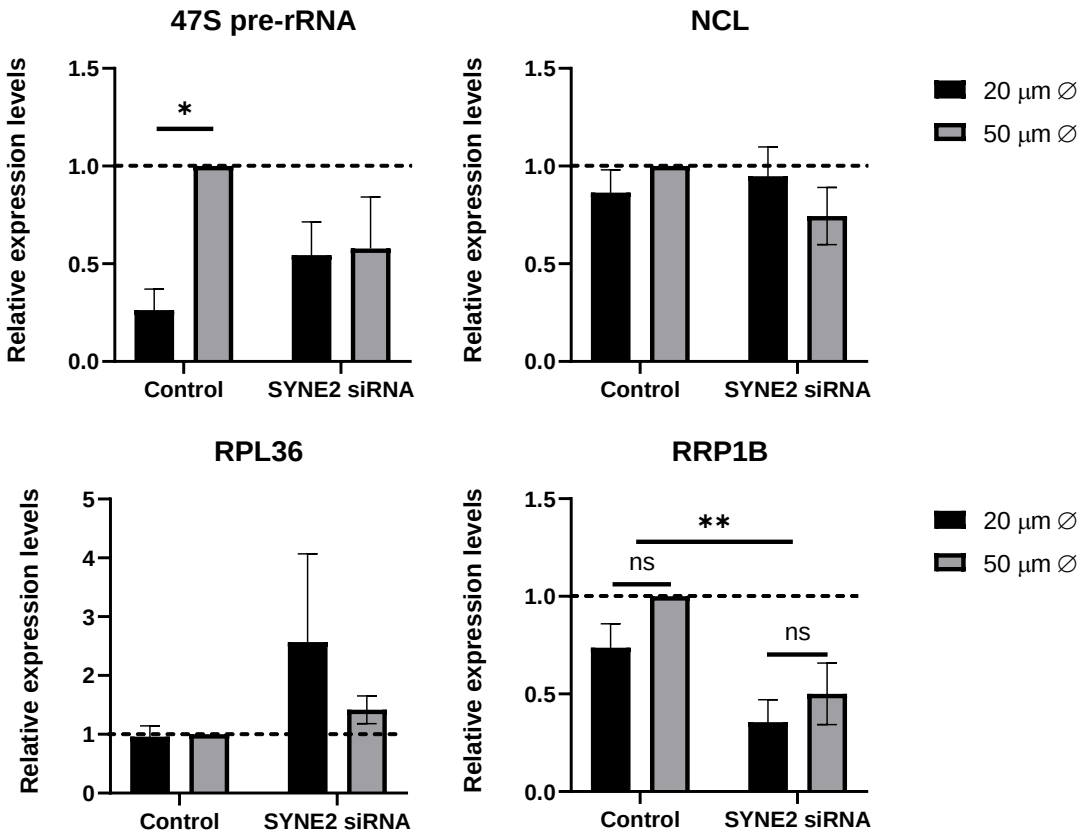

Figure 5.24. *Bar graph of relative expression levels of 47S pre-ribosomal RNA (top left), Nucleolin (top right), Ribosomal Protein Large 36 (bottom left) and Ribogenesis Regulating Protein 1B (bottom right) of control versus SYNE2 siRNA-treated cells grown on micropatterned surfaces as evaluated by qPCR. All genes were normalised to 7SK transcript levels. Shown as mean + S.E.M, N = 4 experiments. n.s: non-significant. *: p-value<0.05. **: p-value<0.01. (2-Way ANOVA, Tukeys multiple comparisons test).*

Non-targeting siRNA-treated cells showed a significant reduction of nascent protein levels on small islands compared to large islands in accordance with previous results. SYNE2 siRNA treatment had no significant effect on cells grown on 20 μm islands compared to control conditions. But interestingly a significant decrease was perceived in SYNE2 siRNA-treated cells grown on large islands compared to control, while still being significantly higher than cells grown

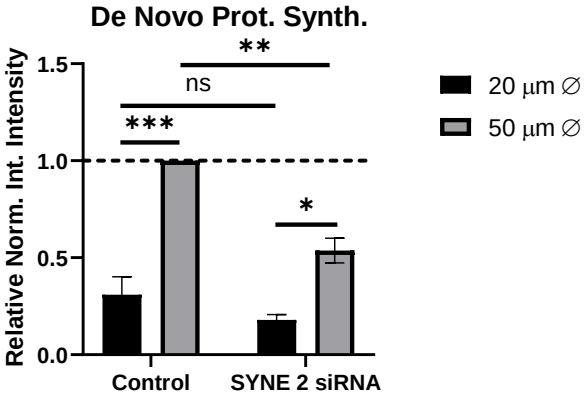

Figure 5.25. *Bar graph of normalised integrated intensity measurements of epifluorescence microscopy images of nascent proteins of control versus SYNE2 siRNA-treated cells grown on micropatterned surfaces. N = 3 experiments. n.s: non-significant. *: p-value < 0.05 **: p-value < 0.01 ***: p-value < 0.001 (2-Way ANOVA, Tukey multiple comparisons test).*

on small islands. These results indicate that the effect of SYNE2 siRNA treatment on translational capabilities of cells scales with its effect on nuclear size, albeit not completely.

Discussion

In this chapter we investigated the role of key components of the cytoskeleton and nucleoskeleton in the regulation of nuclear morphology, chromatin architecture and translation using small molecule inhibitors and genetic methods. Overall, we found that nucleoli number scale with nuclear volume, and that this appears to have direct effects on translation as seen by changes in protein synthesis levels and ribogenesis genes expression. Heterochromatin marker H3K9me3 inversely scaled with nuclear volume, while euchromatin marker H3K27Ac was mainly upregulated after nucleoskeletal or actin perturbation. Finally, Lamin A/C radial distribution was affected by perturbations that targeted the F-actin network. Altogether, while confirming that correct mechanical integration of the nucleus in the cytoskeleton is a key modulator of nuclear architecture with gene transcription and translation effects, direct causational links that explain these phenomena are still to be found.

Our initial approach consisted of using Blebbistatin and Y-27632 to perturb actin network formation and mechanics. Unfortunately, this strategy did not yield expected results: nuclear morphology was not significantly changed, and changes in H3K27Ac marker as well as lamin A/C were minimal. Indeed, H3K27Ac hinted at a slight upregulation. Lamin A/C levels were similar if downregulated. Its radial distribution did show a reduction towards the nuclear periphery for HKs grown on 20 µm islands. Overall, albeit striking changes in actin cytoskeleton organisation could be observed upon treatment of HKs with both inhibitors, little perturbation of tension to the nucleus was perceived by measuring our set of nuclear architecture factors. This either puts into question the general role of the actin cytoskeleton in the modulation of nuclear architecture in our model or raises doubts about how effective is perturbing it using these cytoskeletal inhibitors. There might be some compensation mechanisms that would minimize their action, but other approaches such as use of stronger inhibitors (e.g latrunculin) or translational suppression with siRNA would yield a better perturbation which would answer these questions. There is also the possibility that focusing our investigation solely on the 24-hour timepoint we might be missing temporal responses which could happen at an earlier time point.

Our second strategy, using overexpression of keratin 14 with a dominant mutation, did not heed expected results. Nuclear volume changes were not significant between island size nor keratin WT and mutated form, indicating that possibly the cell line had incompressible nuclei. H3K9me3 marker intensity levels were also unaffected. Interestingly enough, we reported larger differences in nuclear volumes between island sizes for cells which expressed the mutated form, and this was translated in a similar trend for nucleoli number, further cementing the notion that

both characteristics are intrinsically linked. Regarding lamin A/C levels, a slight increase could be observed for large islands. While a formation of aggregates of keratin 14 was clearly visible for cells stably infected with the mutated form, this was not the case for all cells, and levels varied across samples. This puts in doubt how effective transfecting a defective keratin is in perturbing the native keratin cytoskeleton, which still contains fully functional keratin 14. A genetic editing of the keratin gene, or better yet using Dowling-Meara patient samples, may show better results, and this is a potential tool to develop in future studies.

Our third approach consisted of using mouse keratinocytes, which had a total knockout of plectin, a multi-functional cytolinker. *Plec* KO generates cells with higher actin levels as well as more mature focal adhesions, which we believe result in elevated intracellular tension on the nucleus[403]. Simultaneously, loss of linkage between the F-actin and keratin cytoskeleton is thought to perturb the stability of the perinuclear keratin cage. This consequently generates more deformable and larger nuclei[221], as could be appreciated in our model too. Regarding chromatin markers there was minimal effect on H3K27Ac levels, but a significant downregulation on H3K9me3 levels. This is consistent with previous reports that higher tension on the nucleus results in drops in heterochromatin marker levels as a way for chromatin to better disperse mechanical tension to avoid DNA damage[383]. A significant increment in nucleoli number was observed, as expected of larger nuclei. As theorised in the previous chapter, we further investigated if these changes in nuclear volume and nucleoli number had effects on translational capabilities and ribogenesis pathway. We found that indeed incremented nuclear volume and nucleoli number correlate with higher de novo protein synthesis levels, albeit we could not directly link this to incremented pre-rRNA levels nor ribogenesis effectors which did not vary in a significant way. Considering that both pre-rRNA and ribogenesis effectors were selected from previous studies involving primary HK, perhaps this perceived discrepancy originates from an incorrect choice of transcripts to measure. A general downregulation of heterochromatin as seen by reduced H3K9me3 levels could also induce elevated transcriptional levels. A more robust and complete measure, such as with RNA sequencing and other chromatin markers, would help shed light into this phenomenon.

The final perturbation strategy consisted in the use of siRNA to transcriptionally silence lamin A/C and nesprin 2. Lamin A/C silencing would theoretically help disconnect part of the chromatin from the nuclear lamina and LADS and thus hinder mechanotransduction to the chromatin while allowing nuclear changes in morphology[404]. On the other hand, nesprin 2 silencing would allow the whole nucleus to be disconnected. When nuclear volumes were measured changes in nuclear morphology were observed for SYNE2 siRNA treated HKs but not for LMNA. Interestingly these changes saw nuclei on large islands shrink to a similar size of those of small islands, which

can be explained by the loss of tension from the actin cytoskeleton exerted on the nucleus. Why such a change is not seen on smaller islands is debatable. One reason might be that the HKs have reached a minimal nuclear size upon which further compaction is not possible. Another reasoning is that reduced available adhesive space, upon which focal adhesions are built, reduces the possible tangential "pulling points" on the nucleus, thus explaining why nuclei are smaller on smaller islands. In that direction of thought then, removing the actin anchoring to the nucleus would do little to reduce its volume further. Similarly, knockdown of lamin A/C, the major mediator in regulating structural integrity of the nucleus would have had effects on its nuclear volume, but we only observed a slight increment in 50 µm island nuclei. This could also be due to the need of a large adhesive space to create a tangential tensive force upon the nucleus, and thus a more deformable nuclei would enlarge. Potentially also, other unknown mechanisms involving chromatin as a regulator of nuclear architecture might be at play.

Interestingly, while nesprin 2 connects the LINC with the actin cytoskeleton, our selection of F-actin inhibitors did not appear to generate similar results regarding nuclear volume (or the rest of measured parameters for that matter). Perhaps this is indicative that the severity of the perturbation using cytoskeletal inhibitors was not enough to induce measurable changes. As indicated before, other strategies to disrupt the F-actin network would have to be investigated to better assess its role in our model.

We observed then that in both siRNA treatments both open and close chromatin markers H3K27Ac and H3K9me3 respectively were upregulated in all island sizes, and more so in LMNA siRNA treated ones. Recent studies have shown that heterochromatin downregulation can happen because of compressive forces exerted on the cell, and that this is in part modulated by the mechanical resistance of the nucleus[383]. In the first chapter of results we hypothesised that this could be the reason behind downregulation chromatin markers in small islands. Here we see that the opposite, i.e perturbing nuclear mechanical integration into the cytoskeleton or its mechanical integrity, results in elevated heterochromatin marker levels. What is intriguing is the fact that H3K27Ac behaves similarly, which is counterintuitive to the concept that close chromatin markers are reduced to give chromatin more deformability. Furthermore, we observed elevated levels of lamin A/C in SYNE2 siRNA treated cells which could increment nuclear mechanical rigidity. This dual response could be the reason behind why SYNE2 siRNA treatment sees a lower increment in chromatin marker levels.

When characterising chromatin foci and nucleoli we observed that nuclear size correlates with heterochromatin foci number and size as well as nucleoli number, as it was apparent from similar size of all nuclei in SYNE2 siRNA-treated HKs. As previously observed euchromatin markers did react but to a lesser extent. Taken together with the *Plec* KO data on nucleoli, these

findings suggest that nucleoli number scales directly with nuclear size. Considering that nucleoli are delimited by phase-separation[172] and possess Brownian motion[174], these results were expected. Heterochromatin-promoting proteins such as HP1 have shown phase-separation properties[405,406], which could potentially also explain the perceived coalescence of heterochromatin foci.

Finally, we observed that nascent protein levels correlated with nuclear size. In parallel, a change in pre-ribosomal RNA 47S and RRP1B levels was perceived, hinting that the changes in translational capability are linked to a perturbed ribogenesis. Ribosomal RNA is produced in nucleoli, and so that their levels is scalable with nucleolar number, and in our model nuclear volume, was to be expected. We know also that nucleolar size, number and activity is regulated by the proteins and RNA that composes it[174,407], and changes in their concentration, as could arise from changes in nuclear volume, could potentially affect nucleolar dynamics. While we expected pre-ribosomal RNA levels to be affected by changes in nucleolar numbers, it is very interesting to note that at least one protein (RRP1B) transcriptional levels appear to be scalable with nuclear volume. As with *Plec* KO studies the selection of ribogenesis effectors and ribosomal proteins whose transcripts were measured was limited. A more thorough investigation could unveil more direct links between nuclear size and ribogenesis. As before we also note that these measures are proxy measures of actual ribosome levels, which were technically not possible under the scope of this project, but if done would better answer important questions that stem off this research.

One important aspect of what has been observed in this chapter is the difference between changes to nuclear architecture that stem off changes in nuclear size, and changes that come from force transmission to the nucleus. While both of the phenomenon are intrinsically linked (i.e the nucleus changes size because of the forces that are exerted on it), we must separate changes in chromatin configuration such as nucleoli or heterochromatin foci fusing which come from altered nuclear volume, from changes such as chromatin marker levels, which could come from force transmission to the chromatin. Indeed, nucleoli, and we believe heterochromatin foci, form by phase separation and thus their fusing mechanics are governed by nuclear volume but are inherently mechano-irresponsive, which can be seen by their lack of reactivity to cytoskeletal and nucleoskeletal inhibitors. On the other hand, chromatin markers and lamin radial distribution respond to mechanical stimuli as well as perturbation of the mechanosensing pathways.

It is interesting to note that most perturbations reduced nuclear size and saw upregulated chromatin markers, while *Plec* KO, which incremented nuclear size, saw a drop in heterochromatin marker H3K9me3. This could possibly point at a directionality of forces exerted

upon the nucleus. We saw most perturbations decrease the tension of the actin cytoskeleton on the nucleus thus allowing other forces, such as the one generated by the nucleoskeleton or perhaps the keratin perinuclear cage, to shrink the nucleus. At the same time, this disconnection from the actin cytoskeleton would be expected to affect the potential of the nucleus as a mechanosensing unit, as it is less integrated in the cytoskeleton, and perhaps is the reason behind a dysregulation of H3K9me3 levels. Inversely, *Plec* KO which theoretically sees an increment in actin levels as well as a perturbation of perinuclear keratin resulted in elevated nuclear volume and downregulation of heterochromatin marker H3K9me3, found in recent research to be a response of HKs to extracellular biophysical cues[383]. But we must keep in mind other possible explanations, such as variations in soluble actin fraction, which could potentially also affect nuclear actin which is known to have effects on chromatin[319], and moreover H3K9me3 levels[408]. It is also possible that nesprin 2 KD could see upregulation of other nesprins such as nesprin 3, which also links with plectin and the IF network and could have possible chromatin remodelling effects unknown to us. KO of nesprin 2 has also been shown to reduce HK proliferation[409], and possibly has effects on differentiation too, which as we know bring their own changes to chromatin architecture. More complete future studies will have to further dissect the complex relationship between nuclear volume, mechanosensing and chromatin architecture to paint a clearer picture.

In this final chapter we have successfully employed several approaches at perturbing components involved in force transmission to the nucleus and chromatin by systematically destabilising cyto- and nucleoskeletal components. We observed the effect of these perturbations on previously measured characteristics of nuclear compaction due to reduced available adhesive space on HKs as well as other cell types. This permitted to obtain insights into how mechanical integration of the nucleus affects its role as a central mechanosensing unit of the cell in the context of nuclear and chromatin architecture.

Chapter 6: Discussion

This project has aimed to uncover how external biophysical cues influenced human keratinocyte nuclear architecture. Furthermore, it aimed at understanding the role of cytoskeletal and nucleoskeletal mediators in nuclear mechanosensing as well as describing the downstream phenotypic impact on cell function.

To achieve this, single HKs available adhesive space was modulated using micropatterned surfaces. This in vitro model permitted the generation of a simple and homogenous biophysical cue on single cells. HKs grown on small, 20 µm diameter islands, adopted a rounded morphology while cells grown on larger, 50 µm diameter islands were more spread and flattened. This was translated into modified nuclear morphology; round cells had smaller nuclei and spread cells had larger nuclei. Interestingly, this morphological change had clear effects on HK differentiation as about half of primary HKs grown on small islands entered terminal differentiation after 24 hours, unlike their spread counterparts which remained largely undifferentiated.

Based on these observations, this project set out to investigate how HK reduced nuclear size as induced by limited available adhesive area affected its nuclear architecture and phenotype through three distinct aims. The first aim set out to acquire general characteristics of macroscopic nuclear architecture differences between spread and rounded HKs. The second focused on gene-specific differences by means of transcriptome profiling and subsequent analysis of affected pathways. Finally, the third aim investigated the roles of the cytoskeletal and nucleoskeletal networks in the regulation of HK nuclear architecture by perturbing selected cytoskeletal and nucleoskeletal mediators. Each of these separate aims constituted separate chapters of results in this thesis.

In the first results chapter (Chapter 3), we initially confirmed that HKs grown on 20 µm diameter micropatterned islands have smaller nuclear volume and enter terminal differentiation after 24 hours compared to HKs grown on 50 µm islands, as previously reported[193,221]. Next, heterochromatin markers H3K27me3 and H3K9me3 as well as euchromatin markers H3K27Ac and H3K4me3 were investigated. HKs grown on small islands saw a downregulation of H3K27me3, H3K27Ac and H3K9me3 but not H3K4me3 after 24 hours compared to large islands. Downregulation of histone acetylation had also been previously described in this model[221].

To investigate differences between differentiating and non-differentiating cells segregation of HKs based on their TGM1 levels was performed but no significant differences in H3K27me3 and H3K27Ac levels was found. Considering that HK differentiation has been shown to influence chromatin architecture at the gene level[16] this was unexpected. This could be indicative of nuclear size being more deterministic of chromatin architecture compared to differentiation. Perhaps it could also be caused by a delay between initiation of terminal differentiation and

chromatin marker changes which are not apparent at the timepoints that were considered. Moreover, changes in chromatin markers are often gene-specific, and lack of overall changes do not necessarily mean lack of specific changes at differentiation-associated genes. More gene specific techniques such as ChIPseq would shed light into how cell and nuclear morphology could potentially impact transcription. Unfortunately for this set of studies ChIPseq was not a possible choice due to the low amount of cells per micropatterns.

As most measured differences indicated downregulation of chromatin marker on small islands, total levels of histone 3 were quantified. A non-statistically significant downregulation of total histone 3 levels in small islands was observed. This could partly explain the previously observed downregulation of chromatin markers. These results provide proof that cell and nuclear morphological changes induce a response by chromatin markers levels. They also underline how analysis of global changes in histone PTMs is a very limited tool as these changes are often gene and context specific, and thus do not provide valuable information about gene regulation. Similarly, they also exemplify best one of the main drawbacks of a multitude of experiments here presented; low N numbers. Indeed, a higher statistical size would have helped properly assess the trends that were observed here and in other sections of this work. A power series would have best allowed to determine the correct N number to address these shortcomings.

Next, radial distribution of chromatin markers was investigated. While the distribution of markers at early 4-hour timepoint was significantly different across island size for most markers, all of them had similar profiles at 24 hours. It is apparent that long term radial distribution of chromatin markers is not affected by nuclear shape. Interestingly, all markers appeared to have elevated levels near the nuclear periphery. While expected of heterochromatin markers, this was not for euchromatin ones. It was also interesting to observe a clear peak of heterochromatin marker H3K9me3 near the nuclear periphery at 4h point for small islands which subsequently was reduced. This could be in line with previous reports that described H3K9me3 aggregation at the nuclear lamina to mechanically protect the genome[383] which also eventually dispersed.

Using a custom pipeline for the IN Cell Developer software, chromatin marker foci size and number were quantified next. A significant difference in heterochromatin foci organisation was observed in 20 µm islands, resulting in less numerous and larger foci compared to 50 µm islands. Comparatively, a similar trend was observed in euchromatin foci albeit less pronounced. Heterochromatin has been described in the past as behaving by phase separation[102], a process modulated by HP1[406] and useful in creating associated chromatin domains. However, this concept has been challenged in recent literature[410], which indicates that chromocenters might actually be generated through collapsed chromatin globules. Nevertheless, our results suggest that reduction of nuclear volume may be responsible for forcing heterochromatin foci to

associate together. Phase separation would better explain this phenomenon while the possibility of proximity of collapsed chromatin globules associating together and sharing bridging molecules such as HP1 would also make sense. Euchromatin foci is not known to possess phase separation properties. Furthermore, some open chromatin foci are theorized to be transcription factories[411], where RNA polymerases are relatively immobile while genes are shuttled in and out using increased affinity between promoters and transcription factors. In this model, alteration of chromatin architecture leads to dysregulated transcription[412]. Consequently, open chromatin foci would have to remain comparatively unaffected for correct transcriptional state to be maintained.

Nucleoskeletal proteins lamin A/C as well as B1 were investigated next. Both exhibited no significant differences in overall levels across time point. Lamin B1 did appear to have downregulated levels in small islands while lamin A/C did not. Furthermore, lamin B1 did not appear to have modified radial distribution under any condition. In contrast, lamin A/C showed elevated levels near the nuclear periphery on small islands. Considering the role of lamin A/C in mechanical integrity[329], this could be a mechanoresponsive mechanism to protect the nucleus from compressive forces. Indeed, one would expect that close localisation of lamin A/C would be indicative of their association into fibres with stronger mechanical properties, albeit this remains to be proven. Furthermore, as levels do not appear to change across island size and keeping in mind that lamin A/C has been shown to also have gene regulating properties[363], this relocalisation could potentially have gene expression effects such as in the regulation of LADs. Similarly, Lamin B1 is usually considered to have a more gene-regulatory role than structural[329,413]. Downregulation in small islands might also have gene regulatory effects. As lamin A/C and B1 usually interact with LADs and euchromatin TADs respectively, changes in radial distribution and levels might possibly impact hetero- and euchromatin levels as well as radial distribution. While changes in overall chromatin levels were perceived, no significant change in their radial distribution was observed making the latter unlikely.

Finally, nucleoli number and size were analysed. Nucleoli were shown to fuse on small islands while their size remained comparatively unaffected, and this phenomenon was observed in a variety of cell lines. Like heterochromatin, nucleoli behave by liquid-liquid phase separation[172] and their condensation is expected to stem off reduced nuclear volume.

Overall, the first chapter of results described how several nuclear architecture parameters were affected by altered cell and nuclear morphological changes. These initial observations served as a starting point to interrogate the mechanical regulation of these responses and the downstream effects on gene expression.

In the second results chapter (Chapter 4) next generation RNA sequencing was used to characterize the transcriptome of HKs grown on micropatterned surfaces. Differences in gene expression patterns were then used to investigate how restricted available adhesive area affected key signalling pathways and phenotype.

Initial analysis of data suggested that island size was not pre-selecting different populations of HKs as seen by their lack of differences in gene expression profiles at the early 4-hour time point. In contrast RNA extracted from 24-hour samples exhibited significant differences in expression profiles, indicating that available adhesive space effectively induces changes in the transcriptome. Bulk analysis indicated that reduced adhesive space leads to HK premature differentiation and confirmed this facet of the model. Further analysis of bulk and hierarchically clustered data revealed several affected pathways to be subsequently investigated, notably DNA damage repair, retinoic acid biosynthesis and ribogenesis.

The first affected pathway investigated was DNA damage repair. This pathway was upregulated on large islands compared to small ones after 24 hours. We quantified DNA DSB repair sites from colocalization of γH2AX and 53BP1 foci to explore if changes to RNA transcript levels did translate in changes in DNA repair activity. We found that HKs grown on large islands had more DSB repair sites compared to smaller islands, albeit only significantly so at the early 4-hour time point. Interestingly, we observed that differences in DSB repair sites preceded changes in RNA expression of DNA damage factors. Localisation to DSB sites and phosphorylation of DNA damage factors is often fast (<1h)[383,389,414], but little is known on the upregulation of their genes. Observation of a broader amount of time points would surely help answer some of these questions.

Chapter 3 described several observed changes in nuclear architecture with potential DNA damage protecting effects that could explain this phenomenon. Recent research has described changes in H3K9me3 levels central to protecting DNA from extracellular forces[383]. The role of Lamin A/C in DNA damage prevention is also known[389], and its radial redistribution could be a potential mechanism for it. Tension generated by stiff substrates can induce DNA damage[389] and while substrate stiffness is the same across island size perhaps changes in available adhesive area can modulate DNA damage. Furthermore, this tension can be modulated by focal adhesions[403], which cultured HKs have been shown in this model and in literature[415] to possess specific patterns of expression. Finally, as over half of HKs grown on small islands initiate terminal differentiation, their exit from the cell cycle could explain downregulated DNA damage sensing as well as active repair. Indeed, several reports indicate that differentiating HKs exhibit diminished DNA repair[416] and DSB repair sites[417,418]. This reasoning is difficult to integrate with the difference in DSB repair sites at 4-hour timepoint due to the lack of differences in

differentiating cells. Inducing differentiation on large islands, using per example high calcium concentrations, would be a straightforward way of shedding light into this complex issue.

While the previous reasoning, that exit from the cell cycle induces diminished DNA damage sensing and repair, another explanation could be that differentiating cells often undergo heterochromatization[18], and that this compaction of chromatin may hinder access to the DNA damage repair machinery[419]. In our model we see both a reduction of heterochromatin markers as well as what appears to be their coalescence on small islands, so this reasoning is difficult to incorporate. Inhibition of histone deacetylases could potentially help ascertain how correct this hypothesis is.

Recent research has also unveiled a very interesting facet of DNA damage repair: the appearance of nucleoplasmic and nucleolar actin filaments[388]. Previous research[220] has shown that HKs grown on large islands possess higher levels of G-actin compared to small islands. This elevated population of cytoplasmic actin could potentially increment nuclear actin levels, and thus influence DNA damage response. Moreover, new data[420] (yet to be peer-reviewed) indicates that these nucleolar actin filaments modulate nucleolar size. If this data is to be true, our model would be a very interesting tool to further investigate these relationships between nucleolar size, activity and DNA damage repair processes.

The second affected pathway was retinoic acid biosynthesis, which was upregulated on small islands. Using a transfected luciferase reporter system, we measured elevated levels of transcriptional activity of RA response elements in HKs grown on 20 μm islands. Considering that RA has been shown to inhibit HK differentiation[394], this upregulation in a differentiating population is intriguing. RA signalling has been implicated in lamin biogenesis[390], and lamin radial redistribution may be responsible for the upregulated RA pathway. Moreover, extracellular matrix rigidity has been linked to lamin A/C regulation through Retinoic Acid Receptor γ[421]. Similar levels of lamin A/C were observed across island size in the previous chapter. Perhaps this seemingly odd observation is the results of a hidden compensation mechanism, but nevertheless underlines the complex nature of mechanical regulation of lamin A/C.

The final affected pathway that was investigated was ribogenesis. Small and large islands saw upregulation of genes for ribosomal proteins and ribogenesis regulators, respectively. The model was initially interrogated for total de novo protein synthesis and found that it was reduced on small islands after 24 hours. Previous reports have shown that HKs entering terminal differentiation have elevated nascent protein levels as well as enlarged nucleoli[186], and it is accepted that nucleolar size scales with cellular translational needs[158,173,422]. This is then in stark contrast with our previous finding that overall nucleolar size does not vary between island size.

To further investigate if this was a result of a shortage of ribosomes or reduced ribosomal activity, qPCR of total 47S pre-rRNA transcripts was performed. Small islands were found to have reduced levels of 47S pre-rRNA. While not a direct measure of actual ribosomes, reduced pre-ribosomal RNA levels are thought to most likely couple with reduced ribosomal levels[423]. It is likely that this is perturbing ribogenesis, and that upregulation of ribosomal proteins in small islands is a compensation mechanism. Indeed, recent research has unveiled the idea that nascent ribosomes are sequestered by ribosomal proteins in order to force their export from the nucleolus, as mature ribosomes by reducing their affinity to nucleolar scaffold proteins[407]. Another report indicates that nucleolin, which was found to be downregulated on small islands, induces chromatin decondensation[424]. Perhaps downregulation on small islands of nucleolin is modulating heterochromatin condensation. The ribogenesis pathway response is highly complex and will surely be a very interesting ground for future research.

This chapter added a transcriptomic dimension to the characterization of the HKs nuclear compaction model. It showed that restrictive adhesive space can effectively generate a transcriptional response from HKs. Combined with the initial findings of Chapter 4, they served as a foundation that the following chapter could build upon to dissect the relationship between these changes and force transmission through the cytoskeleton to the nucleus. As a final comment on this chapter it is important to note that a low N number of 3 samples per condition may have robbed us of needed sensitivity to properly appreciate certain minute changes, as was for exemplified by the seemingly erroneous categorization of one of the 20 μm 4 hour sample in both the PCA and hierarchical cluster plots.

The last results chapter, Chapter 5, employed several strategies to perturb specific key mediators in force transmission to the nucleus to assess their effect on previously established cell shape-induced changes in nuclear architecture. The aim was to extract information on which and how these mediators affected HK chromatin organisation.

The first strategy consisted of using small molecule cytoskeletal inhibitors blebbistatin and Y-27632. Blebbistatin is an inhibitor of myosin II, and Y-27632, a ROCK-inhibitor, inhibits both contractility and F-actin polymerisation. Unfortunately, while treatment of HKs with them resulted in visible changes to the actin cytoskeleton, little effect was appreciated in nuclear size, chromatin markers and lamin A/C levels. Lack of effect on nuclear morphology by blebbistatin in our model was expected as it was already reported[221]. We previously discussed the possibility of changes in heterochromatin marker H3K9me3 to be the result of a mechanical dampening mechanism to protect chromatin[383]. We hoped to see some changes using blebbistatin, which has been shown to induce changes in heterochromatin and lamin A/C[389] levels. But a slight downregulation of lamin A/C radial distribution near the nuclear periphery was evident for HKs

grown on small islands, which might be indicative of the actin cytoskeleton role in that particular response. No change was appreciated in large islands. All these results taken together indicate that actin cytoskeleton perturbation did not appear to have significant effects in the regulation of our list of parameters. There is of course the possibility that the two selected inhibitors are not as effective at perturbing the F-actin network as we thought, albeit visual inspection assured us that they were, or that some compensation mechanism is minimizing the perturbation. Perhaps the use of other inhibitors, such as phalloidin, cytochalasin B or latrunculin would yield more perceptible changes, or the use of other perturbations such as siRNA. There is also the strong possibility that measuring changes at the 24 hour timepoint is untimely, as some of these responses can occur at earlier times[383].

For the next series of perturbation studies, a HaCaT cell line expressing the dominant R416P mutation in the keratin-14, analogous to the one found in patients suffering from severe Dowling-Meara form of EB. As keratin is the main source of keratinocyte mechanical integrity, this perturbation was expected to significantly affect nuclear mechanotransduction.

Unfortunately, little effect was appreciated, from similar nuclear size across conditions to a slight upregulation of heterochromatin marker H3K9me3 levels, mainly in small islands. Lamin A/C exhibited a more pronounced reaction, with upregulated levels, which was unexpected since the general understanding of lamin A/C regulation is that it reacts to altered actomyosin activity[389]. Even more intriguing considering recent reports which indicate downregulated actomyosin upon KO or mutation of keratins[425,426]. But perhaps the change in cell type and the type of disruption, as well as the use of sheets of cells respectively, are to blame for the differences between literature and the data here presented. While lamin A/C levels were changed, no significant change in radial distribution could be observed.

Little is known of keratin-based regulation of nuclear architecture and chromatin. Previous research has shown the importance of the perinuclear keratin cage in regulating nuclear shape[400], which we did not observe here. Nuclear shape was influenced by island size as we could appreciate by changes in cross sectional area, which implies that perhaps HaCaTs nuclear volume is incompressible. Recent work has uncovered some roles of keratin 14 in regulating the Hippo pathway through sequestration of YAP based on the degree of disulfide bonding its IF network undergoes[427], with effects on lamin A/C levels and differentiation. While that research indicated that point mutations hindering disulfide crosslinking hinted at a perturbed mechanosensing and cellular structural defects, it does not appear to be the reason behind its effect on YAP. Likely here, the perturbed keratin cytoskeleton appears to have little to no effect on our limited set of nuclear architecture parameters. Other keratins, such as keratin 17, appear as of now to be much more promising candidates in having nuclear roles[266,428]. Moreover,

previous research found K17 to be upregulated in K14 null mice keratinocytes[429], which might be the case here. Perhaps the choice of cell type (immortalized keratinocytes) and the type of perturbation were inappropriate for this set of experiments. Using Dowling-Meara patient samples compared to healthy donors could be perhaps a more direct way of assessing the effect of the mutation.

The following studies used a mouse keratinocyte cell line with a total KO of the *Plec* gene. Past research have shown these cells to exhibit elevated levels of F-actin and disruption of perinuclear keratin filaments, resulting in more deformable and larger nuclei[221], providing an interesting contrast to the previous strategies.

Larger nuclei were indeed observed in our model, accompanied by lower levels of H3K9me3. Larger tension on the nucleus has already been linked to reduced H3K9me3 levels, and could very much be the case here too[383]. Considering also that plectin KO in keratinocytes has been linked to modified MAPK signalling[274], which in turn has been linked to several chromatin remodellers[430], there is a possibility that some of these changes are affected by it. It is also appropriate to consider that MAPK, actin contractility, focal adhesions and FAK, as well as other signalling pathways were not investigated in this course of studies and could have potential effects in many of the observed phenomena.

Changes in nuclear size and heterochromatin levels were not accompanied with significant changes in H3K9me3 association into foci. It was however accompanied by more numerous nucleoli and moreover elevated levels of protein synthesis. The lack of response from heterochromatin and euchromatin foci association due to larger nuclear volume might be indicative that foci are as dissociated as possible. It is interesting then, that although we could perceive a clear downregulation of at least one of the markers (H3K9me3), and thus would assume general changes in chromatin organisation, we did not perceive such a change at the foci organisation level. Perhaps subtler changes are at play which could not be appreciated using our methods. Both the increased number of nucleoli and reduced heterochromatin levels might also be responsible for the elevated protein synthesis. Analysis of pre-ribosomal 45S rRNA did not yield significant changes, so we are inclined to believe that the reduced levels of heterochromatin to be mainly responsible. More numerous nucleoli might also have other effects on ribogenesis which we could not ascertain, so a more complete investigation would be needed to fully characterise this phenomenon.

Finally, lamin A levels did not appear to be significantly changed, but its radial distribution near the nuclear periphery was reduced, this time for cells grown on both small and large islands. Considering that *Plec* KO has been associated to changes in keratin IF network as well as elevated

levels of actin, and that previous data here presented appeared to indicate lamin A/C to respond to changes in keratin but not actin networks, this lack of change in levels is puzzling. Conceivably it is the result of some compensation mechanism unknown to us. Changes in radial distribution could possibly be attributed to changes in nuclear size, as larger nuclei appear to possess more dispersed levels of lamin towards the nuclear periphery. Changes in actin tension might also possibly be involved in this phenomenon, but for now there is no explicit explanation to this. This also further questions the findings from the actin network perturbations, as perhaps the inadequacy of the chosen inhibitors led to erroneous interpretation of the role of the actin cytoskeleton in the regulation of lamin A/C, and indeed it is the theorised elevated actin tension generated by *Plec* KO that drives this dispersion of lamin A/C. Perhaps it is the loss of crosstalk between both cytoskeletal networks which is to blame. Treating the K14-mutant HaCaTs with actin inhibitors would be one way to examine this complex crosstalk issue.

The last set of studies used siRNA to effectively KD production of lamin A/C and Nesprin 2. Both proteins serve important roles in how forces are transmitted to chromatin and the nucleus, respectively. These complementary set of studies aimed to compare how attachment of the nuclear envelope to the cytoskeleton, or chromatin to the nuclear envelope, affects nuclear architecture.

While LMNA siRNA did not yield observable changes in nuclear size, significantly smaller nuclei on HKs grown on large islands could be appreciated for SYNE2 siRNA treatments. KD of nesprin 2, and thus hypothetical disconnection of the nucleus from the actin cytoskeleton could indicate then that the shrinking of the nucleus on large islands is the result of the loss of F-actin tension. Lamin A/C KD does not result in larger nuclei, so perhaps the size of HK nuclei is more dependent on the balance between tensive and compressive forces generated by the actin and keratin networks[221]. There is also the possibility of some regulation generated by the microtubule network, which was absent in this set of studies. The lack of change in HKs grown on small islands treated with SYNE2 siRNA is perhaps indicative of the need of tangential anchoring of actin filaments to effectively be able to assert tensive forces upon the nucleus to enlarge it. In this perspective the disconnection from the actin cytoskeleton does little effect to further compress the nucleus.

In contrast with plec KO results, siRNA KD of lamin A/C and nesprin 2 resulted in elevated levels of H3K9me3 and particularly H3K27Ac. As previously indicated, heterochromatin downregulation can happen as a result of tensive forces applied upon the nucleus, and that this response is dependent on nuclear mechanical integrity[383]. Here we can observe an inverse effect; predicted disruption of tensive forces upon the nucleus, or perturbation of its mechanical integrity, results in upregulated H3K9me3 levels. That euchromatin marker H3K27Ac behaved

similarly was not expected, nor can be explained in a similar fashion. Considering that both proteins dwell close to the nuclear periphery and are known to interact with heterochromatin[118,352,409] and each other[431], the similar response regarding chromatin markers may be indicative of a common chromatin regulating pathway. Further analysis such as comparison of ChIPseq data, co-immunoprecipitation of interaction partners would shed more light into this possibility. There is also the likely possibility that both responses are simply unrelated, and that while the H3K9me3 upregulation is related to the aforementioned reasons, H3K27Ac changes could stem off the perturbation of the LINC and the nuclear lamina, two major nuclear scaffolding structures with known chromatin organization properties[354,432].

Lamin A/C KD did not significantly affect either heterochromatin or euchromatin foci number or size. In contrast, nesprin 2 KD saw reduced H3K9me3 foci number and caused a slight increase in H3K27Ac foci size on large islands. Analogously, nesprin 2 KD reduced the number of nucleoli on large islands. As discussed before both heterochromatin foci and nucleoli are believed to behave by phase separation[405,407], so changes in their organisation correlate with changes in nuclear size and further corroborate some of our previous findings and support this model of nuclear architecture.

Changes in nucleoli number were also accompanied by reduced de novo protein synthesis levels and altered expression of 47S pre-ribosomal RNA and RRP1B. Both pre-ribosomal RNA 47S and RRP1B transcriptional levels appeared to scale with nuclear size. This hints again at the possibility that nuclear shape can alter nucleolar number which in turn can affect ribogenesis. Nucleolar fusion induces chromatin reorganization, as separate NORs come together[433], and these reorganizations could impact chromatin structure and gene expression. Nucleolar Associated Domains (NADs) are frequently shared with LADs and are often gene rich regions. Nuclear shrinkage and nucleolar fusion would inherently bring changes in nucleolar and nuclear lamina surface. These surfaces are where NADs and LADs are located, and changes in them could be translated in changes in nucleolar dynamics, as has been theorised recently in senescent cells[434,435]. Moreover, nucleoli are also a dense structure, and fusing in a smaller nucleus could make them even denser, physically hindering diffusion and chromatin access of the transcriptional machinery. Apart from perturbed chromatin architecture, changes in nuclear volume could also affect the concentrations of nucleolar scaffold proteins (such as nucleolin), rRNA (47S) and ribosomal proteins (RPL36), and in turn modulate nucleolar dynamics[173,174,407]. A more extensive analysis of nucleolar compartments, nucleoli-associated biomolecules and nucleolar chromatin organisation would be necessary to better understand this response.

Important take-aways from this chapter are the difference between effects that stem off changes to the nuclear volume and changes due to perturbation of force. Of course, both

phenomena are in essence connected, as in our model nuclear volume is dependent of how tensive and compressive forces are exerted unto it but can have divergent downstream effects. This is clearly observed in the strategies which did not yield changes to nuclear volume but did affect other nuclear architecture features and vice versa.

In this regard we can postulate a model which classifies nuclear responses to biophysical cues in two types. The first type are nuclear volume-dependent. In this category we can find changes to nucleoli number and heterochromatin foci distribution. These types of responses are generated because of the biophysical nature of these nuclear structures, i.e membraneless organelles, which behave as liquid droplets. Direct phenotypic changes are due to these variations in nuclear volume, such as changes in protein synthesis or RRP1B levels. The second type of responses are dependent on the integration of the nucleus in the cytoskeleton. We classify changes in lamin A/C levels, radial distribution, and chromatin markers in this category. We theorise these changes to be caused by modifications to how forces are transmitted to the nucleus, but might also be caused by other means, such as biochemical signalling cascades.

This final chapter therefore uncovered mechanistic insights into the inner working of the previously observed changes in chromatin architecture and gene expression in HKs induced by limited adhesive space. Multiple strategies to perturb cyto- and nucleoskeletal components allowed to further our understanding of our model and provided important information on the role of the nucleus as a mechanosensing unit.

Outlook and Future Directions

We have provided through this project a characterisation of changes to HK nuclear architecture and gene expression induced by limited adhesive space as well as understandings as to the roles of several cyto- and nucleoskeletal components in their regulation. While important features have been uncovered, many other remain to be elucidated.

The initial characterisation of changes to nuclear architecture presented changes in several key chromatin markers saw induced differentiation in small islands. While these changes give information on macroscopic changes to nuclear architecture, they are quite limited if not accompanied by more gene-specific information. Similarly, RNAseq data reflects bulk changes in gene expression, and does not provide insight into the behaviour of single cells or specific sub-populations. More in-depth genetic analyses, such as ChIPseq of the presented chromatin markers and lamin A/C, and single cell RNAseq are needed to fully characterise the genetic scope of this project.

Analysis to changes at regulatory regions of the genes that are affected could give insight in how the macroscopic changes to chromatin markers affect individual genes. We saw reduced levels of H3K27Ac, H3K27me3 and H3K9me3 in small islands, with upregulation of retinoic acid signalling genes. Analysis of these markers at promoters or enhancers of the affected genes would provide valuable information as to which chromatin remodellers are responsible for this characteristic response. Changes in lamin A/C radial distribution would hopefully also be reflected in its interaction with regulatory regions. Further inhibition of chromatin remodellers, such as histone deacetylases using trichostatin A, would help verifying their participation. We could also envision more localised strategies, such as using an inactive Cas9 (dCas9) protein to target specific promoter or enhancer regions with chromatin remodellers[436,437]. This would allow to control the chromatin state at these regions, and thus determine the role of local chromatin architecture in the biophysical regulation of gene transcription. Then, with the use of cytoskeletal inhibitors we could help identify more direct links between biophysical cues and local chromatin changes. Single-cell analysis would help with the differentiation aspect of the project, which was not examined in-depth once we could not appreciate changes in chromatin organisation. Moreover, we could potentially also find other subpopulations which are lost in bulk analysis. We believe that there are very possibly interesting aspects of cell fate decisions to be found.

The DNA damage response was found to be quite intriguing and the model could serve as an interesting tool to investigate the roles of both lamin A/C and the cytoskeleton in its modulation.

Indeed, laminopathies such as Hutchinson–Gilford progeria syndrome are accompanied by premature aging of the skin, a phenotype akin to senescence and thought to be linked to DNA damage response[438]. Perturbation experiments where HKs would be seeded on both island sizes, treated with blebbistantin and in parallel LMNA siRNA and stained for H2AX/53BP1 foci would surely provide very interesting initial results. Following experiments could then probe known DSB repair pathways and their relationship to cyto- and nucleoskeletal elements.

The retinoic acid response, especially in the context of lamin A/C as well as psoriasis[439], skin cancer[440], aging[441] and other cosmetical applications[442], is also a promising alley of research. Experiments would have to determine if lamin A/C redisposition or retinoic acid upregulation are the initial steps of the response to reduced available adhesive area. HKs could be treated with retinoic acid or LMNA siRNA and lamin A/C or retinoic acid levels could be determined, respectively. Then targeted KD of other components such as RARG, CRABP2 or the cytoskeleton while observing changes in lamin A/C levels, DNA damage or differentiation would further characterise this response.

Our most important set of results concerned the nucleolar coalescence observed on small islands and the consequent reduction of pre-ribosomal RNA and protein synthesis levels. RNAseq data revealed a plethora of affected components of the ribogenesis pathway, and we provided mechanistic information into how nuclear size could affect translational activity. There exist many more ways this complex phenomenon could be probed. Expanding the characterisation of affected ribogenesis effectors and ribosomal proteins in perturbation experiments would be important, as they are numerous, and their roles poorly understood. rRNAseq would also give valuable insight into rRNA transcription and maturation, helping localise which specific steps are affected. Measuring changes in nuclear protein concentration and partition coefficients of scaffold proteins would give a better understanding into the thermodynamics behind nucleolar dynamics. Overall, we believe this model could become a very useful tool in the field of nucleolar dynamics where much is still to be discovered in how nucleoli regulate their size and how it affects ribogenesis.

Finally, this model represents a unique platform to study genome organisation, especially as a contrasted example of senescent nuclei which are often enlarged[443]. For example, recent research into how chromatin compaction level modulates penetration of RNA polymerases could possibly benefit from such a model[444]. Our project did not preoccupy itself on small nor large scale DNA interactions, which are possibly modified. Hi-C analysis, as well as ChIPseq analysis of CTCF binding regions would very probably reveal some interesting changes in interactions. Analogously, very recent research has indicated the possible existence of “super-silencer regions”, in contrast to the well-established super-enhancer regions, as regions of DNA

which contain high levels of repressive chromatin markers with long-range interactions (not yet published data)[445]. Surely the forcing together of heterochromatic regions, as we theorise could be the consequence of heterochromatin foci condensation, could potentially generate unnatural super-silencer regions, with hopefully measurable changes in chromatin architecture and gene expression.

This model has been used in the past to gain valuable insight into how biophysical cues as transmitted by the cytoskeleton affect HK differentiation and nuclear morphology. This work has pushed this understanding further by associating specific nuclear architecture features as well as phenotypic changes to it. Correct mechanotransduction and chromatin organisation are paramount to HK differentiation and skin homeostasis, and defects are associated with a plethora of ailments[188,192]. Further characterization of this model, and moreover the expansion to include patient samples would greatly improve our understanding of these diseases and potentially bring new insights as to their treatment and skin biology in general.

Conclusion

This work has laid down the foundations of a full characterisation of nuclear architecture and transcriptional changes resulting of altered available adhesive area of HKs. It also expanded this characterisation by providing basic mechanistic insights into the role of the cytoskeleton in modulating such a response.

We observed macroscopic changes in nuclear architecture, mainly downregulation of chromatin markers H3K27me3, H3K27Ac and H3K9me3 on small islands, accompanied by heterochromatin foci and nucleolar condensation as well as radial redistribution towards the nuclear periphery of lamin A/C. RNA sequencing revealed changes in gene transcription, most notably in the DNA damage repair, retinoic acid and ribogenesis pathways. DNA damage was upregulated in large islands and accompanied by incremented DSB repair sites. Retinoic acid signalling was upregulated on small islands and we measured elevated levels of transcriptional activity of RA response elements. The ribogenesis pathway was affected in a mixed fashion, with upregulation of ribosomal proteins in small islands and upregulation of ribogenesis effectors in spread cells. Reduced adhesive area was then linked to reduced levels of pre-ribosomal RNA 47S transcript levels and protein synthesis levels. We then used mice keratinocytes with *Plec* KO to ascertain that nucleoli number and protein synthesis levels incremented with nuclear size. Inversely, HKs with nesprin 2 KD showed reduced nuclear volume, reduced nucleoli number, protein synthesis levels and pre-rRNA 47S levels, further proving their relation. Reduced nuclear volume was also linked to heterochromatin foci association. Finally, we observed that Lamin A/C and nesprin 2 KD had upregulated levels of chromatin markers H3K27Ac and H3K9me3, indicating that the cytoskeleton and nucleoskeleton have roles in chromatin regulation.

We proposed that nuclear responses to biophysical cues can be divided into two categories: changes stemming off nuclear volume, such as nucleoli number and heterochromatin foci association, and changes generated by mechanical coupling of the nucleus, such as chromatin marker and lamin A/C levels. These two types of responses are intrinsically linked, as they are both ultimately influenced by the equilibrium of forces exerted on the nucleus. It reveals how mechanotransduction can generate responses not only by direct physical linkage but also by varying other parameters such as nuclear volume with effects on diffusion dynamics of intranuclear bodies. This raises questions also as to how changes in nuclear volume could affect other parameters, such as intranuclear concentration of transcription factors or scaffolding proteins. We also uncovered a characteristic mechanical regulation of lamin A/C levels and radial distribution. We believe this regulation has potential roles in DNA damage response and retinoic acid signalling, to be found in future studies, and could potentially uncover hidden aspects of

laminopathies. Similarly, while not yet reported it is possible that genetic defects, such as in EBS variations caused by plectin defects[446], or even in other more naturally occurring conditions such as seen in synaptic activity-induced neuronal nuclear deformation[447], could affect nuclear volume. These changes in nuclear shape could have downstream effects on nucleoli number and overall cellular translational capabilities. Finally, we found particular interest in the lack of response from cytoskeletal inhibitors and keratin mutation. Both the F-actin and keratin cytoskeleton are arguably two of the most important mediators in mechanostransduction, yet little effect on nuclear architecture could be found while perturbing them. We do not deny their involvement in nuclear mechanics but indicate that better tools for their perturbation and a better understanding of their crosstalk are needed.

This work has presented novel insights into nuclear architecture and its complex relationship with the cytoskeleton, which mediates biophysical cues from the environment. The findings here presented describe for the first time changes to chromatin architecture as induced by available adhesive area, as well as introduces the concept of mechanical regulation of nucleolar dynamics. Mechanostransduction can modulate significant parts of cellular life such as cell fate decisions or metabolism and are partly governed by the changes to chromatin 3D structure that they generate. Future work will expand upon this work to bring even more in-depth knowledge as to the inner workings of this fascinating phenomenon.

Chapter 7: Bibliography

1. McGrath JA, Eady RAJ, Pope FM. Anatomy and Organization of Human Skin. In: *Rook's Textbook of Dermatology*. Malden, Massachusetts, USA: Blackwell Publishing, Inc.; :45-128. doi:10.1002/9780470750520.ch3

2. Essick GK, Rath EM, Kelly DG, James A, Murray RA. Somesthesis and the Neurobiology of the Somatosensory Cortex 0. Franzen, R. Johansson and. 1996:59-72.

3. Potten CS. THE EPIDERMAL PROLIFERATIVE UNIT: THE POSSIBLE ROLE OF THE CENTRAL BASAL CELL. *Cell Prolif*. 1974;7(1):77-88. doi:10.1111/j.1365-2184.1974.tb00401.x

4. Blanpain C, Fuchs E. Epidermal homeostasis: A balancing act of stem cells in the skin. *Nat Rev Mol Cell Biol*. 2009;10(3):207-217. doi:10.1038/nrm2636

5. Fuchs E. Scratching the surface of skin development. *Nature*. 2007;445(7130):834-842. doi:10.1038/nature05659

6. Arwert EN, Hoste E, Watt FM. Epithelial stem cells, wound healing and cancer. *Nat Rev Cancer*. 2012;12(3):170-180. doi:10.1038/nrc3217

7. Fuchs E, Green H. Changes in Keratin Gene Expression during Terminal Differentiation of the Keratinocyte. *Cell*. 1980;19(0):1033-1042. https://ac.els-cdn.com/009286748090094X/1-s2.0-009286748090094X-main.pdf?_tid=73f09992-0c2e-11e8-ac83-00000aacb35d&acdnat=1518025609_3cd10e252c62398d4ce6f265223a4527. Accessed February 7, 2018.

8. Green KJ, Simpson CL. Desmosomes: New Perspectives on a Classic. *J Invest Dermatol*. 2007;127(11):2499-2515. doi:10.1038/sj.jid.5701015

9. Dale BA, Resing KA, Lonsdale-Eccles JD. Filaggrin: a keratin filament associated protein. *Ann N Y Acad Sci*. 1985;455:330-342. http://www.ncbi.nlm.nih.gov/pubmed/2417519. Accessed January 5, 2019.

10. Chamcheu JC, Siddiqui IA, Syed DN, Adhami VM, Liovic M, Mukhtar H. Keratin gene mutations in disorders of human skin and its appendages. *Arch Biochem Biophys*. 2011;508(2):123-137. doi:10.1016/j.abb.2010.12.019

11. Wan H, Dopping-Hepenstal PJC, Gratian MJ, et al. Striate palmoplantar keratoderma arising from desmoplakin and desmoglein 1 mutations is associated with contrasting perturbations of desmosomes and the keratin filament network. *Br J Dermatol*. 2004;150(5):878-891. doi:10.1111/j.1365-2133.2004.05996.x

12. Peña-Penabad C, de Unamuno P, García Silva J, Ludeña MD, González Sarmiento R, Pérez-Arellano JL. Altered expression of immunoreactive involucrin in lamellar ichthyosis. *Eur J Dermatol*. 9(3):197-201. http://www.ncbi.nlm.nih.gov/pubmed/10210784. Accessed January 5, 2019.

13. Fine J-D, Johnson LB, Weiner M, Suchindran C. Gastrointestinal Complications of Inherited Epidermolysis Bullosa: Cumulative Experience of the National Epidermolysis Bullosa Registry. *J Pediatr Gastroenterol Nutr*. 2008;46(2):147-158. doi:10.1097/MPG.0b013e31812f5667

14. Dvorak HF. Tumors: wounds that do not heal-redux. *Cancer Immunol Res*. 2015;3(1):1-11. doi:10.1158/2326-6066.CIR-14-0209

15. Atlasi Y, Stunnenberg HG. The interplay of epigenetic marks during stem cell differentiation and development. 2017. doi:10.1038/nrg.2017.57

16. Botchkarev VA, Gdula MR, Mardaryev AN, Sharov AA, Fessing MY. Epigenetic

Regulation of Gene Expression in Keratinocytes. *J Invest Dermatol*. 2012;132182(10):2505-2521. doi:10.1038/jid.2012.182

17. Lavelle C, Victor J-M. Nuclear architecture and dynamics. In: ; 2018.

18. Lanctôt C, Cheutin T, Cremer M, Cavalli G, Cremer T. Dynamic genome architecture in the nuclear space: Regulation of gene expression in three dimensions. *Nat Rev Genet*. 2007;8(2):104-115. doi:10.1038/nrg2041

19. Hnisz D, Shrinivas K, Young RA, Chakraborty AK, Sharp PA. Perspective A Phase Separation Model for Transcriptional Control. 2017. doi:10.1016/j.cell.2017.02.007

20. Edwards JR, Yarychkivska O, Boulard M, Bestor TH. DNA methylation and DNA methyltransferases. *Epigenetics Chromatin*. 2017;10(1):23. doi:10.1186/s13072-017-0130-8

21. Bird AP, Wolffe AP. Methylation-Induced Repression— Belts, Braces, and Chromatin. *Cell*. 1999;99(5):451-454. doi:10.1016/S0092-8674(00)81532-9

22. Sen GL, Reuter JA, Webster DE, Zhu L, Khavari PA. LETTERS DNMT1 maintains progenitor function in self-renewing somatic tissue. *Nature*. 2010;463. doi:10.1038/nature08683

23. Chédin F. The DNMT3 Family of Mammalian De Novo DNA Methyltransferases. In: *Progress in Molecular Biology and Translational Science*. Vol 101. ; 2011:255-285. doi:10.1016/B978-0-12-387685-0.00007-X

24. Li C-J. DNA demethylation pathways: recent insights. *Genet Epigenet*. 2013;5:43-49. doi:10.4137/GEG.S12143

25. Rasmussen KD, Helin K. Role of TET enzymes in DNA methylation, development, and cancer. *Genes Dev*. 2016;30(7):733-750. doi:10.1101/gad.276568.115

26. Jelinic P, Shaw P. Loss of imprinting and cancer. *J Pathol*. 2007;211(3):261-268. doi:10.1002/path.2116

27. Leick MB, Shoff CJ, Wang EC, Congress JL, Gallicano GI. Loss of imprinting of IGF2 and the epigenetic progenitor model of cancer. *Am J Stem Cells*. 2012;1(1):59-74. http://www.ncbi.nlm.nih.gov/pubmed/23671798. Accessed January 10, 2019.

28. Liu Y, Aryee MJ, Padyukov L, et al. Epigenome-wide association data implicate DNA methylation as an intermediary of genetic risk in rheumatoid arthritis. *Nat Biotechnol*. 2013;31(2):142-147. doi:10.1038/nbt.2487

29. Li X, Xiao B, Chen X-S. DNA Methylation: a New Player in Multiple Sclerosis. *Mol Neurobiol*. 2017;54(6):4049-4059. doi:10.1007/s12035-016-9966-3

30. Soriano-Tárraga C, Jiménez-Conde J, Giralt-Steinhauer E, et al. Epigenome-wide association study identifies *TXNIP* gene associated with type 2 diabetes mellitus and sustained hyperglycemia. *Hum Mol Genet*. 2016;25(3):609-619. doi:10.1093/hmg/ddv493

31. Horvath S, Ritz BR. Increased epigenetic age and granulocyte counts in the blood of Parkinson's disease patients. *Aging (Albany NY)*. 2015;7(12):1130-1142. doi:10.18632/aging.100859

32. Levine ME, Lu AT, Bennett DA, Horvath S. Epigenetic age of the pre-frontal cortex is associated with neuritic plaques, amyloid load, and Alzheimer's disease related cognitive functioning. *Aging (Albany NY)*. 2015;7(12):1198-1211. doi:10.18632/aging.100864

33. Carrel L, Willard H, D'Esposito M, Bickmore WA. Heterogeneous gene expression from the inactive X chromosome: An X-linked gene that escapes X inactivation in some human cell lines but is inactivated in others. *PNAS*. 2007;96(13):7364-7369. doi:10.1073/pnas.96.13.7364

34. Cytosine Methylation Alters Transcription Factor DNA Binding. *Cancer Discov*. May 2017. doi:10.1158/2159-8290.CD-RW2017-090

35. Jin J, Lian T, Gu C, Yu K, Gao YQ, Su X-D. The effects of cytosine methylation on general transcription factors. *Sci Rep*. 2016;6(1):29119. doi:10.1038/srep29119

36. Fuks F, Hurd PJ, Wolf D, Nan X, Bird AP, Kouzarides T. The Methyl-CpG-binding Protein MeCP2 Links DNA Methylation to Histone Methylation. *J Biol Chem*. 2003;278(6):4035-4040. doi:10.1074/jbc.M210256200

37. Rose NR, Klose RJ. Understanding the relationship between DNA methylation and histone lysine methylation. *Biochim Biophys Acta - Gene Regul Mech*. 2014;1839(12):1362-1372. doi:10.1016/J.BBAGRM.2014.02.007

38. Ji S, Shao H, Han Q, Seiler CL, Tretyakova NY. Reversible DNA-Protein Cross-Linking at Epigenetic DNA Marks. *Angew Chemie Int Ed*. 2017;56(45):14130-14134. doi:10.1002/anie.201708286

39. Bannister AJ, Kouzarides T. Regulation of chromatin by histone modifications. *Cell Res*. 2011;2122:381-395. doi:10.1038/cr.2011.22

40. Cutter AR, Hayes JJ. A brief review of nucleosome structure. *FEBS Lett*. 2015;589(20PartA):2914-2922. doi:10.1016/j.febslet.2015.05.016

41. Rossetto D, Avvakumov N, Côté J. Histone phosphorylation: A chromatin modification involved in diverse nuclear events. *Epigenetics*. 2012;7(10):1098. doi:10.4161/EPI.21975

42. Meas R, Mao P. Histone ubiquitylation and its roles in transcription and DNA damage response. *DNA Repair (Amst)*. 2015;36:36. doi:10.1016/J.DNAREP.2015.09.016

43. Lorenzo A Di, Bedford MT. Histone Arginine Methylation. *FEBS Lett*. 2011;585(13):2024. doi:10.1016/J.FEBSLET.2010.11.010

44. Banerjee T, Chakravarti D. A Peek into the Complex Realm of Histone Phosphorylation. *Mol Cell Biol*. 2011;31(24):4858. doi:10.1128/MCB.05631-11

45. Koch CM, Andrews RM, Flicek P, et al. The landscape of histone modifications across 1% of the human genome in five human cell lines. *Genome Res*. 2007;17(6):691-707. doi:10.1101/gr.5704207

46. Barski A, Cuddapah S, Cui K, et al. High-Resolution Profiling of Histone Methylations in the Human Genome. *Cell*. 2007;129(4):823-837. doi:10.1016/J.CELL.2007.05.009

47. Lesch BJ, Page DC. Poised chromatin in the mammalian germ line. *Development*. 2014;141(19):3619. doi:10.1242/DEV.113027

48. Bernstein BE, Mikkelsen TS, Xie X, et al. A Bivalent Chromatin Structure Marks Key Developmental Genes in Embryonic Stem Cells. *Cell*. 2006;125(2):315-326. doi:10.1016/j.cell.2006.02.041

49. Creyghton MP, Cheng AW, Welstead GG, et al. Histone H3K27ac separates active from poised enhancers and predicts developmental state. *Proc Natl Acad Sci*. 2010;107(50):21931-21936. doi:10.1073/PNAS.1016071107

50. Allis CD, Berger SL, Cote J, et al. New Nomenclature for Chromatin-Modifying Enzymes. *Cell*. 2007;131(4):633-636. doi:10.1016/J.CELL.2007.10.039

51. Lu D. Epigenetic modification enzymes: catalytic mechanisms and inhibitors. *Acta Pharm Sin B*. 2013;3(3):141-149. doi:10.1016/J.APSB.2013.04.007

52. Xiao B, Jing C, Wilson JR, et al. Structure and catalytic mechanism of the human histone methyltransferase SET7/9. *Nature*. 2003;421(6923):652-656. doi:10.1038/nature01378

53. Yun M, Wu J, Workman JL, Li B. Readers of histone modifications. *Cell Res*. 2011;21(4):564-578. doi:10.1038/cr.2011.42

54. Zhou M-M, Dhalluin C, Carlson JE, et al. Structure and ligand of a histone acetyltransferase bromodomain. *Nature*. 1999;399(6735):491-496. doi:10.1038/20974

55. Eissenberg JC, Elgin SC. The HP1 protein family: getting a grip on chromatin. *Curr Opin Genet Dev*. 2000;10(2):204-210. doi:10.1016/S0959-437X(00)00058-7

56. Bannister AJ, Zegerman P, Partridge JF, et al. Selective recognition of methylated lysine 9 on histone H3 by the HP1 chromo domain. *Nature*. 2001;410(6824):120-124. doi:10.1038/35065138

57. Aasland R, Stewart AF. The chromo shadow domain, a second chromo domain in heterochromatin-binding protein 1, HP1. *Nucleic Acids Res*. 1995;23(16):3168-3173. http://www.ncbi.nlm.nih.gov/pubmed/7667093. Accessed January 18, 2019.

58. Yamamoto K, Sonoda M. Self-interaction of heterochromatin protein 1 is required for direct binding to histone methyltransferase, SUV39H1. *Biochem Biophys Res Commun*. 2003;301(2):287-292. doi:10.1016/S0006-291X(02)03021-8

59. Smallwood A, Esteve P-O, Pradhan S, Carey M. Functional cooperation between HP1 and DNMT1 mediates gene silencing. *Genes Dev*. 2007;21(10):1169-1178. doi:10.1101/gad.1536807

60. Chittock EC, Latwiel S, Miller TCR, Müller CW. Molecular architecture of polycomb repressive complexes. *Biochem Soc Trans*. 2017;45(1):193-205. doi:10.1042/BST20160173

61. Kueng S, Oppikofer M, Gasser SM. SIR Proteins and the Assembly of Silent Chromatin in Budding Yeast. *Annu Rev Genet*. 2013;47(1):275-306. doi:10.1146/annurev-genet-021313-173730

62. Koutelou E, Hirsch CL, Dent SYR. Multiple faces of the SAGA complex. *Curr Opin Cell Biol*. 2010;22(3):374-382. doi:10.1016/j.ceb.2010.03.005

63. DesJarlais R, Tummino PJ. Role of Histone-Modifying Enzymes and Their Complexes in Regulation of Chromatin Biology. *Biochemistry*. 2016;55(11):1584-1599. doi:10.1021/acs.biochem.5b01210

64. Clapier CR, Cairns BR. The Biology of Chromatin Remodeling Complexes. *Annu Rev Biochem*. 2009;78(1):273-304. doi:10.1146/annurev.biochem.77.062706.153223

65. Erdel F, Rippe K. Binding kinetics of human ISWI chromatin-remodelers to DNA repair sites elucidate their target location mechanism. *Nucleus*. 2011;2(2):105-112. doi:10.4161/nucl.2.2.15209

66. Skiniotis G, Moazed D, Walz T. Acetylated Histone Tail Peptides Induce Structural Rearrangements in the RSC Chromatin Remodeling Complex. *J Biol Chem*. 2007;282(29):20804-20808. doi:10.1074/jbc.C700081200

67. Whitehouse I, Flaus A, Cairns BR, White MF, Workman JL, Owen-Hughes T. Nucleosome mobilization catalysed by the yeast SWI/SNF complex. *Nature*. 1999;400(6746):784-787. doi:10.1038/23506

68. Lorch Y, Zhang M, Kornberg RD. Histone Octamer Transfer by a Chromatin-Remodeling Complex. *Cell*. 1999;96(3):389-392. doi:10.1016/S0092-8674(00)80551-6

69. Owen-Hughes T, Utley RT, Côté J, Peterson CL, Workman JL. Persistent site-specific remodeling of a nucleosome array by transient action of the SWI/SNF complex. *Science*. 1996;273(5274):513-516. doi:10.1126/SCIENCE.273.5274.513

70. Wilson BG, Wang X, Shen X, et al. Epigenetic antagonism between polycomb and SWI/SNF complexes during oncogenic transformation. *Cancer Cell*. 2010;18(4):316-328. doi:10.1016/j.ccr.2010.09.006

71. Stanton BZ, Hodges C, Calarco JP, et al. Smarca4 ATPase mutations disrupt direct eviction of PRC1 from chromatin. *Nat Genet*. 2017;49(2):282-288. doi:10.1038/ng.3735

72. Bultman S, Gebuhr T, Yee D, et al. A Brg1 Null Mutation in the Mouse Reveals Functional Differences among Mammalian SWI/SNF Complexes. *Mol Cell*. 2000;6(6):1287-1295. doi:10.1016/S1097-2765(00)00127-1

73. Fukuoka J, Fujii T, Shih JH, et al. Chromatin Remodeling Factors and BRM/BRG1 Expression as Prognostic Indicators in Non-Small Cell Lung Cancer. *Clin Cancer Res*. 2004;10(13):4314-4324. doi:10.1158/1078-0432.CCR-03-0489

74. Varela I, Tarpey P, Raine K, et al. Exome sequencing identifies frequent mutation of the SWI/SNF complex gene PBRM1 in renal carcinoma. *Nature*. 2011;469(7331):539-542. doi:10.1038/nature09639

75. Thompson M. Polybromo-1: the chromatin targeting subunit of the PBAF complex. *Biochimie*. 2009;91(3):309-319. doi:10.1016/j.biochi.2008.10.019

76. Hota SK, Bhardwaj SK, Deindl S, Lin Y, Zhuang X, Bartholomew B. Nucleosome mobilization by ISW2 requires the concerted action of the ATPase and SLIDE domains. *Nat Struct Mol Biol*. 2013;20(2):222-229. doi:10.1038/nsmb.2486

77. Erdel F, Rippe K. Chromatin remodelling in mammalian cells by ISWI-type complexes - where, when and why? *FEBS J*. 2011;278(19):3608-3618. doi:10.1111/j.1742-4658.2011.08282.x

78. Tsukiyama T, Wu C. Purification and properties of an ATP-dependent nucleosome remodeling factor. *Cell*. 1995;83(6):1011-1020. doi:10.1016/0092-8674(95)90216-3

79. Ito T, Bulger M, Pazin MJ, Kobayashi R, Kadonaga JT. ACF, an ISWI-containing and ATP-utilizing chromatin assembly and remodeling factor. *Cell*. 1997;90(1):145-155. http://www.ncbi.nlm.nih.gov/pubmed/9230310. Accessed January 30, 2019.

80. Sánchez-Molina S, Mortusewicz O, Bieber B, et al. Role for hACF1 in the G2/M damage checkpoint. *Nucleic Acids Res*. 2011;39(19):8445-8456. doi:10.1093/nar/gkr435

81. Lan L, Ui A, Nakajima S, et al. The ACF1 Complex Is Required for DNA Double-Strand Break Repair in Human Cells. *Mol Cell*. 2010;40(6):976-987. doi:10.1016/j.molcel.2010.12.003

82. Nakamura K, Kato A, Kobayashi J, et al. Regulation of Homologous Recombination by RNF20-Dependent H2B Ubiquitination. *Mol Cell*. 2011;41(5):515-528. doi:10.1016/j.molcel.2011.02.002

83. Barber TD, McManus K, Yuen KWY, et al. Chromatid cohesion defects may underlie

chromosome instability in human colorectal cancers. *Proc Natl Acad Sci U S A*. 2008;105(9):3443-3448. doi:10.1073/pnas.0712384105

84. Basta J, Rauchman M. The Nucleosome Remodeling and Deacetylase (NuRD) Complex in Development and Disease. *Transl Res*. 2015;165(1):36. doi:10.1016/J.TRSL.2014.05.003

85. Bouazoune K, Mitterweger A, Längst G, et al. The dMi-2 chromodomains are DNA binding modules important for ATP-dependent nucleosome mobilization. *EMBO J*. 2002;21(10):2430-2440. doi:10.1093/emboj/21.10.2430

86. Wang Y, Zhang H, Chen Y, et al. LSD1 Is a Subunit of the NuRD Complex and Targets the Metastasis Programs in Breast Cancer. *Cell*. 2009;138(4):660-672. doi:10.1016/J.CELL.2009.05.050

87. Smits AH, Jansen PWTC, Poser I, Hyman AA, Vermeulen M. Stoichiometry of chromatin-associated protein complexes revealed by label-free quantitative mass spectrometry-based proteomics. *Nucleic Acids Res*. 2013;41(1):e28. doi:10.1093/nar/gks941

88. Fujita N, Jaye DL, Kajita M, Geigerman C, Moreno CS, Wade PA. MTA3, a Mi-2/NuRD Complex Subunit, Regulates an Invasive Growth Pathway in Breast Cancer. *Cell*. 2003;113(2):207-219. doi:10.1016/S0092-8674(03)00234-4

89. Zhang H, Stephens LC, Kumar R. Metastasis tumor antigen family proteins during breast cancer progression and metastasis in a reliable mouse model for human breast cancer. *Clin Cancer Res*. 2006;12(5):1479-1486. doi:10.1158/1078-0432.CCR-05-1519

90. Kaji K, Caballero IM, MacLeod R, Nichols J, Wilson VA, Hendrich B. The NuRD component Mbd3 is required for pluripotency of embryonic stem cells. *Nat Cell Biol*. 2006;8(3):285-292. doi:10.1038/ncb1372

91. Kashiwagi M, Morgan BA, Georgopoulos K. The chromatin remodeler Mi-2 is required for establishment of the basal epidermis and normal differentiation of its progeny. *Development*. 2007;134(8):1571-1582. doi:10.1242/dev.001750

92. Shen X, Mizuguchi G, Hamiche A, Wu C. A chromatin remodelling complex involved in transcription and DNA processing. *Nature*. 2000;406(6795):541-544. doi:10.1038/35020123

93. Tosi A, Haas C, Herzog F, et al. Structure and Subunit Topology of the INO80 Chromatin Remodeler and Its Nucleosome Complex. *Cell*. 2013;154(6):1207-1219. doi:10.1016/J.CELL.2013.08.016

94. Papamichos-Chronakis M, Watanabe S, Rando OJ, Peterson CL. Global Regulation of H2A.Z Localization by the INO80 Chromatin-Remodeling Enzyme Is Essential for Genome Integrity. *Cell*. 2011;144(2):200-213. doi:10.1016/j.cell.2010.12.021

95. Papamichos-Chronakis M, Peterson CL. The Ino80 chromatin-remodeling enzyme regulates replisome function and stability. *Nat Struct Mol Biol*. 2008;15(4):338-345. doi:10.1038/nsmb.1413

96. Mizuguchi G, Shen X, Landry J, Wu W-H, Sen S, Wu C. ATP-driven exchange of histone H2AZ variant catalyzed by SWR1 chromatin remodeling complex. *Science*. 2004;303(5656):343-348. doi:10.1126/science.1090701

97. Billon P, Côté J. Precise deposition of histone H2A.Z in chromatin for genome expression and maintenance. *Biochim Biophys Acta - Gene Regul Mech*. 2012;1819(3-4):290-302. doi:10.1016/J.BBAGRM.2011.10.004

98. Li Z, Gadue P, Chen K, et al. Foxa2 and H2A.Z Mediate Nucleosome Depletion during Embryonic Stem Cell Differentiation. *Cell*. 2012;151(7):1608-1616. doi:10.1016/J.CELL.2012.11.018

99. Tang L, Nogales E, Ciferri C. Structure and function of SWI/SNF chromatin remodeling complexes and mechanistic implications for transcription. *Prog Biophys Mol Biol*. 2010;102(2-3):122-128. doi:10.1016/j.pbiomolbio.2010.05.001

100. Hnisz D, Abraham BJ, Lee TI, et al. Super-Enhancers in the Control of Cell Identity and Disease. *Cell*. 2013;155(4):934-947. doi:10.1016/J.CELL.2013.09.053

101. Fukaya T, Lim B, Levine M. Enhancer Control of Transcriptional Bursting. *Cell*. 2016;166(2):358-368. doi:10.1016/j.cell.2016.05.025

102. Hnisz D, Shrinivas K, Young RA, Chakraborty AK, Sharp PA. A Phase Separation Model for Transcriptional Control. *Cell*. 2017;169(1):13-23. doi:10.1016/J.CELL.2017.02.007

103. Dowen JM, Fan ZP, Hnisz D, et al. Control of Cell Identity Genes Occurs in Insulated Neighborhoods in Mammalian Chromosomes. *Cell*. 2014;159(2):374-387. doi:10.1016/j.cell.2014.09.030

104. Ji X, Dadon DB, Powell BE, et al. 3D Chromosome Regulatory Landscape of Human Pluripotent Cells. *Cell Stem Cell*. 2016;18(2):262-275. doi:10.1016/j.stem.2015.11.007

105. Flavahan WA, Drier Y, Liau BB, et al. Insulator dysfunction and oncogene activation in IDH mutant gliomas. *Nature*. 2016;529(7584):110-114. doi:10.1038/nature16490

106. Smith EM, Lajoie BR, Jain G, Dekker J. Invariant TAD Boundaries Constrain Cell-Type-Specific Looping Interactions between Promoters and Distal Elements around the CFTR Locus. *Am J Hum Genet*. 2016;98(1):185-201. doi:10.1016/j.ajhg.2015.12.002

107. Dixon JR, Selvaraj S, Yue F, et al. Topological domains in mammalian genomes identified by analysis of chromatin interactions. *Nature*. 2012;485(7398):376-380. doi:10.1038/nature11082

108. Dixon JR, Jung I, Selvaraj S, et al. Chromatin architecture reorganization during stem cell differentiation. *Nature*. 2015;518(7539):331-336. doi:10.1038/nature14222

109. Benedetti F, Dorier J, Burnier Y, Stasiak A. Models that include supercoiling of topological domains reproduce several known features of interphase chromosomes. *Nucleic Acids Res*. 2014;42(5):2848-2855. doi:10.1093/nar/gkt1353

110. Lupiáñez DG, Spielmann M, Mundlos S. Breaking TADs: How Alterations of Chromatin Domains Result in Disease. *Trends Genet*. 2016;32(4):225-237. doi:10.1016/J.TIG.2016.01.003

111. Lupiáñez DG, Kraft K, Heinrich V, et al. Disruptions of Topological Chromatin Domains Cause Pathogenic Rewiring of Gene-Enhancer Interactions. *Cell*. 2015;161(5):1012-1025. doi:10.1016/J.CELL.2015.04.004

112. Peric-Hupkes D, Meuleman W, Pagie L, et al. Molecular Maps of the Reorganization of Genome-Nuclear Lamina Interactions during Differentiation. *Mol Cell*. 2010;38(4):603-613. doi:10.1016/J.MOLCEL.2010.03.016

113. Guelen L, Pagie L, Brasset E, et al. Domain organization of human chromosomes revealed by mapping of nuclear lamina interactions. *Nature*. 2008;453(7197):948-951. doi:10.1038/nature06947

114. Wen B, Wu H, Shinkai Y, Irizarry RA, Feinberg AP. Large histone H3 lysine 9 dimethylated chromatin blocks distinguish differentiated from embryonic stem cells.

Nat Genet. 2009;41(2):246-250. doi:10.1038/ng.297

115. Kind J, Pagie L, Ortabozkoyun H, et al. Single-cell dynamics of genome-nuclear lamina interactions. *Cell*. 2013;153(1):178-192. doi:10.1016/j.cell.2013.02.028

116. Zhao H, Sifakis EG, Sumida N, et al. PARP1- and CTCF-Mediated Interactions between Active and Repressed Chromatin at the Lamina Promote Oscillating Transcription. *Mol Cell*. 2015;59(6):984-997. doi:10.1016/j.molcel.2015.07.019

117. Bian Q, Khanna N, Alvikas J, Belmont AS. β-Globin cis-elements determine differential nuclear targeting through epigenetic modifications. *J Cell Biol*. 2013;203(5):767-783. doi:10.1083/jcb.201305027

118. Harr JC, Luperchio TR, Wong X, Cohen E, Wheelan SJ, Reddy KL. Directed targeting of chromatin to the nuclear lamina is mediated by chromatin state and A-type lamins. *J Cell Biol*. 2015;208(1):33-52. doi:10.1083/jcb.201405110

119. Solovei I, Wang AS, Thanisch K, et al. LBR and lamin A/C sequentially tether peripheral heterochromatin and inversely regulate differentiation. *Cell*. 2013;152(3):584-598. doi:10.1016/j.cell.2013.01.009

120. Amendola M, van Steensel B. Nuclear lamins are not required for lamina-associated domain organization in mouse embryonic stem cells. *EMBO Rep*. 2015;16(5):610-617. doi:10.15252/embr.201439789

121. Zuleger N, Boyle S, Kelly DA, et al. Specific nuclear envelope transmembrane proteins can promote the location of chromosomes to and from the nuclear periphery. *Genome Biol*. 2013;14(2):R14. doi:10.1186/gb-2013-14-2-r14

122. Lieberman-Aiden E, van Berkum NL, Williams L, et al. Comprehensive mapping of long-range interactions reveals folding principles of the human genome. *Science*. 2009;326(5950):289-293. doi:10.1126/science.1181369

123. Fortin J-P, Hansen KD. Reconstructing A/B compartments as revealed by Hi-C using long-range correlations in epigenetic data. *Genome Biol*. 2015;16(1):180. doi:10.1186/s13059-015-0741-y

124. Schwarzer W, Abdennur N, Goloborodko A, et al. Two independent modes of chromatin organization revealed by cohesin removal. *Nature*. 2017;551(7678):51. doi:10.1038/nature24281

125. BOVERI, T. Die Blastomerenkerne von Ascaris megalocephala und die Theorie der Chromosomenindividualitat. *Arch fur Zellforsch*. 1909;3:181-268. https://ci.nii.ac.jp/naid/10024028641/. Accessed February 4, 2019.

126. RABL, C. Uber Zelltheilung. *Morphol Jahrb*. 1885;10:214-330. https://ci.nii.ac.jp/naid/10017168932/. Accessed February 4, 2019.

127. Cremer T, Baumann H, Nakanishi K, Cremer C. Correlation between interphase and metaphase chromosome arrangements as studied by laser-uv-microbeam experiments. In: *Chromosomes Today*. Dordrecht: Springer Netherlands; 1984:203-212. doi:10.1007/978-94-010-9163-3_19

128. Zorn C, Cremer T, Cremer C, Zimmer J. Laser UV microirradiation of interphase nuclei and post-treatment with caffeine. A new approach to establish the arrangement of interphase chromosomes. *Hum Genet*. 1976;35(1):83-89. http://www.ncbi.nlm.nih.gov/pubmed/1002167. Accessed February 4, 2019.

129. Manuelidis L. Individual interphase chromosome domains revealed by in situ

hybridization. *Hum Genet*. 1985;71(4):288-293. http://www.ncbi.nlm.nih.gov/pubmed/3908288. Accessed February 4, 2019.

130. Cremer M, Grasser F, Lanctôt C, et al. Multicolor 3D Fluorescence In Situ Hybridization for Imaging Interphase Chromosomes. In: *Methods in Molecular Biology (Clifton, N.J.)*. Vol 463. ; 2012:205-239. doi:10.1007/978-1-59745-406-3_15

131. Branco MR, Pombo A. Intermingling of Chromosome Territories in Interphase Suggests Role in Translocations and Transcription-Dependent Associations. Becker P, ed. *PLoS Biol*. 2006;4(5):e138. doi:10.1371/journal.pbio.0040138

132. Parada LA, Roix JJ, Misteli T. An uncertainty principle in chromosome positioning. *Trends Cell Biol*. 2003;13(8):393-396. doi:10.1016/S0962-8924(03)00149-1

133. Grasser F, Neusser M, Fiegler H, et al. Replication-timing-correlated spatial chromatin arrangements in cancer and in primate interphase nuclei. *J Cell Sci*. 2008;121(11):1876-1886. doi:10.1242/jcs.026989

134. Barakat TS, Gribnau J. X Chromosome Inactivation and Embryonic Stem Cells. In: Springer, Boston, MA; 2010:132-154. doi:10.1007/978-1-4419-7037-4_10

135. Clemson CM, Hall LL, Byron M, McNeil J, Lawrence JB. The X chromosome is organized into a gene-rich outer rim and an internal core containing silenced nongenic sequences. *Proc Natl Acad Sci*. 2006;103(20):7688-7693. doi:10.1073/PNAS.0601069103

136. Splinter E, de Wit E, Nora EP, et al. The inactive X chromosome adopts a unique three-dimensional conformation that is dependent on Xist RNA. *Genes Dev*. 2011;25(13):1371-1383. doi:10.1101/gad.633311

137. Zhang L-F, Huynh KD, Lee JT. Perinucleolar Targeting of the Inactive X during S Phase: Evidence for a Role in the Maintenance of Silencing. *Cell*. 2007;129(4):693-706. doi:10.1016/J.CELL.2007.03.036

138. Bolzer A, Kreth G, Solovei I, et al. Three-Dimensional Maps of All Chromosomes in Human Male Fibroblast Nuclei and Prometaphase Rosettes. Misteli T, ed. *PLoS Biol*. 2005;3(5):e157. doi:10.1371/journal.pbio.0030157

139. Kreth G, Finsterle J, von Hase J, Cremer M, Cremer C. Radial arrangement of chromosome territories in human cell nuclei: a computer model approach based on gene density indicates a probabilistic global positioning code. *Biophys J*. 2004;86(5):2803-2812. doi:10.1016/S0006-3495(04)74333-7

140. Croft JA, Bridger JM, Boyle S, Perry P, Teague P, Bickmore WA. Differences in the localization and morphology of chromosomes in the human nucleus. *J Cell Biol*. 1999;145(6):1119-1131. http://www.ncbi.nlm.nih.gov/pubmed/10366586. Accessed February 4, 2019.

141. Kuroda M, Tanabe H, Yoshida K, et al. Alteration of chromosome positioning during adipocyte differentiation. *J Cell Sci*. 2004;117(Pt 24):5897-5903. doi:10.1242/jcs.01508

142. Bártová E, Krejčí J, Harničarová A, Kozubek S. Differentiation of human embryonic stem cells induces condensation of chromosome territories and formation of heterochromatin protein 1 foci. *Differentiation*. 2008;76(1):24-32. doi:10.1111/J.1432-0436.2007.00192.X

143. Rouquette J, Genoud C, Vazquez-Nin GH, Kraus B, Cremer T, Fakan S. Revealing the high-resolution three-dimensional network of chromatin and interchromatin space: A novel electron-microscopic approach to reconstructing nuclear architecture. *Chromosom Res*. 2009;17(6):801-810. doi:10.1007/s10577-009-9070-x

144. Cavalli G. Chromosome kissing. *Curr Opin Genet Dev*. 2007;17(5):443-450. doi:10.1016/J.GDE.2007.08.013

145. Jackson DA, Pombo A. Replicon clusters are stable units of chromosome structure: evidence that nuclear organization contributes to the efficient activation and propagation of S phase in human cells. *J Cell Biol*. 1998;140(6):1285-1295. doi:10.1083/JCB.140.6.1285

146. Brown KE, Guest SS, Smale ST, Hahm K, Merkenschlager M, Fisher AG. Association of Transcriptionally Silent Genes with Ikaros Complexes at Centromeric Heterochromatin. *Cell*. 1997;91(6):845-854. doi:10.1016/S0092-8674(00)80472-9

147. Ling JQ, Li T, Hu JF, et al. CTCF mediates interchromosomal colocalization between Igf2/H19 and Wsb1/Nf1. *Science*. 2006;312(5771):269-272. doi:10.1126/science.1123191

148. Olivares-Chauvet P, Fennessy D, Jackson DA, Maya-Mendoza A. Innate Structure of DNA Foci Restricts the Mixing of DNA from Different Chromosome Territories. Bridger JM, ed. *PLoS One*. 2011;6(12):e27527. doi:10.1371/journal.pone.0027527

149. Raška I, Shaw PJ, Cmarko D. New Insights into Nucleolar Architecture and Activity. In: *International Review of Cytology*. Vol 255. ; 2006:177-235. doi:10.1016/S0074-7696(06)55004-1

150. Ma N, Matsunaga S, Takata H, Ono-Maniwa R, Uchiyama S, Fukui K. Nucleolin functions in nucleolus formation and chromosome congression. *J Cell Sci*. 2007;120(Pt 12):2091-2105. doi:10.1242/jcs.008771

151. Mosgoeller W, Schöfer C, Steiner M, Sylvester JE, Hozák P. Arrangement of ribosomal genes in nucleolar domains revealed by detection of "Christmas tree" components. *Histochem Cell Biol*. 2001;116(6):495-505. doi:10.1007/s00418-001-0345-3

152. Reeder RH. Regulation of RNA Polymerase I Transcription in Yeast and Vertebrates. *Prog Nucleic Acid Res Mol Biol*. 1998;62:293-327. doi:10.1016/S0079-6603(08)60511-5

153. Grummt I. Regulation of Mammalian Ribosomal Gene Transcription by RNA Polymerase I. *Prog Nucleic Acid Res Mol Biol*. 1998;62:109-154. doi:10.1016/S0079-6603(08)60506-1

154. Kermekchiev M, Workman JL, Pikaard CS. Nucleosome binding by the polymerase I transactivator upstream binding factor displaces linker histone H1. *Mol Cell Biol*. 1997;17(10):5833-5842. http://www.ncbi.nlm.nih.gov/pubmed/9315641. Accessed February 19, 2019.

155. Reichow SL, Hamma T, Ferré-D'Amaré AR, Varani G. The structure and function of small nucleolar ribonucleoproteins. *Nucleic Acids Res*. 2007;35(5):1452-1464. doi:10.1093/nar/gkl1172

156. Lindström MS. NPM1/B23: A Multifunctional Chaperone in Ribosome Biogenesis and Chromatin Remodeling. *Biochem Res Int*. 2011;2011:195209. doi:10.1155/2011/195209

157. Wolgemuth DJ, Jagiello GM, Henderson AS. Quantitation of ribosomal RNA genes in fetal human oocyte nuclei using rRNA: DNA hybridization in situ: Evidence for increased multiplicity. *Exp Cell Res*. 1979;118(1):181-190. doi:10.1016/0014-4827(79)90596-2

158. Lessard F, Igelmann S, Trahan C, et al. Senescence-associated ribosome biogenesis defects contributes to cell cycle arrest through the Rb pathway. *Nat Cell Biol*. 2018;20(7):789-799. doi:10.1038/s41556-018-0127-y

159. Muscarella DE, Vogt VM, Bloom SE. The ribosomal RNA gene cluster in aneuploid chickens: evidence for increased gene dosage and regulation of gene expression. *J Cell Biol*. 1985;101(5 Pt 1):1749-1756. http://www.ncbi.nlm.nih.gov/pubmed/4055895. Accessed March 6, 2019.

160. Reeder RH. Mechanisms of nucleolar dominance in animals and plants. *J Cell Biol*. 1985;101(5 Pt 1):2013-2016. doi:10.1083/JCB.101.5.2013

161. Michalak K, Maciak S, Kim YB, et al. Nucleolar dominance and maternal control of 45S rDNA expression. *Proceedings Biol Sci*. 2015;282(1820):20152201. doi:10.1098/rspb.2015.2201

162. Lewis MS, Pikaard CS. Restricted chromosomal silencing in nucleolar dominance. *Proc Natl Acad Sci*. 2001;98(25):14536-14540. doi:10.1073/pnas.251424098

163. Grob A, Colleran C, McStay B. Construction of synthetic nucleoli in human cells reveals how a major functional nuclear domain is formed and propagated through cell division. *Genes Dev*. 2014;28(3):220-230. doi:10.1101/gad.234591.113

164. Harničarová Horáková A, Bártová E, Galiová G, Uhlířová R, Matula P, Kozubek S. SUV39h-independent association of HP1β with fibrillarin-positive nucleolar regions. *Chromosoma*. 2010;119(3):227-241. doi:10.1007/s00412-009-0252-2

165. Paredes S, Angulo-Ibanez M, Tasselli L, et al. The epigenetic regulator SIRT7 guards against mammalian cellular senescence induced by ribosomal DNA instability. *J Biol Chem*. 2018;293(28):11242-11250. doi:10.1074/jbc.AC118.003325

166. Schmitz K-M, Mayer C, Postepska A, Grummt I. Interaction of noncoding RNA with the rDNA promoter mediates recruitment of DNMT3b and silencing of rRNA genes. *Genes Dev*. 2010;24(20):2264-2269. doi:10.1101/gad.590910

167. Bacalini MG, Pacilli A, Giuliani C, et al. The nucleolar size is associated to the methylation status of ribosomal DNA in breast carcinomas. *BMC Cancer*. 2014;14(1):361. doi:10.1186/1471-2407-14-361

168. Strohner R, Nemeth A, Jansa P, et al. NoRC--a novel member of mammalian ISWI-containing chromatin remodeling machines. *EMBO J*. 2001;20(17):4892-4900. doi:10.1093/emboj/20.17.4892

169. Xie W, Ling T, Zhou Y, et al. The chromatin remodeling complex NuRD establishes the poised state of rRNA genes characterized by bivalent histone modifications and altered nucleosome positions. *Proc Natl Acad Sci*. 2012;109(21):8161-8166. doi:10.1073/pnas.1201262109

170. Hirschler-Laszkiewicz I, Cavanaugh A, Hu Q, Catania J, Avantaggiati ML, Rothblum LI. The role of acetylation in rDNA transcription. *Nucleic Acids Res*. 2001;29(20):4114-4124. http://www.ncbi.nlm.nih.gov/pubmed/11600700. Accessed March 6, 2019.

171. Harris B, Bose T, Lee KK, et al. Cohesion promotes nucleolar structure and function. *Mol Biol Cell*. 2014;25(3):337-346. doi:10.1091/mbc.E13-07-0377

172. Weber SC, Brangwynne CP. Getting RNA and protein in phase. *Cell*. 2012;149(6):1188-1191. doi:10.1016/j.cell.2012.05.022

173. Weber SC, Brangwynne CP. Inverse size scaling of the nucleolus by a concentration-dependent phase transition. *Curr Biol*. 2015;25(5):641-646. doi:10.1016/j.cub.2015.01.012

174. Berry J, Weber SC, Vaidya N, Haataja M, Brangwynne CP. RNA transcription modulates

phase transition-driven nuclear body assembly. *Proc Natl Acad Sci U S A*. 2015;112(38):E5237-45. doi:10.1073/pnas.1509317112

175. Okada N, Steinberg ML, Defendi V. Re-expression of differentiated properties in SV40-infected human epidermal keratinocytes induced by 5-azacytidine. *Exp Cell Res*. 1984;153(1):198-207. http://www.ncbi.nlm.nih.gov/pubmed/6203767. Accessed February 7, 2019.

176. Pucci M, Rapino C, Di Francesco A, Dainese E, D'Addario C, Maccarrone M. Epigenetic control of skin differentiation genes by phytocannabinoids. *Br J Pharmacol*. 2013;170(3):581-591. doi:10.1111/bph.12309

177. Bock C, Beerman I, Lien W-H, et al. DNA Methylation Dynamics during In Vivo Differentiation of Blood and Skin Stem Cells. *Mol Cell*. 2012;47(4):633-647. doi:10.1016/J.MOLCEL.2012.06.019

178. Rinaldi L, Datta D, Serrat J, et al. Dnmt3a and Dnmt3b Associate with Enhancers to Regulate Human Epidermal Stem Cell Homeostasis. *Cell Stem Cell*. 2016;19(4):491-501. doi:10.1016/J.STEM.2016.06.020

179. Ryan MC, Lee K, Miyashita Y, Carter WG. Targeted disruption of the LAMA3 gene in mice reveals abnormalities in survival and late stage differentiation of epithelial cells. *J Cell Biol*. 1999;145(6):1309-1323. http://www.ncbi.nlm.nih.gov/pubmed/10366601. Accessed February 7, 2019.

180. Sathyanarayana UG et al. Sun exposure related methylation in malignant and non-malignant skin lesions. *Cancer Lett*. 2007;245:112-120.

181. Vandiver AR, Irizarry RA, Hansen KD, et al. Age and sun exposure-related widespread genomic blocks of hypomethylation in nonmalignant skin. *Genome Biol*. 2015;16(1):80. doi:10.1186/s13059-015-0644-y

182. Yang Y, Gil M, Byun SM, Choi I, Pyun KH, Ha H. Transforming Growth Factor-β1 Inhibits Human Keratinocyte Proliferation by Upregulation of a Receptor-Type Tyrosine Phosphatase R-PTP-κ Gene Expression. *Biochem Biophys Res Commun*. 1996;228(3):807-812. doi:10.1006/bbrc.1996.1736

183. Deng T, Kuang Y, Wang L, Li J, Wang Z, Fei J. An essential role for DNA methyltransferase 3a in melanoma tumorigenesis. *Biochem Biophys Res Commun*. 2009;387(3):611-616. doi:10.1016/j.bbrc.2009.07.093

184. Miroshnikova YA, Le HQ, Schneider D, et al. Adhesion forces and cortical tension couple cell proliferation and differentiation to drive epidermal stratification. *Nat Cell Biol*. 2018;20(1):69-80. doi:10.1038/s41556-017-0005-z

185. Chiles MC, Ai L, Zuo C, Fan C-Y, Smoller BR. E-Cadherin Promoter Hypermethylation in Preneoplastic and Neoplastic Skin Lesions. *Mod Pathol*. 2003;16(10):1014-1018. doi:10.1097/01.MP.0000089779.35435.9D

186. Gdula MR, Poterlowicz K, Mardaryev AN, et al. Remodeling of Three-Dimensional Organization of the Nucleus during Terminal Keratinocyte Differentiation in the Epidermis. *J Invest Dermatol*. 2013;133:2191-2201. doi:10.1038/jid.2013.66

187. Lien WH, Guo X, Polak L, et al. Genome-wide maps of histone modifications unwind in vivo chromatin states of the hair follicle lineage. *Cell Stem Cell*. 2011;9(3):219-232. doi:10.1016/j.stem.2011.07.015

188. Ezhkova E, Pasolli HA, Parker JS, et al. Ezh2 Orchestrates Gene Expression for the Stepwise Differentiation of Tissue-Specific Stem Cells. *Cell*. 136:1122-1135.

doi:10.1016/j.cell.2008.12.043

189. Ezhkova E, Lien WH, Stokes N, Pasolli HA, Silva JM, Fuchs E. EZH1 and EZH2 cogovern histone H3K27 trimethylation and are essential for hair follicle homeostasis and wound repair. *Genes Dev*. 2011;25(5):485-498. doi:10.1101/gad.2019811

190. Sen GL, Webster DE, Barragan DI, Chang HY, Khavari PA. Control of differentiation in a self-renewing mammalian tissue by the histone demethylase JMJD3. *Genes Dev*. 2008;22(14):1865-1870. doi:10.1101/gad.1673508

191. Driskell I, Oda H, Blanco S, Nascimento E, Humphreys P, Frye M. The histone methyltransferase Setd8 acts in concert with c-Myc and is required to maintain skin. *EMBO J*. 2012;31(3):616-629. doi:10.1038/emboj.2011.421

192. Leboeuf M, Terrell A, Trivedi S, et al. Hdac1 and Hdac2 Act Redundantly to Control p63 and p53 Functions in Epidermal Progenitor Cells. *Dev Cell*. 2010;19:807-818. doi:10.1016/j.devcel.2010.10.015

193. Connelly JT, Mishra A, Gautrot JE, Watt FM. Shape-induced terminal differentiation of human epidermal stem cells requires p38 and is regulated by histone acetylation. *PLoS One*. 2011;6(11):1-10. doi:10.1371/journal.pone.0027259

194. Robertson ED, Weir L, Romanowska M, Leigh IM, Panteleyev AA. ARNT controls the expression of epidermal differentiation genes through HDAC- and EGFR-dependent pathways. *J Cell Sci*. 2012;125(Pt 14):3320-3332. doi:10.1242/jcs.095125

195. Shin J-W, Choi H-R, Nam K-M, et al. The Co-Expression Pattern of p63 and HDAC1: A Potential Way to Disclose Stem Cells in Interfollicular Epidermis. *Int J Mol Sci*. 2017;18(7). doi:10.3390/ijms18071360

196. Li G, Ye Z, Shi C, et al. The Histone Methyltransferase Ash1l is Required for Epidermal Homeostasis in Mice. *Sci Rep*. 2017;7(1):45401. doi:10.1038/srep45401

197. Indra AK, Dupe V, Bornert J-M, et al. Temporally controlled targeted somatic mutagenesis in embryonic surfaceectoderm and fetal epidermal keratinocytes unveils two distinct developmentalfunctions of BRG1 in limb morphogenesis and skin barrier formation. *Development*. 2005;132(20):4533-4544. doi:10.1242/dev.02019

198. Bao X, Tang J, Lopez-Pajares V, et al. ACTL6a Enforces the Epidermal Progenitor State by Suppressing SWI/SNF-Dependent Induction of KLF4. *Cell Stem Cell*. 2013;12(2):193-203. doi:10.1016/J.STEM.2012.12.014

199. Luis NM, Morey L, Mejetta S, et al. Regulation of Human Epidermal Stem Cell Proliferation and Senescence Requires Polycomb- Dependent and -Independent Functions of Cbx4. *Cell Stem Cell*. 2011;9(3):233-246. doi:10.1016/J.STEM.2011.07.013

200. Mardaryev AN, Liu B, Rapisarda V, et al. Cbx4 maintains the epithelial lineage identity and cell proliferation in the developing stratified epithelium. *J Cell Biol*. 2016;212(1):77-89. doi:10.1083/jcb.201506065

201. Dauber KL, Perdigoto CN, Valdes VJ, Santoriello FJ, Cohen I, Ezhkova E. Dissecting the Roles of Polycomb Repressive Complex 2 Subunits in the Control of Skin Development. *J Invest Dermatol*. 2016;136(8):1647-1655. doi:10.1016/J.JID.2016.02.809

202. Mulder KW, Wang X, Escriu C, et al. Diverse epigenetic strategies interact to control epidermal differentiation. *Nat Cell Biol*. 2012;14(7):753-763. doi:10.1038/ncb2520

203. Koludrovic D, Laurette P, Strub T, et al. Chromatin-Remodelling Complex NURF Is Essential for Differentiation of Adult Melanocyte Stem Cells. Bickmore WA, ed. *PLOS*

Genet. 2015;11(10):e1005555. doi:10.1371/journal.pgen.1005555

204. Marella N V., Seifert B, Nagarajan P, Sinha S, Berezney R. Chromosomal rearrangements during human epidermal keratinocyte differentiation. *J Cell Physiol*. 2009;221(1):139-146. doi:10.1002/jcp.21855

205. Mischke D, Korge BP, Marenholz I, Volz A, Ziegler A. Genes Encoding Structural Proteins of Epidermal Cornification and S100 Calcium-Binding Proteins Form a Gene Complex ("Epidermal Differentiation Complex") on Human Chromosome 1q21. *J Invest Dermatol*. 1996;106(5):989-992. doi:10.1111/1523-1747.EP12338501

206. Mischke D. The complexity of gene families involved in epithelial differentiation. Keratin genes and the epidermal differentiation complex. *Subcell Biochem*. 1998;31:71-104. http://www.ncbi.nlm.nih.gov/pubmed/9932490. Accessed February 6, 2019.

207. Kypriotou M, Huber M, Hohl D. The human epidermal differentiation complex: cornified envelope precursors, S100 proteins and the 'fused genes' family. *Exp Dermatol*. 2012;21(9):643-649. doi:10.1111/j.1600-0625.2012.01472.x

208. Williams RRE, Broad S, Sheer D, Ragoussis J. Subchromosomal Positioning of the Epidermal Differentiation Complex (EDC) in Keratinocyte and Lymphoblast Interphase Nuclei. *Exp Cell Res*. 2002;272(2):163-175. doi:10.1006/EXCR.2001.5400

209. Oh IY, Albea DM, Goodwin ZA, et al. Regulation of the dynamic chromatin architecture of the epidermal differentiation complex is mediated by a c-Jun/AP-1-modulated enhancer. *J Invest Dermatol*. 2014;134(9):2371-2380. doi:10.1038/jid.2014.44

210. Mardaryev AN, Gdula MR, Yarker JL, et al. p63 and Brg1 control developmentally regulated higher-order chromatin remodelling at the epidermal differentiation complex locus in epidermal progenitor cells. *Development*. 2014;141(1):101-111. doi:10.1242/dev.103200

211. Lechler T, Fuchs E. Asymmetric cell divisions promote stratification and differentiation of mammalian skin. *Nature*. 2005;437(7056):275-280. doi:10.1038/nature03922

212. Bikle DD, Xie Z, Tu C-L. Calcium regulation of keratinocyte differentiation. *Expert Rev Endocrinol Metab*. 2012;7(4):461-472. doi:10.1586/eem.12.34

213. Clapham DE. Calcium Signaling. *Cell*. 2007;131(6):1047-1058. doi:10.1016/j.cell.2007.11.028

214. Wang N. Review of cellular mechanotransduction. *J Phys D Appl Phys*. 2017;50(23):233002. doi:10.1088/1361-6463/aa6e18

215. Charest JL, Jennings JM, King WP, Kowalczyk AP, García AJ. Cadherin-Mediated Cell–Cell Contact Regulates Keratinocyte Differentiation. *J Invest Dermatol*. 2009;129(3):564-572. doi:10.1038/JID.2008.265

216. Trappmann B, Gautrot JE, Connelly JT, et al. Extracellular-matrix tethering regulates stem-cell fate. *Nat Mater*. 2012;11(7):642-649. doi:10.1038/nmat3339

217. Zarkoob H, Bodduluri S, Ponnaluri S V, Selby JC, Sander EA. Substrate Stiffness Affects Human Keratinocyte Colony Formation. *Cell Mol Bioeng*. 2015;8(1):32-50. doi:10.1007/s12195-015-0377-8

218. Frank DE. Laminin 5 deposition regulates keratinocyte polarization and persistent migration. *J Cell Sci*. 2004;117(8):1351-1363. doi:10.1242/jcs.01003

219. Chermnykh E, Kalabusheva E, Vorotelyak E. Extracellular Matrix as a Regulator of Epidermal Stem Cell Fate. *Int J Mol Sci*. 2018;19(4). doi:10.3390/ijms19041003

220. Connelly JT, Gautrot JE, Trappmann B, et al. Actin and serum response factor transduce physical cues from the microenvironment to regulate epidermal stem cell fate decisions. *Nat Cell Biol*. 2010;12(7):711-718. doi:10.1038/ncb2074

221. Almeida F V., Walko G, McMillan JR, et al. The cytolinker plectin regulates nuclear mechanotransduction in keratinocytes. *J Cell Sci*. 2015;128(24):4475-4486. doi:10.1242/jcs.173435

222. Hardin J, Bertoni G, Kleinsmith LJ, Becker WM. *Becker's World of the Cell*. Benjamin Cummings; 2012.

223. Veigel C, Schmidt CF. Moving into the cell: single-molecule studies of molecular motors in complex environments. *Nat Publ Gr*. 2011;12. doi:10.1038/nrm3062

224. Mayor R, Etienne-Manneville S. The front and rear of collective cell migration. *Nat Rev Mol Cell Biol*. 2016;17(2):97-109. doi:10.1038/nrm.2015.14

225. Fenelon KD, Hopyan S. Structural components of nuclear integrity with gene regulatory potential. *Curr Opin Cell Biol*. 2017;48:63-71. doi:10.1016/j.ceb.2017.06.001

226. Uhler C, Shivashankar G V. Chromosome Intermingling: Mechanical Hotspots for Genome Regulation. *Trends Cell Biol*. 2017;27(11):810-819. doi:10.1016/j.tcb.2017.06.005

227. Franker MAM, Hoogenraad CC. Microtubule-based transport - basic mechanisms, traffic rules and role in neurological pathogenesis. *J Cell Sci*. 2013;126(Pt 11):2319-2329. doi:10.1242/jcs.115030

228. Forth S, Kapoor TM. The mechanics of microtubule networks in cell division. *J Cell Biol*. 2017;216(6):1525-1531. doi:10.1083/jcb.201612064

229. Muroyama A, Lechler T. A transgenic toolkit for visualizing and perturbing microtubules reveals unexpected functions in the epidermis. *Elife*. 2017;6. doi:10.7554/eLife.29834

230. Shahbazi MN, Perez-Moreno M. Microtubules CLASP to Adherens Junctions in epidermal progenitor cells. *Bioarchitecture*. 2014;4(1):25-30. doi:10.4161/bioa.28177

231. Fuchs E. Keratins and the Skin. *Annu Rev Cell Dev Biol*. 1995;11(1):123-154. doi:10.1146/annurev.cb.11.110195.001011

232. Ramms L, Fabris G, Windoffer R, et al. Keratins as the main component for the mechanical integrity of keratinocytes. *Proc Natl Acad Sci*. 2013;110(46):18513-18518. doi:10.1073/pnas.1313491110

233. Reichelt J. Mechanotransduction of keratinocytes in culture and in the epidermis. *Eur J Cell Biol*. 2007;86(11-12):807-816. doi:10.1016/J.EJCB.2007.06.004

234. Pollard TD, Goldman RD. Overview of the Cytoskeleton from an Evolutionary Perspective. In: *The Cytoskeleton*. ; 2017:1-7. doi:10.1101/cshperspect.a030288

235. Schweizer J, Bowden PE, Coulombe PA, et al. New consensus nomenclature for mammalian keratins. *J Cell Biol*. 2006. doi:10.1083/jcb.200603161

236. Parry DAD, Strelkov S V., Burkhard P, Aebi U, Herrmann H. Towards a molecular description of intermediate filament structure and assembly. *Exp Cell Res*. 2007;313(10):2204-2216. doi:10.1016/J.YEXCR.2007.04.009

237. Bray DJ, Walsh TR, Noro MG, Notman R. Complete Structure of an Epithelial Keratin Dimer: Implications for Intermediate Filament Assembly. Kreplak L, ed. *PLoS One*. 2015;10(7):e0132706. doi:10.1371/journal.pone.0132706

238. Windoffer R, Beil M, Magin TM, Leube RE. Cytoskeleton in motion: the dynamics of keratin intermediate filaments in epithelia. *J Cell Biol*. 2011;194(5):669-678. doi:10.1083/jcb.201008095

239. Seltmann K, Roth W, Kröger C, et al. Keratins mediate localization of hemidesmosomes and repress cell motility. *J Invest Dermatol*. 2013;133(1):181-190. doi:10.1038/jid.2012.256

240. Waseem A, Alam Y, Lalli A, et al. Keratin 15 Expression in Stratified Epithelia: Downregulation in Activated Keratinocytes. *J Invest Dermatol*. 1999;112(3):362-369. doi:10.1046/J.1523-1747.1999.00535.X

241. Porter RM, Lunny DP, Ogden PH, et al. K15 expression implies lateral differentiation within stratified epithelial basal cells. *Lab Invest*. 2000;80(11):1701-1710. http://www.ncbi.nlm.nih.gov/pubmed/11092530. Accessed February 8, 2019.

242. Kartasova T, Roop DR, Holbrook KA, Yuspa SH. Mouse differentiation-specific keratins 1 and 10 require a preexisting keratin scaffold to form a filament network. *J Cell Biol*. 1993;120(5):1251-1261. http://www.ncbi.nlm.nih.gov/pubmed/7679677. Accessed February 8, 2019.

243. Paramio JM, Casanova ML, Segrelles C, Mittnacht S, Lane EB, Jorcano JL. Modulation of cell proliferation by cytokeratins K10 and K16. *Mol Cell Biol*. 1999;19(4):3086-3094. http://www.ncbi.nlm.nih.gov/pubmed/10082575. Accessed February 8, 2019.

244. SMITH, UNDERWOOD, McLEAN. Ontogeny and regional variability of keratin 2e (K2e) in developing human fetal skin: a unique spatial and temporal pattern of keratin expression in development. *Br J Dermatol*. 1999;140(4):582-591. doi:10.1046/j.1365-2133.1999.02755.x

245. Mahler B, Gocken T, Brojan M, Childress S, Spandau DF, Foley J. Keratin 2e: A Marker for Murine Nipple Epidermis. *Cells Tissues Organs*. 2004;176(4):169-177. doi:10.1159/000077033

246. Yamaguchi Y, Itami S, Tarutani M, Hosokawa K, Miura H, Yoshikawa K. Regulation of Keratin 9 in Nonpalmoplantar Keratinocytes by Palmoplantar Fibroblasts Through Epithelial–Mesenchymal Interactions. *J Invest Dermatol*. 1999;112(4):483-488. doi:10.1046/j.1523-1747.1999.00544.x

247. Rogers MA, Edler L, Winter H, Langbein L, Beckmann I, Schweizer J. Characterization of New Members of the Human Type II Keratin Gene Family and a General Evaluation of the Keratin Gene Domain on Chromosome 12q13.13. *J Invest Dermatol*. 2005;124(3):536-544. doi:10.1111/J.0022-202X.2004.23530.X

248. Ma L, Xu J, Coulombe PA, Wirtz D. Keratin filament suspensions show unique micromechanical properties. *J Biol Chem*. 1999;274(27):19145-19151. doi:10.1074/JBC.274.27.19145

249. Ma L, Yamada S, Wirtz D, Coulombe PA. A “hot-spot” mutation alters the mechanical properties of keratin filament networks. *Nat Cell Biol*. 2001;3(5):503-506. doi:10.1038/35074576

250. Windoffer R, Leube RE. Detection of cytokeratin dynamics by time-lapse fluorescence microscopy in living cells. *J Cell Sci*. 1999;112(24).

251. Yoon KH, Yoon M, Moir RD, Khuon S, Flitney FW, Goldman RD. Insights into the dynamic properties of keratin intermediate filaments in living epithelial cells. *J Cell Biol*. 2001;153(3):503-516. http://www.ncbi.nlm.nih.gov/pubmed/11331302. Accessed February 9, 2019.

252. Windoffer R, Wöll S, Strnad P, Leube RE. Identification of novel principles of keratin filament network turnover in living cells. *Mol Biol Cell*. 2004;15(5):2436-2448. doi:10.1091/mbc.e03-09-0707

253. Windoffer R, Kölsch A, Wöll S, Leube RE. Focal adhesions are hotspots for keratin filament precursor formation. *J Cell Biol*. 2006;173(3):341-348. doi:10.1083/JCB.200511124

254. Lee C-H, Coulombe PA. Self-organization of keratin intermediate filaments into cross-linked networks. *J Cell Biol*. 2009;186(3):409-421. doi:10.1083/jcb.200810196

255. Kölsch A, Windoffer R, Würflinger T, Aach T, Leube RE. The keratin-filament cycle of assembly and disassembly. *J Cell Sci*. 2010;123(Pt 13):2266-2272. doi:10.1242/jcs.068080

256. Nolting J-F, Möbius W, Köster S. Mechanics of Individual Keratin Bundles in Living Cells. *Biophys J*. 2014;107(11):2693-2699. doi:10.1016/J.BPJ.2014.10.039

257. Blessing M, Rüther U, Franke WW. Ectopic synthesis of epidermal cytokeratins in pancreatic islet cells of transgenic mice interferes with cytoskeletal order and insulin production. *J Cell Biol*. 1993;120(3):743-755. doi:10.1083/JCB.120.3.743

258. Listwan P, Rothnagel JA. Keratin bundling proteins. *Methods Cell Biol*. 2004;78:817-827. http://www.ncbi.nlm.nih.gov/pubmed/15646640. Accessed February 9, 2019.

259. Ishikawa K, Sumiyoshi H, Matsuo N, et al. Epiplakin accelerates the lateral organization of keratin filaments during wound healing. *J Dermatol Sci*. 2010;60(2):95-104. doi:10.1016/j.jdermsci.2010.08.011

260. Svitkina TM, Verkhovsky AB, Borisy GG. Plectin sidearms mediate interaction of intermediate filaments with microtubules and other components of the cytoskeleton. *J Cell Biol*. 1996;135(4):991-1007. http://www.ncbi.nlm.nih.gov/pubmed/8922382. Accessed February 9, 2019.

261. Sivaramakrishnan S, Schneider JL, Sitikov A, Goldman RD, Ridge KM. Shear stress induced reorganization of the keratin intermediate filament network requires phosphorylation by protein kinase C zeta. *Mol Biol Cell*. 2009;20(11):2755-2765. doi:10.1091/mbc.e08-10-1028

262. Moch M, Herberich G, Aach T, Leube RE, Windoffer R. Measuring the regulation of keratin filament network dynamics. *Proc Natl Acad Sci U S A*. 2013;110(26):10664-10669. doi:10.1073/pnas.1306020110

263. Wöll S, Windoffer R, Leube RE. p38 MAPK-dependent shaping of the keratin cytoskeleton in cultured cells. *J Cell Biol*. 2007;177(5):795-807. doi:10.1083/jcb.200703174

264. Loschke F, Homberg M, Magin TM. Keratin Isotypes Control Desmosome Stability and Dynamics through PKCα. *J Invest Dermatol*. 2016;136(1):202-213. doi:10.1038/JID.2015.403

265. Alam H, Sehgal L, Kundu ST, Dalal SN, Vaidya MM. Novel function of keratins 5 and 14 in proliferation and differentiation of stratified epithelial cells. *Mol Biol Cell*. 2011;22(21):4068-4078. doi:10.1091/mbc.E10-08-0703

266. Hobbs RP, DePianto DJ, Jacob JT, et al. Keratin-dependent regulation of Aire and gene expression in skin tumor keratinocytes. *Nat Genet*. 2015;47(8):933-938. doi:10.1038/ng.3355

267. Escobar-Hoyos LF, Shah R, Roa-Peña L, et al. Keratin-17 Promotes p27KIP1 Nuclear Export and Degradation and Offers Potential Prognostic Utility. *Cancer Res*. 2015;75(17):3650-3662. doi:10.1158/0008-5472.CAN-15-0293

268. Broussard JA, Yang R, Huang C, et al. The desmoplakin–intermediate filament linkage regulates cell mechanics. Nusrat A, ed. *Mol Biol Cell*. 2017;28(23):3156-3164. doi:10.1091/mbc.e16-07-0520

269. Kostan J, Gregor M, Walko G, Wiche G. Plectin isoform-dependent regulation of keratin-integrin α6β4 anchorage via Ca2+/calmodulin. *J Biol Chem*. 2009;284(27):18525-18536. doi:10.1074/jbc.M109.008474

270. Letai A, Coulombe PA, McCormick MB, Yu QC, Hutton E, Fuchs E. Disease severity correlates with position of keratin point mutations in patients with epidermolysis bullosa simplex. *Proc Natl Acad Sci U S A*. 1993;90(8):3197-3201. doi:10.1073/pnas.90.8.3197

271. Moll R, Divo M, Langbein L. The human keratins: biology and pathology. *Histochem Cell Biol*. 2008;129:705-733. doi:10.1007/s00418-008-0435-6

272. Wilhelmsen K, Litjens SHM, Kuikman I, et al. Nesprin-3, a novel outer nuclear membrane protein, associates with the cytoskeletal linker protein plectin. *J Cell Biol*. 2005;171(5):799-810. doi:10.1083/JCB.200506083

273. Ketema M, Sonnenberg A. Nesprin-3: a versatile connector between the nucleus and the cytoskeleton. *Biochem Soc Trans*. 2011;39(6):1719-1724. doi:10.1042/BST20110669

274. Osmanagic-Myers S, Gregor M, Walko G, Burgstaller G, Reipert S, Wiche G. Plectin-controlled keratin cytoarchitecture affects MAP kinases involved in cellular stress response and migration. *J Cell Biol*. 2006;174(4):557-568. doi:10.1083/jcb.200605172

275. Lodish, Berk, Kaiser, Krieger. *MOLECULAR CELL BIOLOGY*. W.H. Freeman; 2016.

276. Luxenburg C, Heller E, Pasolli HA, et al. Wdr1-mediated cell shape dynamics and cortical tension are essential for epidermal planar cell polarity. *Nat Cell Biol*. 2015;17(5):592-604. doi:10.1038/ncb3146

277. Kim JS, Lee C-H, Su BY, Coulombe PA. Mathematical modeling of the impact of actin and keratin filaments on keratinocyte cell spreading. *Biophys J*. 2012;103(9):1828-1838. doi:10.1016/j.bpj.2012.09.016

278. DePina AS, Langford GM. Vesicle transport: The role of actin filaments and myosin motors. *Microsc Res Tech*. 1999;47(2):93-106. doi:10.1002/(SICI)1097-0029(19991015)47:2<93::AID-JEMT2>3.0.CO;2-P

279. Gunning PW, Ghoshdastider U, Whitaker S, Popp D, Robinson RC. The evolution of compositionally and functionally distinct actin filaments. *J Cell Sci*. 2015;128(11):2009-2019. doi:10.1242/jcs.165563

280. Dominguez R, Holmes KC. Actin Structure and Function. *Annu Rev Biophys*. 2011;40:169-186. doi:10.1146/annurev-biophys-042910-155359

281. Pollard TD, Blanchoin L, Mullins RD. Molecular Mechanisms Controlling Actin Filament Dynamics in Nonmuscle Cells. *Annu Rev Biophys Biomol Struct*. 2000;29(1):545-576. doi:10.1146/annurev.biophys.29.1.545

282. Carlsson L, Nyström L-E, Sundkvist I, Markey F, Lindberg U. Actin polymerizability is influenced by profilin, a low molecular weight protein in non-muscle cells. *J Mol Biol*. 1977;115(3):465-483. doi:10.1016/0022-2836(77)90166-8

283. Lappalainen P, Drubin DG. Cofilin promotes rapid actin filament turnover in vivo. *Nature*. 1997;388(6637):78-82. doi:10.1038/40418

284. Gunning PW, Schevzov G, Kee AJ, Hardeman EC. Tropomyosin isoforms: divining rods for actin cytoskeleton function. *Trends Cell Biol*. 2005;15(6):333-341. doi:10.1016/j.tcb.2005.04.007

285. Michelot A, Drubin DG. Building distinct actin filament networks in a common cytoplasm. *Curr Biol*. 2011;21(14):R560-9. doi:10.1016/j.cub.2011.06.019

286. Tojkander S, Gateva G, Lappalainen P. Actin stress fibers – assembly, dynamics and biological roles. *J Cell Sci*. 125:1855-1864. doi:10.1242/jcs.098087

287. Beach JR, Bruun KS, Shao L, et al. Actin dynamics and competition for myosin monomer govern the sequential amplification of myosin filaments. *Nat Cell Biol*. 2017;19(2):85-93. doi:10.1038/ncb3463

288. Nanba D, Toki F, Matsushita N, Matsushita S, Higashiyama S, Barrandon Y. Actin filament dynamics impacts keratinocyte stem cell maintenance. *EMBO Mol Med*. 2013;5(4):640-653. doi:10.1002/emmm.201201839

289. McGough A, Pope B, Chiu W, Weeds A. Cofilin changes the twist of F-actin: implications for actin filament dynamics and cellular function. *J Cell Biol*. 1997;138(4):771-781. http://www.ncbi.nlm.nih.gov/pubmed/9265645. Accessed February 10, 2019.

290. Hayakawa K, Tatsumi H, Sokabe M. Actin filaments function as a tension sensor by tension-dependent binding of cofilin to the filament. *J Cell Biol*. 2011;195(5):721-727. doi:10.1083/jcb.201102039

291. Uyeda TQP, Iwadate Y, Umeki N, Nagasaki A, Yumura S. Stretching Actin Filaments within Cells Enhances their Affinity for the Myosin II Motor Domain. Gasset M, ed. *PLoS One*. 2011;6(10):e26200. doi:10.1371/journal.pone.0026200

292. del Rio A, Perez-Jimenez R, Liu R, Roca-Cusachs P, Fernandez JM, Sheetz MP. Stretching single talin rod molecules activates vinculin binding. *Science*. 2009;323(5914):638-641. doi:10.1126/science.1162912

293. Buckley CD, Tan J, Anderson KL, et al. The minimal cadherin-catenin complex binds to actin filaments under force. *Science (80-)*. 2014;346(6209):1254211-1254211. doi:10.1126/science.1254211

294. Schiffhauer ES, Luo T, Mohan K, et al. Mechanoaccumulative Elements of the Mammalian Actin Cytoskeleton. *Curr Biol*. 2016;26(11):1473-1479. doi:10.1016/j.cub.2016.04.007

295. Courtemanche N, Lee JY, Pollard TD, Greene EC. Tension modulates actin filament polymerization mediated by formin and profilin. *Proc Natl Acad Sci*. 2013;110(24):9752-9757. doi:10.1073/pnas.1308257110

296. Miralles F, Posern G, Zaromytidou A-I, Treisman R. Actin Dynamics Control SRF Activity by Regulation of Its Coactivator MAL. *Cell*. 2003;113(3):329-342. doi:10.1016/S0092-8674(03)00278-2

297. Haller K, Rambaldi I, Daniels E, Featherstone M. Subcellular localization of multiple PREP2 isoforms is regulated by actin, tubulin, and nuclear export. *J Biol Chem*. 2004;279(47):49384-49394. doi:10.1074/jbc.M406046200

298. Favot L, Hall SM, Haworth SG, Kemp PR. Cytoplasmic YY1 Is Associated with Increased Smooth Muscle-Specific Gene Expression. *Am J Pathol*. 2005;167(6):1497-1509.

doi:10.1016/S0002-9440(10)61236-9

299. Ikura T, Ogryzko V V, Grigoriev M, et al. Involvement of the TIP60 Histone Acetylase Complex in DNA Repair and Apoptosis. *Cell*. 2000;102(4):463-473. doi:10.1016/S0092-8674(00)00051-9

300. Fuchs M, Gerber J, Drapkin R, et al. The p400 Complex Is an Essential E1A Transformation Target. *Cell*. 2001;106(3):297-307. doi:10.1016/S0092-8674(01)00450-0

301. Mattera L, Escaffit F, Pillaire M-J, et al. The p400/Tip60 ratio is critical for colorectal cancer cell proliferation through DNA damage response pathways. *Oncogene*. 2009;28(12):1506-1517. doi:10.1038/onc.2008.499

302. Serebryannyy LA, Cruz CM, de Lanerolle P. A Role for Nuclear Actin in HDAC 1 and 2 Regulation. *Sci Rep*. 2016;6(1):28460. doi:10.1038/srep28460

303. Philimonenko V V., Zhao J, Iben S, et al. Nuclear actin and myosin I are required for RNA polymerase I transcription. *Nat Cell Biol*. 2004;6(12):1165-1172. doi:10.1038/ncb1190

304. Hofmann WA, Stojiljkovic L, Fuchsova B, et al. Actin is part of pre-initiation complexes and is necessary for transcription by RNA polymerase II. *Nat Cell Biol*. 2004;6(11):1094-1101. doi:10.1038/ncb1182

305. Hu P, Wu S, Hernandez N. A role for beta-actin in RNA polymerase III transcription. *Genes Dev*. 2004;18(24):3010-3015. doi:10.1101/gad.1250804

306. Dopie J, Skarp K-P, Kaisa Rajakyla E, Tanhuanpaa K, Vartiainen MK. Active maintenance of nuclear actin by importin 9 supports transcription. *Proc Natl Acad Sci*. 2012;109(9):E544-E552. doi:10.1073/pnas.1118880109

307. Almuzzaini B, Sarshad AA, Rahmanto AS, et al. In β-actin knockouts, epigenetic reprogramming and rDNA transcription inactivation lead to growth and proliferation defects. *FASEB J*. 2016;30(8):2860-2873. doi:10.1096/fj.201600280R

308. Le HQ, Ghatak S, Yeung CYC, et al. Mechanical regulation of transcription controls Polycomb-mediated gene silencing during lineage commitment. *Nat Cell Biol*. 2016;18(8):864-875. doi:10.1038/ncb3387

309. Baarlink C, Wang H, Grosse R. Nuclear actin network assembly by formins regulates the SRF coactivator MAL. *Science*. 2013;340(6134):864-867. doi:10.1126/science.1235038

310. Lundquist MR, Storaska AJ, Liu T-C, et al. Redox Modification of Nuclear Actin by MICAL-2 Regulates SRF Signaling. *Cell*. 2014;156(3):563-576. doi:10.1016/J.CELL.2013.12.035

311. Plessner M, Melak M, Chinchilla P, Baarlink C, Grosse R. Nuclear F-actin formation and reorganization upon cell spreading. *J Biol Chem*. 2015;290(18):11209-11216. doi:10.1074/jbc.M114.627166

312. Fiore APZP, Spencer VA, Mori H, Carvalho HF, Bissell MJ, Bruni-Cardoso A. Laminin-111 and the Level of Nuclear Actin Regulate Epithelial Quiescence via Exportin-6. *Cell Rep*. 2017;19(10):2102-2115. doi:10.1016/J.CELREP.2017.05.050

313. Mogessie B, Schuh M. Actin protects mammalian eggs against chromosome segregation errors. *Science*. 2017;357(6353):eaal1647. doi:10.1126/science.aal1647

314. Mehta IS, Amira M, Harvey AJ, Bridger JM. Rapid chromosome territory relocation by nuclear motor activity in response to serum removal in primary human fibroblasts. *Genome Biol*. 2010;11(1):R5. doi:10.1186/gb-2010-11-1-r5

315. Tajik A, Zhang Y, Wei F, et al. Transcription upregulation via force-induced direct

stretching of chromatin. *Nat Mater*. 2016;15(12):1287-1296. doi:10.1038/nmat4729

316. Baarlink C, Plessner M, Sherrard A, et al. A transient pool of nuclear F-actin at mitotic exit controls chromatin organization. *Nat Cell Biol*. 2017;19(12):1389-1399. doi:10.1038/ncb3641

317. de Leeuw R, Gruenbaum Y, Medalia O. Nuclear Lamins: Thin Filaments with Major Functions. *Trends Cell Biol*. 2018;28(1):34-45. doi:10.1016/j.tcb.2017.08.004

318. Muller J, Oma Y, Vallar L, Friederich E, Poch O, Winsor B. Sequence and Comparative Genomic Analysis of Actin-related Proteins. *Mol Biol Cell*. 2005;16(12):5736-5748. doi:10.1091/mbc.e05-06-0508

319. Chen M, Shen X. Nuclear actin and actin-related proteins in chromatin dynamics. *Curr Opin Cell Biol*. 2007;19(3):326-330. doi:10.1016/J.CEB.2007.04.009

320. Kölsch A, Windoffer R, Leube RE. Actin-dependent dynamics of keratin filament precursors. *Cell Motil Cytoskeleton*. 2009;66(11):976-985. doi:10.1002/cm.20395

321. Andrä K, Nikolic B, Stöcher M, Drenckhahn D, Wiche G. Not just scaffolding: Plectin regulates actin dynamics in cultured cells. *Genes Dev*. 1998;12(21):3442-3451. doi:10.1101/gad.12.21.3442

322. Burke B, Stewart CL. The nuclear lamins: flexibility in function. *Nat Rev Mol Cell Biol*. 2013;14(1):13-24. doi:10.1038/nrm3488

323. Herrmann H, Aebi U. Intermediate Filaments: Molecular Structure, Assembly Mechanism, and Integration Into Functionally Distinct Intracellular Scaffolds. *Annu Rev Biochem*. 2004;73(1):749-789. doi:10.1146/annurev.biochem.73.011303.073823

324. Adam SA, Butin-Israeli V, Cleland MM, Shimi T, Goldman RD. Disruption of lamin B1 and lamin B2 processing and localization by farnesyltransferase inhibitors. *Nucleus*. 2013;4(2):142-150. doi:10.4161/nucl.24089

325. Rusiñol AE, Sinensky MS. Farnesylated lamins, progeroid syndromes and farnesyl transferase inhibitors. *J Cell Sci*. 2006;119(Pt 16):3265-3272. doi:10.1242/jcs.03156

326. Gruenbaum Y, Foisner R. Lamins: Nuclear Intermediate Filament Proteins with Fundamental Functions in Nuclear Mechanics and Genome Regulation. *Annu Rev Biochem*. 2015;84(1):131-164. doi:10.1146/annurev-biochem-060614-034115

327. Kolb T, Maaß K, Hergt M, Aebi U, Herrmann H. Lamin A and lamin C form homodimers and coexist in higher complex forms both in the nucleoplasmic fraction and in the lamina of cultured human cells. *Nucleus*. 2011;2(5):425-433. doi:10.4161/nucl.2.5.17765

328. Shimi T, Pfleghaar K, Kojima S, et al. The A- and B-type nuclear lamin networks: microdomains involved in chromatin organization and transcription. *Genes Dev*. 2008;22(24):3409-3421. doi:10.1101/gad.1735208

329. Lammerding J, Fong LG, Ji JY, et al. Lamins a and C but not lamin B1 regulate nuclear mechanics. *J Biol Chem*. 2006;281(35):25768-25780. doi:10.1074/jbc.M513511200

330. Martin C, Chen S, Maya-Mendoza A, Lovric J, Sims PFG, Jackson DA. Lamin B1 maintains the functional plasticity of nucleoli. *J Cell Sci*. 2009;122(Pt 10):1551-1562. doi:10.1242/jcs.046284

331. Louvet E, Yoshida A, Kumeta M, Takeyasu K. Probing the stiffness of isolated nucleoli by atomic force microscopy. *Histochem Cell Biol*. 2014;141(4):365-381. doi:10.1007/s00418-013-1167-9

332. Broers JL, Machiels BM, van Eys GJ, et al. Dynamics of the nuclear lamina as monitored by GFP-tagged A-type lamins. *J Cell Sci*. 1999;112 (Pt 20):3463-3475. http://www.ncbi.nlm.nih.gov/pubmed/10504295. Accessed March 1, 2019.

333. Peter M, Nakagawa J, Dorée M, Labbé JC, Nigg EA. In vitro disassembly of the nuclear lamina and M phase-specific phosphorylation of lamins by cdc2 kinase. *Cell*. 1990;61(4):591-602. http://www.ncbi.nlm.nih.gov/pubmed/2188731. Accessed March 2, 2019.

334. Zhang Y-Q, Sarge KD. Sumoylation regulates lamin A function and is lost in lamin A mutants associated with familial cardiomyopathies. *J Cell Biol*. 2008;182(1):35-39. doi:10.1083/jcb.200712124

335. Swift J, Ivanovska IL, Buxboim A, et al. Nuclear lamin-A scales with tissue stiffness and enhances matrix-directed differentiation. *Science*. 2013;341(6149):1240104. doi:10.1126/science.1240104

336. Fong LG. Prelamin A and lamin A appear to be dispensable in the nuclear lamina. *J Clin Invest*. 2006;116(3):743-752. doi:10.1172/JCI27125

337. Cho S, Abbas A, Irianto J, et al. Progerin phosphorylation in interphase is lower and less mechanosensitive than lamin-A,C in iPS-derived mesenchymal stem cells. *Nucleus*. 2018;9(1):235-250. doi:10.1080/19491034.2018.1460185

338. Schirmer EC, Guan T, Gerace L. Involvement of the lamin rod domain in heterotypic lamin interactions important for nuclear organization. *J Cell Biol*. 2001;153(3):479-489. doi:10.1083/JCB.153.3.479

339. Grossman E, Dahan I, Stick R, Goldberg MW, Gruenbaum Y, Medalia O. Filaments assembly of ectopically expressed Caenorhabditis elegans lamin within Xenopus oocytes. *J Struct Biol*. 2012;177(1):113-118. doi:10.1016/J.JSB.2011.11.002

340. Ben-Harush K, Wiesel N, Frenkiel-Krispin D, et al. The Supramolecular Organization of the C. elegans Nuclear Lamin Filament. *J Mol Biol*. 2009;386(5):1392-1402. doi:10.1016/J.JMB.2008.12.024

341. Wilson KL, Foisner R. Lamin-binding Proteins. *Cold Spring Harb Perspect Biol*. 2010;2(4):a000554. doi:10.1101/cshperspect.a000554

342. Schirmer EC, Foisner R. Proteins that associate with lamins: Many faces, many functions. *Exp Cell Res*. 2007;313(10):2167-2179. doi:10.1016/J.YEXCR.2007.03.012

343. Bank EM, Ben-Harush K, Wiesel-Motiuk N, et al. A laminopathic mutation disrupting lamin filament assembly causes disease-like phenotypes in *Caenorhabditis elegans*. Goldman RD, ed. *Mol Biol Cell*. 2011;22(15):2716-2728. doi:10.1091/mbc.e11-01-0064

344. Wiesel N, Mattout A, Melcer S, et al. Laminopathic mutations interfere with the assembly, localization, and dynamics of nuclear lamins. *Proc Natl Acad Sci U S A*. 2008;105(1):180-185. doi:10.1073/pnas.0708974105

345. Worman HJ, Courvalin J-C. How do mutations in lamins A and C cause disease? *J Clin Invest*. 2004;113(3):349-351. doi:10.1172/JCI20832

346. Chang W, Worman HJ, Gundersen GG. Accessorizing and anchoring the LINC complex for multifunctionality. *J Cell Biol*. 2015;208(1):11-22. doi:10.1083/jcb.201409047

347. Sood V, Brickner JH. Nuclear pore interactions with the genome. *Curr Opin Genet Dev*. 2014;25:43-49. doi:10.1016/j.gde.2013.11.018

348. Light WH, Brickner JH. Nuclear pore proteins regulate chromatin structure and

transcriptional memory by a conserved mechanism. *Nucleus*. 2013;4(5):357-360. doi:10.4161/nucl.26209

349. Lomakin A, Nader G, Piel M. Forcing Entry into the Nucleus. *Dev Cell*. 2017;43(5):547-548. doi:10.1016/j.devcel.2017.11.015

350. Elosegui-Artola A, Andreu I, Beedle AEM, et al. Force Triggers YAP Nuclear Entry by Regulating Transport across Nuclear Pores. *Cell*. 2017;171(6):1397-1410.e14. doi:10.1016/j.cell.2017.10.008

351. Dobrokhotov O, Samsonov M, Sokabe M, Hirata H. Mechanoregulation and pathology of YAP/TAZ via Hippo and non-Hippo mechanisms. *Clin Transl Med*. 2018;7(1):23. doi:10.1186/s40169-018-0202-9

352. Taniura H, Glass C, Gerace L. A chromatin binding site in the tail domain of nuclear lamins that interacts with core histones. *J Cell Biol*. 1995;131(1):33-44. doi:10.1083/JCB.131.1.33

353. Meuleman W, Peric-Hupkes D, Kind J, et al. Constitutive nuclear lamina-genome interactions are highly conserved and associated with A/T-rich sequence. *Genome Res*. 2013;23(2):270-280. doi:10.1101/gr.141028.112

354. Kind J, van Steensel B. Stochastic genome-nuclear lamina interactions: modulating roles of Lamin A and BAF. *Nucleus*. 2014;5(2):124-130. doi:10.4161/nucl.28825

355. Amendola M, van Steensel B. Nuclear lamins are not required for lamina-associated domain organization in mouse embryonic stem cells. *EMBO Rep*. 2015;16(5):610-617. doi:10.15252/embr.201439789

356. Hirano Y, Hizume K, Kimura H, Takeyasu K, Haraguchi T, Hiraoka Y. Lamin B receptor recognizes specific modifications of histone H4 in heterochromatin formation. *J Biol Chem*. 2012;287(51):42654-42663. doi:10.1074/jbc.M112.397950

357. Lee KK, Haraguchi T, Lee RS, Koujin T, Hiraoka Y, Wilson KL. Distinct functional domains in emerin bind lamin A and DNA-bridging protein BAF. *J Cell Sci*. 2001;114(Pt 24):4567-4573. http://www.ncbi.nlm.nih.gov/pubmed/11792821. Accessed March 1, 2019.

358. Bione S, Maestrini E, Rivella S, et al. Identification of a novel X-linked gene responsible for Emery-Dreifuss muscular dystrophy. *Nat Genet*. 1994;8(4):323-327. doi:10.1038/ng1294-323

359. Shimojima M, Yuasa S, Motoda C, et al. Emerin plays a crucial role in nuclear invagination and in the nuclear calcium transient. *Sci Rep*. 2017;7(1):44312. doi:10.1038/srep44312

360. Lammerding J, Hsiao J, Schulze PC, Kozlov S, Stewart CL, Lee RT. Abnormal nuclear shape and impaired mechanotransduction in emerin-deficient cells. *J Cell Biol*. 2005;170(5):781-791. doi:10.1083/jcb.200502148

361. Holaska JM, Rais-Bahrami S, Wilson KL. Lmo7 is an emerin-binding protein that regulates the transcription of emerin and many other muscle-relevant genes. *Hum Mol Genet*. 2006;15(23):3459-3472. doi:10.1093/hmg/ddl423

362. Demmerle J, Koch AJ, Holaska JM. The Nuclear Envelope Protein Emerin Binds Directly to Histone Deacetylase 3 (HDAC3) and Activates HDAC3 Activity. *J Biol Chem*. 2012;287(26):22080-22088. doi:10.1074/jbc.M111.325308

363. Lund E, Oldenburg AR, Delbarre E, et al. Lamin A/C-promoter interactions specify chromatin state-dependent transcription outcomes. *Genome Res*. 2013;23(10):1580-

1589. doi:10.1101/gr.159400.113

364. Pradhan R, Ranade D, Sengupta K. Emerin modulates spatial organization of chromosome territories in cells on softer matrices. *Nucleic Acids Res*. 2018;46(11):5561-5586. doi:10.1093/nar/gky288

365. Buxboim A, Swift J, Irianto J, et al. Matrix Elasticity Regulates Lamin-A,C Phosphorylation and Turnover with Feedback to Actomyosin. *Curr Biol*. 2014;24(16):1909-1917. doi:10.1016/J.CUB.2014.07.001

366. Philip JT, Dahl KN. Nuclear mechanotransduction: Response of the lamina to extracellular stress with implications in aging. *J Biomech*. 2008;41(15):3164-3170. doi:10.1016/J.JBIOMECH.2008.08.024

367. Ivorra C, Kubicek M, González JM, et al. A mechanism of AP-1 suppression through interaction of c-Fos with lamin A/C. *Genes Dev*. 2006;20(3):307-320. doi:10.1101/gad.349506

368. González JM, Navarro-Puche A, Casar B, Crespo P, Andrés V. Fast regulation of AP-1 activity through interaction of lamin A/C, ERK1/2, and c-Fos at the nuclear envelope. *J Cell Biol*. 2008;183(4):653-666. doi:10.1083/jcb.200805049

369. Serebryannyy L, Misteli T. Protein sequestration at the nuclear periphery as a potential regulatory mechanism in premature aging. *J Cell Biol*. 2018;217(1):21-37. doi:10.1083/jcb.201706061

370. Dechat T, Korbei B, Vaughan OA, Vlcek S, Hutchison CJ, Foisner R. Lamina-associated polypeptide 2alpha binds intranuclear A-type lamins. *J Cell Sci*. 2000;113 Pt 19:3473-3484. http://www.ncbi.nlm.nih.gov/pubmed/10984438. Accessed March 6, 2019.

371. Pekovic V, Harborth J, Broers JL V, et al. Nucleoplasmic LAP2alpha-lamin A complexes are required to maintain a proliferative state in human fibroblasts. *J Cell Biol*. 2007;176(2):163-172. doi:10.1083/jcb.200606139

372. Holaska JM, Kowalski AK, Wilson KL. Emerin Caps the Pointed End of Actin Filaments: Evidence for an Actin Cortical Network at the Nuclear Inner Membrane. Marc W. Kirschner, ed. *PLoS Biol*. 2004;2(9):e231. doi:10.1371/journal.pbio.0020231

373. Ho CY, Jaalouk DE, Vartiainen MK, Lammerding J. Lamin A/C and emerin regulate MKL1–SRF activity by modulating actin dynamics. *Nature*. 2013;497(7450):507-511. doi:10.1038/nature12105

374. Lombardi ML, Jaalouk DE, Shanahan CM, Burke B, Roux KJ, Lammerding J. The interaction between nesprins and sun proteins at the nuclear envelope is critical for force transmission between the nucleus and cytoskeleton. *J Biol Chem*. 2011;286(30):26743-26753. doi:10.1074/jbc.M111.233700

375. Uzer G, Thompson WR, Sen B, et al. Cell Mechanosensitivity to Extremely Low-Magnitude Signals Is Enabled by a LINCed Nucleus. *Stem Cells*. 2015;33(6):2063-2076. doi:10.1002/stem.2004

376. Horn HF, Brownstein Z, Lenz DR, et al. The LINC complex is essential for hearing. *J Clin Invest*. 2013;123(2):740-750. doi:10.1172/JCI66911

377. Rheinwatd JG, Green H. Seria cultivation of strains of human epidemal keratinocytes: the formation keratinizin colonies from single cell is. *Cell*. 1975;6(3):331-343. doi:10.1016/S0092-8674(75)80001-8

378. Boukamp P, Petrussevska RT, Breitkreutz D, Hornung J, Markham A, Fusenig NE. Normal

keratinization in a spontaneously immortalized aneuploid human keratinocyte cell line. *J Cell Biol*. 1988;106(3):761-771. doi:10.1083/jcb.106.3.761

379. Ana Catarina Laly Aguedo. Dissecting the role of the keratin cytoskeleton in cellular mechanotransduction. 2019.

380. Andrä K, Kornacker I, Jörgl A, et al. Plectin-isoform-specific rescue of hemidesmosomal defects in plectin (-/-) keratinocytes. *J Invest Dermatol*. 2003;120(2):189-197. doi:10.1046/j.1523-1747.2003.12027.x

381. Hoon Lee J, Ju Back S, Im M, et al. Epigenetic Modulation of Gene Expression during Keratinocyte Differentiation. *Epigenetic Chang Keratinocyte Differ Ann Dermatol*. 2012;24(3). doi:10.5021/ad.2012.24.3.261

382. Liang G, Lin JCY, Wei V, et al. Distinct localization of histone H3 acetylation and H3-K4 methylation to the transcription start sites in the human genome. *Proc Natl Acad Sci U S A*. 2004;101(19):7357-7362. doi:10.1073/pnas.0401866101

383. Nava MM, Miroshnikova YA, Biggs LC, et al. Heterochromatin-Driven Nuclear Softening Protects the Genome against Mechanical Stress-Induced Damage. *Cell*. April 2020. doi:10.1016/j.cell.2020.03.052

384. Frye M, Fisher AG, Watt FM. Epidermal stem cells are defined by global histone modifications that are altered by Myc-induced differentiation. *PLoS One*. 2007;2(8). doi:10.1371/journal.pone.0000763

385. Kovalchuk N, Starov V, Holdich R. Effect of aggregation on viscosity of colloidal suslension. *Colloid J*. 2010;72(5):647-652. doi:10.1134/S1061933X10050108

386. Su C, Gao G, Schneider S, et al. DNA damage induces downregulation of histone gene expression through the G1 checkpoint pathway. *EMBO J*. 2004;23(5):1133-1143. doi:10.1038/sj.emboj.7600120

387. Padeken J, Heun P. Nucleolus and nuclear periphery: Velcro for heterochromatin. *Curr Opin Cell Biol*. 2014;28(1):54-60. doi:10.1016/j.ceb.2014.03.001

388. Belin BJ, Lee T, Mullins RD. DNA damage induces nuclear actin filament assembly by formin-2 and spire-1/2 that promotes efficient DNA repair. *Elife*. 2015;4(AUGUST2015). doi:10.7554/eLife.07735

389. Cho S, Vashisth M, Abbas A, et al. Mechanosensing by the Lamina Protects against Nuclear Rupture, DNA Damage, and Cell-Cycle Arrest. *Dev Cell*. 2019;49(6):920-935.e5. doi:10.1016/j.devcel.2019.04.020

390. Swift J, Ivanovska IL, Buxboim A, et al. Nuclear Lamin-A Scales with Tissue Stiffness and Enhances Matrix-Directed Differentiation. *Science*. 2013;341(6149):1240104. doi:10.1126/SCIENCE.1240104

391. Panier S, Boulton SJ. Double-strand break repair: 53BP1 comes into focus. *Nat Rev Mol Cell Biol*. 2014;15(1):7-18. doi:10.1038/nrm3719

392. Gonzalo S. DNA damage and lamins. *Adv Exp Med Biol*. 2014;773:377-399. doi:10.1007/978-1-4899-8032-8_17

393. Engler AJ, Sen S, Sweeney HL, Discher DE. Matrix Elasticity Directs Stem Cell Lineage Specification. *Cell*. 2006;126(4):677-689. doi:10.1016/j.cell.2006.06.044

394. Aneskievich BJ, Fuchs E. Terminal differentiation in keratinocytes involves positive as well as negative regulation by retinoic acid receptors and retinoid X receptors at retinoid response elements. *Mol Cell Biol*. 1992;12(11):4862-4871.

doi:10.1128/mcb.12.11.4862

395. Mills MA, Yang N, Weinberger R, et al. Differential expression for the actin-binding proteins, α-actinin-2 and -3, in different species: Implications for the evolution of functional redundancy. *Hum Mol Genet*. 2001;10(13):1335-1346. doi:10.1093/hmg/10.13.1335

396. Jonkman MF, Heeres K, Pas HH, et al. Effects of keratin 14 ablation on the clinical and cellular phenotype in a kindred with recessive epidermolysis bullosa simplex. *J Invest Dermatol*. 1996;107(5):764-769. doi:10.1111/1523-1747.ep12365805

397. Fine JD, Bruckner-Tuderman L, Eady RAJ, et al. Inherited epidermolysis bullosa: Updated recommendations on diagnosis and classification. *J Am Acad Dermatol*. 2014;70(6):1103-1126. doi:10.1016/j.jaad.2014.01.903

398. Coulombe PA, Lee CH. Defining keratin protein function in skin epithelia: Epidermolysis bullosa simplex and its aftermath. *J Invest Dermatol*. 2012;132(3 PART 2):763-775. doi:10.1038/jid.2011.450

399. Khatau SB, Hale CM, Stewart-Hutchinson PJ, et al. A perinuclear actin cap regulates nuclear shape. *Proc Natl Acad Sci U S A*. 2009;106(45):19017-19022. doi:10.1073/pnas.0908686106

400. Lee C-H, Kim M-S, Min Chung B, Leahy DJ, Coulombe PA. Structural basis for heteromeric assembly and perinuclear organization of keratin filaments. *Nat Struct Mol Biol*. 2012;19(7). doi:10.1038/nsmb.2330

401. Frijns E, Sachs N, Kreft M, Wilhelmsen K, Sonnenberg A. EGF-induced MAPK signaling inhibits hemidesmosome formation through phosphorylation of the integrin ??4. *J Biol Chem*. 2010;285(48):37650-37662. doi:10.1074/jbc.M110.138818

402. Zhang Q, Ragnauth CD, Skepper JN, et al. Nespirin-2 is a multi-isomeric protein that binds lamin and emerin at the nuclear envelope and forms a subcellular network in skeletal muscle. *J Cell Sci*. 2005;118(4):673-687. doi:10.1242/jcs.01642

403. Wang W, Zuidema A, Te Molder L, et al. Hemidesmosomes modulate force generation via focal adhesions. *J Cell Biol*. 2020;219(2). doi:10.1083/jcb.201904137

404. Lammerding J, Schulze PC, Takahashi T, et al. Lamin A/C deficiency causes defective nuclear mechanics and mechanotransduction. *J Clin Invest*. 2004;113(3):370-378. doi:10.1172/jci19670

405. Strom AR, Emelyanov A V., Mir M, Fyodorov D V., Darzacq X, Karpen GH. Phase separation drives heterochromatin domain formation. *Nature*. 2017;547(7662):241-245. doi:10.1038/nature22989

406. Larson AG, Elnatan D, Keenen MM, et al. Liquid droplet formation by HP1α suggests a role for phase separation in heterochromatin. *Nature*. 2017;547(7662):236-240. doi:10.1038/nature22822

407. Riback JA, Zhu L, Ferrolino MC, et al. Composition-dependent thermodynamics of intracellular phase separation. *Nature*. 2020;581(7807):209-214. doi:10.1038/s41586-020-2256-2

408. Xie X, Almuzzaini B, Drou N, et al. β-Actin-dependent global chromatin organization and gene expression programs control cellular identity. *FASEB J*. 2018;32(3):1296-1314. doi:10.1096/fj.201700753R

409. Rashmi RN, Eckes B, Glöckner G, et al. The nuclear envelope protein Nesprin-2 has roles

in cell proliferation and differentiation during wound healing. *Nucleus*. 2012;3(2):172-186. doi:10.4161/nucl.19090

410. Erdel F, Rademacher A, Vlijm R, et al. Mouse Heterochromatin Adopts Digital Compaction States without Showing Hallmarks of HP1-Driven Liquid-Liquid Phase Separation. *Mol Cell*. 2020;78(2):236-249.e7. doi:10.1016/j.molcel.2020.02.005

411. Iborra FJ, Pombo A, McManus J, Jackson DA, Cook PR. The topology of transcription by immobilized polymerases. *Exp Cell Res*. 1996;229(2):167-173. doi:10.1006/excr.1996.0355

412. Deng B, Melnik S, Cook PR. Transcription factories, chromatin loops, and the dysregulation of gene expression in malignancy. *Semin Cancer Biol*. 2013;23(2):65-71. doi:10.1016/j.semcancer.2012.01.003

413. Camps J, Erdos MR, Ried T. The role of lamin Bl for the maintenance of nuclear structure and function. *Nucleus*. 2015;6(1):8-14. doi:10.1080/19491034.2014.1003510

414. Rosen EM. BRCA1 in the DNA damage response and at telomeres. *Front Genet*. 2013;4(JUN):85. doi:10.3389/fgene.2013.00085

415. Tsuruta D, Hashimoto T, Hamill KJ, Jones JCR. Hemidesmosomes and focal contact proteins: Functions and cross-talk in keratinocytes, bullous diseases and wound healing. *J Dermatol Sci*. 2011;62(1):1-7. doi:10.1016/j.jdermsci.2011.01.005

416. Liu SC, Parsons S, Hanawalt PC. DNA repair in cultured keratinocytes. *J Invest Dermatol*. 1983;81(1 Suppl.):S179-S183. doi:10.1111/1523-1747.ep12541076

417. Suzuki K, Nakashima M, Yamashita S. Dynamics of ionizing radiation-induced DNA damage response in reconstituted three-dimensional human skin tissue. *Radiat Res*. 2010;174(4):415-423. doi:10.1667/RR2007.1

418. Acheva A, Ghita M, Patel G, Prise KM, Schettino G. Mechanisms of DNA Damage Response to Targeted Irradiation in Organotypic 3D Skin Cultures. Li JJ, ed. *PLoS One*. 2014;9(2):e86092. doi:10.1371/journal.pone.0086092

419. Asaithamby A, Hu B, Chen DJ. Unrepaired clustered DNA lesions induce chromosome breakage in human cells. *Proc Natl Acad Sci U S A*. 2011;108(20):8293-8298. doi:10.1073/pnas.1016045108

420. Cerutti E, Daniel L, Donnio L-M, et al. β-Actin and Nuclear Myosin I are responsible for nucleolar reorganization during DNA Repair. *bioRxiv*. May 2019:646471. doi:10.1101/646471

421. Ivanovska IL, Swift J, Spinler K, Dingal D, Cho S, Discher DE. Cross-linked matrix rigidity and soluble retinoids synergize in nuclear lamina regulation of stem cell differentiation. *Mol Biol Cell*. 2017;28(14):2010-2022. doi:10.1091/mbc.E17-01-0010

422. Németh A, Grummt I. Dynamic regulation of nucleolar architecture. *Curr Opin Cell Biol*. 2018;52:105-111. doi:10.1016/J.CEB.2018.02.013

423. Aubert M, O'donohue MF, Lebaron S, Gleizes PE. Pre-ribosomal RNA processing in human cells: From mechanisms to congenital diseases. *Biomolecules*. 2018;8(4). doi:10.3390/biom8040123

424. Erard MS, Belenguer P, Caizergues-Ferrer M, Pantaloni A, Amalric F. A major nucleolar protein, nucleolin, induces chromatin decondensation by binding to histone H1. *Eur J Biochem*. 1988;175(3):525-530. http://www.ncbi.nlm.nih.gov/pubmed/3409881. Accessed May 15, 2019.

425. Karsch S, Büchau F, Magin TM, Janshoff A. An intact keratin network is crucial for mechanical integrity and barrier function in keratinocyte cell sheets. *Cell Mol Life Sci*. January 2020:1-15. doi:10.1007/s00018-019-03424-7

426. Fujiwara S, Deguchi S, Magin TM. Disease-associated keratin mutations reduce traction forces and compromise adhesion and collective migration. *J Cell Sci*. 2020;133(14). doi:10.1242/jcs.243956

427. Guo Y, Redmond CJ, Leacock KA, et al. Keratin 14-dependent disulfides regulate epidermal homeostasis and barrier function via 14-3-3α and YAP1. *Elife*. 2020;9. doi:10.7554/eLife.53165

428. Jacob JT, Nair RR, Poll BG, et al. Keratin 17 regulates nuclear morphology and chromatin organization. *J Cell Sci*. October 2020:jcs.254094. doi:10.1242/jcs.254094

429. Troy TC, Turksen K. In vitro characteristics of early epidermal progenitors isolated from keratin 14 (K14)-deficient mice: Insights into the role of keratin 17 in mouse keratinocytes. *J Cell Physiol*. 1999;180(3):409-421. doi:10.1002/(SICI)1097-4652(199909)180:3<409::AID-JCP12>3.0.CO;2-V

430. Plotnikov A, Zehorai E, Procaccia S, Seger R. The MAPK cascades: Signaling components, nuclear roles and mechanisms of nuclear translocation. *Biochim Biophys Acta - Mol Cell Res*. 2011;1813(9):1619-1633. doi:10.1016/j.bbamcr.2010.12.012

431. Zhang Q, Ragnauth CD, Skepper JN, et al. Nespirin-2 is a multi-isomeric protein that binds lamin and emerin at the nuclear envelope and forms a subcellular network in skeletal muscle. *J Cell Sci*. 2005;118(4):673-687. doi:10.1242/jcs.01642

432. van Steensel B, Belmont AS. Lamina-Associated Domains: Links with Chromosome Architecture, Heterochromatin, and Gene Repression. *Cell*. 2017;169(5):780-791. doi:10.1016/j.cell.2017.04.022

433. Hernandez-Verdun D. Assembly and disassembly of the nucleolus during the cell cycle. *Nucleus*. 2011;2(3):189-194. doi:10.4161/nucl.2.3.16246

434. Nishimura K, Kumazawa T, Kuroda T, et al. Perturbation of Ribosome Biogenesis Drives Cells into Senescence through 5S RNP-Mediated p53 Activation. *Cell Rep*. 2015;10(8):1310-1323. doi:10.1016/j.celrep.2015.01.055

435. Dillinger S, Straub T, Nemeth A. Nucleolus association of chromosomal domains is largely maintained in cellular senescence despite massive nuclear reorganisation. *PLoS One*. 2017;12(6). doi:10.1371/journal.pone.0178821

436. Braun SMG, Kirkland JG, Chory EJ, Husmann D, Calarco JP, Crabtree GR. Rapid and reversible epigenome editing by endogenous chromatin regulators. *Nat Commun*. 2017;8(1):1-8. doi:10.1038/s41467-017-00644-y

437. Donovan DA, Crandall JG, Banks OGB, et al. Engineered Chromatin Remodeling Proteins for Precise Nucleosome Positioning. *Cell Rep*. 2019;29(8):2520-2535.e4. doi:10.1016/j.celrep.2019.10.046

438. McKenna T, Sola Carvajal A, Eriksson M. Skin Disease in Laminopathy-Associated Premature Aging. *J Invest Dermatol*. 2015;135(11):2577-2583. doi:10.1038/jid.2015.295

439. Saurat JH. Retinoids and psoriasis: Novel issues in retinoid pharmacology and implications for psoriasis treatment. In: *Journal of the American Academy of Dermatology*. Vol 41. Mosby Inc.; 1999:S2-S6. doi:10.1016/S0190-9622(99)70358-0

440. Levine N. Role of retinoids in skin cancer treatment and prevention. In: *Journal of the*

American Academy of Dermatology. Vol 39. Mosby Inc.; 1998:S62-S66. doi:10.1016/s0190-9622(98)70447-5

441. Bielli A, Scioli MG, D'Amico F, et al. Cellular retinoic acid binding protein-II expression and its potential role in skin aging. *Aging (Albany NY)*. 2019;11(6):1619-1632. doi:10.18632/aging.101813

442. Zasada M, Budzisz E. Retinoids: Active molecules influencing skin structure formation in cosmetic and dermatological treatments. *Postep Dermatologii i Alergol*. 2019;36(4):392-397. doi:10.5114/ada.2019.87443

443. Mitsui Y, Schneider EL. Increased nuclear sizes in senescent human diploid fibroblast cultures. *Exp Cell Res*. 1976;100(1):147-152. doi:10.1016/0014-4827(76)90336-0

444. Miron E, Oldenkamp R, Brown JM, et al. Chromatin arranges in chains of mesoscale domains with nanoscale functional topography independent of cohesin. *Sci Adv*. 2020;6(39):eaba8811. doi:10.1126/sciadv.aba8811

445. Cai Y, Zhang Y, Loh YP, et al. H3K27me3-rich genomic regions can function as silencers to repress gene expression via chromatin interactions. *bioRxiv*. April 2020:684712. doi:10.1101/684712

446. Winter L, Türk M, Harter PN, et al. Downstream effects of plectin mutations in epidermolysis bullosa simplex with muscular dystrophy. *Acta Neuropathol Commun*. 2016;4(1):44. doi:10.1186/s40478-016-0314-7

447. Wittmann M, Queisser G, Eder A, et al. Synaptic activity induces dramatic changes in the geometry of the cell nucleus: Interplay between nuclear structure, histone H3 phosphorylation, and nuclear calcium signaling. *J Neurosci*. 2009;29(47):14687-14700. doi:10.1523/JNEUROSCI.1160-09.2009